DESIGN AND ANALYSIS OF TIME DOMAIN REFLECTOMETRY PROBES FOR MEASURING WATER CONTENT AND BULK ELECTRICAL CONDUCTIVITY UNDER STEADY AND TRANSIENT FLOW CONDITIONS

by

Ty Ferré

A thesis

presented to the University of Waterloo

in fulfillment of the

thesis requirement for the degree of

Doctor of Philosophy

in

Earth Sciences

Waterloo, Ontario, Canada, 1997

BORROWER'S PAGE

The University of Waterloo requires the signature of all persons using or photocopying this thesis. Please sign below, and give address and date.

ABSTRACT

A time domain reflectometry (TDR) instrument includes an EM pulse generator, transmission lines to deliver the pulse to the point of measurement, and probes to guide the pulse through the medium. Standard, continuous-rod probes are comprised of two or three parallel metal rods that are pushed into the medium. The velocity of propagation of the pulse along the rods defines the relative dielectric permittivity of the medium. Given the large contrast in the relative dielectric permittivities of water (81), air (1) and soil solids (3-5), the relative dielectric permittivity of a soil sample is highly correlated with its water content. In addition, the pulse loses energy through electrical conduction as it travels along the rods. These energy losses can be related to the bulk electrical conductivity (EC) of the medium in the sample volume of the probe.

The bulk EC of a porous medium is a function of the water content and of the EC of the pore water. If the pore water chemistry is dominated by a single electrolytic solute, the pore water EC can be related to the solute concentration at a given water content. As a result, TDR offers the possibility of measuring both the water content and the solute concentration simultaneously, allowing for rapid, nondestructive monitoring of flow and transport in partially saturated media.

Standard, continuous-rod TDR probes have been shown to measure the length-weighted average water content along their length, even if the water content varies along the probe. The distribution of probe sensitivity in the plane perpendicular to the rods has only been described for homogeneous distributions and under restrictive heterogeneous conditions. A numerical model is used here to define the spatial distribution of probe sensitivity in the plane transverse to standard continuous-rod probes. The results show that the size of the sample area is directly related to the rod separation; an increase in the rod diameter results in a more uniform distribution of sensitivity in the transverse plane. A three-rod design has a far smaller sample area than a two-rod probe with the same separation of the outermost rods. Regardless of the probe configuration, the probe sensitivity is not uniform in the transverse plane. Therefore, the rods should be installed in a manner that minimizes water content variations between them to ensure that the measured relative dielectric permittivity correlates with a representative average water content in the sample volume.

Direct current EC measurements show a nonlinear dependence of the bulk EC on the water content. The results of a laboratory experiment conducted in a sand-filled column show that the TDR-measured EC follows the same relationship shown for direct current measurements. The relationship applies to both two-rod probes with and without baluns and three-rod probes. Results from this experiment also demonstrate that probe calibrations can be conducted in a saline solutions. In contrast to the laboratory results, a field experiment showed a linear dependence of the bulk EC on the water content. This result is critical for solute concentration monitoring if the water content varies along the rods. A

method of probe calibration is presented and used to monitor the advance of a solute step under steady-state flow.

The ability of continuous-rod probes to measure the water content and solute concentration in their sample volume has been demonstrated. However, these probes face limitations for profiling the water content and solute concentration with depth, measuring the water content very near the ground surface, and measuring the water content in electrically conductive media. Several alternative probes have been designed to address these shortcomings. Analytical and numerical analyses are presented to describe the response of these probes to changing water contents and to define their sample areas in the transverse plane. The results can be summarized generally based on the geometry of the metal rods and nonmetallic probe components for a given probe design. Any probe that places the probe materials in series with the medium, such as coated continuous-rod probes, will have a sensitivity that varies with the water content of the surrounding medium. As a result, the sample areas will not be constant, usually decreasing with increases in the soil water content. In addition, the measured relative dielectric permittivity will not be related uniquely to the average water content along the rods if the water content varies along the probe. Probes that place their components in parallel with the surrounding medium avoid these problems, showing sensitivities that are independent of the water content and measuring the correct length-weighted average water content along their length. The numerical approach can also be used to investigate the sensitivity of the response and sample area of an alternative probe on each of its design parameters, allowing for efficient optimization of the design.

An alternative TDR probe is presented that was designed to measure both the water content and the bulk EC over limited depth intervals. The probe is shown to produce water content profiles comparable to those measured with a neutron probe to 2 m depth. The EC response is calibrated to measure the solute concentration under temporally variable water content and solute concentrations, providing a unique ability to profile the resident solute concentration during transport under transient flow conditions in the field. Unfortunately, given that the probe materials are placed in series with the surrounding medium, the probe will not measure the correct length-weighted average water content or bulk EC if these properties vary along the probe. Therefore, the measurement interval should be as short as possible to limit the spatial variability of the water content and solute concentrations in the sample volume of the probe.

The results of numerical calibrations of published alternative probes consistently differ from physical probe calibrations. This may demonstrate errors in the methods of physical calibration. Poorly understood influences from the connection of the transmission line to the probe or from the field distribution at the ends of the rods may also add to the discrepancies between the measured and modeled probe responses. Further investigation of the causes of these differences will lead to greater understanding of the behavior of TDR probes, allowing for further improvements in their design.

ACKNOWLEDGMENTS

Funding was provided to me by the National Science Foundation through the Graduate Fellowship program. This funding allowed me the freedom to follow a course of study driven solely by my scientific interests. The importance of this academic freedom to my education cannot be overstated.

In general, I would like to recognize the spirit of cooperation among students, faculty and staff that I believe is one of the great strengths of the Department of Earth Sciences at the University of Waterloo. Specifically, my education has benefited greatly from interaction with many people in the Department of Earth Sciences. I would like to thank Dr. John Greenhouse for inspiring me to come to Waterloo and then selflessly encouraging me to follow my interests in defining a course of research. Dr. Gary Kachanoski introduce me to the possibilities of TDR and continually provided sound guidance on the direction of my work. Dr. John Cherry, through the University Consortium Solvents in Groundwater Program, funded my initial work leading to my thesis research. Dr. Bob Gillham gave me my first exposure to the field of unsaturated flow through his lectures and later gave me the opportunity to teach the subject; two experiences which rank as some of the most valuable during my graduate studies. Dave Redman was invaluable in teaching me how to use TDR and, more importantly, the importance of careful, critical thinking to scientific investigations. Rob McLaren provided me with the codes necessary to complete my numerical analyses. Paul Johnson and Bob Ingleton made difficult field work seem effortless through their experience and hard work. George Schneider designed and built the multiplexed DC resistivity system that I used in my field experiments. Dave Lawson continually sought sources of funding that helped me to afford to continue my studies. Finally, I would like to thank Dr. Dave Rudolph, my advisor, for his unwavering encouragement, his technical guidance and his confidence to allow me to choose the directions of my thesis.

My work also benefited greatly from the influence of two people external to the University of Waterloo. The numerical analysis of TDR behavior would have been impossible without the guidance and encouragement of Dr. John Knight, from Canberra, Australia. In addition, I was honored to have Dr. Clarke Topp agree to act as external examiner of my work.

PERSONAL ACKNOWLEDGMENTS

One's professional life does not exist separately from their personal life. Therefore, my thesis acknowledgments would be incomplete without recognizing the important roles that several people have played in my life during and leading to my graduate studies.

Firstly, I would like to thank my family. My mom has been an irreplaceable champion, teacher and friend throughout my life. I would also like to thank my dad, Cindy and Alex for making me a part of their lives. Finally, I'd like to thank Nan and Charlie for their encouragement and for keeping me in their thoughts.

I would like to thank some of the many people who influenced me through their teaching and guidance: Kiki Tamashiro, Aileen England, Brian Smith, Lincoln Phillips, Laura Thomas, Faye Bresnick, Carolyn Lavallee, Celeste Penkunas, Jean O'Toole, Chris von Lersner, Vicky Wingert, Lyle Silka and Tom Philipose.

Finally, I would like to thank the Halls, the Englands, the Dicksons, the Hamel-Smiths, the Ellams, Amy Roos, Erik Rader, Kevin Roe, Billy Barbieri, Ken Wihby, Blaine Ross, Sue DeRyck, Andy Mace, Ed Carr, Eric MeWhinney and Che McRae, some of the friends that give special meaning to my life.

DEDICATION

This work is dedicated to my grandfather, John A. O'Brien, whose strength of character, kindness, and love of education are my constant guides.

Honey, I hope you're watching.

TABLE OF CONTENTS

LIST OF TABLES

LIST OF FIGURES

1. CHAPTER ONE

BACKGROUND

1.1 *INTRODUCTION*

Laboratory and field measurements of the distribution of water and solutes in unsaturated media are essential to characterize the properties describing water flow and solute transport through partially saturated soils. Direct measurements of the spatial distribution of water in the field can delineate potential areas of slope failure, demonstrate the efficiency of irrigation or drainage programs, and define the likely pathways of water-borne contaminants through the shallow subsurface. Measurements of the distribution of solutes throughout the unsaturated zone can define areas of soil salinization as well as identifying sources of shallow contamination. Quantitative descriptions of porous media properties made in either the laboratory or in the field can be used in analytical and numerical analyses to predict the future impacts of water and solute movement for topics including crop productivity, slope stability, and contaminant transport and remediation.

Quantitative characterization of unsaturated flow requires a detailed description of the relationships between the hydraulic conductivity and the water content and between the water content and the water-phase pressure. Definition of these relationships depends upon accurate measurements of the water content. The heterogeneous distribution of soil properties in most natural systems further requires that these relationships be defined on a spatial scale comparable to the scale of variability of the medium properties. Detailed deterministic analyses rely on definition of the soil properties in undisturbed media; stochastic analyses make use of the statistical distribution of measurements commonly made on disturbed samples. Validation of quantitative flow analyses also requires detailed measurements of the spatial distribution of water content. Similarly, the spatial and temporal distributions of solute mass are required to define the solute transport characteristics of a medium and to validate the results of quantitative analyses of solute transport.

A method for water content monitoring should measure over a well-defined sample volume under a wide range of conditions. The method should have a small sample volume to provide fine spatial resolution while measuring over a volume that is large enough to be representative of the medium on a scale that is meaningful for flow and solute transport analyses. Nondestructive methods that can be used in undisturbed samples offer greater flexibility to sampling programs. In both the laboratory and the field, the ability to profile the water content along a single instrument inserted into the medium admits the possibility of extending to three-dimensional water content monitoring. For temporal monitoring, the method should be nondestructive, to minimize disruption of the flow field, and rapid, to ensure full characterization of the transient behavior. Current field methods for water content measurement include

neutron moderation, soil coring, tensiometry and time domain reflectometry (TDR); gravimetric measurements, tensiometry and TDR are commonly used to measure water content in the laboratory.

Gravimetric methods are the standard laboratory method for water content determination. Soil cores provide relatively undisturbed samples that can be subsampled for gravimetric water content analysis. The sample size over which the water content is measured is defined exactly. In addition to providing a direct measure of the water content, chemical analyses can be performed on extracted pore water for simultaneous solute concentration monitoring. However, coring is slow, expensive and destructive, making it inappropriate for detailed monitoring of either transient flow or solute transport.

The pressure of the water phase in an unsaturated medium can be measured with a tensiometer. This method is nondestructive, generally introduces minimal disturbance to the flow field, and is easily automated. In an air-water system, there is a characteristic relationship between the water-phase pressure and the water content of a given medium. However, this relationship is subject to hysteresis, limiting the conditions under which the water content can be inferred uniquely from a water-pressure measurement.

Neutron probes measure the hydrogen content of the surrounding medium. The probes employ a radioactive source of epithermal neutrons. Neutrons have a mass that is similar to that of hydrogen atoms; therefore, when the neutrons collide with hydrogen atoms they experience large energy losses, becoming thermalized. A detector on the probe counts the thermalized neutrons reaching the probe. The ratio of the thermalized neutrons detected to the epithermal neutrons produced by the source in a given time can be correlated to the hydrogen content of the medium. In the absence of other significant sources of hydrogen, this gives a nondestructive measure of the soil water content.

Their radioactive source and passive receiver allow neutron probes to be lowered to almost any depth of measurement in an access tube, making them the accepted standard for deep water content profiling. However, the probes face several limitations in common hydrogeological applications. The release of neutrons from a radioactive source is a random process; therefore, measurements must be made over a relatively long time (commonly longer than one minute) to ensure that the average number of epithermal neutrons provided by the source is constant among measurements. This long sampling time can limit the ability of neutron probes to monitor transient changes in the water content under some conditions. In addition, the sample volume of a neutron probe depends on the water content of the medium; as the water content of the medium decreases, an epithermal neutron will travel farther before it encounters a hydrogen atom, increasing the sample volume. Even in very wet soils, the sample volume of a neutron probe (a sphere with an approximate radius of 30 cm) is too large to provide fine scale measurements of the water content. Finally, the radioactive source of neutron probes presents safety and permitting constraints on their continued use in the field.

A TDR instrument measures the propagation velocity of a fast rise-time electromagnetic pulse through a porous medium. This velocity defines the average relative dielectric permittivity of the medium surrounding the TDR probe. The large contrast between the high relative dielectric permittivity of water

and the low relative dielectric permittivities of air and soil grains results in a strong correlation between the relative dielectric permittivity of a mixture of these components and the volumetric water content of the mixture. As a result, TDR can measure the water content of many soils without the need for site-specific calibration. Standard TDR field probes are comprised of two or three parallel metal rods that are installed vertically at the ground surface, extending to the depth of interest. The probes measure the average water content from the ground surface to the ends of the rods. The large sample volumes of the probes introduce limitations for profiling the water content with depth. In addition, as the pulse travels through the medium, it is subject to power losses through electrical conduction. Excessive power losses result in insufficient energy remaining to accurately determine the propagation velocity of the pulse from the instrument response, limiting the depth of investigation attainable with TDR in electrically conductive environments.

The characteristics required of a method for solute concentration monitoring are similar to those required for water content measurement: rapid, nondestructive measurement over a small, well-defined sample volume under a wide range of conditions. Current field methods for solute concentration measurement include solution sampling, soil coring, soil gas sampling, direct current (DC) electrical methods, and TDR; these methods are also employed in the laboratory.

Solution sampling involves the removal of pore water for chemical analysis. Pore water samples can be collected from an unsaturated medium under tension using porous cup solution samplers; for laboratory column studies, effluent samples can be collected as well. Given that sampling with porous cups removes water and solutes from the system, it must be considered to be destructive, especially under low water content conditions; however, solution sampling is less disruptive than coring while still offering complete characterization of the pore water chemistry. It is difficult to quantify the sample volume of a solution sampler. In general, for a given extracted volume of pore water, the volume of medium from which the sample is withdrawn will increase with a decrease in the water content. The main limitation facing solute concentration monitoring is the difficulty of collecting samples under low water content conditions. To limit the loss of volatile components due to sample collection under vacuum, soil-gas sampling is commonly used to monitor the concentrations of volatile compounds.

Many solute transport processes can be characterized by monitoring the movement of a conservative tracer. The bulk electrical conductivity (EC) of a medium is dependent on both the water content and the pore water EC. If the pore water chemistry is dominated by a simple electrolytic solute, the pore water EC is linearly related to the solute concentration. As a result, if the influence of the water content on the bulk EC can be accounted for, either by direct measurement or by imposing controlled flow conditions, bulk EC monitoring can provide a nondestructive measure of the concentration of an electrolytic tracer in a partially saturated medium. DC instruments designed to measure the bulk EC are inexpensive to construct and can be multiplexed readily for automated monitoring. The major limitation to the widespread use of DC measurements for monitoring solute concentrations during controlled

transport experiments in partially saturated media is the requirement of an independent measure of the water content.

As an electromagnetic pulse travels along a TDR probe it continually loses energy to the surrounding medium through electrical conduction. The amount of energy lost can be determined from the response of the instrument and then related to the bulk EC of the medium around the probe. As for DC measurements, if the influence of the water content can be removed, the TDR-measured EC can be related directly to the concentration of an electrolytic solute in the sample volume of the probe. The unique ability of TDR to measure both the water content and the bulk EC in the same volume of porous medium may allow for monitoring of the concentration of an electrolytic tracer in a partially saturated medium. However, this application requires a full description of the dependence of the EC response of TDR on the water content. TDR has been shown to measure the average pore water EC under spatially uniform water content conditions, even if the concentration of an electrolytic solute varies along the probe. However, solute concentration measurement under transient flow requires an investigation of the EC response of TDR probes in a medium with water contents and solute concentrations that vary independently in time along the rods.

1.2 Monitoring the Soil Water Content with Continuous-rod TDR Probes

1.2.1 TDR Instrumentation

A TDR instrument includes a wave generator that produces fast rise-time electromagnetic pulses. The pulses are delivered to a coaxial line and continue to travel along the line until either all of their energy is dissipated or they reach the end of the line. At the end of the line, any remaining energy is reflected back to the instrument along the coaxial line. The propagation velocity of the pulse along the line is related to the relative dielectric permittivity, K, of the medium surrounding the line through [*Fellner-Feldegg*, 1969],

$$v = \frac{L}{t} = \frac{c}{\sqrt{K}}, \tag{1-1}$$

where c is the speed of light in a vacuum, L is the length of the line, and t is the travel time of the pulse to the end of the line.

Physically, the dielectric permittivity describes the ability of the charge within a medium to be polarized by a time varying external electric field; the relative dielectric permittivity describes the ratio of

the dielectric permittivity to the dielectric permittivity of free space. The dielectric response of a medium is comparable to a capacitance; an electromagnetic pulse moves more slowly through a medium with a high dielectric permittivity because more time is required for the molecules to align with the external field and for energy to be released when the external field is removed.

TDR instruments are used widely by the utilities industry to locate breaks in buried cables; standard TDR instruments are still produced as cable testers. The travel time of the round trip from the instrument to the break in a cable and back defines the distance to the break by Equation 1-1 because the wires are insulated, surrounded by a medium with a known relative dielectric permittivity.

In an alternative use of the TDR method, the dielectric permittivity of a medium can be defined from the propagation velocity of a pulse through a sample of the medium. For this application, a coaxial cable leading from the instrument is connected to a larger diameter coaxial sample holder of known length that is filled with the medium, as shown on Figure 1-1. In a coaxial line, all of the energy of the pulse is contained by the outer shield; as a result, the propagation velocity of the pulse is a function of the relative dielectric permittivity of the medium between the central wire and the outer shield. Equation 1-1 defines the relative dielectric permittivity of the sample from the measured travel time through a cell of known length. Measurement of the dielectric permittivity using this method is especially useful for fluids because they can be distributed uniformly within the coaxial cell.

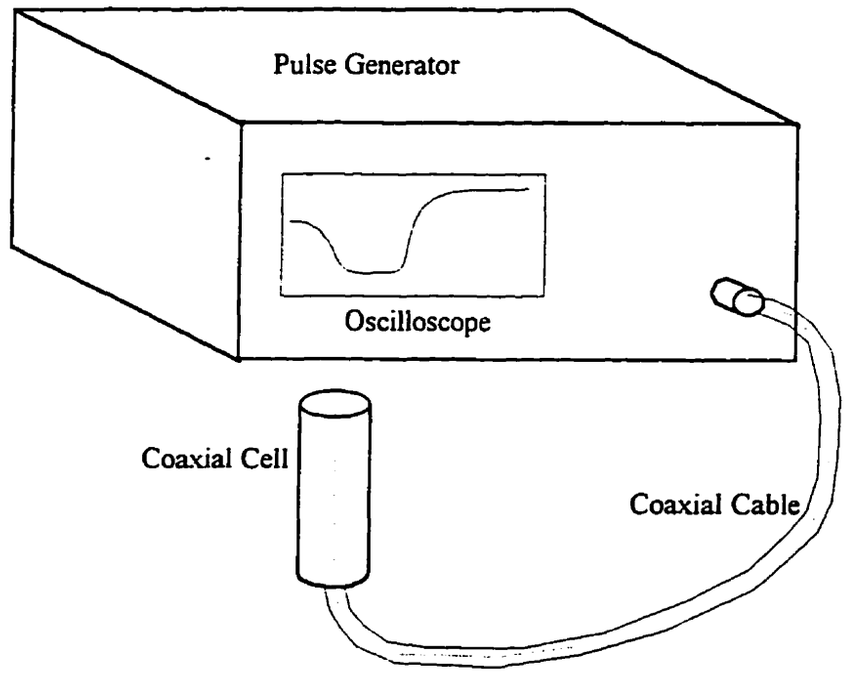

Figure 1-1. TDR instrumentation.

1.2.2 Design and Application of Continuous-rod TDR Waveguides

Initial investigations of the response of TDR to changes in the soil water content used coaxial cells packed with soil samples [*Topp et al.*, 1980]. Unfortunately, coaxial probes cannot be installed easily into a medium and, therefore, require repacking of the sample in the cell. To extend the application of TDR to water content measurement in undisturbed media, *Topp et al.* [1982] introduced twin parallel-rod probes.

The pulse delivered to a coaxial probe is unbalanced with respect to ground, with a positive voltage spike supplied to the inner wire while the outer shield is grounded. The geometry of a twin-rod probe requires a balanced pulse with respect to ground; a positive voltage is applied to one rod and a negative voltage of equal magnitude is applied to the other rod, such that the plane of zero voltage runs between the rods. A balancing transformer (balun) is commonly used to alter the unbalanced output from the cable tester to a balanced signal appropriate for twin-rod probes. The signal from the balun is delivered to the probe through a shielded, parallel-wire transmission line. *Zegelin et al.* [1989] later demonstrated that the electrical potential distribution surrounding a three-rod probe closely approximates that around a coaxial cell, allowing for direct connection of these probes to the coaxial output from the TDR instrument. Standard two- and three-rod TDR probes are shown on Figure 1-2; these probe designs are referred to collectively as standard, continuous-rod probes.

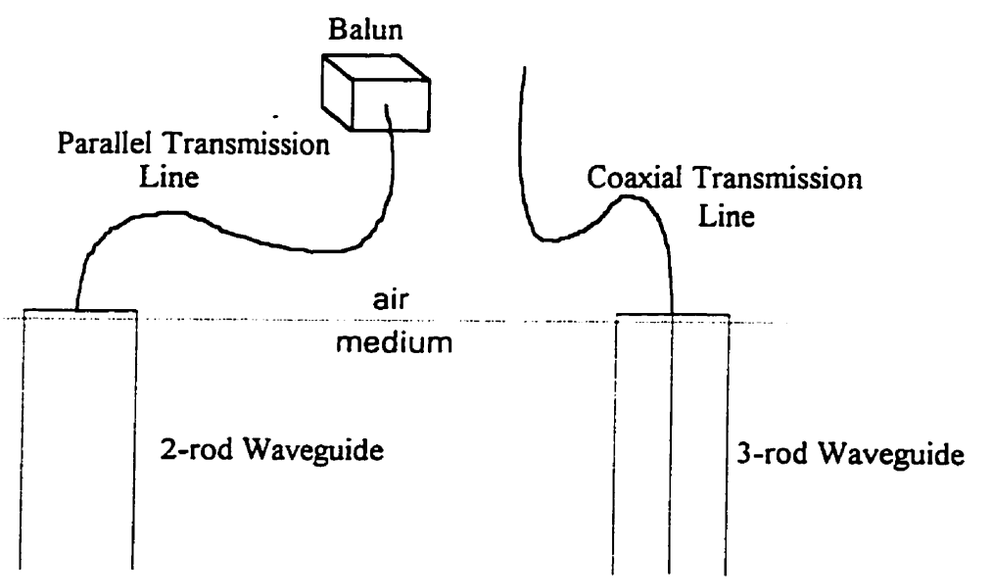

Figure 1-2. Standard, continuous-rod TDR probes: two- and three-rod designs.

A change in the relative dielectric permittivity of the medium between the rods or in the separation or diameters of the rods along the probe causes a change in the impedance of the probe. At any point along the probe that the pulse encounters a change in the impedance, a portion of the energy of the pulse is reflected back along the waveguide to the pulse generator. This returning energy is displayed as a function of time as a waveform on the oscilloscope of the TDR instrument (Figure 1-3). The energy of the reflected pulse increases with an increase in the impedance difference across the discontinuity. As a result, two- and three-rod probes typically show clear reflections from the connection of the transmission line to the probe, the entry of the rods into the medium, and the ends of the rods. *Topp et al.* [1982] described a method of interpreting the travel time between the partial reflection of the pulse at the ground surface and the total reflection from the end of the waveguide based on fitting four straight lines to sections of the waveform and locating their points of intersection, as shown on Figure 1-3.

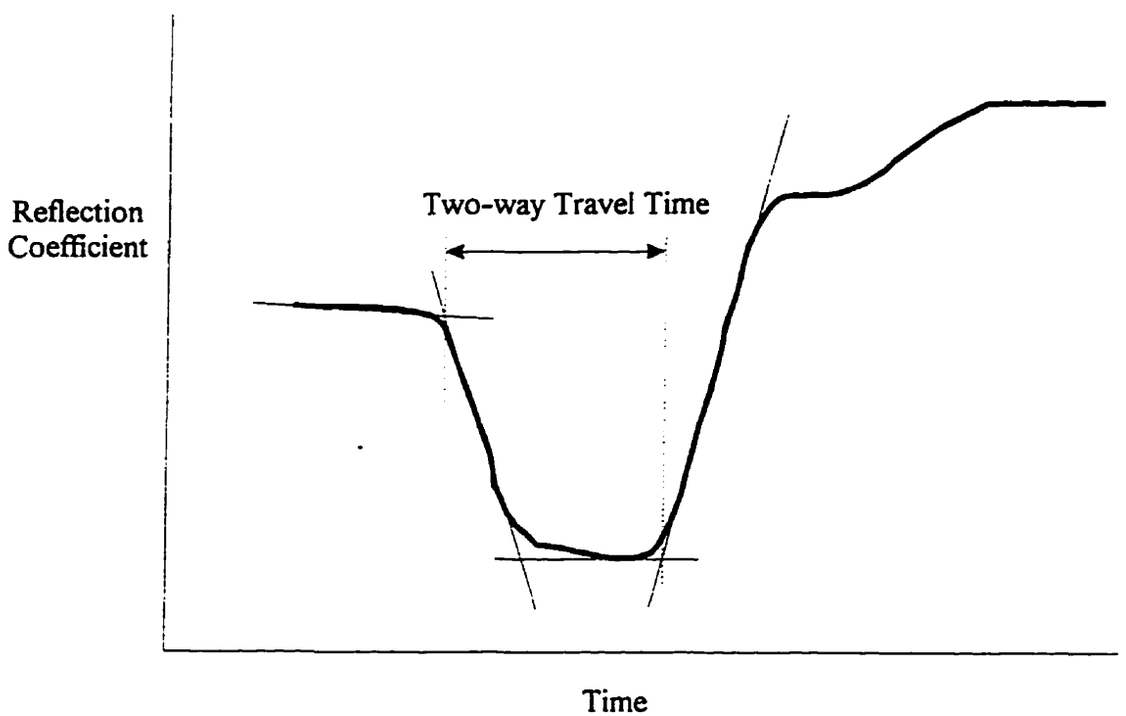

Figure 1-3. Sample TDR waveform.

For a probe of known length, the travel time to the ends of the rods determined from the waveform defines the average velocity of propagation of the electromagnetic pulse along the probe. This velocity is controlled by the relative dielectric permittivity of the medium surrounding the probe [*Fellner-Feldegg*, 1969]. Due to the large differences in the relative dielectric permittivities of water (81), air (1), and soil particles (3-5) [*Weast*, 1990], the relative dielectric permittivities of most soils are strongly

correlated with their volumetric water content. *Topp et al.* [1980] described a general relationship between the relative dielectric permittivity of a soil, K_{soil}, and the soil water content, θ, that is applicable for a wide range of soil types,

$$K_{soil} = 3.03 + 9.3\theta + 146\theta^2 - 76.7\theta^3. \qquad (1\text{-}2)$$

This relationship can be stated in a form that defines the water content from the measured relative dielectric permittivity of the bulk soil as,

$$\theta = -0.053 + 0.0292K_{soil} - 0.00055K_{soil}^2 + 0.0000043K_{soil}^3. \qquad (1\text{-}3)$$

Given that TDR measures the average propagation velocity of the pulse over the length of the probe, the sample volume of a TDR probe extends over its entire length. The measured propagation velocity has been shown to correspond to the correct length-weighted average water content over the length of a continuous-rod probe, even if the water content varies along the rods [*Topp et al.*, 1982a]. The choice of an appropriate length for TDR rods must balance the limitations of the large sample volumes of long probes with the need for some minimum travel time required to separate clearly on the waveform the reflections from the point of entry into the medium and from the ends of the rods.

Horizontally installed continuous-rod probes are ideally suited to profiling the water content along a laboratory column (Figure 1-4). The vertical extent of the sample volume of the horizontal rods is very small, especially for rods placed in the horizontal plane. These small sample areas lead to fine vertical spatial resolution of the water content profile. To ensure that the travel times are long enough to accurately identify the characteristic reflections on the waveforms, horizontal TDR rods should not be used to measure the water content in small diameter (< 10 cm) columns.

TDR rods can be installed horizontally in the field by repacking the soil around buried probes; however, this precludes the possibility of measuring flow through an undisturbed medium. Horizontal rods can be inserted through the walls of trenches dug outside of the measurement domain as well; but, these trenches can impose unacceptable boundary conditions on water flow and solute transport. In addition, both methods of installing horizontal probes in the field are time and labor intensive. As a result, it would be impractical to profile the water content beneath a number of locations using horizontal rods, limiting the ability to conduct reconnaissance measurements or to measure the water content in three spatial dimensions in the field. Due to these limitations, it is common to install continuous-rod waveguides vertically at the ground surface in the field, with the rods extending to the depth of interest (Figure 1-4).

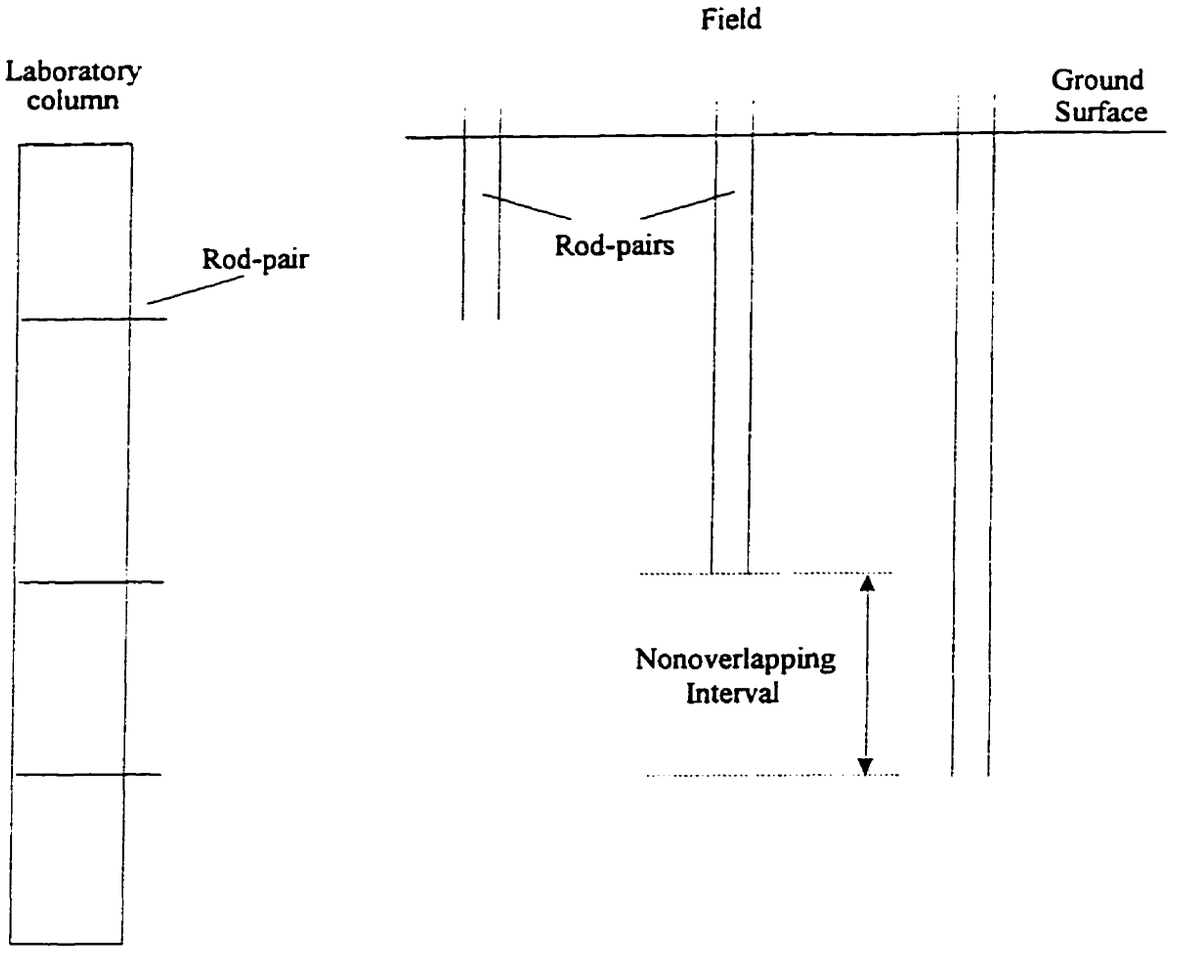

Figure 1-4. Typical laboratory and field continuous-rod TDR probe installations.

1.2.3 Profiling the Water Content in the Field

The average water content in the sample volume of a TDR probe is defined by the measured travel time along the probe through Equations 1-1 and 1-3. TDR measures the length-weighted average water content over the length of the rods. The total water volume beneath a unit surface area over the length of the rods is the product of the water content and the rod length.

Topp [1987] proposed that the water content of a discrete depth interval could be determined from the responses of two adjacent rod-pairs with the shorter rod-pair extending to the top of the depth-interval and the longer pair extending to the base of the interval (Figure 1-4). Assuming that there is no horizontal variability in the water content between the rod-pairs, the water volume in the nonoverlapping interval per unit area in the plane perpendicular to the rods equals the difference between the volumes per

unit area measured with each probe. The water content in the nonoverlapping interval is equal to the volume per unit area in the interval divided by the interval length.

$$\theta_n = \frac{\theta_l L_l - \theta_s L_s}{L_l - L_s} = \frac{\theta_l L_l - \theta_s L_s}{L_n}. \qquad (1\text{-}4)$$

where θ is the water content, L is the probe length and the subscripts n, s and l denote the nonoverlapping region and the short and long rod-pairs, respectively, [*Topp*, 1987].

The dielectric permittivity of the nonoverlapping interval is defined by Equation 1-1 using the difference in the travel times measured with the long and short rod-pairs,

$$\sqrt{K_n} = \frac{c(t_l - t_s)}{L_n}. \qquad (1\text{-}5)$$

where t is the one-way travel time over the rod-pair.

This method of water content profiling faces three practical limitations. Firstly, the need for an additional rod-pair for each depth interval requires a large number of rod-pairs for fine-scale vertical profiling. Secondly, the differencing of the average water content over the overlapping interval explicitly assumes that the water content is horizontally uniform over this interval. Therefore, any horizontal variability in the water content in the overlapping interval between two rod-pairs will be incorrectly attributed to the nonoverlapping vertical interval. Finally, to profile to significant depths with this method, water content measurements must be made over long continuous rods. The pulse continually loses energy through reflection and through electrical conduction, with preferential degradation of the high frequency portion of the power spectrum. As a result, the reflection from the ends of the rods becomes less sharp with increased rod lengths, introducing errors into the determination of the travel time along the rods for long rod-pairs. Differencing two travel times, each subject to uncertainty due to signal degradation, can lead to large errors in the calculated relative dielectric permittivity over short nonoverlapping intervals at depth, limiting the minimum achievable profiling interval.

Alternative TDR probes have been designed specifically to address the shortcomings of the interval differencing approach to water content profiling with continuous-rod probes. All of the probes are variants of the two- or three-rod design, installed vertically at the soil surface to measure the water content beneath a single surface point. Some of the probes have been designed to isolate a section of the subsurface for measurement, others focus on improving the ability to locate the terminal reflection accurately. Many of the probe designs also reduce energy losses along through electrical conduction.

Most of the published alternative TDR probe designs include nonmetallic probe materials in contact with the metal rods. As a result, the dielectric permittivities measured by the probes reflect some average of the dielectric permittivities of the probe materials and the surrounding medium. Due to the influence of the probe materials, the measured travel times must be calibrated to define the water content of the surrounding medium; the "universal" calibration represented by Equations 1-2 and 1-3 no longer apply. Unfortunately, physical calibration of the response of an alternative probe is difficult and time intensive, especially for long, unwieldy field probes.

1.2.4 The Sample Areas of TDR Probes

Baker and Lascano [1989] conducted a laboratory experiment to investigate the sample area of a two-rod probe. A two-rod probe (3.175 mm diameter rods separated by 50 mm) was inserted vertically into a box and surrounded by water-filled glass tubes. Individual tubes were drained to determine the sensitivity of the probe to the medium at the location of the tube. The results of this experiment showed that this configuration of a two-rod probe was sensitive only to the properties of the medium located within an ellipse in the plane perpendicular to the rods that is centered at the midpoint between the rods (Figure 1-5). The length of the axis of the ellipse extending through the rods was approximately twice the rod separation; the shorter axis of the ellipse had a length less than the rod separation. The probe sensitivity was not uniformly distributed throughout the ellipse, with greater sensitivity concentrated in the regions adjacent to the surfaces of the rods. In a similar experiment, they showed that the rods were insensitive to the medium beyond the ends of the rods, suggesting that the sample volume is defined by the projection of the ellipse along the length of the probe.

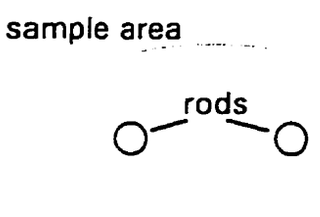

Figure 1-5. The sample area in the plane perpendicular to a two-rod probe determined by *Baker and Lascano* [1989].

Knight [1991] demonstrated that the methodology of *Baker and Lascano* [1989] could not uniquely define the spatial sensitivity of a continuous-rod probe in the transverse plane. Rather, *Knight* [1992] developed an analytical solution describing the spatial sensitivity in the plane perpendicular to any

configuration of a continuous-rod probe surrounded by a medium with a spatially uniform relative dielectric permittivity. The results of his analysis demonstrated that the spatial distribution of probe sensitivity around a two-rod probe is dependent upon the separation of the rods and their diameters. By calculating the fraction of the probe sensitivity contained within circular regions centered on the rods, he concluded that two-rod probes should be designed with a rod separation no greater than ten times the rod diameter. This general guideline was intended to ensure that the probe sensitivity was not restricted to the region immediately adjacent to the rods.

In developing his analytical description of probe sensitivity, *Knight* [1992] assumed that the relative dielectric permittivity in the transverse plane was uniform. He then imposed a slight perturbation at each point in the K field to define the spatial sensitivity of the probe response to changes in the relative dielectric permittivity throughout the transverse plane. This approach inherently assumes that the perturbation in the field does not alter the spatial weighting functions; this is reasonable for small perturbations in an otherwise homogeneous field. The inclusion of very low dielectric permittivity probe materials within the sample areas of the alternative probes clearly violates this assumption. As a result, the spatial sensitivities of the published alternative probes will differ from those of standard continuous-rod probes; however, the analytical approach of *Knight* [1992] cannot be applied to define these spatial sensitivities.

1.3 *Monitoring the Bulk Electrical Conductivity with Continuous-rod TDR Probes*

1.3.1 Descriptions of the Bulk Electrical Conductivity of a Sand

Based on paired measurements in consolidated and clean, unconsolidated sands, *Archie* [1942] formed an empirical relationship between the direct current electrical conductivity of a medium, σ, and properties including the water saturation, S, porosity, ϕ, and pore water EC, σ_w,

$$\sigma = \sigma_w S^n \phi^m . \tag{1-6}$$

The constants, m and n, are soil-specific with typical values for m ranging from 1.3 to 2.0 and n approximately equal to 2 for a sand.

Substituting for the saturation, S, as the ratio of the water content, θ, to the porosity, ϕ, Equation 1-6 becomes,

$$\sigma = \sigma_w \theta^n \phi^{m-n} . \tag{1-7}$$

Rhoades et al. [1976] developed a similar relationship that is appropriate for loamy soils based on a simple capillary model,

$$\sigma = \sigma_w \theta (a_R \theta + b_R) + \sigma_S . \tag{1-8}$$

This relationship includes a contribution due to surface conduction, σ_s, generally due to the presence of exchangeable ions at the interface between the pore water and clay minerals.

A later interpretation of their capillary model [*Rhoades et al.*, 1989] lead to,

$$\sigma = \sigma_{wc} \theta_{wc} + \left(\frac{(\theta_s + \theta_{ws})^2}{\theta_s} \sigma_s \right). \tag{1-9}$$

where θ_{wc} and σ_{wc} are the mobile water content and the EC of the mobile water, θ_{ws} and σ_{ws} are the immobile water content and the EC of the immobile water, and σ_s is the surface conductivity.

The second term of Equation 1-9 is significant only in media with large immobile water contents and surface conductivities under low water content conditions. Therefore, for a clean sand with very little surface conductance, Equation 1-9 simplifies to,

$$\sigma = \sigma_w \theta . \tag{1-10}$$

The linear dependence of the bulk EC on the water content of a medium suggested by Equation 1-10 contrasts starkly with published laboratory measurements such as those compiled by *Wyllie and Spangler* [1952]for natural and synthetic, unconsolidated and consolidated media. The linear relationship arises from the simplified capillary model underlying Equation 1-10 that does not include any consideration of the dependence of the tortuosity of the pore system on the bulk electrical conductivity. Furthermore, field measurements supporting Equation 1-10 [*Rhoades et al.*, 1989] were only measured at a single water content equal to the field capacity for each sample. Therefore, it is questionable whether this relationship applies over a wide range of water content conditions.

For a given water content, Equations 1-7 , 1-8 and 1-10 show linear relationships between the bulk EC of a clean sand and the EC of the pore water in the sand. There is also a near-linear relationship between the EC of a solution dominated by a single electrolyte, such as potassium chloride (KCl), and the concentration of that solute [*Barthel, et al.*, 1980]. These relationships lead to a near-linear relationship between the bulk EC of a clean sand at a given water content and the average solute concentration in the pore water.

The average solute concentration in the pore water in a sample of porous medium is defined as the total solute mass in the sample divided by the total water volume in the sample. Over any volume within the sample, the solute mass per unit volume of porous medium equals the product of the point values of the water content and the solute concentration in the pore water, these values can be integrated over the entire sample to give the total solute mass; similarly, the integral of the water content over the sample volume defines the total volume of water in the sample. If the water content is spatially uniform, the average solute concentration is equivalent to the average of the local solute concentrations in the pore water over the measurement volume. Similarly, if the solute concentration in the pore water is spatially uniform, Equations 1-8 through 1-10 can be used to define the pore water EC corresponding to the average solute concentration in the pore water for a measured water content. However, if the water content and solute concentration vary independently through a sample, the average solute concentration can be determined only as the average of the local values of the solute mass per unit volume of medium divided by the water content. *Archie* [1942] and *Rhoades et al.* [1976] both found that the bulk EC has a nonlinear dependence on the water content. Therefore, over any volume within the sample, the bulk EC does not correspond uniquely to the solute mass per unit volume of porous medium. Therefore, in the general case, the average bulk EC measured over the sample cannot be correlated with the solute mass per unit volume in the sample, precluding the use of EC measurements to define the average solute concentration in the pore water within the sample. This suggests that EC measurements for the determination of solute concentrations in the pore water must be made over a sample volume with a nearly uniform water content or solute concentration in the pore water.

1.3.2 The Electrical Conductivity Response of TDR Instruments

The voltage difference applied as a pulse to TDR rods causes current to flow through the medium between the rods as the pulse propagates along the rods. At each impedance discontinuity along the rods, a portion of the energy of the pulse is reflected back to the pulse generator. The reflection coefficient of an impedance discontinuity, ρ, defined as the fraction of the incident energy of the pulse that is reflected at the discontinuity, increases with an increase in the impedance mismatch at the discontinuity. The voltage difference between the rods decreases as the pulse travels along the probe, decreasing the amount of energy available to reflect back to the pulse generator from each successive impedance discontinuity. The decrease in the magnitudes of the reflections seen on the waveform can be related to the energy lost through current flow between the rods, giving a measure of the bulk EC of the medium.

A TDR waveform is commonly presented on an oscilloscope as the reflection coefficient as a function of time (see Figure 1-3). Using a simplified, single reflection analysis *Yanuka et al.* [1988] showed that the voltage difference of the pulse arriving at the pulse generator from the ends of the rods at

time f (V_f) and the output voltage of the pulse generator, V_0, define the reflection coefficient of the discontinuity at the ends of the rods, ρ, as.

$$\rho = \frac{V_f}{V_0} - 1. \tag{1-11}$$

The locations at which the voltages V_0 and V_f, are measured on a typical TDR waveform are shown on Figure 1-6. A pulse traveling back to the generator also faces partial reflection at each intervening change in the impedance, resulting in multiple reflections on the waveforms. *Yanuka et al.* [1988] present a quantitative discussion of the effects of these multiple reflections on the waveforms produced by TDR probes. In practice, given that the energy of the reflected pulse decreases for each successive multiple reflection, generally no more than three multiple reflections can be distinguished on a waveform from an impedance discontinuity. The voltages V_1 and V_2 correspond to the signal returning from the end of the probe and the signal at late time on the waveform after all multiple reflections have died out, respectively.

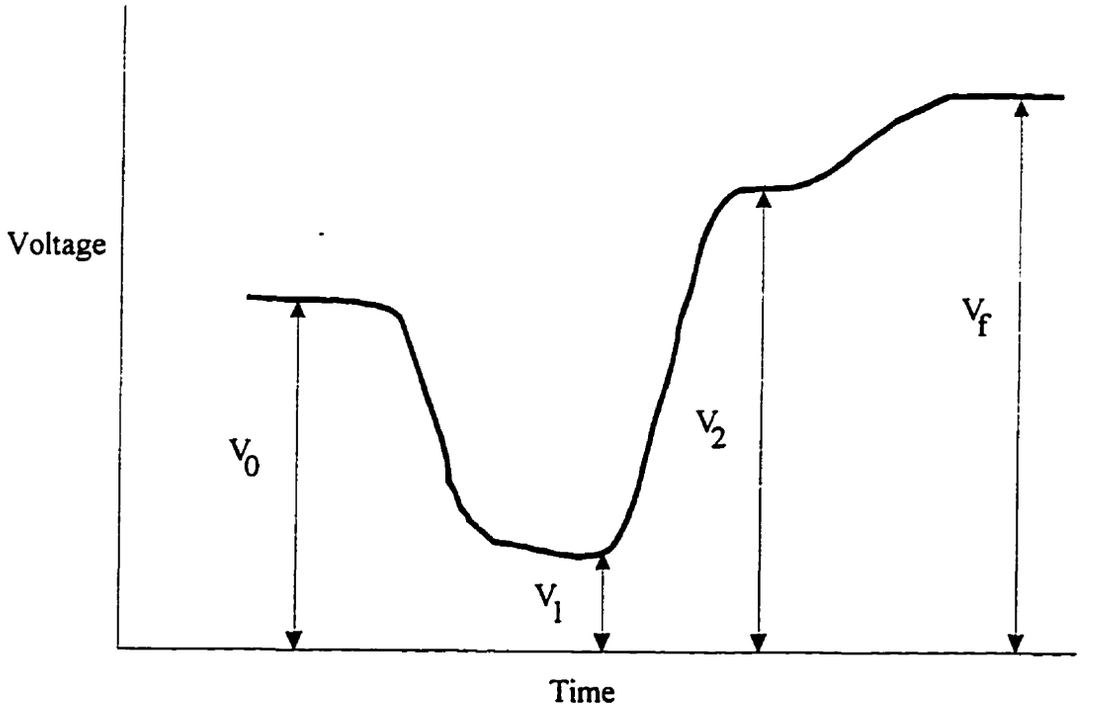

Figure 1-6. Locations of voltage measurements for EC analyses on a TDR waveform.

Dalton et al. [1984] developed a theoretical relationship between the voltages measured at two times on a waveform and the bulk EC of the medium surrounding a TDR probe, σ.

$$\sigma = \frac{K^{0.5}}{120\pi L} \ln \frac{V_2}{V_2 - V_1}, \tag{1-12}$$

where K is the relative dielectric permittivity of the medium and L is the probe length. They tested this relationship with twin-rod probes embedded in soil columns saturated with a range of saline solutions, showing a linear relationship between the TDR-estimated bulk EC and the pore water EC. Further advances in the analysis of the EC response of TDR led to relationships accounting for multiple reflections on the waveforms [*Yanuka et al.*, 1988].

A more recent approach to the analysis of the EC response of TDR was based on the conductivity analysis of *Giese and Tiemann* [1975]. *Topp et al.* [1988] rewrote this analysis to give,

$$\sigma = \frac{K_0 c}{L} \frac{Z_0}{Z_u} \left(\frac{2V_0}{V_f} - 1 \right), \tag{1-13}$$

where K_0 is the relative dielectric permittivity of free space, c is the speed of light in a vacuum, Z_0 is the characteristic impedance defined solely by the probe geometry and Z_u is the output impedance of the pulse generator. They found that EC values calculated using this relationship from TDR waveforms collected with coaxial probes in saline solutions compared well with measurements made with a standard resistance bridge. Similar agreement was found between measurements made on saturated soil samples placed in coaxial holders and the EC of the pore water in the samples.

As part of an examination of the EC response of TDR probes crossing soil layers, *Nadler et al.* [1991] proposed a simplified method of EC analysis based on a single measurement on the waveform,

$$\sigma = \frac{K_c}{Z_u} Z_0 \frac{1+\rho_f}{1-\rho_f}, \tag{1-14}$$

where K_c is a constant that is dependent on the probe geometry and ρ_f is the reflection coefficient at the time of measurement for V_f as shown on Figure 1-6. *Heimovaara* [1992] showed that this relationship is identical to Equation 1-13 if the empirical geometric constant, K_c, follows,

$$K_c = \frac{K_0 c}{L} Z_0 . \qquad (1\text{-}15)$$

The Giese-Tiemann (GT) analysis (Equation 1-13) is generally accepted to be the most accurate method of determining the bulk EC from TDR waveforms [*Spaans and Baker*, 1993]. However, given that the late time impedance (LTI) analysis of *Nadler et al.* [1991] only requires a single impedance measurement from the waveform, this analysis is often applied for rapid EC measurement during solute transport experiments.

1.3.3 Monitoring Solute Transport with TDR

By measuring both the travel time and the signal loss, TDR can determine both the bulk EC and the water content in approximately the same volume of porous medium. If the water content is nearly uniform throughout the sample volume, this presents the possibility of correcting the measured bulk EC with the measured water content to define the pore water EC, allowing for measurement of the concentration of an electrolytic tracer under a range of water content conditions. Initial applications of TDR to solute transport monitoring involved measurements of the resident solute mass under spatially and temporally uniform water content conditions. Further advances saw the measurement of solute flux concentrations. Then TDR was applied to solute concentration measurement under spatially variable water content conditions. All of these published solute transport experiments used the LTI method to determine the bulk EC from the TDR waveforms.

Ward et al. [1988] presented the first use of TDR to monitor solute transport. They used curved TDR rods in a repacked box to monitor three-dimensional transport during steady-state flow from a surface point. The geometry of the rods with respect to the flow field resulted in near-constant water contents along each rod-pair under steady-state flow conditions in the homogeneous medium. As a result, each probe only required a single calibration between the EC response and the solute concentration to account for the water content. These EC measurements were related to the solute mass residing in the sampling volume of each probe at any given time.

The simplest condition for pore water EC monitoring is steady-state vertical flow through a homogeneous, saturated medium. Under this condition, the relationship between the TDR-measured bulk EC and the pore water EC for the given water content condition is sufficient to monitor the tracer concentration with TDR. *Kachanoski et al.* [1992] monitored one-dimensional solute transport under steady-state, saturated flow using vertically installed rods placed along the axis of a laboratory column. A short duration solute pulse was released into the flow field and monitored as it traveled along the column. The results showed a constant EC following the introduction of the tracer until the dispersed solute front

reached the end of the rods, confirming the ability of TDR to measure the average pore water EC under spatially uniform water content conditions even if the solute concentration is spatially variable. In addition, the experimental results showed that TDR could be used to measure the mass flux of the tracer past the ends of the vertical rods. A corresponding field experiment was conducted under unsaturated flow conditions using a rod-pair installed vertically beneath a spray nozzle. A short duration solute pulse was released after steady-state flow was achieved. For the homogeneous medium, with the rods located far above the water table, the water content was uniform in both time and space over the length of the rods during the experiment. The results agreed with the laboratory findings, further demonstrating the ability of TDR to monitor solute transport under unsaturated conditions in the field.

Kachanoski et al. [1994] used TDR to monitor the transport of a solute from a point source during constant infiltration. They applied a drip source between a pair of TDR rods until steady-state flow was achieved and then monitored the advance of a tracer step at the same flow rate. The three-dimensional flow field resulted in water contents that varied along the rods during this experiment, although they remained constant at each depth through time; the water content and solute concentration varied independently along the rods during solute transport. Based on the results of the steady-state vertical flow experiments, they determined the total solute mass directly from the measured EC responses; as discussed above, this does not appear to be strictly valid given the nonlinear relationship between the bulk EC and the water content found for DC measurements [*Archie*, 1942; *Rhoades et al.*, 1976]. For these conditions, a rigorous definition of the mass of solute between the rods from the EC response requires an investigation of the EC response of continuous-rod probes to spatially variable water contents and solute concentrations.

Both *Knight* [1992] and *Baker and Lascano* [1989] showed that TDR probes are most sensitive to media located in the plane through the rods; the probe sensitivity drops sharply with distance perpendicular to this plane. *Ward et al.* [1994] took advantage of this by installing horizontal rod-pairs through the wall of a column to provide high resolution profiles of the solute mass along the column with time during solute transport. Horizontal rods were especially useful for this application because they allowed for measurements in a layered column while maintaining nearly uniform water contents and solute concentrations throughout the sample volume of each probe. As a part of this work, *Ward et al.* [1994] found linear relationships between the TDR-measured bulk EC based on Equation 1-14 and the concentration of an electrolytic tracer for four spatially uniform water contents over a wide range of tracer concentrations.

Rudolph et al. [1996] applied a salt pulse under steady-state flow over vertically installed rod-pairs to monitor solute transport on a heterogeneous field site. The mass flux measured with short TDR rods showed good agreement with that measured with solution samplers. This agreement demonstrated the ability of TDR to monitor solute transport under conditions of spatially variable water content and solute concentration. However, it is possible that although the water content was variable along the rods,

the short-duration tracer pulse only occupied a small volume of the porous medium at any time over which the water content was nearly uniform. Therefore, the agreement of the TDR-inferred solute concentrations with those measured in pore water collected with solution samplers shown in this experiment does not provide a general confirmation of the ability of TDR to measure the correct solute concentration if the water content and solute concentration vary independently in the same volume of porous medium.

The most difficult condition for solute transport monitoring by EC methods is transport during transient flow. Given that the water content and the solute concentration will vary independently both spatially and temporally, the dependence of the EC response of TDR on both the water content and the pore water EC must be defined completely to relate bulk EC measurements to solute concentrations. *Ward et al.* [1994] presented insufficient data to define the dependence of the bulk EC on the water content. *Risler et al.* [1996] presented a more complete data set collected continuously during cyclical wetting and drainage of soil columns. They found a highly linear relationship between the TDR-measured EC calculated using the GT method and the product of the water content and pore water EC in soils ranging from a very fine sand to a clay loam. Equation 1-8 predicts a quadratic relationship between σ and the product $\sigma_w\theta$. Equation 1-7 only predicts a linear relationship between the bulk EC and this product if the water content is held constant. Judging by the data presented by *Risler et al.* [1996], their linear result may be due to the narrow range of imposed water contents, ranging only from 0.25 to 0.37. The dependence of the EC response of TDR probes on the water content must be defined over a wider range of water contents to broaden the applicability of solute transport monitoring with TDR during transient flow.

Kachanoski et al. [1992] showed that under some conditions vertically emplaced TDR rods can measure the mass flux of a solute past the ends of the rods. However, as for water content measurement, the large sample volumes of continuous-rod TDR probes limit their ability to profile the resident solute mass with depth. Most of the alternative probes designed to profile the water content are not well-suited to profiling the bulk EC. Therefore, to allow for solute concentration profiling under widely ranging flow conditions, new probes should be designed that can measure both the water content and the bulk EC simultaneously over discrete depth intervals.

1.4 *Research Objectives*

The general goal of this work is to advance the understanding of the water content and EC responses time domain reflectometry using both standard and alternative probes and to use this insight to improve the design of TDR probes to fulfill a range of specific measurement needs. This goal is achieved by addressing four objectives. The dependence of the EC response of standard, continuous-rod probes on

spatially variable water contents and electrolytic solute concentrations is examined to allow for solute concentration monitoring during transient flow. The influence of the configuration of standard continuous-rod probes on their sample areas is studied in order to choose the appropriate probe for measurement on any desired scale while ensuring that the distribution of measurement sensitivity is as uniform as possible within the sample volume. This analysis is also applied to all published alternative TDR probes to compare their sample areas, to show the dependence of their sample areas on the soil water content, and to suggest alterations to the probe designs to improve the sizes of their sample areas and the distributions of their probe sensitivities. The sensitivities of alternative probes to changes in the soil water content are investigated to compare their performance; design changes are suggested to improve the responses of each probe. Finally, a new multilevel TDR probe is designed and the ability of this probe to profile both the water content and bulk EC with depth is shown in the field.

2. CHAPTER TWO

THE WATER CONTENT RESPONSE OF CONTINUOUS-ROD TDR PROBES

2.1 *Motivation*

Standard, continuous-rod TDR probes have been shown to measure a relative dielectric permittivity that corresponds with the length-weighted average water content over their length, even if the water content varies along the rods. An empirical relationship has been presented that relates the measured relative dielectric permittivity to the water content for a wide range of soils. The response of TDR probes in media with relative dielectric permittivity values that vary in the plane perpendicular to the rods has been described analytically for one specific case: a circular ring of material placed nonconcentrically around each rod of a two-rod probe in an otherwise homogeneous medium. However, the implications of this analysis for water content monitoring with standard and alternative TDR probes have not been discussed. The goal of the investigations presented in this chapter is to develop a definition of probe sensitivity that can be applied to any TDR probe to define its response to changes in the water content and to judge its ability to measure the correct volume-averaged water content in its sample volume. This analysis is applied to standard continuous-rod probes with and without dielectric coatings to define the optimal probe design and placement for water content measurement.

2.2 *Axial Averaging by Uncoated Continuous-rod Probes*

2.2.1 Length-weighted Averaging of the Travel Time

The relative dielectric permittivity of a mixture of materials is related to an average of the dielectric permittivities of its components. A general form of a dielectric mixing model of x different components can be written as [*Birchak et al.*, 1974],

$$K_m^n = w_1 K_1^n + w_2 K_2^n + \ldots + w_x K_x^n, \qquad (2\text{-}1)$$

where w_i is a weighting factor describing the fractional contribution of component i to the bulk relative dielectric permittivity of the mixture.

The weighting factors are taken to be independent of the component dielectric permittivities and are constrained by,

$$\sum_i w_i = 1. \tag{2-2}$$

The exponent, n, defines the method of averaging of the mixing model and ranges from -1 for dielectric materials placed in series to 1 for a parallel mixing model [*Roth et al.*, 1990].

An experimental investigation of undisturbed soils has shown that the relationship between the measured relative dielectric permittivity and the component relative dielectric permittivities approximately follows a square root mixing model with $n = 0.46$. The weighting factor of each component was found to equal its volume fraction [*Roth et al.*, 1990]. This conforms to the theoretical model of *Birchak et al.* [1974] based on refractive volumetric mixing.

Many field applications of TDR use vertically installed probes to examine predominantly vertical changes in the water content. Water contents are assumed to be constant in the plane perpendicular to the probe and only the averaging of water contents varying axially along the probe is considered. Axial averaging of the relative dielectric permittivity can be examined by considering the probe as a series of consecutive regions. Each region has a length, L_i. Over each region, the relative dielectric permittivity, K_i, corresponding to a uniform water content, θ_i, is constant. From Equation 1-1, the time required for the wave to propagate through region i is,

$$t_i = \frac{L_i}{c}\sqrt{K_i}\,. \tag{2-3}$$

The travel time that would be measured over the length of the rods is,

$$t_m = \sum_i t_i = \frac{1}{c}\sum_i L_i \sqrt{K_i}\,. \tag{2-4}$$

The relative dielectric permittivity determined from the total travel time is,

$$K_m = \left(\frac{ct_m}{L_{total}}\right)^2 = \left(\frac{\sum_i L_i \sqrt{K_i}}{L_{total}}\right)^2. \tag{2-5}$$

Equation 2-5 can be written in the general form of a mixing model replacing n with the square root and the weighting factors, w_i, as the fractional length of each section.

$$K_m^{1/2} = \frac{L_1}{L_{total}} K_1^{1/2} + \frac{L_2}{L_{total}} K_2^{1/2} + \ldots + \frac{L_x}{L_{total}} K_x^{1/2}. \qquad (2\text{-}6)$$

In this form it can be seen that the measured relative dielectric permittivity for media that vary in series along the rods follows a length-weighted averaging model based on the square root of the interval relative dielectric permittivities.

The length-weighted average water content over the rods is defined as,

$$\theta_{ave} = \frac{\sum_i L_i \theta_i}{L_{total}}. \qquad (2\text{-}7)$$

Given the square root averaging model of the relative dielectric permittivity shown in Equation 2-6, the TDR-measured average relative dielectric permittivity will only give the correct length-weighted average water content shown in Equation 2-7 if the water content is related to the relative dielectric permittivity through,

$$\theta = aK^{1/2} + b, \qquad (2\text{-}8)$$

where a and b are constants. Substitution of Equation 2-8 into Equation 2-7 gives,

$$\theta_{ave} = \frac{\sum_i L_i \left(aK_i^{1/2} + b\right)}{L_{total}} = a\sum_i \frac{L_i K_i^{1/2}}{L_{total}} + \frac{b\sum_i L_i}{L_{total}} = aK_m^{1/2} + b. \qquad (2\text{-}9)$$

Figure 2-1 shows that Equation 2-8 with fitted a and b values of 0.1181 and -0.1841, respectively, is nearly identical to Equation 1-3 determined empirically by *Topp et al.* [1980]; calculated water contents based on the two equations differ by less than 0.5% between 5 and 40% water content. *Topp et al.* [1982] also suggested that the large coefficient on the squared water content term causes Equation 1-2 to describe a linear relationship between the square root of the relative dielectric permittivity and the soil water content, explaining laboratory results showing that vertical TDR rods measure the length-weighted arithmetic average water content even in the presence of sharp vertical water content gradients.

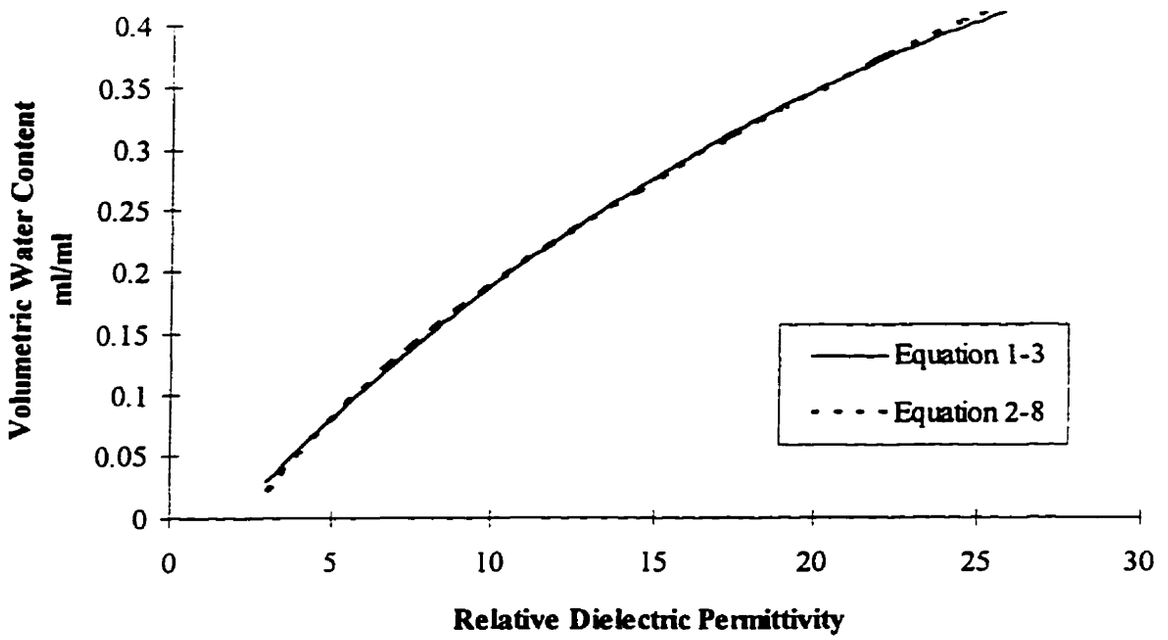

Figure 2-1. Comparison of Equations 1-3 and 2-8 for describing the relationship between the relative dielectric permittivity and the water content.

Other calibration relationships have been proposed to relate the water content to the measured relative dielectric permittivity for specific soil conditions [*Ledieu et al.*, 1986; *Herkelrath et al.*, 1991; *Van Loon*, 1991; *Malicki et al.*, 1992]. However, only those relationships of the form of Equation 2-8 will give the exact length-weighted average water content for axially variable water contents.

2.2.2 Sensitivity of Uncoated Continuous-rod Probes

The travel time is measured by a TDR instrument to infer the soil water content. Therefore, the most useful definition of the sensitivity of a TDR probe is the change in the travel time for a given change in the soil water content.

Combining Equations 2-3 and 2-8 shows a linear relationship between the TDR-measured travel time and average water content along the rods,

$$t_m = \frac{L}{ac}(\theta - b). \qquad (2\text{-}10)$$

Substituting for θ in Equation 2-10 with Equation 2-7 gives,

$$t_m = \frac{1}{ac}\left[L_1\theta_1 + L_2\theta_2 + \ldots + L_x\theta_x\right] - \frac{bL}{ac} \qquad (2\text{-}11)$$

Applying the definition of sensitivity to the travel time defined by Equation 2-11 shows that the sensitivity of the measured travel time to changes in the water content of region i is,

$$\frac{dt_m}{d\theta_i} = \frac{L_i}{ac}. \qquad (2\text{-}12)$$

Equation 2-12 demonstrates that the measured travel time has a constant, length-weighted sensitivity to the water content in each region. This sensitivity is independent of the water content within the region or the water contents along the rods outside of the region. This result is consistent with the observed ability of TDR to measure the correct length-weighted average water content even in the presence of sharp wetting fronts [*Topp et al.*, 1982a].

2.2.3 Averaging of Dielectric Permittivities in the Transverse Plane

Little has been published regarding the dependence of the TDR-measured relative dielectric permittivity on the distribution of materials in the plane perpendicular to parallel TDR rods. Previous experimental results have shown that the sample volume of a twin-rod TDR probe is concentrated between the rods with the greatest sensitivity in close proximity to the surface of the rods [*Baker and Lascano*, 1989]. A subsequent analytical treatment showed that, in a homogeneous medium, the nonuniform distribution of instrument sensitivity in the transverse plane is controlled by the diameter and separation of the rods. As the ratio of the rod diameter to separation decreases, the field becomes increasingly restricted to a region immediately adjacent to the rods; larger diameter-to-separation ratios result in a more evenly distributed field between the rods [*Knight*, 1992].

An appropriate averaging model must be defined to develop an expression describing the response of a TDR probe to material properties that vary in the transverse plane. The preceding analysis has shown that a square root averaging model applies to properties that vary along a TDR probe. Unfortunately, a similar direct analysis is not available to describe the general case of the response of a TDR probe to dielectric materials distributed heterogeneously in the transverse plane. However, an analytical description of dielectric mixing can be defined for certain distributions of relative dielectric permittivities.

Considering the problem of air- or water-filled gaps around standard twin rod TDR probes, *Annan* [1977b] developed an expression describing the response of a twin rod probe to dielectric materials placed as nonconcentric rings around each of the rods. This development is based on the nonconcentric circular equipotentials that surround a pair of line sources in the transverse plane in a homogeneous medium. These equipotentials conform to the bipolar coordinate, ξ, as shown on Figure 2-2.

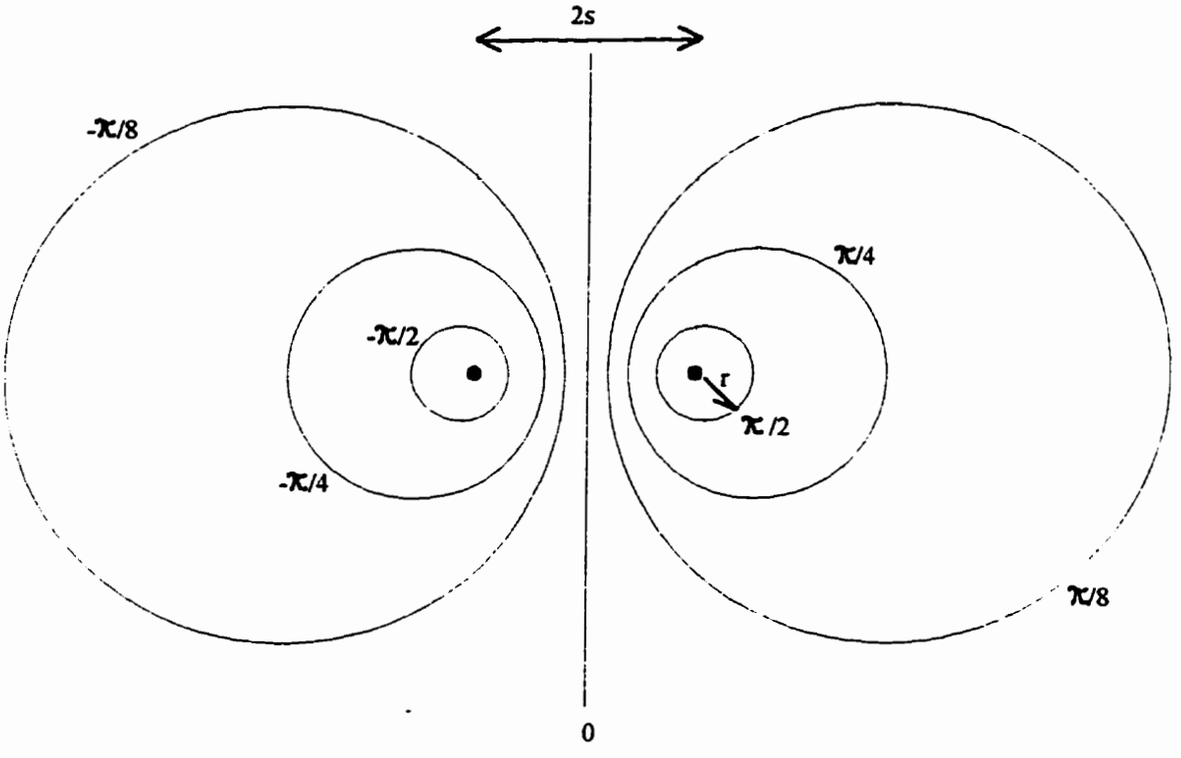

Figure 2-2. Bipolar coordinate system with equipotentials of constant ξ.

If the material between any pair of equipotentials around both rods is replaced with a different medium, the background material and the added medium will be placed in series with respect to the geometry of the probes. As a result, the property boundaries will still represent equipotentials in the heterogeneous medium. Therefore, by considering the inner circles on each half of Figure 2-2 to represent the rod surfaces and replacing the medium in nonconcentric circular areas around the rods with air- or water-filled gaps, the potential distribution can be determined analytically. Annan found that a twin-rod probe with gaps filled with a material with a dielectric permittivity, K_{ring}, would measure a relative dielectric permittivity, K_m, equal to,

$$K_m = \frac{K_{ring}\xi_0}{K_{soil}(\xi_0 - \xi_1) + K_{ring}\xi_1} K_{soil}. \quad (2\text{-}13)$$

where the bipolar coordinates ξ_0 and ξ_1 correspond to the locations of the rod surfaces and the outer surfaces of the surrounding rings, respectively. These equipotentials are related to the separation, $2s$, and radius, r, of any symmetric pair of equipotentials by,

$$\pm\xi = \pm \operatorname{csch}^{-1}\left(\frac{r}{\sqrt{s^2 - r^2}}\right) \quad (2\text{-}14)$$

Equation 2-13 can be restated in the form of a mixing model as,

$$K_m^{-1} = w_{ring}K_{ring}^{-1} + w_{soil}K_{soil}^{-1} = \frac{\xi_0 - \xi_1}{\xi_0} K_{ring}^{-1} + \frac{\xi_1}{\xi_0} K_{soil}^{-1} \quad (2\text{-}15)$$

Annan recognized that due to this series averaging low dielectric permittivity rings, such as air-filled gaps around continuous rods, have a much greater impact on the TDR-measured relative dielectric permittivity than high dielectric permittivity rings, such as water-filled gaps.

2.3 *Axial Averaging by Coated Continuous-rod Probes*

2.3.1 Objective

As an EM pulse travels along a TDR probe, energy is both reflected from changes in the line impedance and dissipated through electrical conduction. The maximum useable length of TDR probes is often limited by excessive energy losses resulting in insufficient energy remaining to identify the characteristic reflection from the end of the probe. To extend the depth of measurement for probes installed at the ground surface, the rods can be coated with electrically resistive dielectric coatings to minimize conductive losses. The objective of this investigation is to examine the influence of these coatings on the measured water content.

2.3.2 Averaging of Dielectric Permittivities in the Transverse Plane

Equation 2-15 is in the form of an averaging model following an inverse relationship with the weighting factors, w_{ring} and w_{soil}, defined only by the geometry of the rods and gaps. This treatment can be extended to include two nonconcentric circular gaps surrounding the rods giving,

$$K_m^{-1} = w_{ring\,1} K_{ring\,1}^{-1} + w_{ring\,2} K_{ring\,2}^{-1} + w_{soil} K_{soil}^{-1}$$

$$= \frac{\xi_0 - \xi_1}{\xi_0} K_{ring\,1}^{-1} + \frac{\xi_1 - \xi_2}{\xi_0} K_{ring\,2}^{-1} + \frac{\xi_2}{\xi_0} K_{soil}^{-1} \qquad (2\text{-}16)$$

where ξ_0, ξ_1 and ξ_2 are defined by the geometries of the rods and gaps. Equations 2-15 and 2-16 describe the applicable averaging model when the materials are distributed following the geometry employed by *Annan* [1977b] expressly designed to eliminate tangential components of the electromagnetic field at the property boundaries. Less idealized material distributions introduce further complications that are not amenable to analytical solutions.

Coatings on continuous rods can be modeled as concentric rings of (typically) low dielectric materials. However, given that the coatings are commonly thin compared to the rod diameter, the application of the nonconcentric ring model should not introduce significant errors. Rods with coatings that can be approximately described by the nonconcentric circle geometry used by Annan (1977b) and can be calibrated with two calibration points and an inverse averaging model such as Equation 2-15. Other researchers have calibrated alternative probes with coatings or partial coatings using a form of Equation 2-3 that relates the travel time to a linear function of the square root of the relative dielectric permittivity [*Hook et al.*, 1992]. Figure 2-3 compares two calibration procedures for a PVC coated continuous-rod probe with a geometry represented by ring and soil weighting factors of 0.15 and 0.85, respectively. Square root and inverse averaging model calibrations are shown using calibration points for a soil with volumetric water contents of 0.05 and 0.40. Using these calibration points for the assumed probe geometry, the maximum error in the water content due to the miscalibration will be approximately 0.04; the error will be larger for probes that have larger weighting factors for the coatings. For ease of measurement, calibrations are often performed in air-filled and water-filled containers. However, this approach is inadvisable because the miscalibration due to the application of Equation 2-3 will be more pronounced for calibration points chosen further outside of the range of measurement.

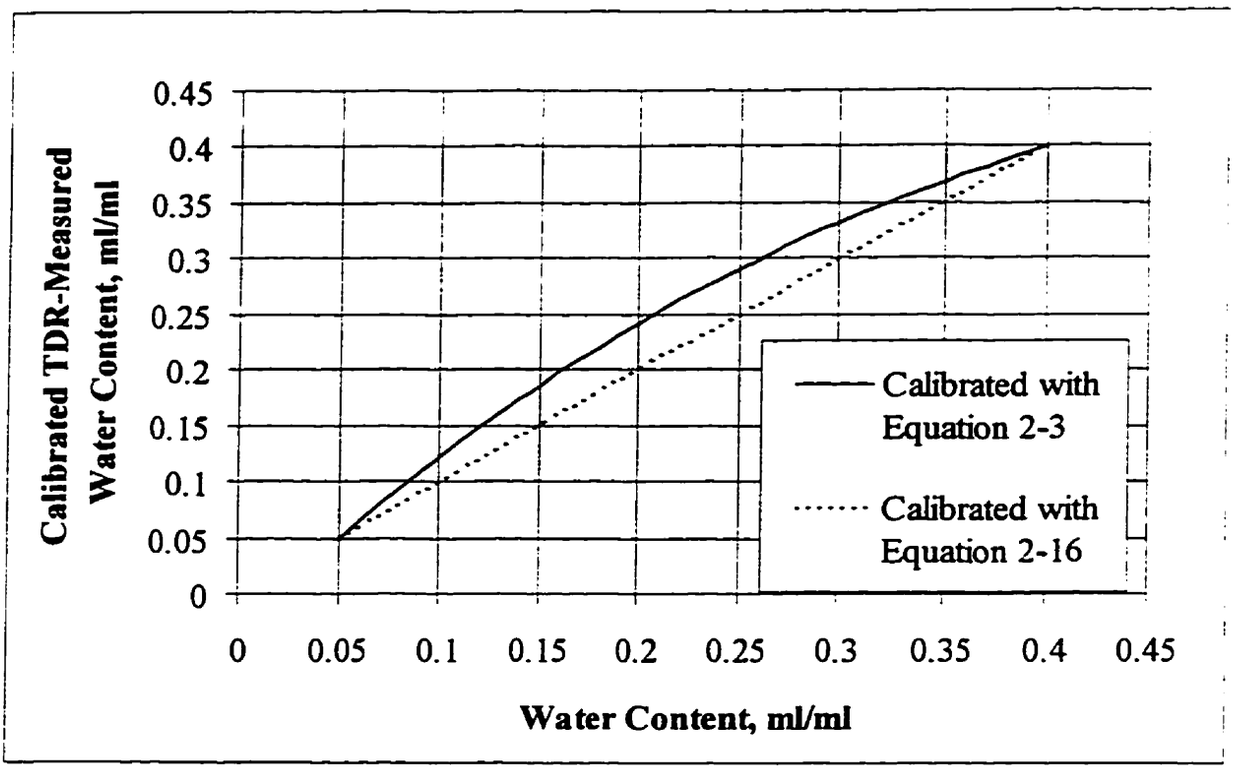

Figure 2-3. Miscalibration due to the application of a two-point calibration following Equation 2-3.

TDR probes that cannot be described analytically should not be calibrated with a two-point calibration. In general, alternative probes can be calibrated over a range of water contents between full saturation and the free drainage water content by comparison with carefully installed uncoated continuous rod probes or other independent measurements of the soil water content. This more complete calibration can be practically achieved by installing both the standard and alternative probes in a homogeneous medium. Constant infiltration can be applied at the soil surface to achieve steady-state, high water content conditions throughout the sample volume. Then, the measured relative dielectric permittivities measured with the probe over the course of the ensuing drainage can be compared to the independently measured water contents to define the appropriate response characteristics of the alternative probe design. A similar calibration procedure has been described by *Redman and DeRyck* [1994] in which the relative dielectric permittivity measured by an alternative TDR probe is compared to the relative dielectric permittivity measured in a coaxial line for mixtures of fluids with different relative dielectric permittivities.

2.3.3 Dependence of the Weighting Factors on the Soil Water Content

The preceding analysis leading to Equation 2-6 has shown that, for materials varying along the waveguides, the weighting of the TDR method for uncoated continuous-rod probes is equal to the fractional length of each section, suggesting that the sensitivity of the TDR rods is constant along the length of the rods. Similarly, for homogeneous mixtures of dielectric materials, the weighting factors are equal to the volume fraction occupied by each material [*Roth et al.*, 1990]. For TDR to measure the average water content in the transverse plane, the weighting factors should be independent of the water content distribution and equal to the relative area occupied by each material.

Equation 2-16 describes the averaging model for two nonconcentric gaps around parallel rods. The ratio of the weighting factors of the inner and outer rings is,

$$\frac{w_{outer}}{w_{inner}} = \frac{\xi_1 - \xi_2}{\xi_0 - \xi_1}. \tag{2-17}$$

Each equipotential has a radius of $\alpha\text{csch}\xi$, where 2α is the distance between the poles in the bipolar coordinate system. Taking the inner equipotentials at $\pm\xi_0$ to be the rod surfaces and the equipotentials, $\pm\xi_1$ and $\pm\xi_2$, to represent the boundaries of the inner and outer rings, respectively, the area of the rings are,

$$A_{inner} = \pi\alpha^2\left[\csc h^2\xi_1 - \csc h^2\xi_0\right], \text{ and} \tag{2-18}$$

$$A_{outer} = \pi\alpha^2\left[\csc h^2\xi_2 - \csc h^2\xi_1\right]. \tag{2-19}$$

Comparing the ratio of weighting factors per unit area for the inner and outer rings gives,

$$\left(\frac{w_{outer}}{A_{outer}}\right)\Big/\left(\frac{w_{inner}}{A_{inner}}\right) = \left(\frac{\csc h^2\xi_0 - \csc h^2\xi_1}{\xi_0 - \xi_1}\right)\Big/\left(\frac{\csc h^2\xi_1 - \csc h^2\xi_2}{\xi_1 - \xi_2}\right) \tag{2-20}$$

Both the numerator and denominator of the right hand side of Equation 2-20 are the slope of the nonlinear function $\text{csch}^2 x$. The absolute value of the slope of this function decreases with increasing positive values of x. Given that $\xi_0 > \xi_1 > \xi_2$, the expression shown is less than one, demonstrating that the weighting per unit area is greater in the region closer to TDR rods than for regions farther from the rod surfaces. This result is independent of the dielectric permittivities of the media in the rings.

Knight [1992] suggested that the unequal weighting of media in the transverse plane can be minimized by reducing the ratio of the rod separation to the rod diameter. However, some degree of unequal spatial weighting in the plane transverse to the probe is inherent in the measurement of the relative dielectric permittivity with TDR and cannot be eliminated. Therefore, to ensure that the measured relative dielectric permittivity corresponds with the average water content of the medium, TDR probes should be installed in a manner that minimizes the variability of the soil water content between the rods. Given that the water content tends to vary vertically in the field, TDR probes should not be installed horizontally, stacked in the vertical plane unless the probe separation is much smaller than the expected scale of variability of the water content.

Substituting Equation 1-1 into the averaging model for rods surrounded by a single heterogeneous ring of material described by Equation 2-15 gives,

$$\frac{1}{t_m} = \frac{c}{L}\left[\frac{\xi_0 - \xi_1}{\xi_0 K_{ring}} + \frac{\xi_1}{\xi_0 K_{soil}}\right]^{1/2} . \tag{2-21}$$

The relative dielectric permittivity in the ring and surrounding soil can be replaced by the equivalent water content based on Equation 2-8. Taking the soil water content in the ring to be independent of the water content of the soil in the surrounding medium the measured travel time will vary with the soil water content outside of the ring following,

$$\frac{dt_m}{d\theta_s} = \frac{L\xi_1}{ac\xi_0\left(\theta_{soil} - b\right)^3\left[\dfrac{\xi_0 - \xi_1}{\xi_0\left(\theta_{ring} - b\right)^2} + \dfrac{\xi_1}{\xi_0\left(\theta_{soil} - b\right)^2}\right]^{3/2}} . \tag{2-22}$$

For a uniform medium (no heterogeneous rings), $\xi_0 = \xi_1$, and Equation 2-22 reduces to Equation 2-12, showing a constant sensitivity of the travel time to the soil water content.

Equation 2-22 shows that the sensitivity of the TDR-measured travel time to changes in the soil water content outside of the inner ring is not constant; the sensitivity is a function of the geometry of the probes and rings, and the water content of the media within the ring. This result demonstrates the limitation to examining the sensitivity of a TDR probe to changes in the water content of a region of the medium between the rods taken by *Baker and Lascano* [1989]. Namely, *Baker and Lascano* [1989] measured the relative dielectric permittivity with continuous rods surrounded by water-filled glass tubes, attributing the change in the relative dielectric permittivity due to draining a tube to the sensitivity to that region of the medium. However, as shown here, the sensitivity of TDR to a change in the water content in any region of the

transverse plane is dependent on the water content distribution throughout the plane. Therefore, changes in the measured relative dielectric permittivity due to a local change in the relative dielectric permittivity distribution only describes the probe sensitivity at that point for that unique water content distribution throughout the transverse plane.

Standard continuous-rod TDR probes place the metal rods in direct contact with the soil. In contrast, most published alternative TDR probe designs have nonmetallic probe components in contact with the metal rods. Therefore, these probes measure some average of the dielectric permittivities of the probe materials and the surrounding medium, requiring application-specific calibrations to correlate the measured relative dielectric permittivity to the water content.

The procedure described above for calibrating alternative probes by continuous measurement during free drainage can be used to define the probe sensitivity empirically. Specifically, paired measurements of the relative dielectric permittivity measured with a probe, K_m, and independent measurements of the water content are collected. The relative dielectric permittivity of the soil, K_{soil}, can be determined from the measured water contents using Equation 1-2. The probe sensitivity, as defined by Equation 2-12, can be rewritten as,

$$\frac{dt}{d\theta} = \frac{d\sqrt{K_m}}{d\sqrt{K_{soil}}} \frac{dt}{d\sqrt{K_m}} \frac{d\sqrt{K_{soil}}}{d\theta}. \tag{2-23}$$

From Equations 1-1 and 2-8, Equation 2-23 can be written as,

$$\frac{dt}{d\theta} = \frac{L}{ac} \frac{d\sqrt{K_m}}{d\sqrt{K_{soil}}}. \tag{2-24}$$

If the slope of the relationship between the square roots of the K values is not constant, the probe will have a variable sensitivity as a function of the soil water content and the problem of incorrect axial averaging will apply; the degree of variability of the slope describes the magnitude of the incorrect averaging.

Equation 2-22 demonstrates how an air- or water-filled gap or an electrically resistive coating surrounding continuous rods will influence the measured relative dielectric permittivity. The influence of the geometry of the rods and gaps requires that probes with coatings or gaps be individually calibrated to determine the water content. However, even when calibrated, the measured travel time will be a function of both the average water content and the distribution of water in the transverse plane. Therefore, as with uncoated continuous-rod probes, coated-rod probes should be installed in a manner that minimizes water content variations between the rods to ensure that the measured relative dielectric permittivity corresponds with the volume averaged water content throughout the sample volume of the probe.

If the water content in the medium is distributed homogeneously, the effects of a gap or coating on the probe sensitivity are described by Equation 2-22. For example, consider the case of 5 mm diameter rods, 50 cm in length, placed with their centers 20 mm apart. Each rod is surrounded by a gap with an average thickness of 0.5 mm placed nonconcentrically to lie on equipotential surfaces in the bipolar coordinate system. The separation of the poles for the applicable bipolar coordinate system, 2α, is defined as,

$$2\alpha = 2\sqrt{s^2 - r^2}\,, \tag{2-25}$$

where $2s$ and r are the separation and radius or the rods, respectively (Figure 2-2).

The bipolar coordinates defining the surfaces of the rods and gaps, respectively, are,

$$\xi_0 = \pm \operatorname{csch}^{-1}\left(\frac{r}{\alpha}\right) = \pm 3.915\,, \text{ and} \tag{2-26}$$

$$\xi_1 = \pm \operatorname{csch}^{-1}\left(\frac{d}{\alpha}\right) = \pm 3.278\,, \tag{2-27}$$

where d is the outer radius of the surrounding ring.

The measured travel time along the rods can be calculated for the example probe geometry with water-filled gaps, air-filled gaps and PVC coatings from Equations 2-3 and 2-15, taking the relative dielectric permittivities of air, water and PVC to be 1, 81 and 3.3, respectively [*Weast*, 1990].

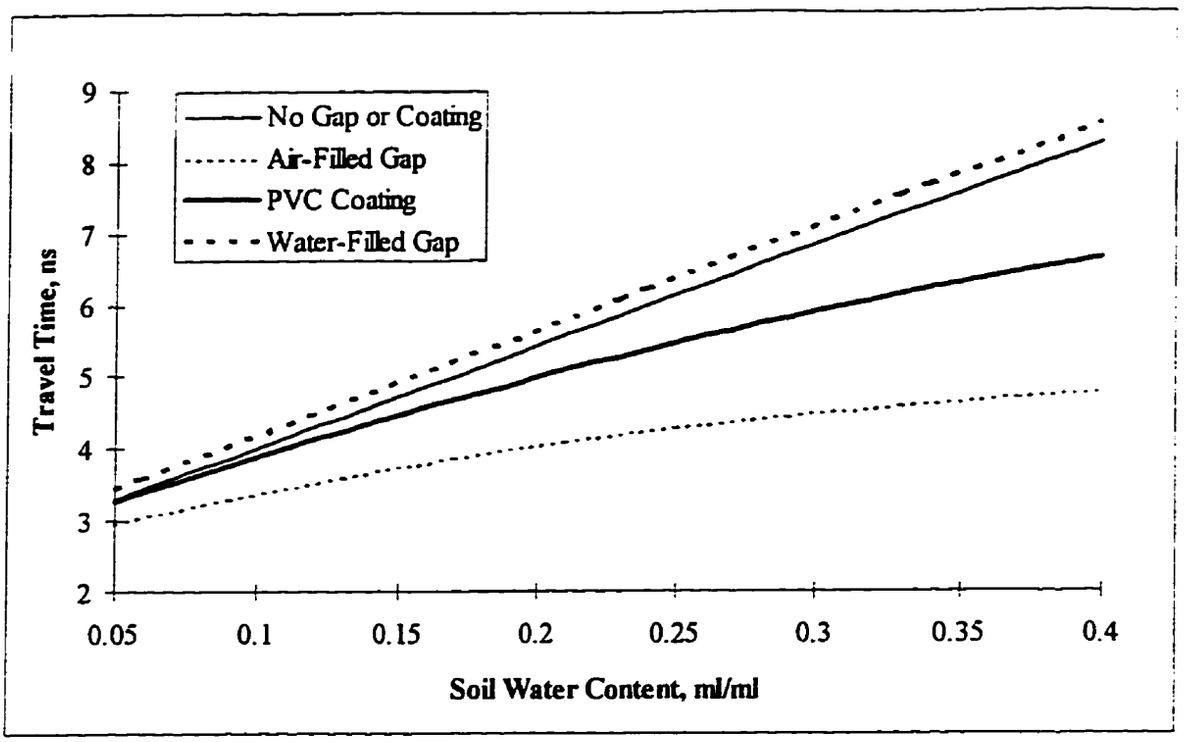

Figure 2-4. Travel time as a function of the soil water content for 50 cm long, 5 mm diameter rods with and without 0.5 mm thick gaps or coatings.

Figure 2-4 shows the travel time as a function of the soil water content for gaps filled with these materials; this is equivalent to a calibration curve that could be constructed by measuring the travel time for a probe under a range of known water content conditions. The results agree with *Annan* [1977b] who concluded that an air-filled gap would cause the most drastic change in the measured travel time.

2.3.4 Sensitivity of Coated Continuous-rod Probes

The definition of probe sensitivity (Equation 2-12) can be applied to responses calculated for the example probe geometry.

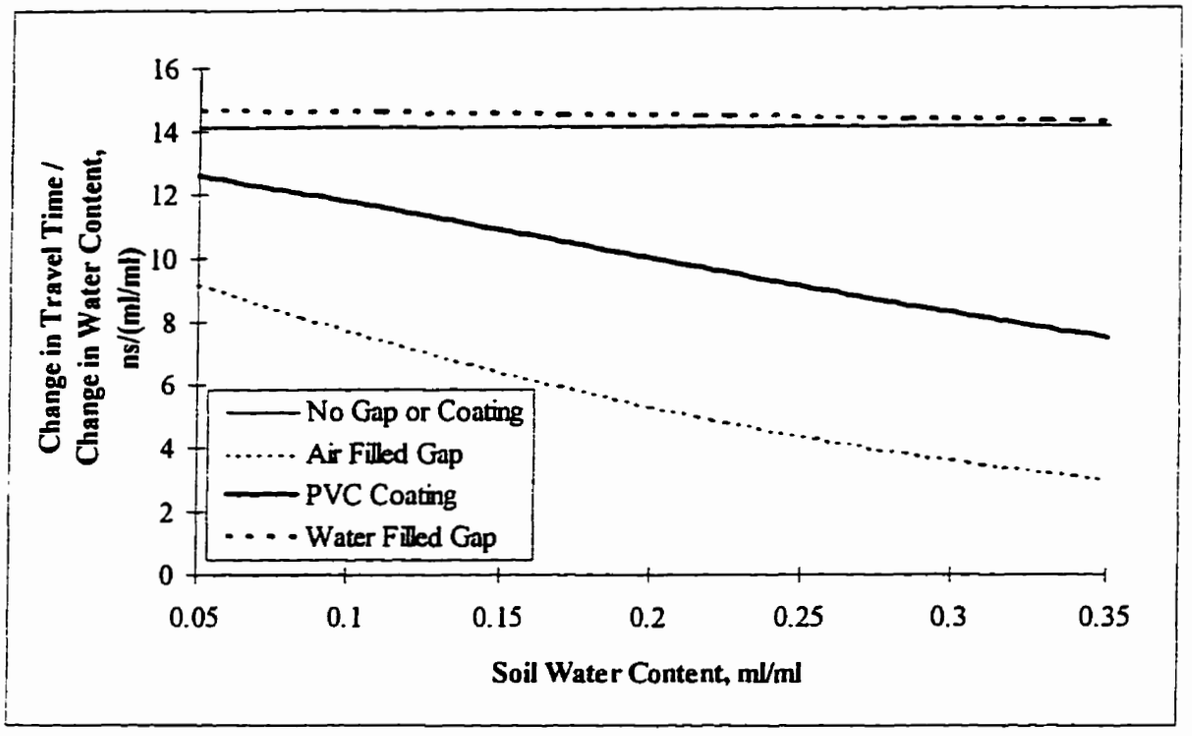

Figure 2-5. Probe sensitivity as a function of the relative dielectric permittivity of the medium in the gaps or coatings surrounding the rods: 50 cm long, 5 mm diameter rods with 0.5 mm thick gaps or coatings.

Figure 2-5 shows the sensitivities calculated from the probe sensitivities shown on Figure 2-4. The rods with water-filled gaps show a nearly constant response to the water content of the medium which is slightly higher than that of a probe with no gap. Probes with air- or PVC-filled gaps show a reduced sensitivity; in addition, the sensitivity is strongly dependent on the water content of the medium.

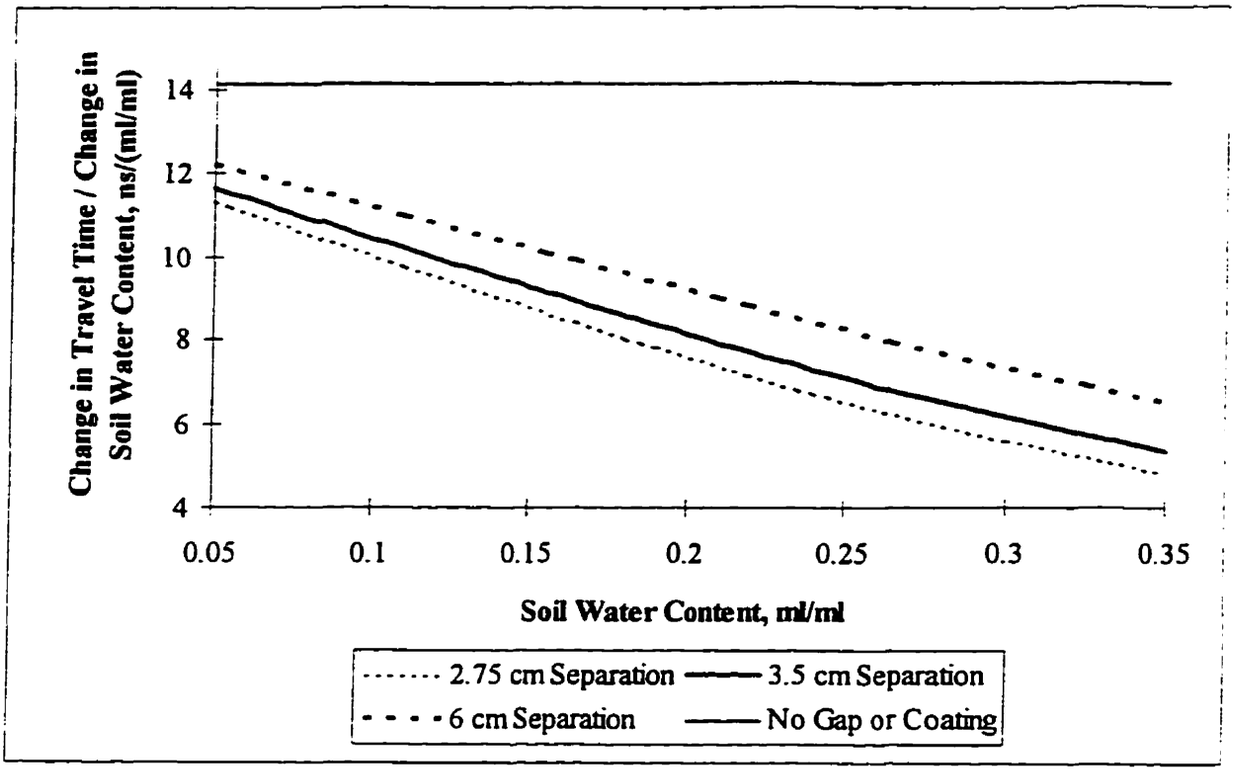

Figure 2-6. Probe sensitivity as a function of the rod separation for 50 cm long, 5 mm diameter rods with and without 0.5 mm thick gaps or coatings.

The configuration of a coated-rod probe is defined by the diameters and separation of the rods, and the thickness of the coatings. The simplest aspect of this geometry to alter is the rod separation. Figure 2-6 shows that the response of the above defined example probe with a PVC coating is not highly sensitive to the rod separation. This appears to differ from the conclusions presented by *Knight* [1992] who, defining probe sensitivity as the relative distribution of field energy around twin-rod probes, found that the spatial sensitivity of a probe with a given rod diameter is more restricted to the region immediately adjacent to the rods for larger rod separations. This apparent discrepancy is reconciled by the decrease in the relative area occupied by the coatings for increased rod separations which balances the more restricted energy distribution, resulting in near constant weighting of the coating regardless of the rod separation.

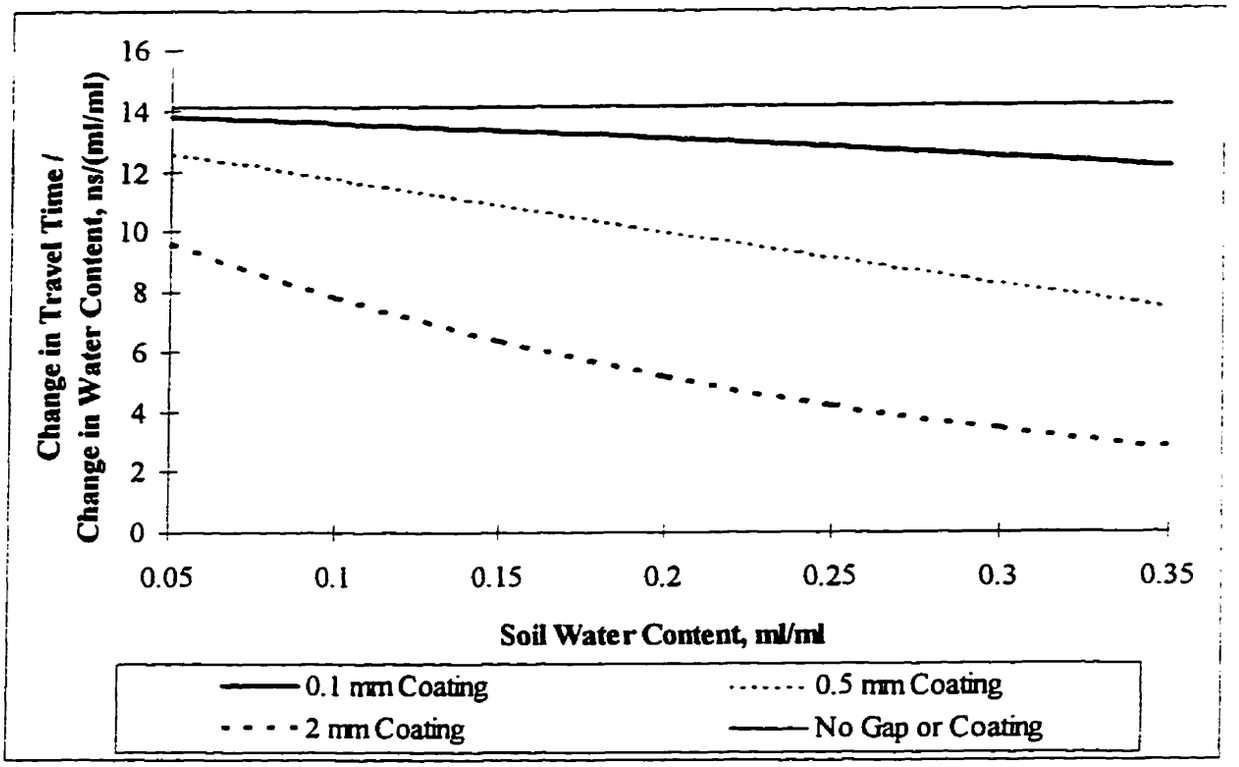

Figure 2-7. Probe sensitivity as a function of the soil water content for 50 cm long, 5 mm diameter rods with PVC coatings of various thicknesses.

Figure 2-7 shows that decreasing the thickness of a coating minimizes its impact on the measured relative dielectric permittivity. The results also show that a decrease in the gap thickness will minimize the dependence of the probe response on the soil water content. The results do show, however, that even PVC coatings as thin as 0.1 mm can introduce measurable variability in the probe sensitivity with changes in water content.

The choice of rod diameter is often arbitrary, compromising between the advantage of minimal disturbance presented by thin rods with the need for more rigid, larger diameter rods for ease of installation. Figure 2-8 shows that the nonlinearity introduced by a PVC coating decreases as the rod diameter increases for a constant rod separation and gap thickness. Therefore, if the thickness of the gap cannot be reduced, the rod diameter should be increased to minimize the influence of the gap or coating.

The sensitivity of a coated probe will be maximized if the rod diameter is large, the coating thickness is small and the relative dielectric permittivity of the coating is large; the rod separation does not significantly affect the probe response. The choice of these probe design characteristics will also decrease the dependence of the probe response on the water content of the soil.

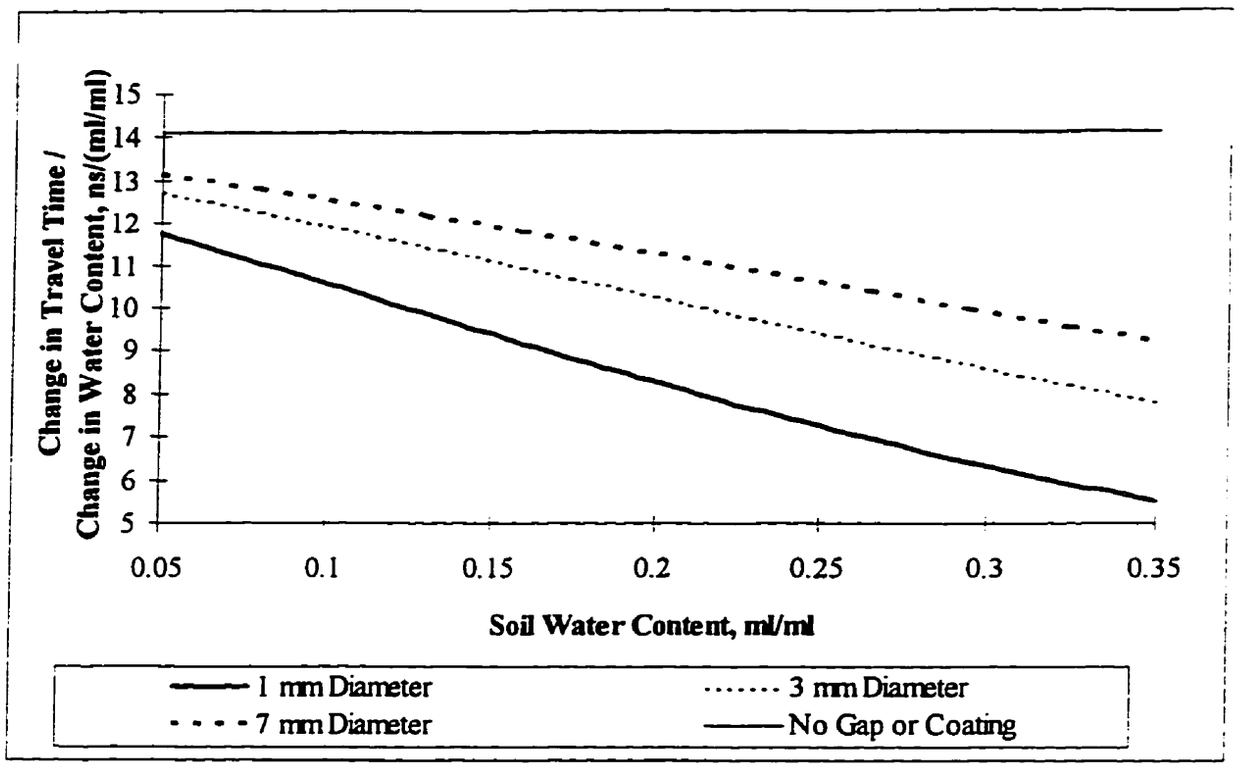

Figure 2-8. Coated-rod probe sensitivity as a function of the rod diameter: 50 cm long, 5 mm diameter rods.

2.3.5 Axial Averaging of the Water Content

The utility of a TDR probe is defined by its ability to measure the average water content of the medium within its sample volume. The response of probes with coatings or gaps to water contents that vary along the rods can be examined using the approach previously applied to uncoated continuous-rod probes. Taking the definition of the response of a probe with nonconcentric gaps or coatings to the soil relative dielectric permittivity as defined by Equation 2-15, the measured length-weighted average relative dielectric permittivity is defined from Equation 2-5 as,

$$K_m = \left(\frac{ct_m}{L_{total}}\right)^2 = \left(\frac{\sum_i L_i \sqrt{\left(w_{ring} K_{ring}^{-1} + w_{soil} K_{soil_i}^{-1}\right)^{-1}}}{L_{total}}\right)^2 . \qquad (2\text{-}28)$$

It has been shown above in the development of Equation 2-6 that in order to return the correct length-weighted average water content, the interval soil relative dielectric permittivity must be averaged as $K_a^{1/2}$. Equation 2-28 only satisfies this condition if $w_{ring} = 0$ or $K_{ring} = K_{soil}$, conditions describing the absence of a gap. Similarly, if K_{soil} does not vary with depth, the relationship simplifies to the averaging model and the measured relative dielectric permittivity can be calibrated to the water content with Equation 2-15. Except for these conditions, the averaging method does not define the length-weighted average of the square root of the soil relative dielectric permittivity.

The influence of a gap or coating on the measured length-weighted average water content can be examined for the example probe configuration. From Equation 2-15, the weighting factors for Equation 2-28 defining the contributions of the rings and soil are 0.163 and 0.837, respectively. Consider a 100 cm long column of soil with a volumetric water content of 0.05 except for a 20 cm layer in which the water content is uniform, but has a value ranging from 0.05 to 0.40.

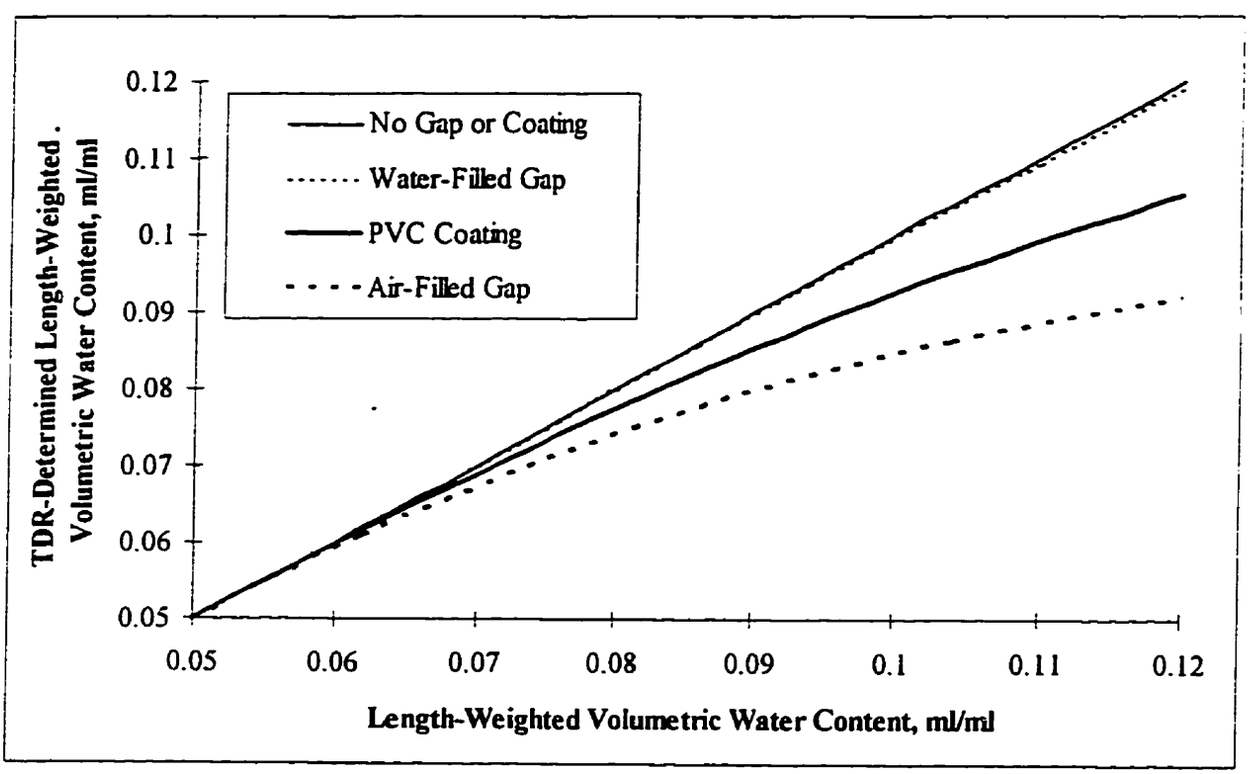

Figure 2-9. Length-weighted average water content calculated for rods with and without gaps or coatings for the example layered column.

Equation 2-15 defines the soil relative dielectric permittivity corresponding to the measured length-weighted average relative dielectric permittivity calculated with Equation 2-28. The water content can be

calculated from this soil relative dielectric permittivity with Equation 2-8. Similarly, Equations 2-5 and 2-8 can be used to determine the water content measured under the same conditions for rods without gaps or coatings. Figure 2-9 compares the average water content calculated for the example probe with an air-filled gap, a water-filled gap, a PVC coating and with no gap or coating. Given that rods with a gap or coating are more sensitive in low water content conditions (Figures 2-5 through 2-8), a change in the water content in a dry region will have a greater impact on the measured travel time than the same change in the water content of a wetter region. Therefore, if the water content varies along the rods, coated continuous-rod probes will always underestimate the average soil water content regardless of the relative dielectric permittivity of the material filling the gap. The error increases with a decrease in the relative dielectric permittivity of the medium filling the gap; a water-filled gap does not have a significant effect on the measured average water content. Furthermore, this analysis shows that even if a coated continuous-rod probe is fully calibrated following the appropriate averaging model or based on a direct experimental calibration, axially variable water contents will not be properly represented by the measured relative dielectric permittivity. As a result, to accurately measure the volume-averaged water content with coated-rod probes it is imperative to minimize the variability in the water content along the probes. In most natural conditions, the axial variability in the water content can be reduced by installing rods horizontally in the horizontal plane or by limiting the length of vertical rods.

Discontinuous gaps along continuous rods may introduce further inaccuracies into the measured relative dielectric permittivity. As shown in Figure 2-4, the presence of an air gap in an interval can entirely dominate the measured travel time through the interval. Therefore, if a gap is present along part of the rods, the water content in that region will be greatly underrepresented in the length-weighted average water content. Similarly, a change in the relative dielectric permittivity of the fluid filling the gap, perhaps due to water filling the gap as the pressure of the water phase increases with time, may have a greater effect on the measured travel time than the entire range of variability of the soil water content in the medium. These observations underscore the importance of careful installation of continuous rods to avoid the formation of gaps.

The relative dielectric permittivity measured by uncoated continuous-rod probes in a medium with a homogeneous water content distribution is independent of the geometry of the probe (Figures 2-6 and 2-8). Although the response of coated rod probes is sensitive to the coating thickness and rod diameter, it is insensitive to the rod separation. As a result, like uncoated rods, perfectly vertical emplacement of the rods to ensure a constant rod separation along the probe is not critical to measure the correct length-weighted average water content.

2.3.6 Summary and Conclusions

In the application of TDR, the travel time of a guided electromagnetic wave through a medium is measured to determine the average soil water content. A square root averaging model of the soil relative dielectric permittivity has been shown to conform to the relationship determined empirically by *Topp et al.* [1980]. This agreement explains the ability of TDR rods without gaps or coatings to measure the length-weighted average water content.

The presence of gaps around TDR rods has long been recognized as a potential source of measurement error. Based on an analytical description of the response of continuous-rod waveguides to heterogeneous media presented by *Annan* [1977b], it has been shown that an inverse dielectric averaging model applies to media distributed heterogeneously as nonconcentric rings around the probes in the plane perpendicular to the probes. If a two point calibration is to be used for coated probes, this inverse averaging model should be applied and calibration points should be chosen close to the range of expected measured values. For probes with geometries that cannot be approximated by the bipolar coordinate system proposed by *Annan* [1977b], a more complete calibration based on a series of calibration points measured simultaneously with standard continuous-rod probes and the alternative design during the drainage of a homogeneous soil profile should be used.

The sensitivity of a TDR probe to the water content is defined as the change in the measured travel time for a unit change in the average soil water content. Based on this definition, the sensitivity of TDR probes with no gap to soil water contents that vary along the rods is shown to be constant regardless of the water content distribution. In contrast, the presence of a gap or coating results in greater probe sensitivity in regions of lower water content along the rods. Furthermore, probe sensitivity has been shown to increase with decreasing gap thickness, increasing gap relative dielectric permittivity and increasing rod diameter. The rod separation does not have a significant effect on the probe sensitivity.

Due to the greater sensitivity of rods with fluid-filled gaps or coatings in lower water content conditions, water contents that vary along the probes will always be underestimated, even if the coated probes are calibrated exactly to the soil water content in a homogeneous medium. The degree of error introduced will increase with a decrease in the relative dielectric permittivity of the coating.

The results of these analyses suggest that uncoated continuous-rod probes should be installed in a manner designed to minimize water content variations in the transverse plane between the rods. As a result, for most field applications, probes should be installed vertically or horizontally in the horizontal plane; rods should not be installed horizontally, stacked in the vertical plane. Coated continuous-rod probes should be installed in a manner that also minimizes water content variations along the probes either by minimizing the length of vertical rods or by installing the rods horizontally in the horizontal plane.

The analytical relationships developed here are only strictly applicable to media distributed in symmetric nonconcentric rings around continuous rods. For thin concentric gaps, this geometry probably

provides a reasonable approximation of the probe response. Most rods with probe materials in the measurement volume, such as coatings or gaps, will have some component of inverse averaging, so the general conclusions presented here should apply to a wide variety of alternative probe designs. An empirical analysis to determine the sensitivity of probes that are not amenable to analytical description is described.

3. CHAPTER THREE

THE ELECTRICAL CONDUCTIVITY RESPONSE OF CONTINUOUS-ROD TDR PROBES

3.1 *Motivation*

In the previous chapter, the spatial weighting of water contents along and transverse to continuous-rod TDR probes was described. The nature of the spatial weighting leads to measured relative dielectric permittivities that correspond with the correct length-weighted average water content along uncoated continuous-rod TDR probes. To use continuous-rod probes to monitor solute concentrations, it is necessary to demonstrate that their EC response corresponds with the length-weighted solute concentration as well. This has been demonstrated under spatially uniform water content conditions [*Kachanoski et al.*, 1992]. As a first step toward demonstrating the ability of TDR to monitor solute concentrations under spatially variable water content conditions, the dependence of the EC response of TDR on the water content must be defined. The goal of the experiments presented in this chapter is to determine the dependence of the EC response of uncoated continuous-rod probes on the water content under both controlled laboratory conditions and in the field. The ability of continuous-rod probes to monitor the average solute concentration under conditions of independently variable water contents and solute concentrations along the probe are discussed based on these findings.

3.2 *Laboratory Column Experiment*

3.2.1 Experimental Objectives

Initial research into the use of the attenuation of TDR pulses through electrical conduction to measure soil properties focused on the response of probes to changes in the EC of the pore water in saturated soil samples [*Dalton et al.*, 1984; *Topp et al.*, 1988]. *Nadler et al.* [1991] compared the EC responses of a two-rod probe with a balun to a three-rod probe without a balun in samples of a silty loam mixed with a saline solutions to six spatially uniform water contents ranging from 0.07 to 0.28. They calculated the EC using both the LTI and GT methods as well as three older methods of EC analysis. In addition, they examined the EC and water content responses of probes inserted through two layers of media of differing water contents. In response to the work of *Nadler et al.* [1991], *Heimovaara* [1992] showed that, in theory, the GT and LTI methods of analysis are identical. *Ward et al.* [1994] presented EC measurements in a fine sand packed to four water contents ranging from 0.05 to 0.25. *Nadler et al.* [1991] showed a linear relationship between the EC response and independent measurements of the bulk EC of the medium; *Ward et al.* [1994] showed a linear relationship between the EC response and the concentration of an electrolytic solute in the pore water

under uniform water content conditions. However, neither of these relationships presented sufficient data to define the dependence of the TDR-measured EC on the water content. *Heimovaara et al.* [1995] applied a theoretical relationship between the bulk EC and the water content [*Mualem and Friedman*, 1991] to monitor solute movement under variable water content conditions with TDR. *Risler et al.* [1996] monitored the EC with TDR during cyclic wetting and drainage of an electrolytic solution, finding a linear dependence of the TDR-measured EC on the water content over a narrow range of water contents.

The objective of this experiment was to examine, under controlled laboratory conditions, the relationship between the TDR-measured EC and the water content over a wide range of soil water contents and pore water salinities. In addition, the ability of two-rod probes both with and without baluns and three- rod probes without baluns to characterize the bulk EC of the medium was tested.

3.2.2 Experimental Design

The dependence of the TDR-measured EC on the water content was examined in a sand-filled column. A homogeneous medium was used to avoid the complications caused by reflections from material boundaries in layered columns as seen by *Nadler et al.* [1991]. The use of a clean sand eliminated the contributions of surface conductance to the measured EC and the influence of bound water on water content determinations [*Dasberg and Hopmans*, 1992]. The fine- to medium-grained sand was collected from Canadian Forces Base Borden, Ontario, Canada, as part of ongoing experiments at the site. To achieve complete drainage of the sand without the need for a pressure plate at the base of the column, a 2m long polyvinyl chloride (PVC) column was used with a hanging water table placed 20 cm below its base. Based on the drainage curve for the sand, shown on Figure 3-1, the upper half of the column should have drained freely to near residual water content. A sealed end cap fitted with a 0.952 cm diameter Swagelock fitting covered the base of the column; a steel screen placed in the fitting retained the sand.

Three horizontal metal rods were used for TDR measurements (Figure 3-1). Longer rods increase the separation in time of the characteristic reflections from the beginning and end of the rods on a TDR waveform, improving the precision of propagation velocity determinations. Therefore, a relatively large diameter (20 cm) PVC column was used to allow for the use of longer TDR rods than are commonly used in column experiments. Each rod was 22.5 cm in length, with a diameter of 0.25 cm; the rod separation was 1.5 cm. Four probe configurations were used: TDR12, TDR13, TDR12n and TDR123. Table 3-1 summarizes the configurations of the probes.

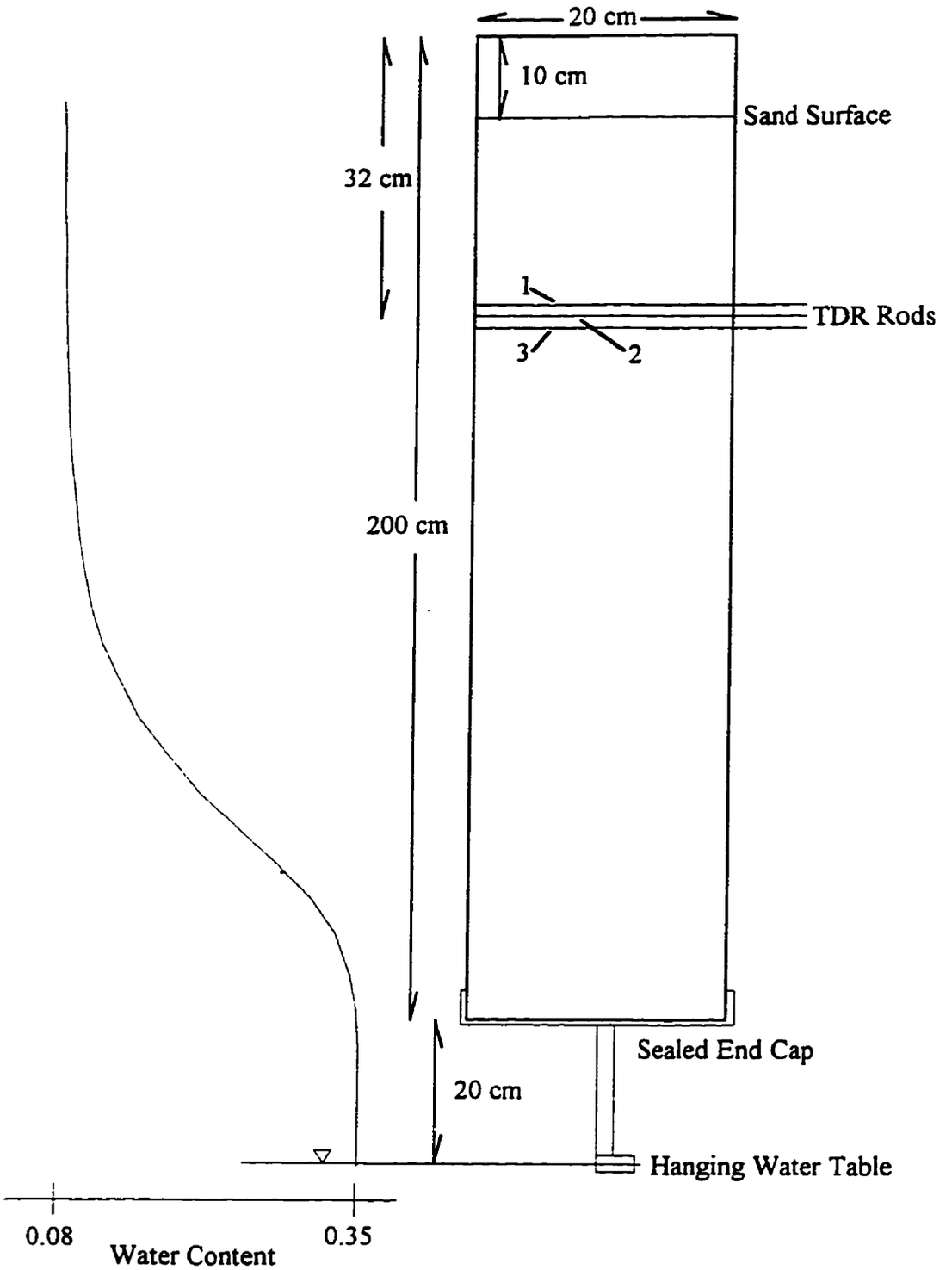

Figure 3-1. Design of laboratory column and pressure-water content relationship of Borden sand.

Probe	Rods Used	Balun
TDR12	1, 2	Yes
TDR13	1, 3	Yes
TDR12n	1, 2	No
TDR123	1, 2, 3	No

Table 3-1. Configurations of the TDR probes used for the column experiment.

For probe TDR12, rods 1 and 2 were connected to the cable tester through a balun (ANZAC TP-103 impedance matching transformer). Twin-wire shielded cable (#9090 Belden) connected the rods to the balun and the balun was placed directly on a cable tester (Tektronix 1502B). A 2.9 m long twin-wire cable was used to separate the reflections from the balun from the characteristic reflections from the beginning and end of the rods on the waveform. Similarly, rods 1 and 3 were connected to the cable tester through a balun to form probe TDR13. Rods 1 and 2 were also connected directly to the cable tester through RG-58 C/U coaxial cable without a balun (TDR12n). The coaxial cable was 2.9 meters long for direct comparison to the designs using a balun and the twin-wire cable. For probe TDR123, rods 1, 2 and 3 were directly connected to the cable tester through a coaxial cable. To improve the connection between the rods and the coaxial cable for TDR123, a small metal plate was used to connect the outer shield of the cable to rods 1 and 3; the central conductor of the cable connected directly to rod 2. For probe TDR12n, the plate connected rod 2 to the cable shield and the central conductor of the coaxial cable connected to rod 1. This variety of probe designs, all measuring within nearly the same volume of the porous medium, allowed for direct comparison of the performance of three-rod probes described by *Zegelin et al.* [1989] to standard two-rod probes [*Topp et al.*, 1982]; in addition, the impact of baluns on the EC response of two-rod probes could be assessed. Software written by *Redman* [1995] collected the waveforms on a personal computer via an RS232 cable for later analysis.

For the Tektronics 1502B cable tester, Z_u is a constant output impedance of 50 ohms. Given that the characteristic impedance of a probe, Z_0, is independent of the properties of the surrounding medium [*Baker and Spaans*, 1993], the GT analysis (Equation 1-13) can be simplified to include only a single, probe-specific calibration constant,

$$\sigma = c_{GT}\left(\frac{2V_0}{V_f} - 1\right). \tag{3-1}$$

Similarly, if the temperature remains constant throughout the experiment, the LTI method can be simplified to,

$$\sigma = \frac{c_N}{R_L}, \tag{3-2}$$

where c_N is a probe-specific calibration constant and R_L is the impedance. Rather than measuring the voltage or impedance at a single point on the waveform, an average over a time window was used to eliminate the influence of small perturbations. Assuming that the output voltage from the cable tester, V_0, is constant, *Heimovaara* [1992] showed that the GT and LTI analyses are identical. Therefore, only the simpler, LTI analysis is examined here.

Heimovaara et al. [1995] showed that the series resistance of the cable leading to the probes must be considered when determining the EC of the medium surrounding TDR rods. Including this series resistance gives,

$$\frac{1}{\sigma} = \frac{R_L}{c_N} = \frac{1}{\sigma_{medium}} + \frac{1}{\sigma_{cable}}, \tag{3-3}$$

where σ is the inverse of the total resistivity measured by the TDR instrument, σ_{medium} is the inverse of the resistivity of the medium surrounding the probe, and σ_{cable} is the inverse of the equivalent series resistivity of the cable leading to the probes.

The EC of the medium is then defined by,

$$\frac{1}{\sigma_{medium}} = \frac{R_L}{c_N} - \frac{1}{\sigma_{cable}}, \tag{3-4}$$

Simple electrolytic solutions, like KCl in deionized water, are known to show a near-linear relationship between the solute concentration and the EC of the solution [*Barthel et al.*, 1980]. A regression of the EC measured with a conductivity cell as a function of the concentration of KCl in deionized water was highly linear with an r^2 value of 0.9998 for KCl concentrations ranging from 0.0 to 4.8 g/l.

3.2.3 Calibration of Continuous-rod Probes in Saline Solutions

The conductivity response of a TDR probe is commonly calibrated in saline solutions because it is a simple method by which the probes can be calibrated for a wide range of EC conditions while maintaining

spatially uniform conditions throughout their sample volume. Initially, waveforms were collected with the rods extending through the far wall of the unpacked column filled with a series of KCl solutions. Equation 3-4 describes linear relationships between the late time impedance, R_L, and the inverse of the EC of the calibration solution for a fluid-filled column. The slope of the linear relationship is directly related to the constant c_N and the intercept defines the inverse of the equivalent resistivity of the cable, balun and connectors between the cable tester and the probe.

Figure 3-2 shows the inverse of the probe response used for the LTI analysis as a function of the inverse of the EC of the calibration solution for the four TDR probe configurations. Linear regressions of Equation 3-4 to the data are shown; all regressions show r^2 values greater than 0.997. The slopes define values of c_N of 1.185, 0.938, 0.215, and 0.326 m^{-1} for probes TDR12, TDR13, TDR12n, and TDR123, respectively. Corresponding values for the equivalent resistivity of the cable and connectors for the probes are 0.41, 0.36, 0.55, and 0.25 ohm-m.

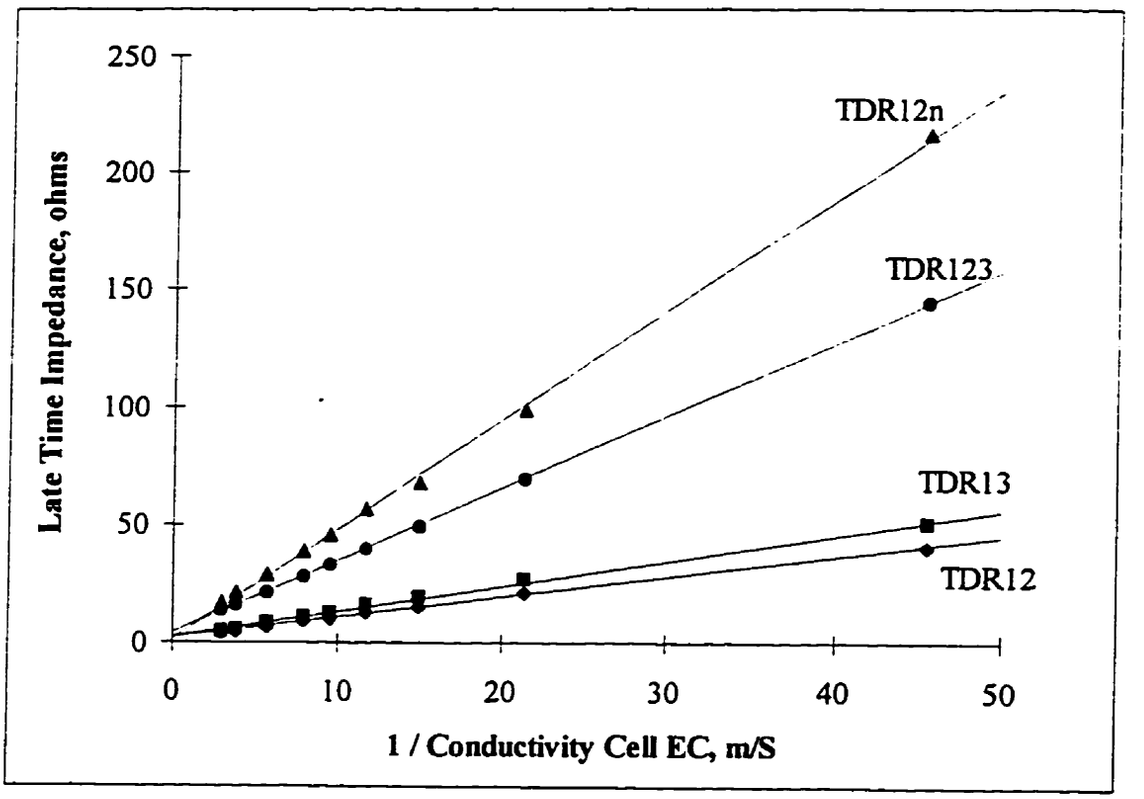

Figure 3-2. Calibration of the EC response used for the LTI analysis and determination of the equivalent resistivity of the TDR cables for four probe designs.

3.2.4 Dependence of the TDR-measured EC on the Pore Water EC

After calibration in saline solutions, the column was packed with Borden sand. To achieve uniform packing, the sand was dropped through crossed screens held above the surface of the sand pack using a technique similar to that described by *Wygal* [1963]. With the column packed, the rods were driven into the column until they were flush with the far column wall. After packing, the column was flooded with deionized water by slowly raising the water table from below the base of the column to a point above the surface of the sand. The column remained saturated for seven days to leach any highly soluble components. Then the column was drained and flooding was repeated.

With the water table near the surface of the column, a saline solution was ponded at the surface of the saturated column and allowed to infiltrate. Solution was added continuously until the waveform collected with probe TDR123 remained constant in time, indicating that the saline solution had replaced the resident pore water above the base of the sample volume of the TDR probes. Then the hanging water table was lowered to the initial position below the base of the column and both the EC and the water content were monitored with all of the TDR probes as the column drained. By measuring continuously during free drainage, a large number of paired water content and EC measurements was collected, allowing for a full description of the relationship between the TDR-measured EC and the water content. After each solution drained, the column was reflooded from below and the procedure was repeated for the next solution, using a total of seven KCl solutions with EC values ranging from 0.06 to 0.63 S/m. (KCl concentrations of 0.38 to 4.08 g/l). Five of the solutions were flooded a second time to examine the repeatability of the TDR measurements.

Maintaining uniform conditions throughout the sample volume avoids any complications introduced by spatial weighting of variable water contents and EC values within the sample volumes of the probes. For the homogeneous sand in the column, the water content and EC should be constant with elevation at any given time during drainage over the 3 cm maximum rod separation. Agreement among the water content values measured with the two- and three-rod probes confirmed that the water content was spatially uniform throughout the measurement volume.

Given that Equation 1-7 was developed for clean sands, this relationship was used to describe the dependence of the water content on the bulk EC. Combining Equations 1-7 and 3-4 shows the dependence of the corrected late time impedance, R'_L on the pore water EC and the water content,

$$\frac{1}{R'_L} = \left(\frac{R_L}{c_N} - \frac{1}{\sigma_{cable}} \right)^{-1} = \sigma_w \theta^n \phi^{m-n}. \qquad (3\text{-}5)$$

Assuming that the porosity is uniform among the sample areas of the rods, for a given water content condition, Equation 3-5 describes a linear relationship between the inverse of the corrected late time

impedance and the pore water EC with a zero intercept. Figures 3-3 through 3-5 show paired measurements of the late time impedance and pore water EC collected at three water contents with probes TDR12, TDR12n and TDR123, respectively. The results for probe TDR13 are very similar to those shown for TDR12. Linear regressions to the data show near zero intercepts of 0.0018, -0.0010, and -0.0003 S/m, respectively. To account for the small, nonzero intercepts seen on Figures 3-3 through 3-5, Equation 3-5 can be rewritten as,

$$\frac{1}{R'_L} = \left(\frac{R_L}{c_N} - \frac{1}{\sigma_{cable}} \right)^{-1} = \sigma_w \theta^n \phi^{m-n} + b. \qquad (3\text{-}6)$$

From the form of Equation 3-6, the constant, b, appears to represent an additional series resistance. However, the negative fitted values have no physical meaning as a resistance. Therefore, it is unclear what this constant represents, and may simply indicate some artifact of the method of EC analysis.

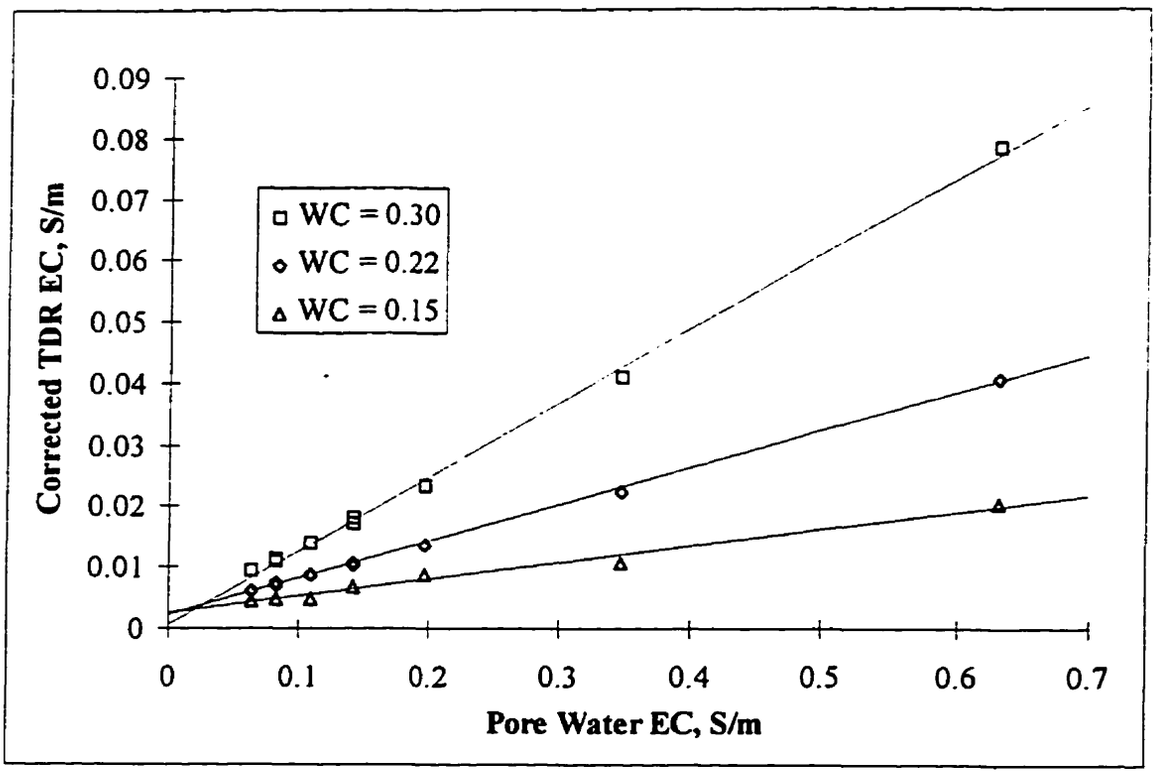

Figure 3-3. Inverse of the corrected late time impedance collected with probe TDR12 as a function of the pore water EC for three water contents: 0.15, 0.22 and 0.30. Linear regressions to the data are shown.

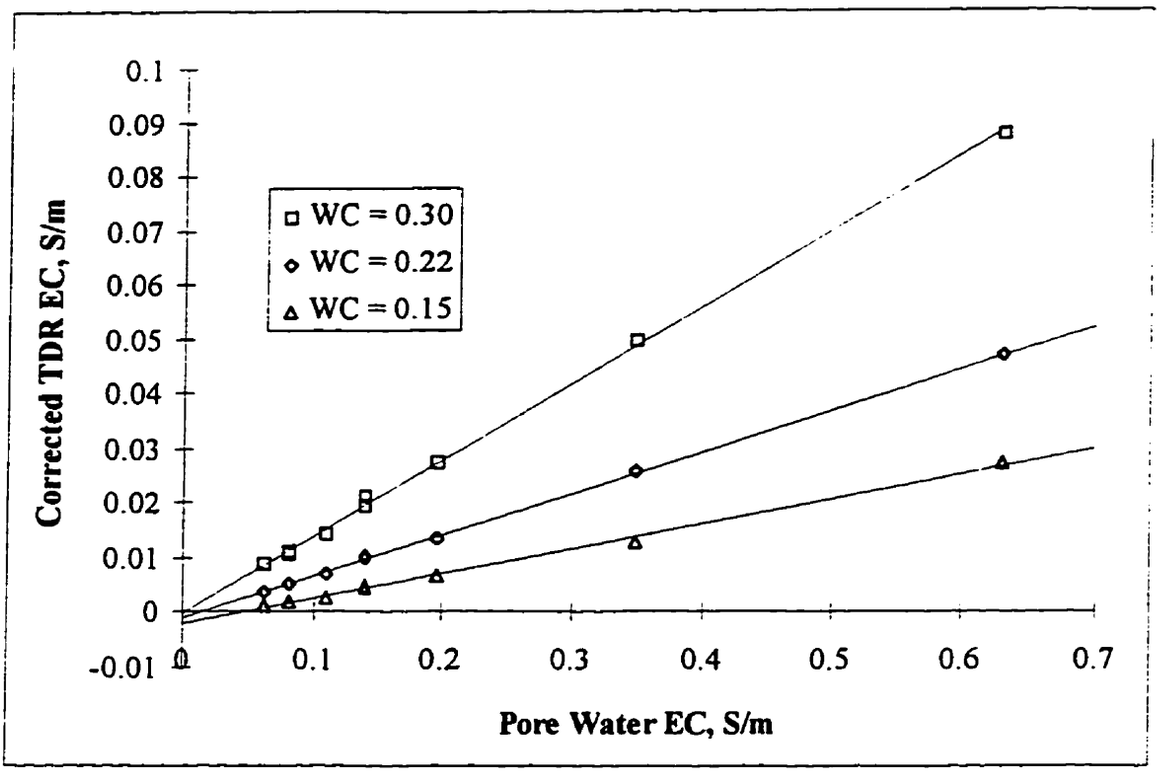

Figure 3-4. Inverse of the corrected late time impedance collected with probe TDR12n as a function of the pore water EC for three water contents: 0.15, 0.22 and 0.30. Linear regressions to the data are shown.

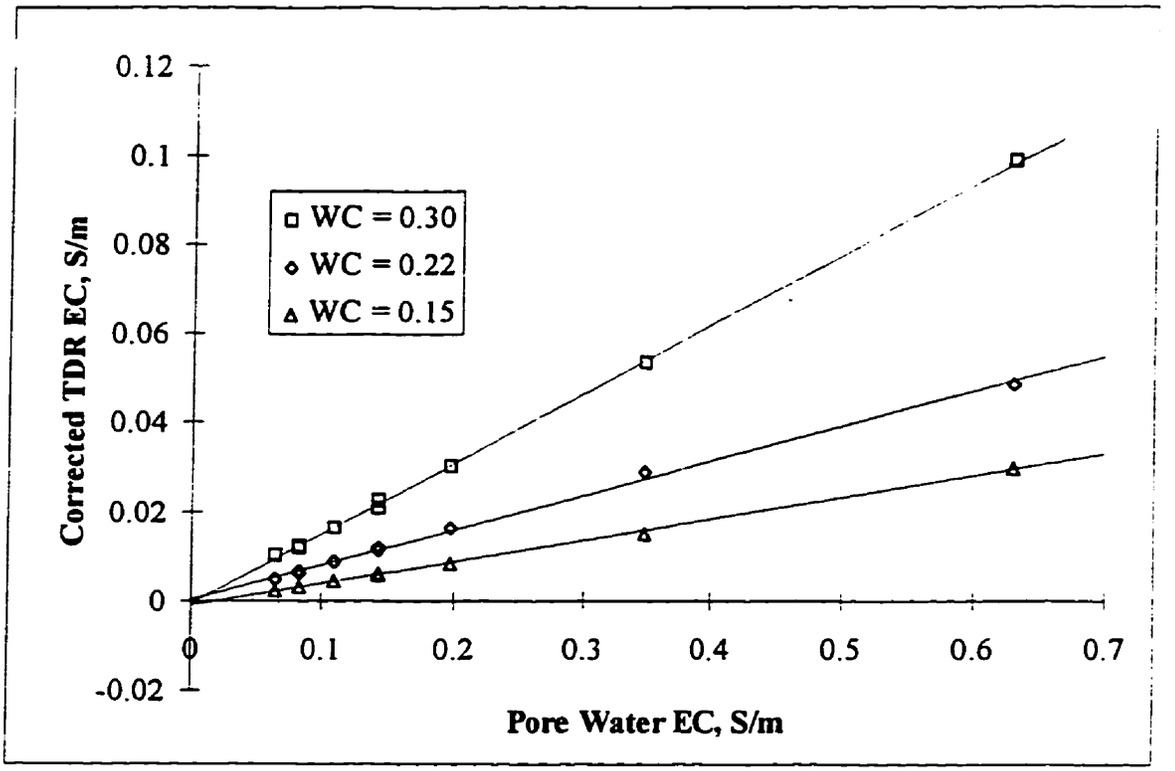

Figure 3-5. Inverse of the corrected late time impedance collected with probe TDR123 as a function of the pore water EC for three water contents: 0.15, 0.22 and 0.30. Linear regressions to the data are shown.

3.2.5 Dependence of the EC Response on the Soil Water Content

Figures 3-3 through 3-5 show that the slope of the linear relationships between the corrected TDR EC and the pore water EC is dependent on the water content of the medium. Therefore, a functional relationship between the slope and the water content is necessary to define the pore water EC from the EC and water content responses obtained with TDR.

From Equation 3-5, the slope of the relationship between the corrected TDR EC and water content is defined as,

$$S = \frac{\partial\left(\frac{1}{R'_L}\right)}{\partial\sigma_w} = \theta^n \phi^{m-n}. \qquad (3\text{-}6)$$

Taking the logarithm of both sides of Equation 3-6 gives.

$$\log S = n\log\theta + \log\phi^{m-n} = n\log\theta + B, \tag{3-7}$$

where the constants ϕ, m, and n are replaced by B for convenience.

Slopes were determined for each probe for nine water content conditions ranging from 0.15 to 0.30 during drainage of the seven flushing solutions. Figure 3-6 shows the logarithm of the slopes determined for each probe as a function of the logarithm of the water content.

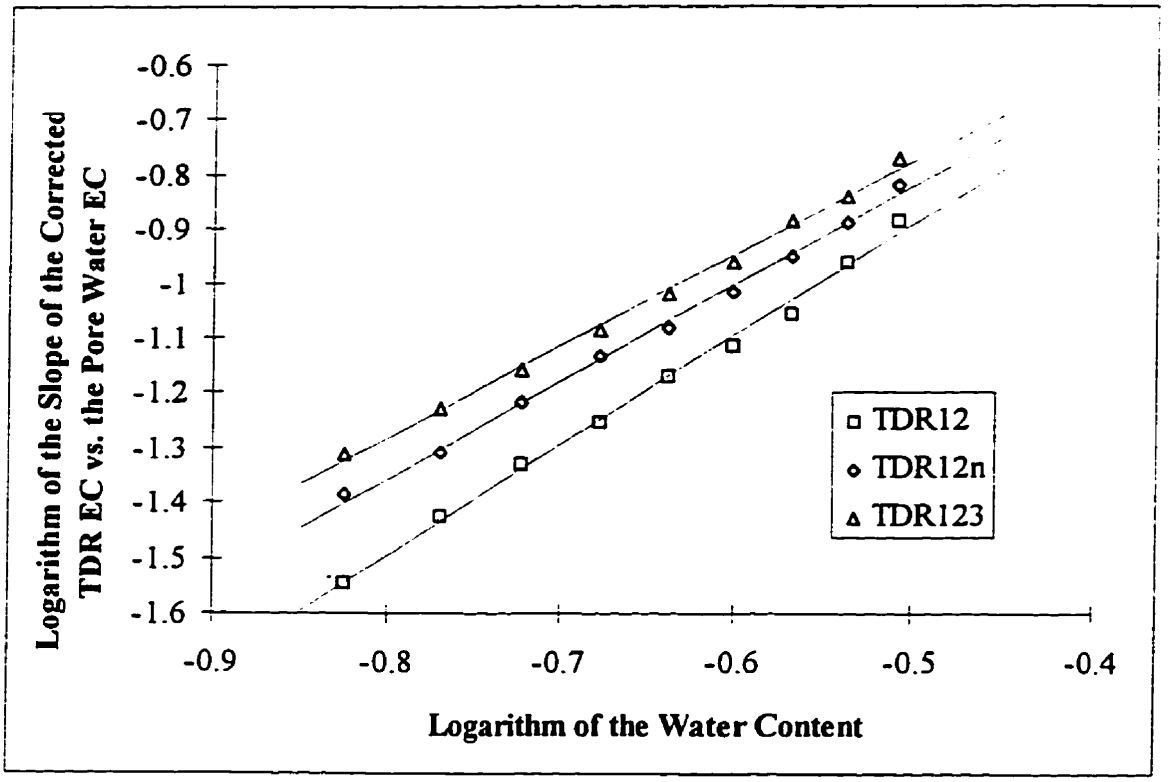

Figure 3-6. Paired measurements of the logarithm of the slope of the corrected TDR EC as a function of the pore water EC and the logarithm of the water content for probes TDR12, TDR12n, and TDR123. Linear regressions to the data are shown.

The data shown on Figure 3-6 are highly linear for all of the probes with r^2 values in excess of 0.99. The results for TDR13 are very similar to those found for TDR12. For clarity of Figure 3-6, they have not been shown.

3.2.6 Applicability of Archie's Model

The linear relationships shown on Figure 3-6 support the use of an equation of the form of Equation 1-7 to describe the dependence of the EC on the water content for the sand used in the experiment. For each probe, the value of n in Equation 1-7 is defined as the slope of the linear regression on Figure 3-6. Values of 2.02, 2.18, 1.78 and 1.69 were found for probes TDR12, TDR13, TDR12n, and TDR123, respectively. These results clearly demonstrate the nonlinear dependence of the EC on the water content over the full range of water content values. These fitted values of n are reasonably consistent with the approximate value of 2 found for clean sands by *Archie* [1942]. However, the exponent should represent a property of the porous medium; therefore, the differences among the probes indicate that the probe design does have an influence the EC response. It is likely that the linear dependence of the EC on the water content reported by found *Risler et al.* [1996] is a result of the limited range of water contents (approximately 0.25 to 0.35) over which the measurements were made.

The fitted values for the constant, B, in Equation 3-7 were 0.117, 0.249, 0.068, and 0.069 for probes TDR12, TDR13, TDR12n and TDR123, respectively. This parameter also represents properties of the porous medium and, therefore, should be constant among the probes. However, given that the value of B incorporates the value of n, it is unclear whether the variability shows further dependence of the EC response on the probe design.

Given the EC of each flushing solution, the corrected TDR EC can be calculated by substituting the fitted parameters found through linear regression into Equation 3-6.

$$\frac{1}{R'_L} = \left(\frac{\dot{R}_L}{c_N} - \frac{1}{\sigma_{cable}} \right)^{-1} = \sigma_w \theta^n \phi^{m-n} + b = \sigma_w \theta^n 10^B + b . \qquad (3\text{-}7)$$

Figures 3-7 through 3-9 compare the corrected TDR EC measured during drainage of the seven flushing solutions to the TDR EC calculated using Equation 3-7.

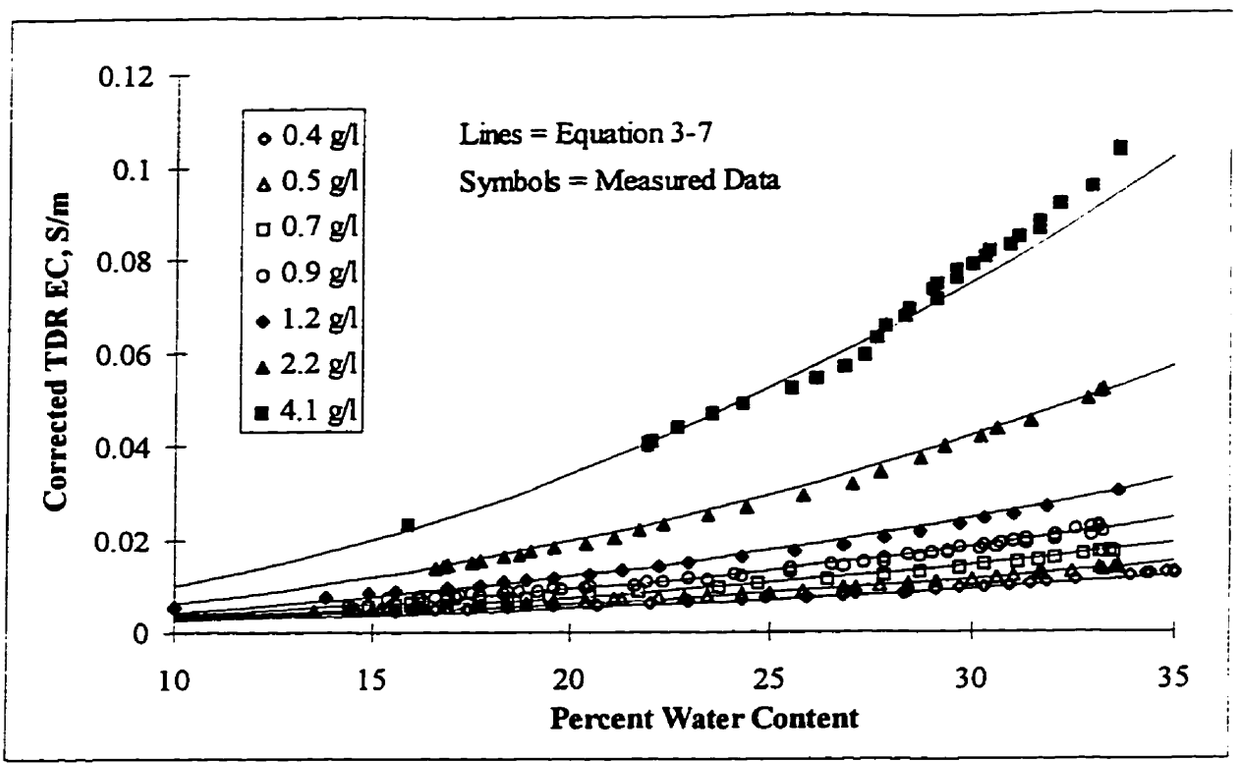

Figure 3-7. Measured and calculated values of the corrected TDR EC for seven flushing solutions as a function of water content: TDR12.

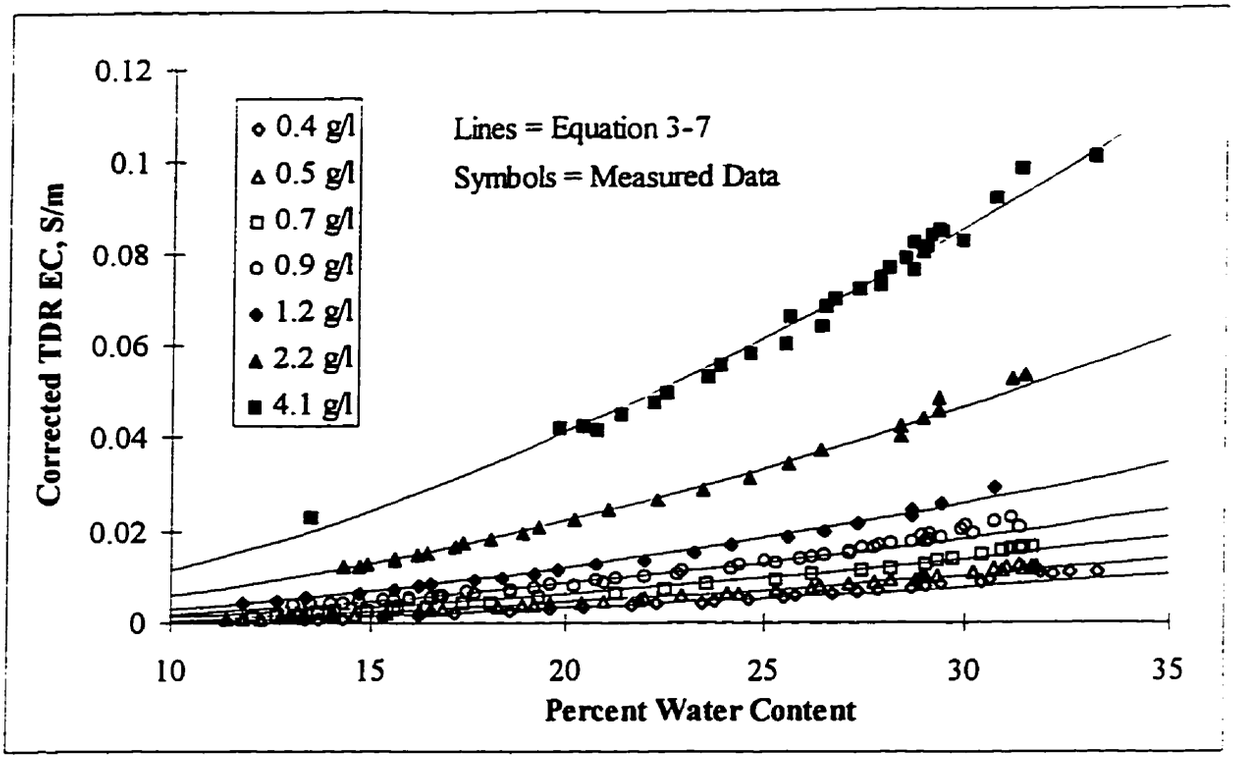

Figure 3-8. Measured and calculated values of the corrected TDR EC for seven flushing solutions as a function of water content: TDR12n.

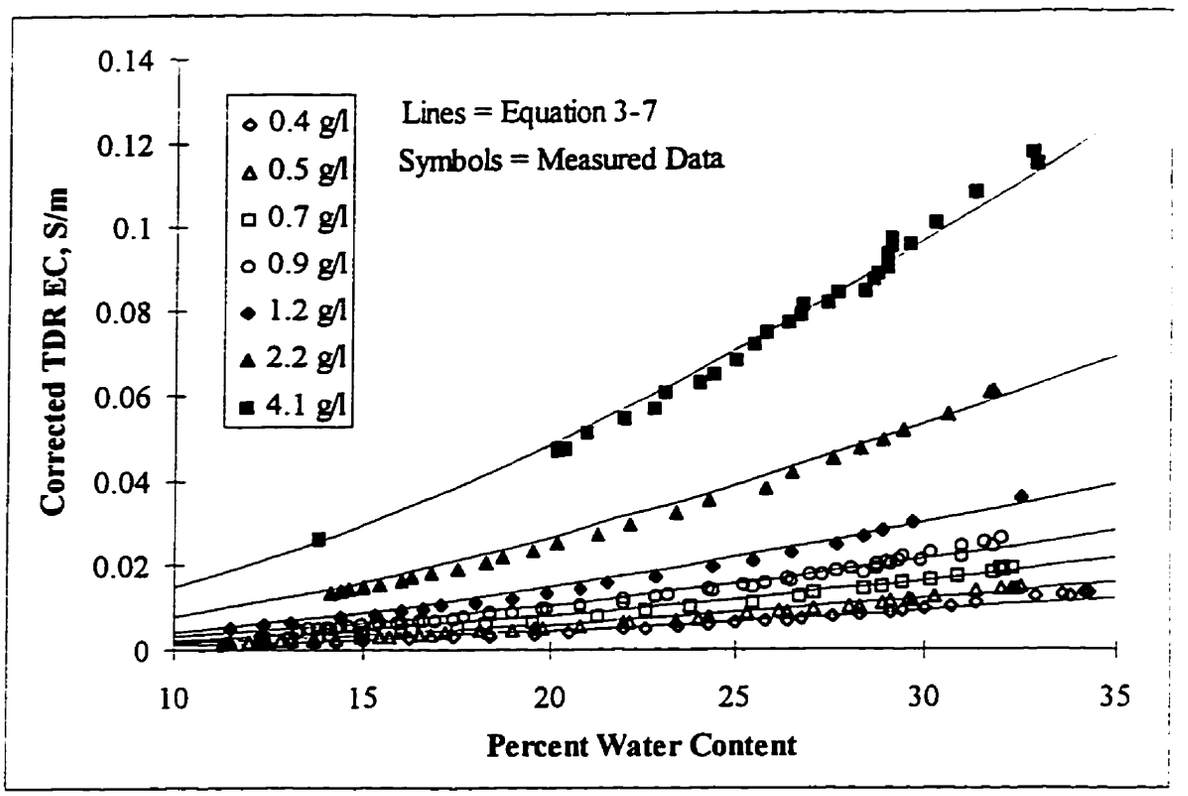

Figure 3-9. Measured and calculated values of the corrected TDR EC for seven flushing solutions as a function of water content: TDR123.

Although the intercepts seen on Figures 3-3 through 3-5 are nearly zero, they must be incorporated in Equation 3-7 to represent the bulk EC correctly. To demonstrate this, Figures 3-10 and 3-11 show the measured and calculated values of the TDR-measured EC both with and without inclusion of the intercept, *b*, for probe TDR12. Given that the intercept has the greatest impact in low EC conditions, only the lower range of corrected TDR EC values are shown.

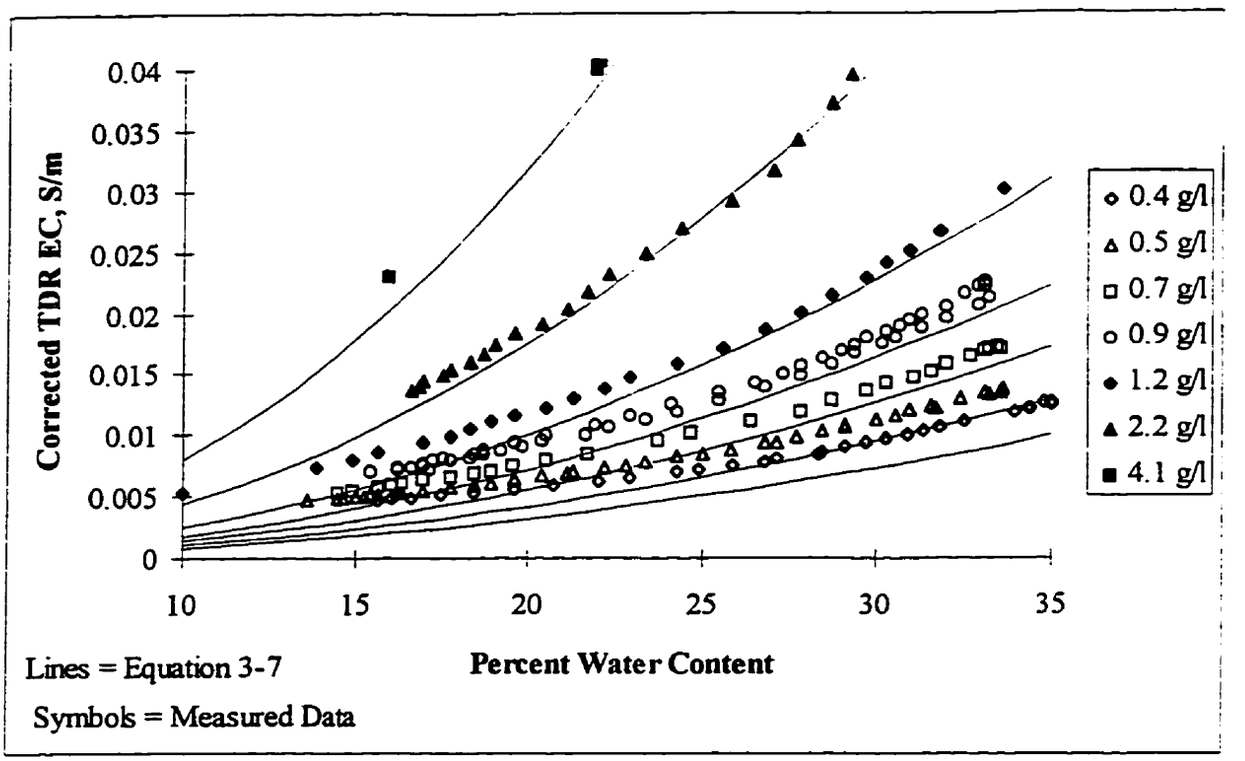

Figure 3-10. Measured and calculated values of the corrected TDR EC for seven flushing solutions as a function of water content: TDR12. Calculated values do not include intercept, *b*.

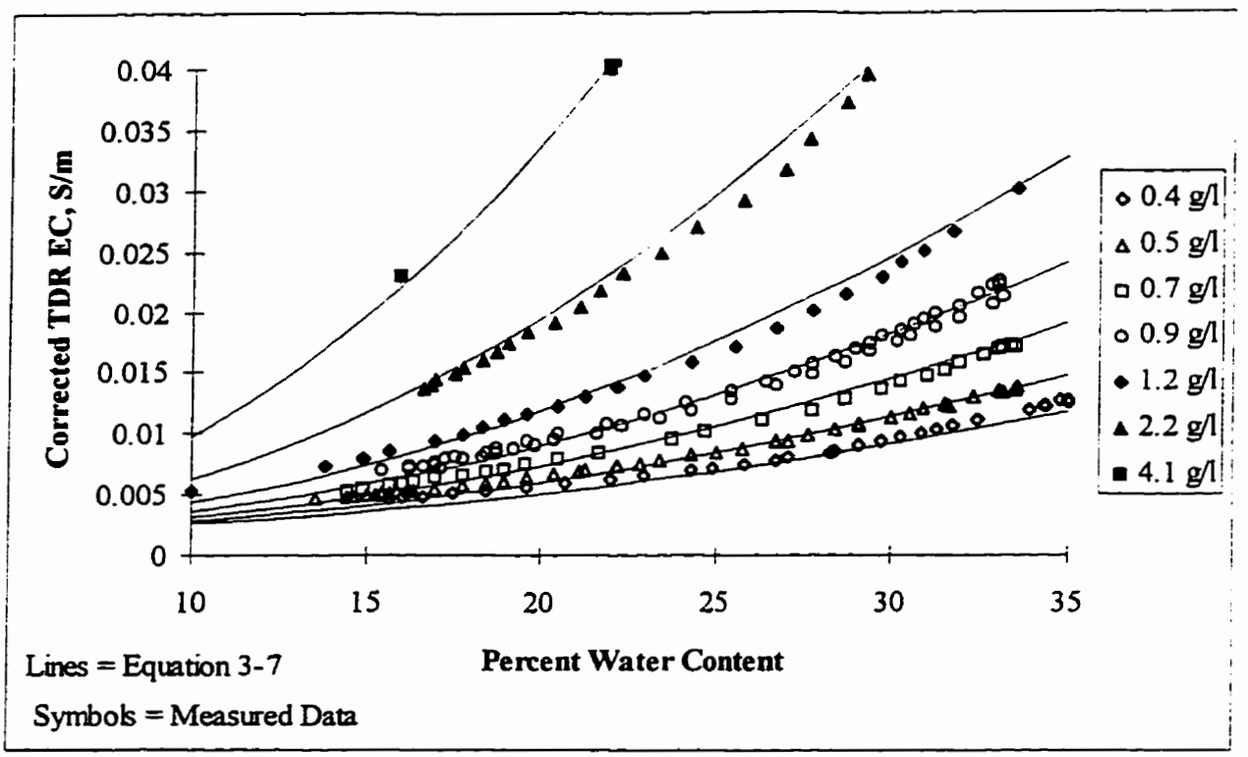

Figure 3-11. Measured and calculated values of the corrected TDR EC for seven flushing solutions as a function of water content: TDR12. Calculated values include intercept, *b*.

3.2.7 Summary and Conclusions

For all of the probe designs, calibration of the EC response of continuous-rod probes in saline solutions can define the equivalent resistivity of the cable and connectors between the TDR instrument and the probe and the calibration constant for the late time impedance analysis. Measurement during drainage provides a complete data set that allows for full definition of the dependence of the TDR-measured EC on the water content. For the clean sand used in this experiment, the relationship was well described by the simple, nonlinear expression determined by *Archie* [1942]. Although the fitting parameters varied with probe design, the response of all of the probes was well described over a wide range of water contents and pore water EC conditions.

3.3 Field Investigation Using Vertically-installed Continuous-rod Probes

3.3.1 Experimental Objectives

Previous studies of the dependence of the EC response of TDR on the water content have been performed under controlled, laboratory conditions. These experiments used short rods installed in a manner that minimized water content variations along the rods. Of all of the previously published experiments designed to study the EC response of TDR, only *Nadler et al.* [1991] made measurements under conditions of variable water content along the rods. However, their experiment was designed to study the effects of these water content distributions on the water content response of TDR; the influence of soil layering on the EC response was not discussed. In contrast, field experiments commonly use longer rods that may be subject to variations in the water content along their length, especially during transient flow and in heterogeneous media. The first objective of this investigation is to examine the dependence of the EC response of long continuous-rod probes on the water content in the field.

The results of the previous laboratory experiment showed a nonlinear relationship between the TDR-measured EC and the water content. In contrast, the dependence of the bulk EC on the pore water EC is linear. Therefore, if the water content varies along the rods, the average EC measured will reflect a weighted average of the pore water EC that gives greater weighting to regions of higher water contents. This differs from the water content response which has been shown to give the correct length-weighted water content under spatially variable water content conditions [*Topp et al.*, 1982a]. The relationship between the bulk EC and the water content will be reexamined based on the results of this field study to judge the viability of solute concentration monitoring with long, continuous-rod probes in the field.

3.3.2 Length-weighted Averaging of the Bulk Electrical Conductivity

For a clean sand, the surface conduction is negligible and Equation 1-8 simplifies to,

$$\sigma = a_R \sigma_w \theta^2 + b_R \sigma_w \theta . \tag{3-8}$$

There is a linear relationship between σ_w and the concentration of a solute per unit volume of pore water, C, for simple solutions such as potassium chloride (KCl) in water [*Barthel, et al.*, 1980],

$$\sigma_w = aC + b . \tag{3-9}$$

For controlled transport experiments, C is the concentration of an electrolytic tracer. The constant, b, represents the EC of the water in which the tracer is dissolved. For laboratory experiments using solutions in deionized water, b is nearly zero. However, the scale of field experiments generally requires the use of available municipal or irrigation waters which commonly have a measurable EC due to any dissolved ions present before amendment with the tracer.

Combining Equations 1-7 and 3-9 defines the relationship between the tracer concentration and the bulk EC of a sand,

$$\sigma = aC\theta^n\phi^{m-n} + b\theta^n\phi^{m-n}. \tag{3-10}$$

Alternatively, combining Equations 3-8 and 3-9 gives,

$$\sigma = a_R(aC+b)\theta^2 + b_R(aC+b)\theta. \tag{3-11}$$

Assuming that the resistance of the medium between the TDR rods can be approximated as independent resistors in parallel, based on the geometry of the transmission line, the EC response of TDR will represent the length-weighted average bulk EC of the medium over the probe. The response for a probe divided into i segments can be defined from Equation 3-10 as,

$$\sigma = a\frac{\sum_i L_i\sigma_i}{\sum_i L_i} = a\frac{\sum_i L_i C_i\theta_i^n\phi_i^{m-n}}{\sum_i L_i} + b\frac{\sum_i L_i\theta_i^n\phi_i^{m-n}}{\sum_i L_i}, \tag{3-12}$$

where L_i is the length of probe segment i.

The probes can be divided into any number of segments such that C and θ are uniform within each segment. In each segment, the product of C and θ equals the tracer mass per unit volume of porous medium, M. Substitution of this product into Equation 3-12 gives,

$$\sigma = a\frac{\sum_i L_i M_i\theta_i^{n-1}\phi_i^{m-n}}{\sum_i L_i} + b\frac{\sum_i L_i\theta_i^n\phi_i^{m-n}}{\sum_i L_i}. \tag{3-13}$$

An expression relating the bulk EC to the water content and solute mass can also be developed from Equation 3-11 based on the EC model of *Rhoades et al.* [1976],

$$\sigma = a_R \frac{\sum_i aL_i M_i \theta_i}{\sum_i L_i} + a_R \frac{\sum_i bL_i \theta_i^2}{\sum_i L_i} + b_R \frac{\sum_i aL_i M_i}{\sum_i L_i} + b_R \frac{\sum_i bL_i \theta_i}{\sum_i L_i}. \qquad (3\text{-}14)$$

A preliminary demonstration of the validity of Equations 3-13 and 3-14 is provided by the findings of *Kachanoski et al.* [1992]. They applied a tracer pulse onto a saturated, repacked column under steady-state flow and monitored the EC with a pair of TDR rods installed along the axis of the column. For the homogeneous column, both the water content and the porosity were spatially uniform; the solute concentration varied spatially due to dispersion during transport. For these conditions, Equations 3-13 and 3-14 can be simplified to,

$$\sigma = a\theta^{n-1}\phi^{m-n} \frac{\sum_i L_i M_i}{\sum_i L_i} + b\theta^n \phi^{m-n}, \text{ and} \qquad (3\text{-}15)$$

$$\sigma = (a_R a\theta + ab_R) \frac{\sum_i L_i M_i}{\sum_i L_i} + a_R b\theta^2 + b_R \theta. \qquad (3\text{-}16)$$

The first term on the right hand side of both equations is a constant times the length-weighted average value of M, $\overline{M}$; the remaining terms are constants. As the tracer pulse traveled along the rods, the total mass of the tracer in the measurement volume of the rods was constant, resulting in a constant value of $\overline{M}$ with time. The results of *Kachanoski et al.* [1992] showed that the EC response also remained constant from the time that the tracer pulse was released until the leading edge of the dispersed pulse reached the ends of the rods, confirming that the TDR-measured EC is directly related to the length-weighted average bulk EC of the medium along the probe.

In forming Equations 3-12 through 3-14, it has been assumed that a_R, b_R, m and n are constant along the rods. However, these constants are soil-specific; therefore, for highly heterogeneous media, this assumption may be invalid, leading to a nonunique relationship between the TDR-measured EC and $\overline{M}$. Even if a_R and b_R, are constant throughout the medium, Equation 3-14 does not lead to a unique relationship

between the EC response of continuous-rod probes and $\overline{M}$ if the water content varies along the length of the rods. For equation 3-13 to lead to a unique relationship n must equal one. In addition, the porosity must be spatially uniform along the rods or the exponents, m and n must be equal. Equation 3-13 with a value of n greater than one and Equation 3-14 both overweight the value of M in higher water content intervals in the length-weighted average. The preceding laboratory experiment showed a value of n equal to two in Equation 3-13. Additional complications will arise in soils with significant surface conductivity, further limiting the applicability of TDR for solute monitoring. Based on this analysis, it appears that the TDR-measured EC will only correspond to the value of $\overline{M}$ under very restrictive conditions.

In practice, TDR has been shown to measure the correct flux concentration of a tracer in the field, even in a highly heterogeneous medium [*Rudolph et al.*, 1996]. These results are based on the monitoring of a short-duration tracer pulse released in a steady-state flow field as suggested by *Kachanoski et al.* [1992]. Under these conditions, the pulse only occupies a short vertical interval at any time, minimizing the spatial variability in the water content in the region where the tracer is present; the limited extent of the pulse generally reduces the effects of spatial variability in the water content or the calibration constants on the length-weighted averaging. Therefore, these results do not demonstrate conclusively the ability of TDR to measure a bulk EC that corresponds with the average solute mass per unit volume of porous medium or the average solute concentration in the pore water.

3.3.3 Experimental Design

Field experiments were conducted to examine the EC response of continuous-rod TDR probes under spatially variable water content and pore water EC conditions. The experimental site was located on Canadian Forces Base Borden, Ontario, Canada. The aquifer material is a homogeneous, well-sorted, fine- to medium-grained sand with no significant clay fraction [*MacFarlane*, 1983]. The low clay fraction leads to minimal surface conduction, making the site well-suited to solute concentration monitoring by electrical conductivity methods.

The top meter of the soil was excavated to provide an undisturbed surface and the entire site was covered with a greenhouse to eliminate natural recharge. The water table was located 2.2 m below the excavated surface. Two calibrated 3 m by 3 m drip-line irrigation systems were placed on the surface of the site; one provided controlled infiltration of unamended municipal water, the other provided infiltration of KCl tracer solutions at the same flux. The drip points within the 3m by 3m area were located on a 15 cm by 15 cm grid.

Six pairs of continuous-rod TDR waveguides were installed vertically at the ground surface using a hand drill. The rod-pairs were 40, 60, 80, 100, 120 and 140 cm in length. Each rod-pair was comprised of

0.4 cm diameter steel welding rods separated by 3 cm. The distance between rod-pairs was 15 cm and the total area occupied by the rod-pairs at the ground surface was 15 cm by 30 cm. The rod-pairs were connected through twin-wire shielded cable (#9090 Belden) to a balun (ANZAC TP-103 impedance matching transformer) that was placed directly on a cable tester (Tektronics 1502B). A program written at the Waterloo Center for Groundwater Research [*Redman, 1994*] transferred the TDR waveforms from the cable tester to a personal computer through an RS-232 serial interface.

The soil was preflushed with municipal source-water with no added tracer (EC = 0.040 S/m) to displace any resident pore water and then allowed to drain. After five days of drainage, the municipal water irrigation system was restarted and TDR waveforms were collected with all of the rod-pairs during the advance of the wetting front. Paired measurements of the bulk EC and the water content were calculated from the waveforms and are referred to as the Infiltration data set. When the waveforms were constant in time for the longest rod-pair, indicating that steady-state flow had been established, fresh-water infiltration ceased and infiltration of a KCl tracer (EC = 0.085 S/m) was started through a separate irrigation system at the same flux. Waveforms collected during the advance of this tracer step form the Transport data set. Infiltration of the tracer-amended solution continued until the waveforms were constant in time for the longest rod-pair, indicating that the tracer solution had displaced the resident pore water. Then the irrigation system was turned off and both the water content and the bulk EC were monitored during drainage; this data set is referred to as Drainage1. Finally, all of these steps were repeated using a tracer solution with an EC of 0.142 S/m to produce the Drainage2 data set.

3.3.4 Experimental Results

Combining Equations 3-1 and 3-12 gives the relationship between the EC response used for the GT analysis and the water contents and tracer concentrations along the rod-pair.

$$\frac{1}{L}\left(\frac{2V_0}{V_f}-1\right)=\frac{a}{c_{GT}}\frac{\sum_i L_i C_i \theta_i^n \phi_i^{m-n}}{\sum_i L_i}+\frac{b}{c_{GT}}\frac{\sum_i L_i \theta_i^n \phi_i^{m-n}}{\sum_i L_i}. \qquad (3\text{-}17)$$

The water contents determined from the waveforms collected with all six rod-pairs during Drainage1 are shown on Figure 3-12. Even for the relatively uniform site conditions, there was measurable spatial variability in the water content with depth throughout the drainage event.

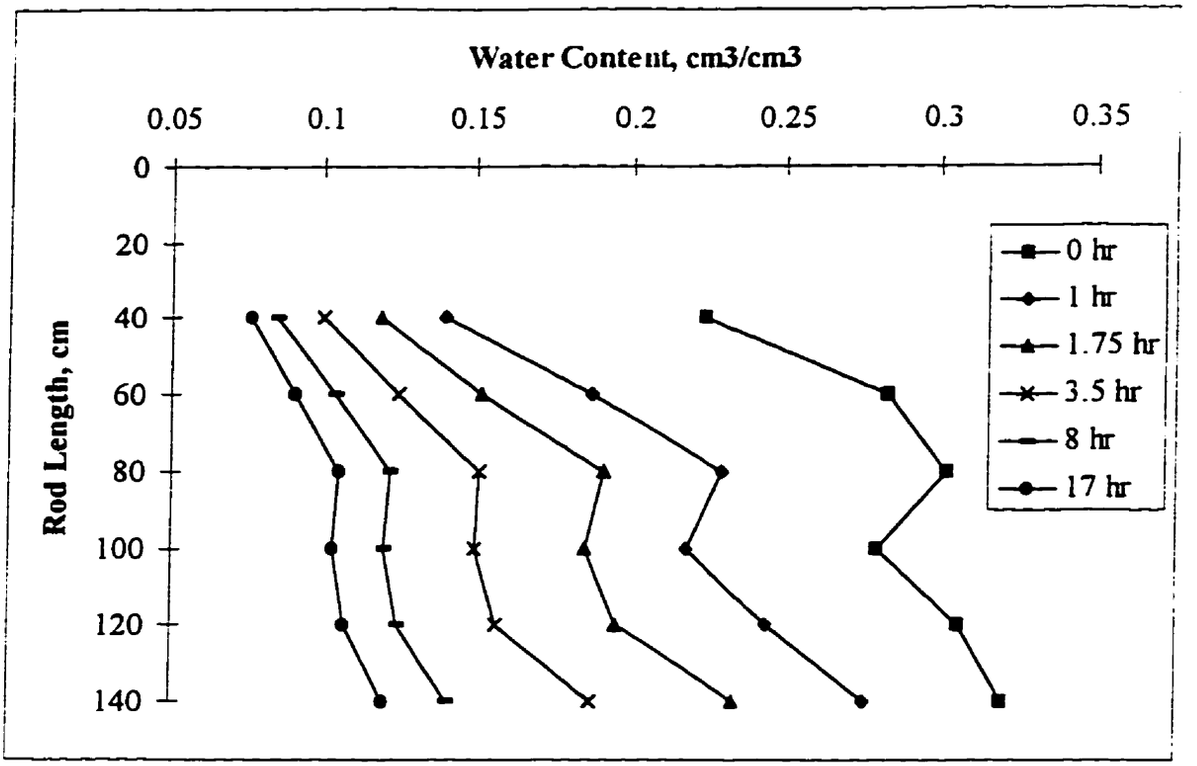

Figure 3-12. The water content as a function of the length of the rod-pair during Drainage1, labeled with the elapsed time since the beginning of drainage.

The solute concentration was spatially uniform during drainage following steady-state infiltration, allowing simplification of Equation 3-17 to,

$$\frac{1}{L}\left(\frac{2V_0}{V_f}-1\right)=\left(\frac{aC+b}{c_{GT}}\right)\frac{\sum_i L_i\theta_i^n\phi_i^{m-n}}{\sum_i L_i}. \qquad (3\text{-}18)$$

Assuming that the porosity was also spatially uniform results in a direct relationship between the EC response and the length-weighted average of the water content raised to the exponent, n. Following a procedure similar to that followed for the laboratory experiment described above, we fit Equation 3-18 to paired measurements of the water content and the EC response used for the GT analysis, $\left[\left(2V_0/V_f - 1\right)/L\right]$, collected with the six rod-pairs during Drainage1.

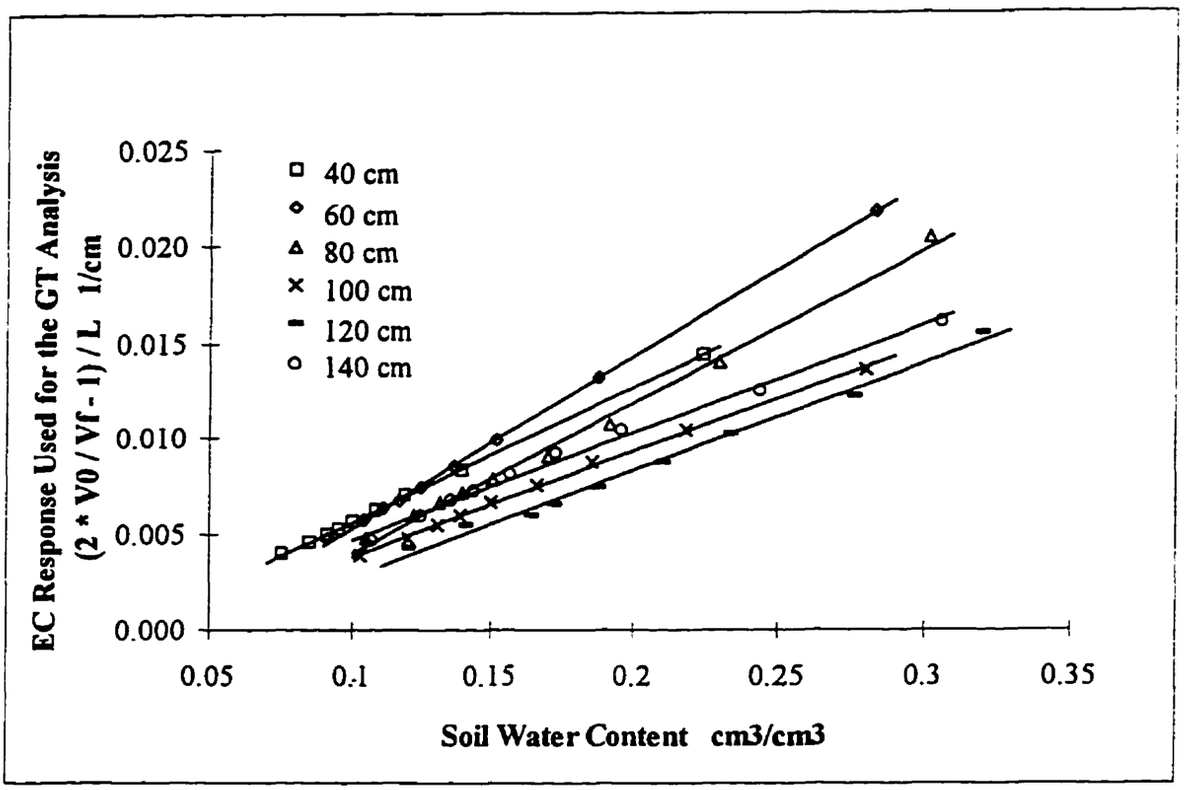

Figure 3-13. The EC response used for the GT analysis as a function of the water content measured with all six rod-pairs during Drainage1. Linear regressions of Equation 3-18 to the EC responses and the water contents are shown as straight lines.

In contrast to the laboratory results presented above, the field data (Figure 3-13) show highly linear relationships between the EC response and the water content for each rod-pair; the linear fits to the data, shown as solid lines on Figure 3-13, all have r^2 values in excess of 0.99. There were also linear relationships between the EC response used for the LTI analysis, $\left[1/R_L\right]$, and the water content. These highly linear relationships justify the use of the EC model of *Archie* [1942] with n equal to one. It is unclear why these findings disagree with those found in the previous laboratory experiment. Figure 3-13 also shows that the

slopes of the linear calibrations differed among the probes. These differences are due to small differences in the separation of the rods among the rod-pairs that occur despite efforts to install the probes carefully in the field site. These variable separations lead to different values of the constants c_N and c_{GT} in the GT and LTI analyses (Equations 3-1 and 3-2) for each rod-pair.

Letting n equal 1 based on the observed linearity of the responses shown on Figure 3-13 and assuming that the porosity, m and n are spatially uniform gives,

$$\frac{1}{L}\left(\frac{2V_0}{V_f}-1\right)=\frac{a\phi_i^{m-1}}{c_{GT}}\frac{\sum_i L_i C_i \theta_i}{\sum_i L_i}+\frac{b\phi_i^{m-1}}{c_{GT}}\frac{\sum_i L_i \theta_i}{\sum_i L_i}. \qquad (3\text{-}19)$$

For drainage following steady-state infiltration, C is spatially uniform giving,

$$\frac{1}{L}\left(\frac{2V_0}{V_f}-1\right)=(AC+B)\frac{\sum_i L_i \theta_i}{\sum_i L_i}=(AC+B)\bar{\theta}. \qquad (3\text{-}20)$$

A similar expression can be developed for the LTI analysis from Equations 3-2 and 3-14.

$$\frac{1}{R_L}=(A_{LTI}C+B_{LTI})\bar{\theta}. \qquad (3\text{-}21)$$

Linear regressions of Equation 3-20 to the EC and water content responses of each probe for the Infiltration, Drainage1 and Drainage2 data sets (Figure 3-14) show nonzero intercepts. Figure 3-14 clearly shows that the EC response is independent of the tracer concentration at a low water content approximately equal to the residual water content, θ_r, as determined in the laboratory by *Nwankwor* [1982]; this value is shown as a vertical dotted line on Figure 3-14. A constant can be added to Equation 3-20 to account for this response,

$$\frac{1}{L}\left(\frac{2V_0}{V_f}-1\right)=(AC+B)\left(\bar{\theta}-\theta_r\right)+d. \qquad (3\text{-}22)$$

We refer to the quantity, $\left(\bar{\theta}-\theta_r\right)$, as the length-weighted average mobile water content, $\overline{\theta_m}$. However, it is important to note that although the value of θ_r is very similar to the residual water content of the

medium measured in the laboratory [*Nwankwor*, 1982] it is only a fitting parameter. Further investigation is necessary to determine relationships between this parameter and other soil properties.

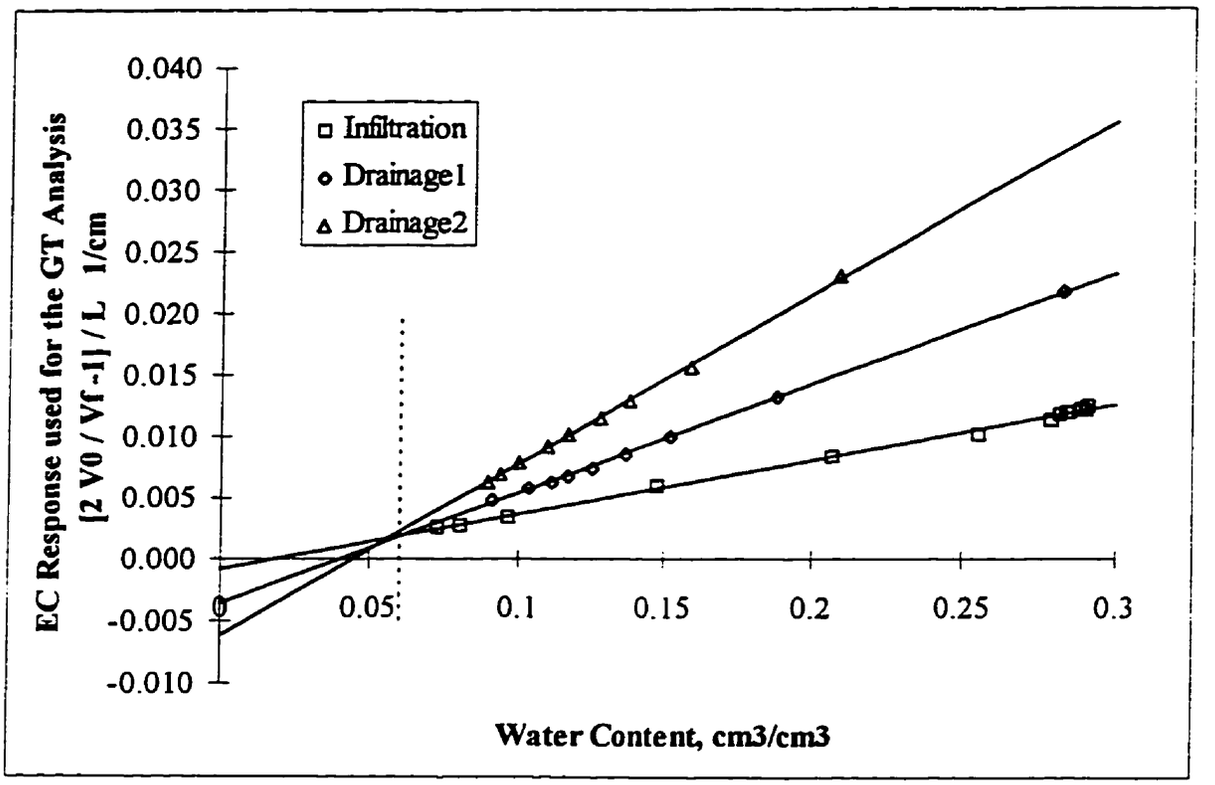

Figure 3-14. The EC response used for the GT analysis as a function of the water content measured with the 60 cm rod-pair during Infiltration, Drainage1 and Drainage2. Linear regressions of Equation 3-20 to the EC responses and the water contents are shown as straight lines. The residual water content is shown as a vertical dotted line.

Figure 3-15 shows paired measurements of the EC response used for the LTI analysis and the water content both measured with the 60 cm rods for the Infiltration, Drainage1 and Drainage2 data sets. This

analysis does not result in a clear separation among the EC responses for the different pore water EC conditions at low water contents. Therefore, we applied the GT method for all further analyses. This result disagrees with the findings of the preceding laboratory experiment which suggests that the LTI analysis should be applied for probes with baluns. The disagreement between the findings under laboratory and field conditions reiterates the importance of carefully examining the method of EC analysis for each application.

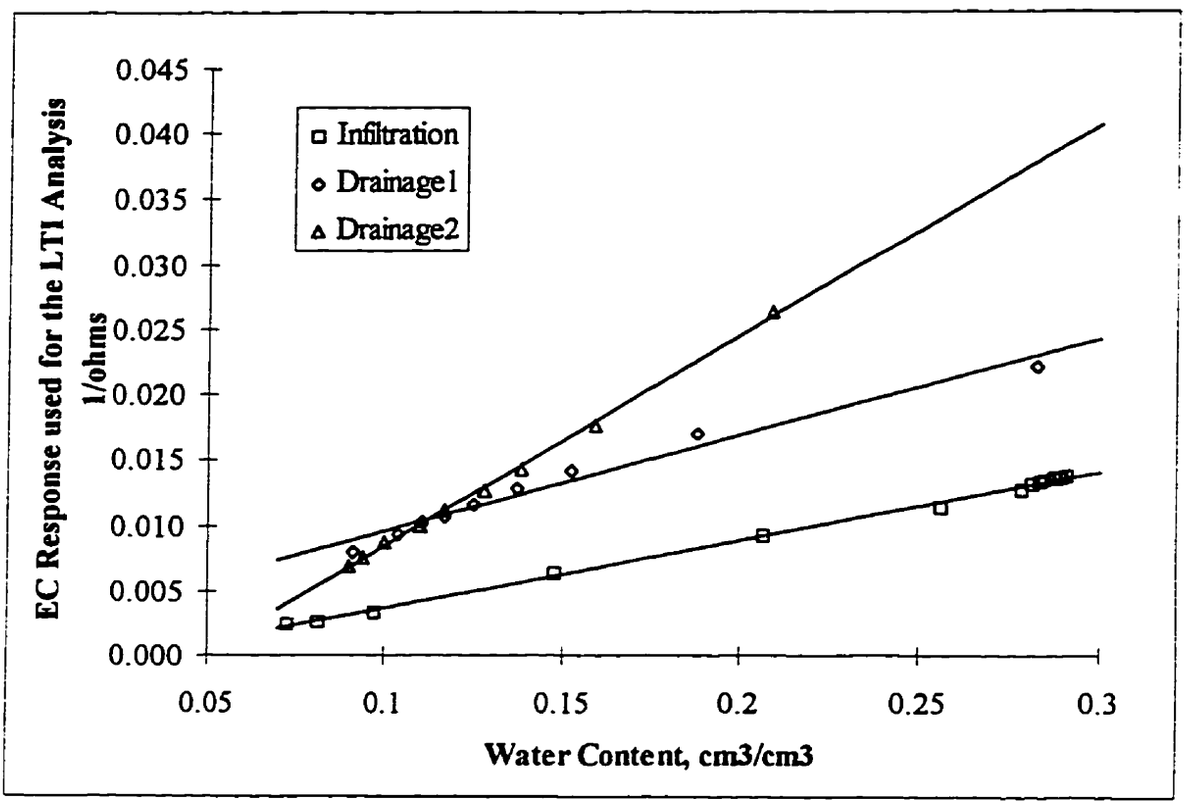

Figure 3-15. The EC response used for the LTI analysis as a function of the water content measured with the 60 cm rod-pair during Infiltration, Drainage1 and Drainage2. Linear regressions of Equation 3-22 to the EC responses and the water contents are shown as straight lines.

The slope of the relationship between the EC response used for the GT analysis and the length-weighted average mobile water content is plotted for each probe as a function of the tracer concentration on Figure 3-16. The slopes, intercepts and r^2 values of the linear regressions included on the figure are shown on Table 3-3. For each probe, the constants A and B in Equation 3-22 equal the slope and intercept of the regression, respectively.

	40 cm	60 cm	80 cm	100 cm	120 cm	140 cm
slope, A	0.113	0.140	0.097	0.074	0.070	0.077
intercept, B	0.036	0.046	0.047	0.030	0.0339	0.029
R^2	0.998	0.996	0.976	0.967	0.995	0.963

Table 3-3. Linear regressions of the slope of Equation 3-22, ($AC+B$), to the tracer concentration for all six rod-pairs.

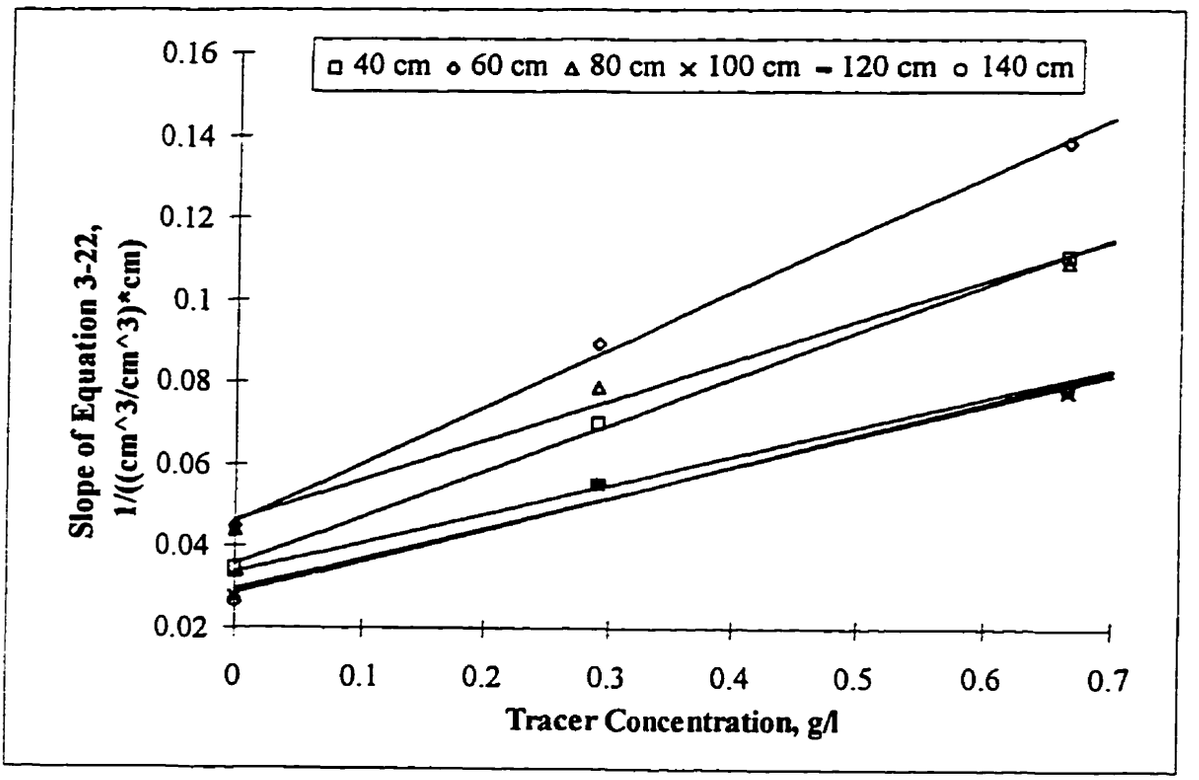

Figure 3-16. The slope of the relationship between the EC response used for the GT analysis and the water content as a function of the tracer concentration measured with all six rod-pairs during Infiltration, Drainage1 and Drainage2. Linear regressions of the slope to the tracer concentration are shown as straight lines.

Based on Equation 3-22, the EC response is related to the length-weighted averages of the tracer mass and water content by,

$$\frac{1}{L}\left(\frac{2V_0}{V_f}-1\right)=A\frac{\sum_i L_i C_i\left(\theta_i-\theta_r\right)}{\sum_i L_i}+B\frac{\sum_i L_i\left(\theta_i-\theta_r\right)}{\sum_i L_i}+d=A\overline{M_m}+B\overline{\theta_m}+d, \quad (3\text{-}23)$$

where M_m is the tracer mass per unit volume of the porous medium in the mobile water. Rearranging Equation 3-19 to define $\overline{M_m}$ gives,

$$\overline{M_m}=\frac{\frac{1}{L}\left(\frac{2V_0}{V_f}-1\right)-B\overline{\theta_m}-d}{A}. \quad (3\text{-}24)$$

The Transport data set is comprised of paired measurements of the water content and EC during the advance of a tracer step released onto a steady-state, unsaturated flow field. The water content measured during transport is shown as the 0 hour profile on Figure 3-12 and remained constant throughout the experiment. The average tracer concentration in the mobile pore water in the sample volume is related to the EC response used for the GT analysis by,

$$\overline{C_m}=\frac{\overline{M}}{\overline{\theta}}=\frac{\overline{M_m}}{\overline{\theta_m}}=\frac{\frac{1}{L}\left(\frac{2V_0}{V_f}-1\right)-B\overline{\theta_m}-d}{A\overline{\theta_m}}. \quad (3\text{-}25)$$

Figure 3-17 shows the tracer concentrations calculated using Equation 3-25 for all six rod-pairs during the advance of the solute step. The calculated concentrations at the beginning of the tracer step are in good agreement with the concentration of the unamended municipal water (C=0). The calculated concentrations are within 10% of the applied tracer concentration for most of the probes at the end of the tracer step. The differences between the known and measured concentrations arise from the variations of the probe responses about the linear regressions shown on Figures 3-14 and 3-16. This level of accuracy should be acceptable for many field investigations of solute transport under transient flow conditions.

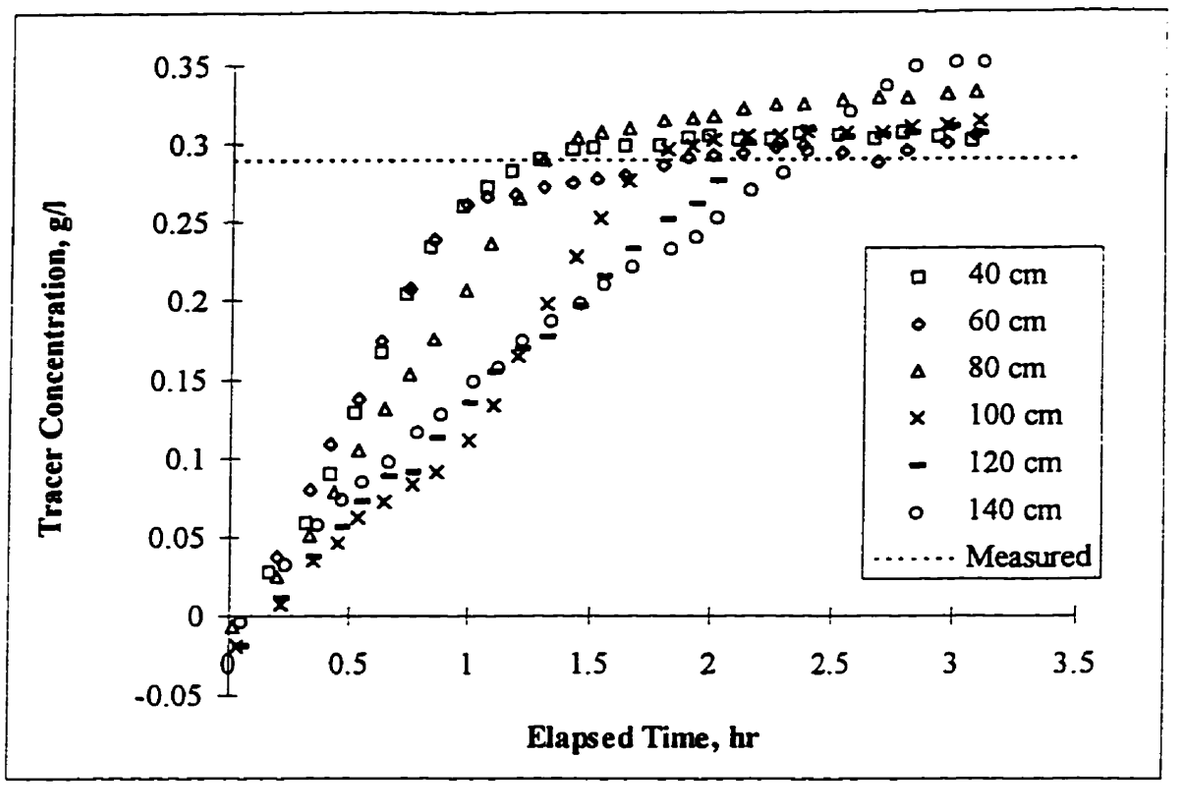

Figure 3-17. The tracer concentration calculated from the responses of all six rod-pairs during the advance of a tracer step using Equation 3-21. The tracer concentration of the municipal water was zero; the applied step had a KCl concentration of 0.29 g/l, shown as a dotted horizontal line.

3.3.5 Summary and Conclusions

In contrast to the laboratory results presented above, the field results show a linear relationship between the TDR-measured bulk EC and the water content for constant pore water EC conditions. As a result, an expression can be defined that relates the EC and water content responses of TDR to the length-weighted average solute mass per unit volume of porous medium. This expression can be applied regardless of the distribution of the soil water for a wide range of tracer concentrations, allowing for the monitoring of solute transport under transient flow conditions. However, in a highly heterogeneous medium, with electrical properties that vary along the rods, it is unlikely that there will be a unique relationship between the average solute mass and the TDR-measured bulk EC, limiting the applicability of long, continuous-rod probes for solute concentration monitoring. Further investigation is required to extend these findings to soils with significant surface conductivities.

4. CHAPTER FOUR

ALTERNATIVE TDR PROBES

4.1 *Motivation*

Standard, continuous-rod probes have been shown to average both the water content and bulk EC along their length. In the laboratory, short probes can be inserted through the walls of columns horizontally in the horizontal plane to minimize the variability of the water content between the rods, ensuring accurate averaging of the water content throughout the sample volume. This placement will also minimize water content variations along the rods, allowing for electrolytic tracer concentration determinations from the EC and water content responses despite the nonlinear dependence of the bulk EC on the water content observed in the laboratory.

Field applications of TDR face several limitations that do not apply under laboratory conditions. Limited access to the subsurface generally requires vertical emplacement of continuous-rod probes at the ground surface. As a result, water content profiling with continuous-rod probes requires interval differencing of the water content measured with several rod pairs, the disadvantages of which have been discussed in section 1.2.3. Similarly, it has been shown that the bulk EC can be related to the resident solute concentration only if the electrical properties of the medium are uniform over the length of the rods. This required spatial uniformity is unlikely over the vertical extent of longer rod-pairs in heterogeneous media, limiting the ability to measure solute concentrations to monitoring short duration solute pulses to shallow depths. In addition to these limitations, continuous-rod probes are subject to large energy losses through electrical conduction, restricting the maximum depth of investigation. Finally, the minimum rod length required to identify clearly the reflections from the ground surface and the ends of the rods precludes water content measurement very near the ground surface.

Alternative TDR probes have been designed to address the limitations that continuous-rod probes face in the field. Each probe has advantages and limitations; no current probe design can fulfill all sampling needs. The first objective of this investigation is to design an alternative probe that is capable of measuring both the water content and the bulk EC over small vertical intervals to allow for water content and solute concentration profiling in the field under both steady-state and transient flow conditions. The second goal is to develop a quantitative method for defining the sample area and sensitivity of any published alternative probe based solely on a description of the geometry of the probe and the dielectric permittivity of any nonmetallic probe materials to allow for direct comparison of probe performance and optimization of probe designs.

4.2 *Previously Published Probe Designs*

Alternative TDR probes perform any of four functions: profile the water content and/or bulk EC with depth, limit conductive losses to increase the maximum depth of measurement, and measure the water content near the ground surface. All of the published alternative probes are variations on the coaxial or multiple parallel rod design. Assuming that the phase velocity is equal to the propagation velocity, the EM pulses travel as plane waves along these conductors. Then, the response of a probe can be described based solely on the response of a representative cross section of the probe in the transverse plane, as shown analytically for coated continuous-rod probes above. These responses can be summed along a probe to describe the response of the probe to axially variable water contents. Representative cross sections of the published alternative probes are shown below.

4.2.1 Standard Continuous-rod Probes

Standard continuous-rod TDR probes are comprised of two or three parallel metal rods [*Topp et al.*, 1982; *Zegelin et al.*, 1989]. The configuration of the probes in the plane perpendicular to the long axis of the rods can be defined by the diameter of the rods, D, and the separation between the centers of the outermost rods, S, as shown on Figure 4-1. In practice, the diameter of rods ranges from 1 mm to greater than 1 cm, depending upon the application.

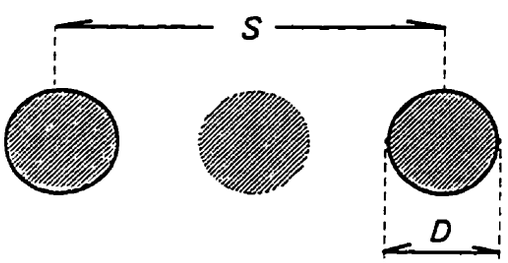

Figure 4-1. Cross-section of a continuous-rod probe.

4.2.2 Topp and Davis Multilevel Probe

Figure 4-2 shows the earliest published waveguide specifically designed to profile the water content with depth [*Topp and Davis*, 1985]. The probes included a series of changes in the diameter of the rods along their length. Each change in the rod diameter causes a change in the impedance of the probe, resulting in an identifiable reflection on the waveform. The travel time between these reflections defines the water content in

the regions between each discontinuity. This is the only published alternative probe that does not include nonmetallic components.

Within each segment, the cross-section of the probe is identical to that shown for standard continuous-rod probes on Figure 4-1. Therefore, the response of this probe will not be analyzed separately; rather, the results for the continuous-rod probes can be applied directly to this design. The number of intervals that can be measured with these probes is limited because the energy reflected at each discontinuity decreases the energy remaining to identify successive characteristic reflections. Furthermore, multiple reflections arise when the energy reflected from a deeper discontinuity encounters a shallower discontinuity as it travels back towards the pulse generator, making interpretation of the waveforms difficult for large numbers of depth intervals.

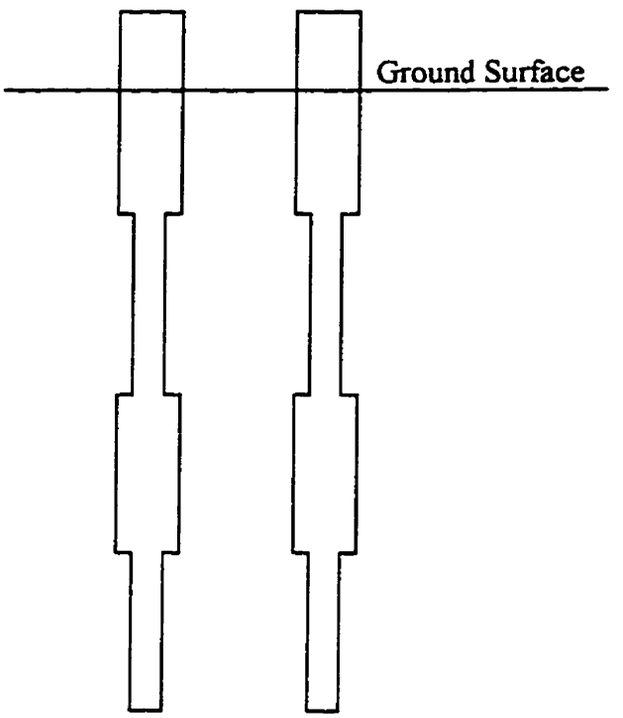

Figure 4-2. Schematic diagram of a cross section along the rods of the *Topp and Davis* [1985] probe for water content profiling.

4.2.3 Coated Continuous-rod Probes

The simplest modification to continuous-rod probes to decrease conductive losses through electrical conduction is the application of electrically resistive coatings to the rods. The configuration of a coated rod probe includes the diameter, D, and separation, S, of the rods and the outer diameter of the coating, G, as

shown on Figure 4-3. Note that the coatings are concentric with the rods and do not conform exactly to the bipolar geometry of *Annan* [1977b].

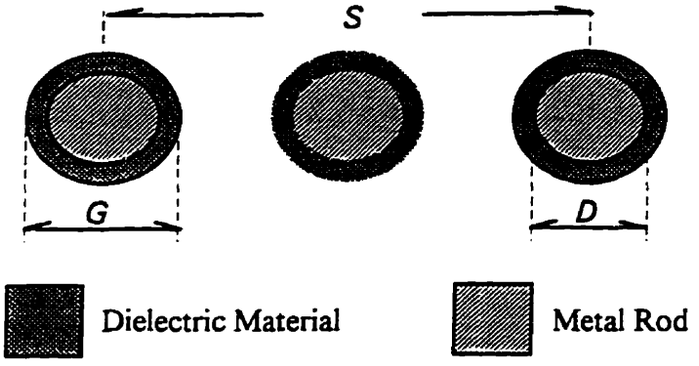

Figure 4-3. Cross-section of a coated continuous-rod probe.

4.2.4 Hook et al. Multilevel Probe

More complex probes have been designed based on the use of electrically-switched shorting diodes [*Hook et el.*, 1992]. A series of these elements are embedded in a dielectric material placed between two or three parallel rectangular metal rods. Using the diodes to sequentially short-circuit the rods, the travel time can be determined over several different rod lengths. A cross-section of the probe between the diodes is shown on Figure 4-4; the probe dimensions are described by the height, H, and width, W of the rods and the separation of the centers of the outermost rods, S. The published design showed a rod separation of 2.5 cm and rod widths and heights on the order of 1 cm and 0.5 cm, respectively. These probes avoid the limitations of multiple physical discontinuity probes by only activating a single discontinuity at any time. The water content of each region is determined by interval differencing of successive water content measurements; but, because the soil water content measurements are made beneath a single surface point, the problem of attribution of horizontal water content variability to the vertical profile is eliminated. *Hook et el.* [1992] also showed that shorting improves the accuracy of travel time determinations. However, to limit costs, probes are commonly constructed with few diodes, limiting the number of depth intervals over which the probe measures the water content. In addition, the electrical shorting removes the information used for EC measurement.

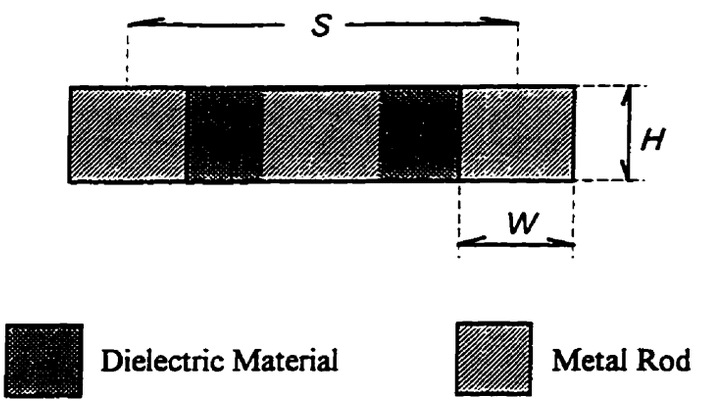

Figure 4-4. Cross section of the *Hook et al.* [1992] probe for water content profiling.

4.2.5 Redman and D'Ryck Probe

Redman and D'Ryck [1994] described a probe including a series of short continuous rod-pairs attached to the outside of a large diameter (5 cm) PVC access tube. The rod-pairs are connected to the surface by a shielded wire located inside the access tube. A representative cross section of the probe in the transverse plane is shown on Figure 4-5.

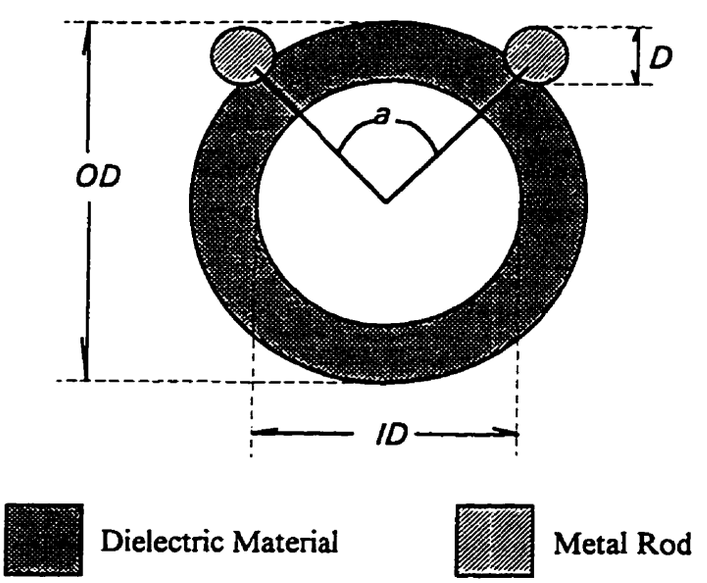

Figure 4-5. Cross section of the *Redman and D'Ryck* [1994] probe for water content and EC profiling.

The probe configuration is defined by the rod diameter, D, the inner and outer diameters of the access tube, ID and OD, and the angular separation of the rods on the surface of the access tube, a. This probe has been shown to measure the water content for a series of nonoverlapping depth intervals; in theory, it should be able to profile the bulk EC as well.

4.2.6 White and Zegelin Surface Probe

White and Zegelin [1992] designed an alternative probe to measure the water content at the ground surface based on a semi-coaxial design. This probe should be able to measure the bulk EC at the near surface as well. A cross section of the *White and Zegelin* [1992] probe is shown on Figure 4-6. The probe includes a central rod of diameter, D, a metallic half-shield with inner diameter, S, and two wings that extend a distance, W, along the ground surface. The thickness of the wings and shield is t. The published probe had dimensions of D, S and W of 1, 4 and 4 cm, respectively and the space between the central rod and the shield was filled with beeswax.

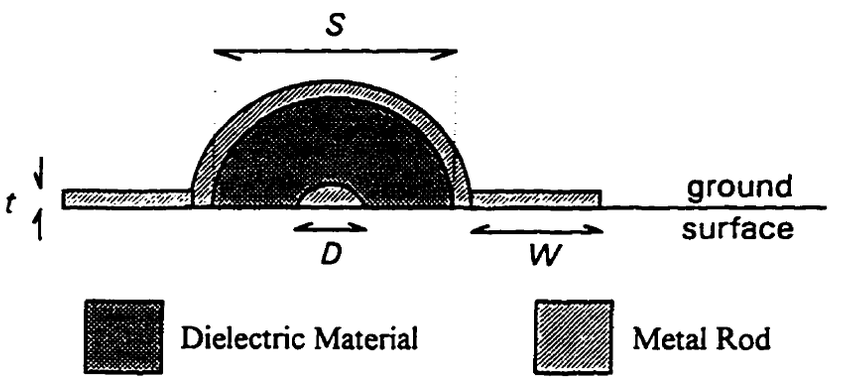

Figure 4-6. Cross section of the *White and Zegelin* [1992] probe for water content and EC measurement at the ground surface.

4.2.7 Selker et al. Surface Probe

A cross section of the *Selker et al.* [1993] probe is shown on Figure 4-7. The probe includes two rectangular metal rods of width, *W*, and height, *H*, embedded in a dielectric probe body. The rods extend past the base of the probe a distance *Ho* and their centers are separated by a distance, *S*. The probe body has a height, *Hb*, and a width, *Wb*. The published probe design had dimensions of 1.25 cm for *Hb*, 2 cm for *Wb*, 1.5 mm for *H*, 0.75 mm for *Ho* and 1 cm for *S*; this design used electrically shorted rods, precluding EC measurement.

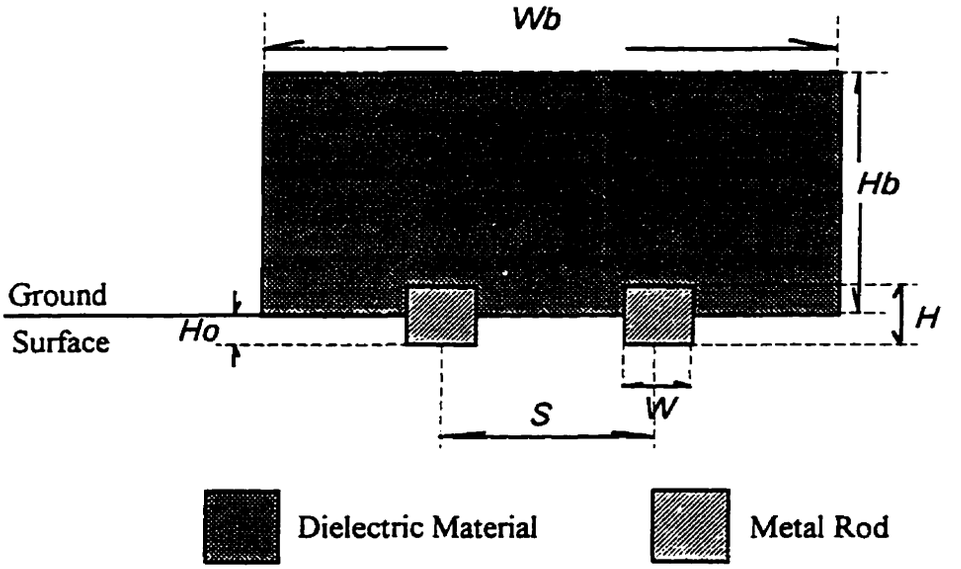

Figure 4-7. Cross section of the *Selker et al.* [1993] probe designed to measure the water content at the ground surface.

To increase the rod length while maintaining a small overall probe size (on the order of 10 cm by 10 cm), *Selker et al.* [1993] arranged a pair of rods in a serpentine pattern along the base of the probe, as shown on Figure 4-8. The bends in the rods result in changes in the rod separation along the probe; the effects of these bends cannot be quantified based on a representative cross section through the rods.

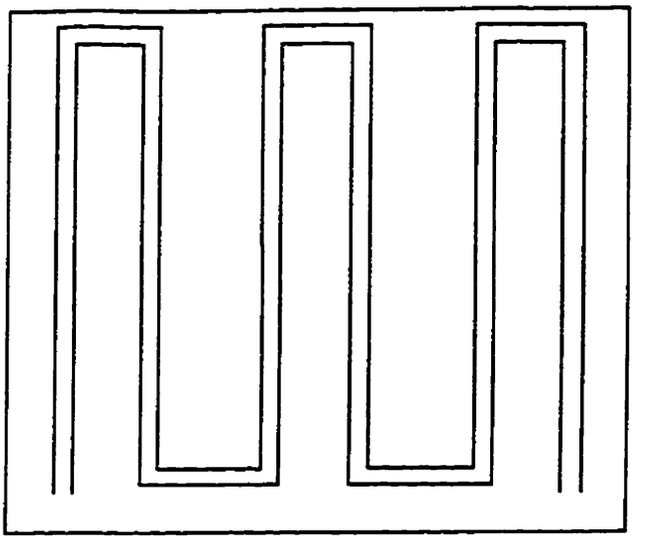

Figure 4-8. Plan view of the base of the *Selker et al.* [1993] probe.

4.3 Design of an Alternative Multilevel Probe

4.3.1 Multilevel Probe Design

A multilevel TDR probe was designed to measure the water content over isolated regions of the subsurface based on the analytical description of the spatial sensitivity of TDR probes presented by *Knight* [1992] and on the design of the multiple impedance discontinuity probes of *Topp and Davis* [1985]. The probe uses a pair of identical rods that are lowered through two parallel access tubes. As shown in Figure 4-9, each multilevel rod is comprised of two sections: a small diameter, coated wire that is connected to the pulse generator through a balun and a larger diameter target rod. The target rod is uncoated; polyethylene tubing with an outer diameter approximately equal to that of the target rods is fitted over the coated wires.

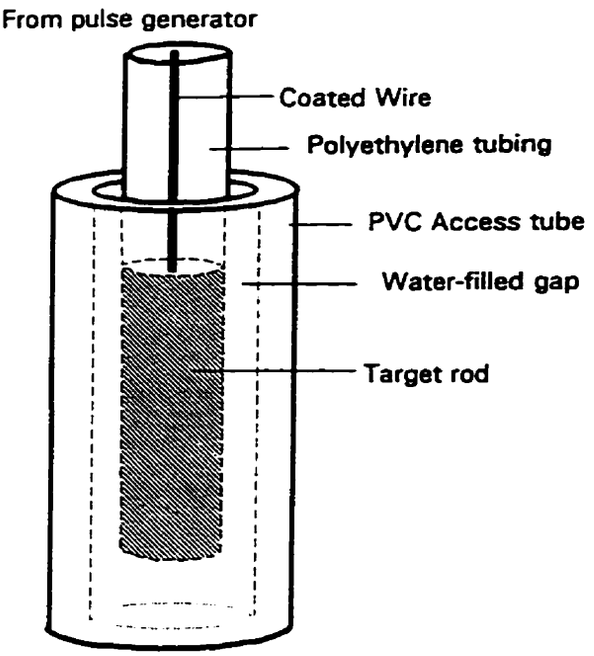

Figure 4-9. Schematic diagram of one of the pair of multilevel rods and access tubes.

The reflections from the impedance discontinuity caused by the change in the rod diameter at the point of connection of the wires to the target rods and from the ends of the target rods can be identified on the waveform. The travel time between these reflections defines the velocity of propagation through the sample interval. The use of a single impedance discontinuity minimizes the problems associated with multiple discontinuities seen by *Topp and Davis* [1985] and measurement through access tubes allows for placement of the target rods at any desired depth.

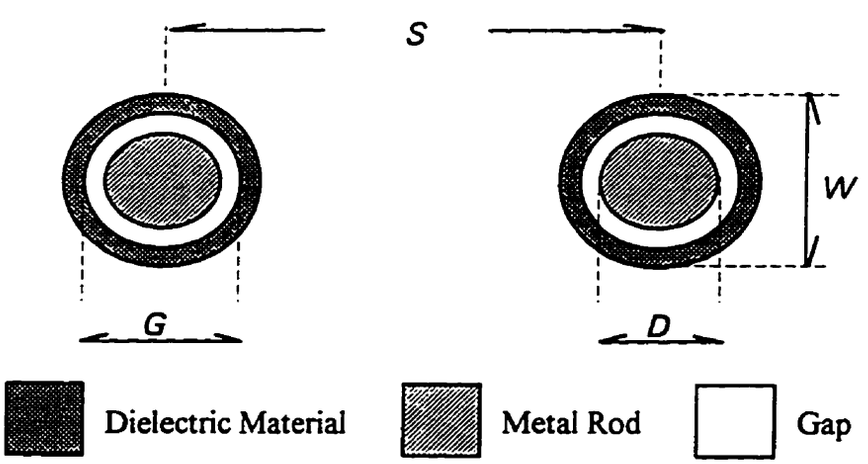

Figure 4-10. Cross-section of the alternative multilevel TDR probe.

A cross-section of the probe in the plane perpendicular to the access tubes is shown on Figure 4-10. The configuration is defined by the diameter of the rods, D, their separation, S, and the inner and outer diameters of the access tubes, G and W, respectively.

Knight [1992] defined the weighting factors in the plane perpendicular to a twin-rod probe placed in a homogeneous medium. These weighting factors, based on the energy distribution of the electric field around the rods, define the weighting of regions of the medium surrounding the rods in the averaging of the relative dielectric permittivity by TDR. Figure 4-11 shows the weighting factors that would apply around the small diameter wires and larger diameter target rods if they were inserted directly into a homogeneous medium without access tubes or coatings. The shaded regions on Figure 4-10 show the dimensions of the access tubes, target rods and wires used for the prototype probe described below. The weighting factors in the medium outside of the access tubes are larger around the target rods than around the small diameter wires, demonstrating the increased sensitivity of the probe to the medium in the target region. The probe sensitivity is focused between the access tubes. *Knight* [1992] presented an equation to define the cumulative sensitivity within a pair of circles of a given diameter surrounding the rods. For the dimensions of the prototype probe, 13% of the sensitivity of the probe in the target interval is contained within the region that would be occupied by the access tubes; 31% of the energy around the wires is contained within the access tubes.

The preceding analysis of the response of coated continuous-rod probes, showed that the presence of low relative dielectric permittivity coatings on TDR rods results in greater restriction of the probe sensitivity to the region adjacent to the surface of the rods. The wires are coated with a plastic housing and polyethylene tubing; therefore, as the pulse travels along the wires, the energy of the electric field should be concentrated within the access tubes, making the probe insensitive to the properties of the surrounding soil. To increase the sensitivity within the target region, the bottoms of the access tubes were sealed and the tubes were filled with water. The presence of a high dielectric material in contact with the target rods increases the sensitivity of the probes to the surrounding medium, as shown for water-filled gaps on Figure 2-5. As a result, as the pulse travels along the target rods, some of the energy of the electric field will reside within the access tubes and some will extend to the surrounding medium, causing the propagation velocity along the target rods to be a function of the relative dielectric permittivity of the porous medium.

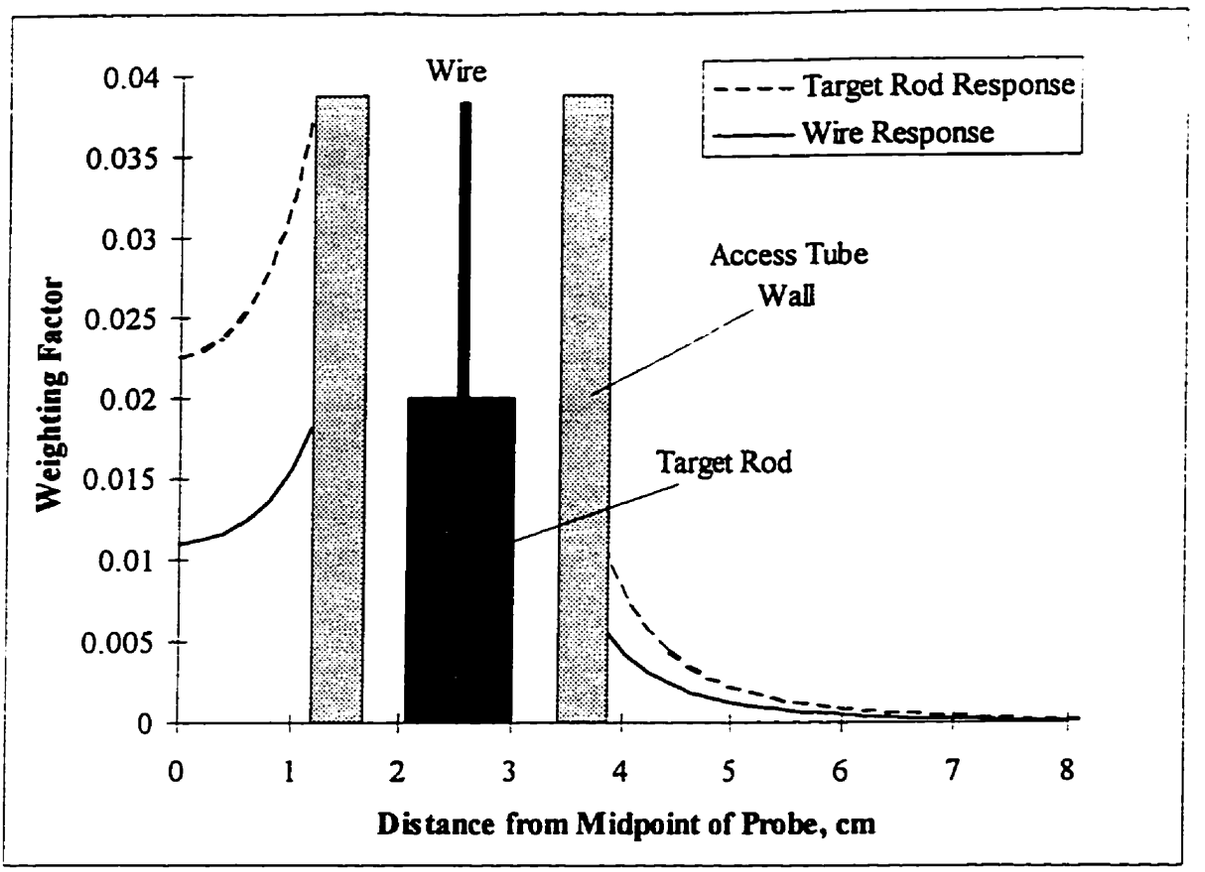

Figure 4-11. Weighting factors that would exist along a line perpendicular to the axes of the wires and target rods if they were installed directly into the medium without access tubes or coatings.

A balun was placed on the pulse generator to connect the shielded twin-wire transmission line to the coaxial output of the TDR unit. The shielding on the wires minimizes the sensitivity of the probe to the conditions above the ground surface. However, the wires must be unshielded and separated for a length that is at least equal to the depth of the top of the target rods below ground surface when placed at the deepest sampling depth to allow for placement of the target rods in the access tubes. Variations in the separation of the unshielded wires will change the impedance of the probe, leading to unwanted reflections on the waveform. Within the access tubes, the polyethylene tubing fitted over the coated wires helps to center the wires and maintain a uniform separation. A surface guide (Figure 4-12) was designed to minimize variations in the separation of the wires above the ground surface.

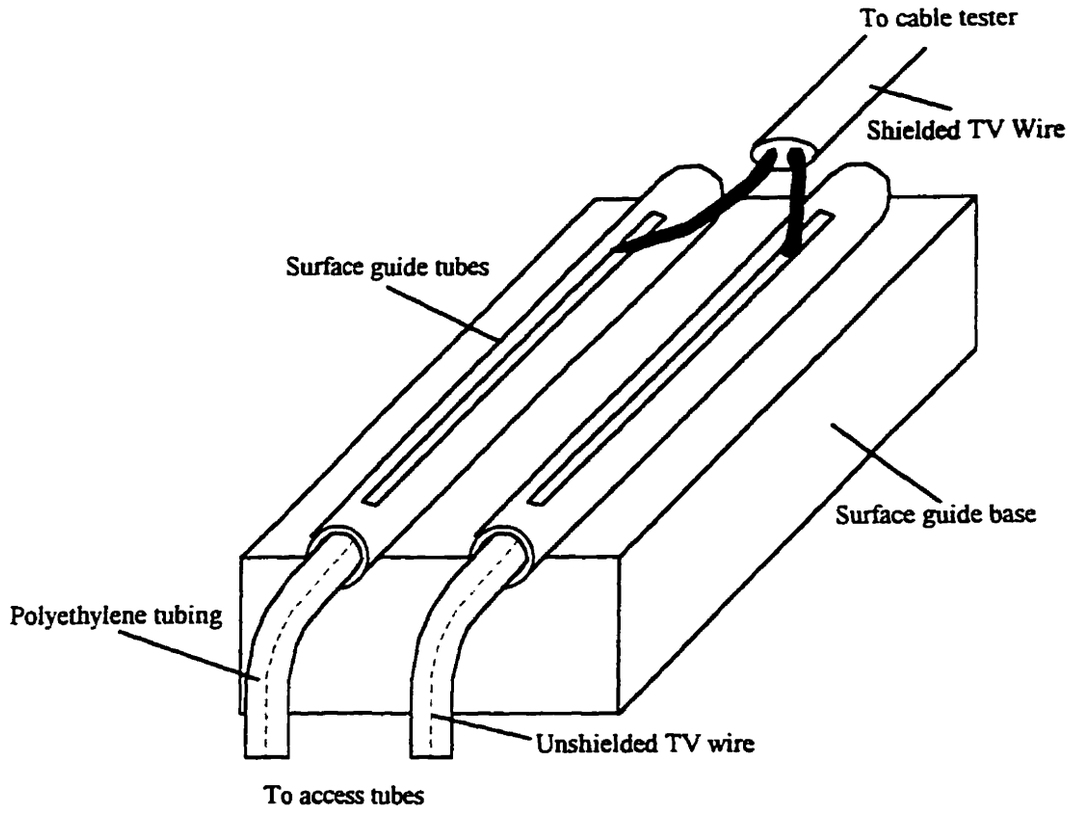

Figure 4-12. Schematic diagram of the surface guide for the multilevel probe.

The multilevel probe allows for great flexibility in the design of a water content monitoring program. The rods can be removed from the access tubes and replaced with rods of a different length to alter the sample volume of the probe at any time. In addition, like a neutron probe, the target rods can be lowered incrementally to any depth within the access tubes to profile with any desired vertical sampling interval.

4.3.2 Prototype Probe Design

Following preliminary laboratory testing, a prototype multilevel TDR probe was built for testing in the field using readily available components. Thick-walled, 1/2 inch (2.67 cm) OD, Schedule 80 PVC access tubes were used for ease of installation. The target rods were 20 cm long sections of 0.95 cm OD steel tubing. A 3 m long section of Belden 9090 82 channel VHF-UHF-FM shielded, 0.1 cm OD twin-wire cable was connected to a Tektronix 1502B cable tester through a balun (ANZAC TP-103 impedance matching transformer). An additional 3 m section of the cable, stripped of the outer shield to allow for separation of the inner wires and housed in flexible 0.95 cm OD polyethylene tubing, extended to the top of the target rods.

Two 1/2 inch (1.77 cm) OD chlorinated PVC tubes were slotted along their length and fastened to a wooden base as a surface guide.

4.4 Water Content Response of the Alternative Multilevel TDR Probe

4.4.1 Field Experimental Design

A field experiment was conducted to test the ability of the multilevel probe to profile the water content and bulk EC with depth. The field site used to examine the EC response of continuous-rod probes, shown previously, was used for this experiment as well.

Six pairs of multilevel TDR access tubes were installed to a depth of 2.5 m. Each access tube was installed in a pilot hole created by driving a 0.95 cm OD steel rod into the soil using a rock drill and a surface guide to ensure vertical placement. The spacing between the access tubes was 5 cm for each pair. Three access tube pairs (ML2, ML4 and ML5) were located 50 cm from a 5.08 cm diameter screened PVC well, the remaining three access tube pairs (ML1, ML3 and ML6) were 1 m from the well, as shown on Figure 4-13.

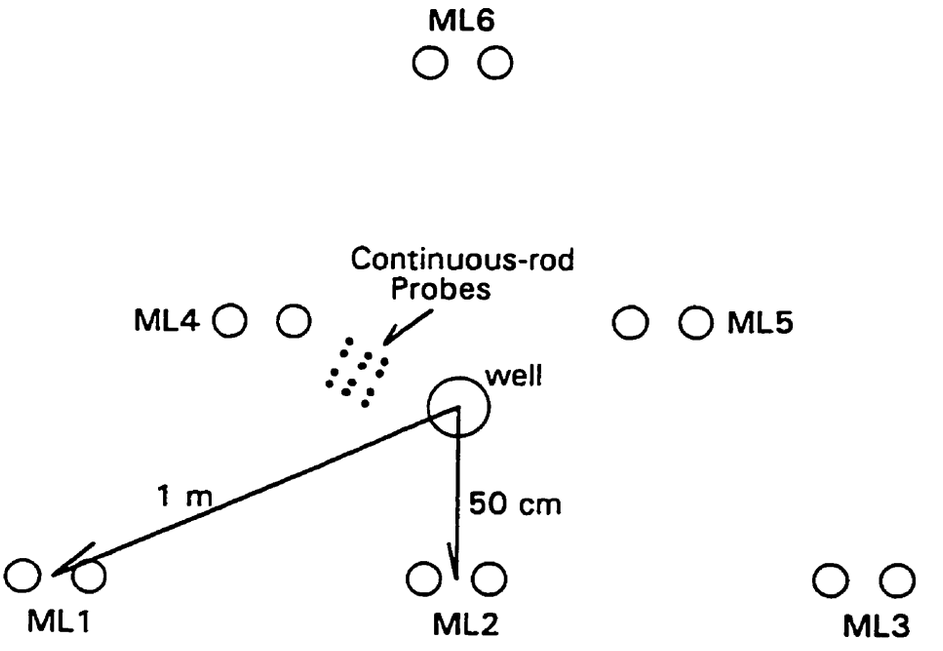

Figure 4-13. Locations of the standard and multilevel probes on the field site.

Six pairs of continuous-rod waveguides were installed between probe ML4 and the central well using a hand drill. The lengths of the continuous-rod pairs were 40, 60, 80, 100, 120 and 140 cm. Each rod had a

diameter of 0.4 cm and each rod-pair had a separation of 3 cm. The distance between rod pairs was 15 cm and the total area occupied by rod pairs at the ground surface was 15 cm by 30 cm.

A program written at the Waterloo Center for Groundwater Research [*Redman, 1994*] transferred the TDR waveforms from the cable tester to a personal computer through an RS-232 serial interface for both the continuous-rod and multilevel TDR probes.

The water content was measured with a neutron probe (CPN Hydroprobe 503DR with an Am241/Be 50 mCi source) as well. By inserting aluminum tubing, sealed at the bottom, in the central screened well, the water content could be logged continuously across the water table without submerging the neutron probe. Neutron counts were averaged over 64 seconds and recorded manually.

4.4.2 Multilevel Probe Waveforms

Despite the availability of automated waveform analysis software, visual inspection of TDR waveforms is critical to judge the quality of the response of a TDR probe. Figure 4-14 shows a waveform collected from the prototype probe under fully drained conditions with the center of the target rods placed 35 cm below the ground surface. Three near-horizontal regions are labeled on the waveform corresponding to the reflections launched as the pulse propagated along the surface guides, along the small-diameter wires in the access tubes, and along the target rods.

The travel times to the top and bottom of the target rod define the velocity of propagation through the target region. Therefore, the point of transition from the wires to the target rod and the final reflection at the end of the target rods (*t1* and *t2* on Figure 4-14, respectively) must be identifiable on the waveform. The intersection points were located using automated analysis software based on the straight-line intersection method described by *Topp et al.* [1982]. To clearly separate the reflections from the ground surface and the top of the target rods, the top of the target rods had to be at least 20 cm below the ground surface. The target rods must also be long enough to separate the reflections from the top and bottom of the measurement region on the waveform; target rods as short as 15 cm could be used, but 20 cm or longer target rods gave more consistent results over the range of measurement depths and water contents.

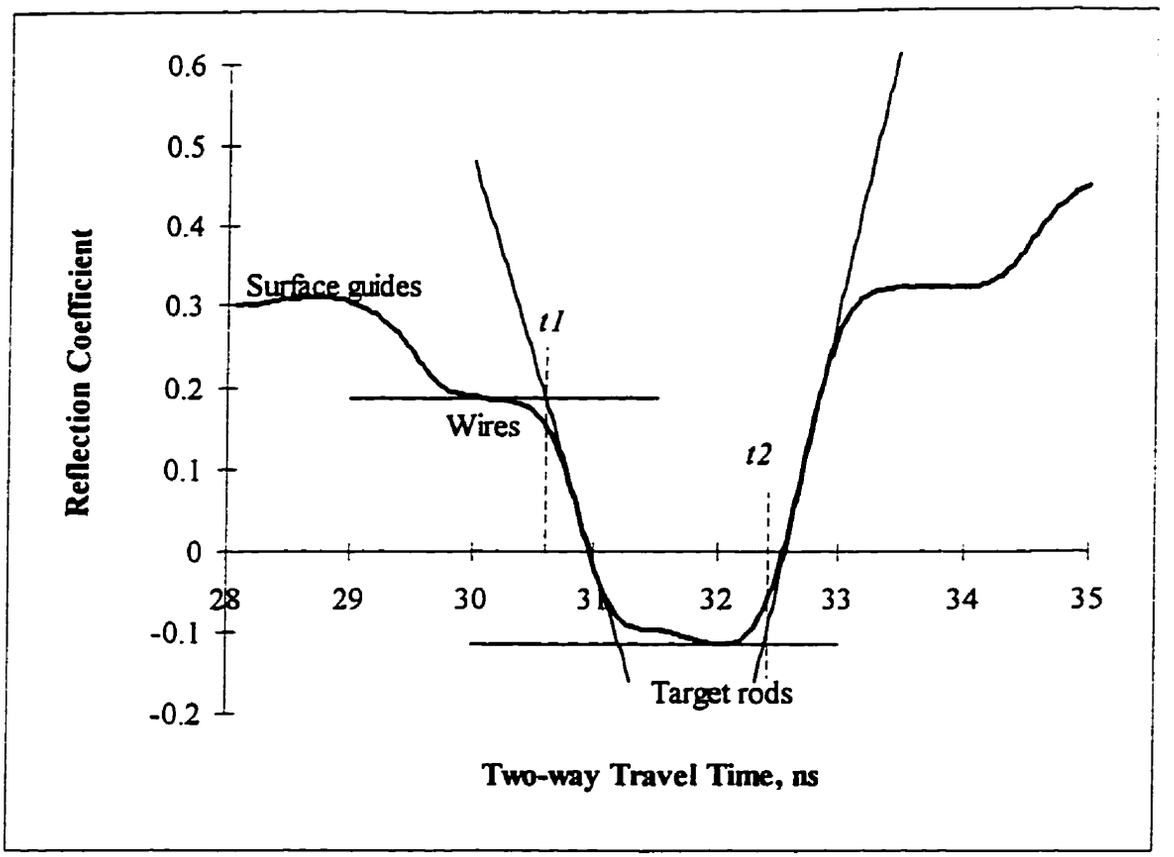

Figure 4-14. Waveform collected with the prototype multilevel probe under fully drained conditions with the center of the target rod placed 35 cm below the ground surface.

The maximum depth of measurement achievable with a TDR probe is limited by the quality of the reflection from the ends of the target rods (t2 on Figure 4-14). A comparison of waveforms collected from four depths (Figure 4-15), shows that the terminal reflection becomes less sharp with increased depths of investigation. This smoothing is likely caused by conductive losses that preferentially remove the high frequency components of the pulse and by the influence of the balun on the 6 m long wires. Despite the degradation of the terminal reflection with depth, the relative dielectric permittivity measured by the multilevel probe was repeatable to a maximum depth (center of the target rod) of 2.25 m. Increased depths of investigation may be possible if improved baluns are used [*Spaans and Baker*, 1993].

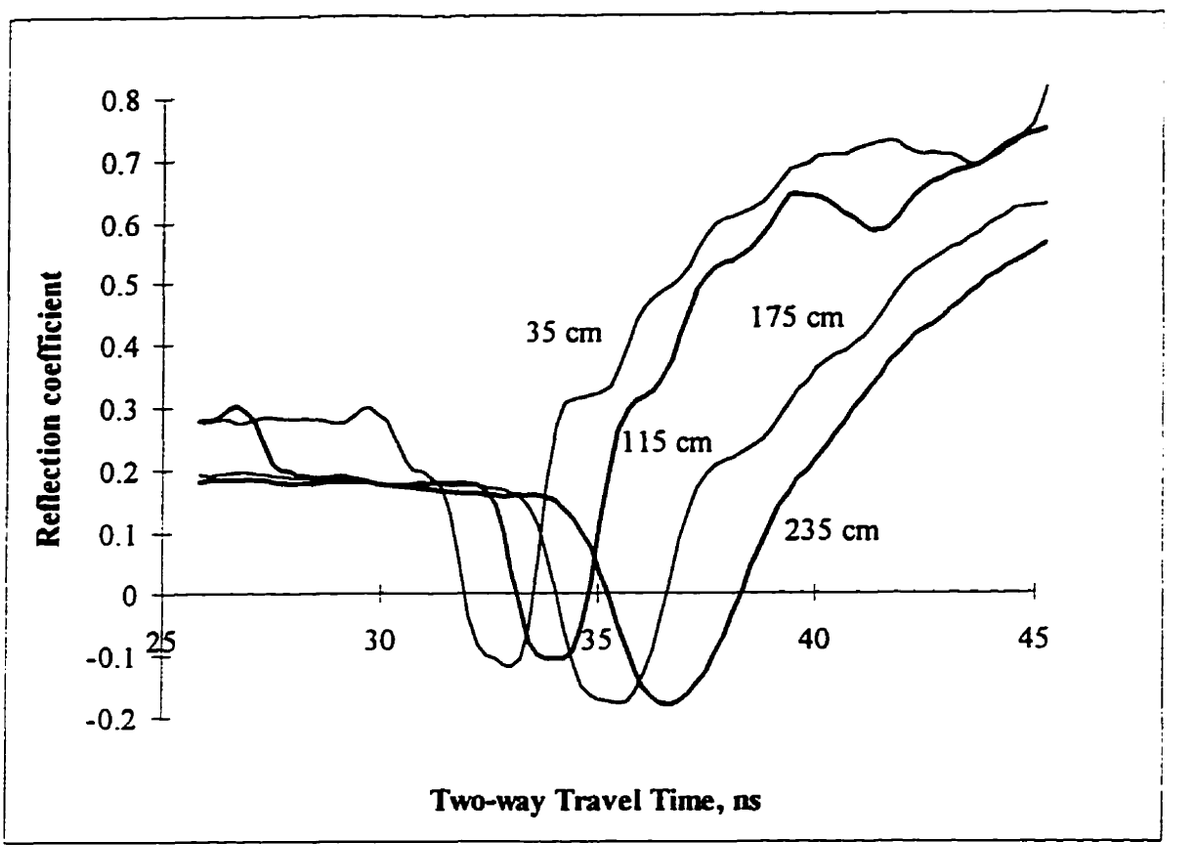

Figure 4-15. Waveforms collected with the multilevel probe ML4 with the center of the target rods placed 35, 115, 175 and 235 cm below ground surface under fully drained conditions.

The differences among the waveforms collected under varying water content conditions gives a qualitative measure of the sensitivity of the water content response of a TDR probe. Figure 4-16 shows two waveforms collected under fully drained conditions before and after an infiltration event and a third waveform collected during steady-state infiltration. The center of the target probe was located 85 cm below the ground surface for all of the measurements. The length of the target rod is unchanged; therefore, the difference in the travel time between the characteristic reflections at the top and bottom of the target rods is due to changes in the relative dielectric permittivity of the medium surrounding the access tubes. The clear difference in the waveforms in response to the change in the soil water content compared to the minimal differences between the two waveforms collected under fully drained conditions demonstrates both the sensitivity of the multilevel probe to the soil water content and the repeatability of the probe response. Closer examination shows that all three waveforms are very similar as the pulse travels through the surface guide. There is a greater reduction in the amplitude of the waveform as the pulse enters the access tubes under constant infiltration than seen after drainage due to a stronger reflection at the ground surface because of the larger impedance mismatch under higher water content conditions. Finally, the minimal change in the travel time from the ground surface to the

top of the target rods (*t1* on Figure 4-14) demonstrates that the probe is nearly insensitive to the properties of the medium above the target rods.

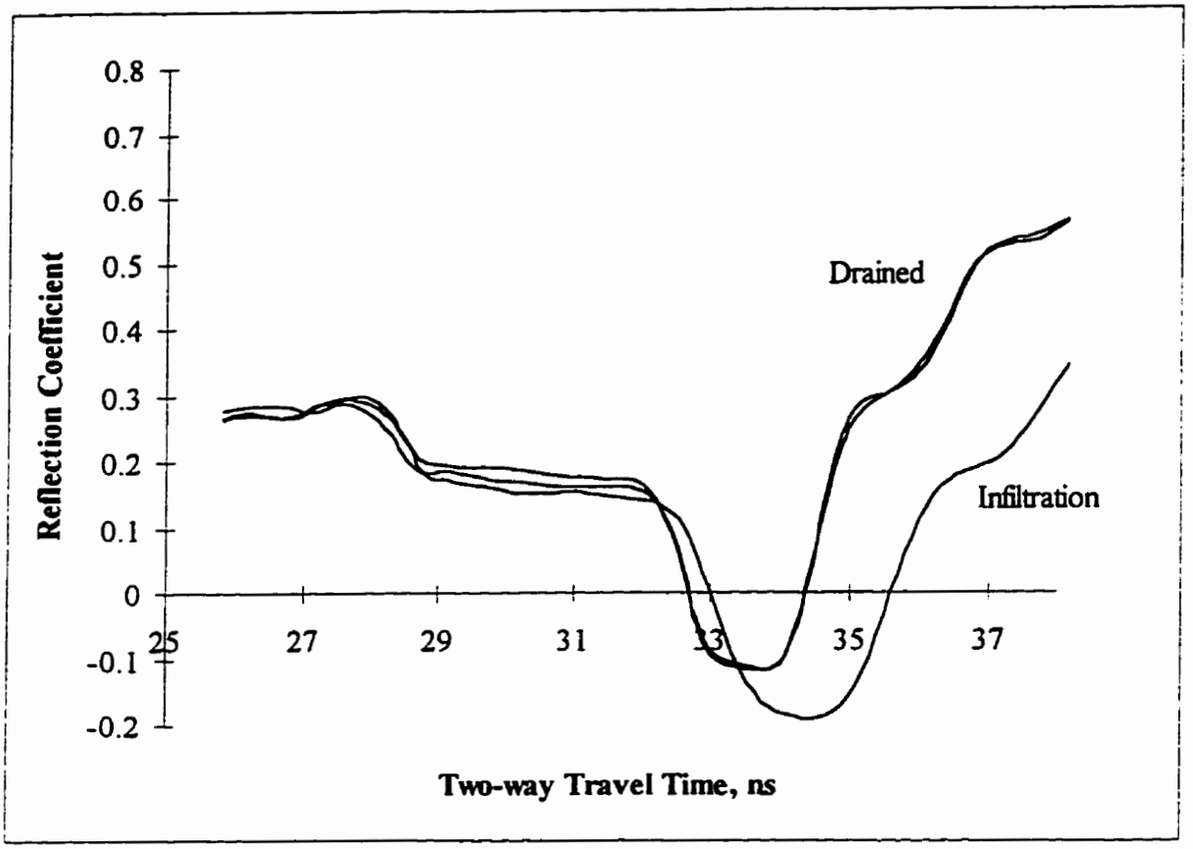

Figure 4-16. Waveforms collected with multilevel probe ML4 with the center of the target rods placed 85 cm below ground surface under fully drained and steady-state infiltration conditions.

4.4.3 Continuous-rod Probe Waveforms

Figure 4-17 shows sample waveforms collected with continuous-rod probes under fully drained conditions and during steady-state infiltration. Unlike the multilevel probe, the travel time is a function of both the water content of the medium and the length of the rods as seen by comparing the waveforms collected with 40 cm and 80 cm rod-pairs under drained conditions. The difference in the travel time for the 80 cm long rod-pair from fully drained to steady-state infiltration conditions gives a qualitative measure of the sensitivity of these probes. However, the absolute difference in travel time cannot be compared directly to that measured with the multilevel probe because the absolute change in the travel time is greater for longer rod lengths for a given change in the relative dielectric permittivity of the surrounding medium. A potential problem that arises with continuous-rod probes can be seen on the waveform labeled '80 cm rods, wetting

front" collected with the 80 cm long rod-pair when the wetting front was located less than 80 cm below the ground surface. The inflection located at approximately 30 ns on the waveform is due to the impedance mismatch caused by the change in the water content across the wetting front. When the wetting front approaches the ends of the rods, this event can obscure the reflection from the ends of the rods, making water content analysis difficult. In contrast, the smoother waveforms shown for the multilevel probe are very amenable to automated analysis.

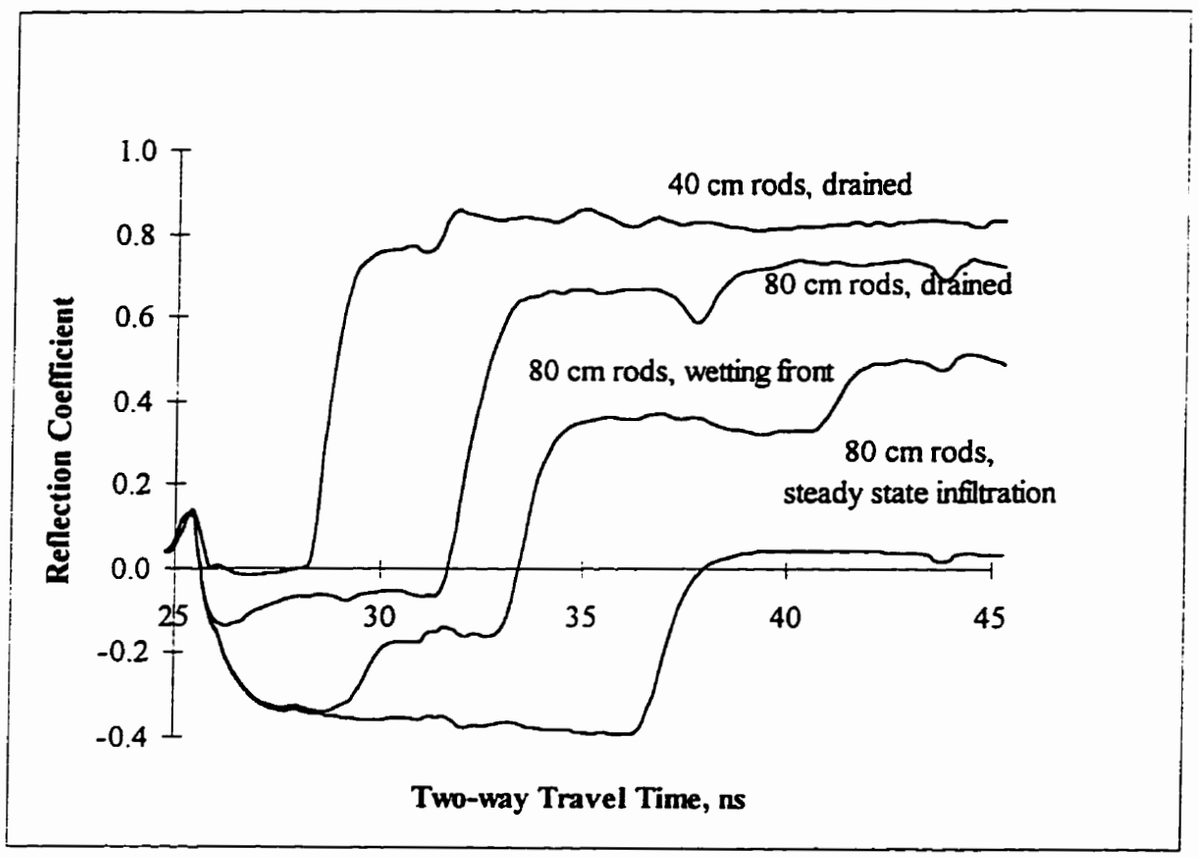

Figure 4-17. Waveforms collected with the 40 and 80 cm continuous-rod probes under fully drained conditions and with the 80 cm rods under steady-state infiltration conditions and during the advance of a wetting front.

4.4.4 Two-point Calibration of the Water Content Response

To match the five nonoverlapping intervals between the ends of the continuous-rod probes, measurements were made with the multilevel probe with the 20 cm long target rods centered at 50, 70, 90, 110 and 130 cm depth. The water content for each continuous-rod pair was determined using Equation 1-3. Then, the difference in the water contents between any two rod-pairs was calculated using Equation 1-4. In this manner, the water content could be determined with the continuous rods for sample volumes that were similar to those of the multilevel probes.

The preceding analysis of a coated twin-rod probe with a nonconcentric water-filled annulus and a nonconcentric outer PVC coating around each rod showed that the probe response corresponded to a weighted average of the inverses of the relative dielectric permittivities of the soil and the probe materials. Although the water-filled gap and access tubes are placed concentrically around the target rods for the multilevel probe, this model is assumed to describe the probe response. The weighted averaging of dielectric permittivities in the transverse plane that applies to the multilevel probe can be described from Equation 2-15 as,

$$K_m^{-1} = w_{water} K_{water}^{-1} + w_{PVC} K_{PVC}^{-1} + w_{soil} K_{soil}^{-1}. \qquad (4\text{-}1)$$

where K_m is the measured relative dielectric permittivity and w_{water}, w_{PVC}, and w_{soil}, are the weighting factors describing the fractional contribution of each component to the probe response. The values of the weighting factors are based on the geometry of the rods, water filled annulus and PVC access tubes. Assuming that the weighting factors are independent of the water content of the medium, Equation 4-1 can be simplified to a linear relationship between K_m and K_{soil}.

$$\frac{1}{K_m} = \frac{m}{K_{soil}} + b. \qquad (4\text{-}2)$$

The slope of this relationship, m, is the inverse of the fractional weighting of the soil in the averaging of the relative dielectric permittivities of the soil and probe materials, w_{soil}.

From the linear relationship shown in Equation 4-2, the response of the multilevel probe can be calibrated under two known soil water content conditions. Based on the pressure-water content relationship of the Borden site material [*Nwankwor*, 1982] and the depth of the water table, the soil should have eventually drained to a residual saturation of 0.068 over the shallowest meter of the subsurface; the saturated water content of the medium was 0.37. To avoid excessive evaporative drying near the ground surface, the drainage profiles were measured after only five days of drainage following steady-state infiltration. The relative dielectric permittivity measured with the multilevel probe near the ground surface after drainage was

correlated to the residual water content. An average of the responses measured from 10 cm below to 10 above the water table were correlated to the saturated water content. A similar linear calibration was applied to the neutron probe, given that the response of neutron probes has been shown to be linearly related to the soil water content [*Kramer et al.*, 1992].

Each of the multilevel TDR probes required a separate calibration to the relative dielectric permittivity of the soil. Table 4-1 shows the slopes and intercepts found for each probe from the two-point calibration to Equation 4-2. The table also includes the probe-specific soil weighting factors calculated as the inverse of the slope.

	ML1	ML2	ML3	ML4	ML5	ML6
Slope, m	3.40	3.08	2.99	3.63	3.27	3.40
Intercept, b	-0.18	-0.15	-0.17	-0.22	-0.20	-0.20
w_{soil}	0.29	0.32	0.34	0.28	0.31	0.29

Table 4-1. Results of application of two-point calibrations to the six multilevel probes.

The weighting factors show that approximately 30% of the total response of the prototype probe is due to the soil surrounding the access tubes in the target region. The weighting factors are controlled by the geometry of the multilevel probe. As shown in the analysis of coated probes presented in Chapter 2, the use of thinner access tubes made of higher relative dielectric permittivity materials would greatly increase the sensitivity of the probes. This analysis also showed that the response of coated rods was not highly sensitive to their separation. The differences in probe geometries among the six probes used in this experiment are largely related to variations in the separation of the access tubes. The similarity among the weighting factors suggests that all of the multilevel probes were installed with nearly the same separation for the experimental site conditions. Consistent installation in highly heterogeneous soils would be more difficult.

4.4.5 Measured Water Content Profiles under Drained Conditions

The drained water content profile was measured three times with multilevel probe ML4: with a pump operating in the central well (BK102), and under drained conditions before (BK101) and after (BK105) pumping.

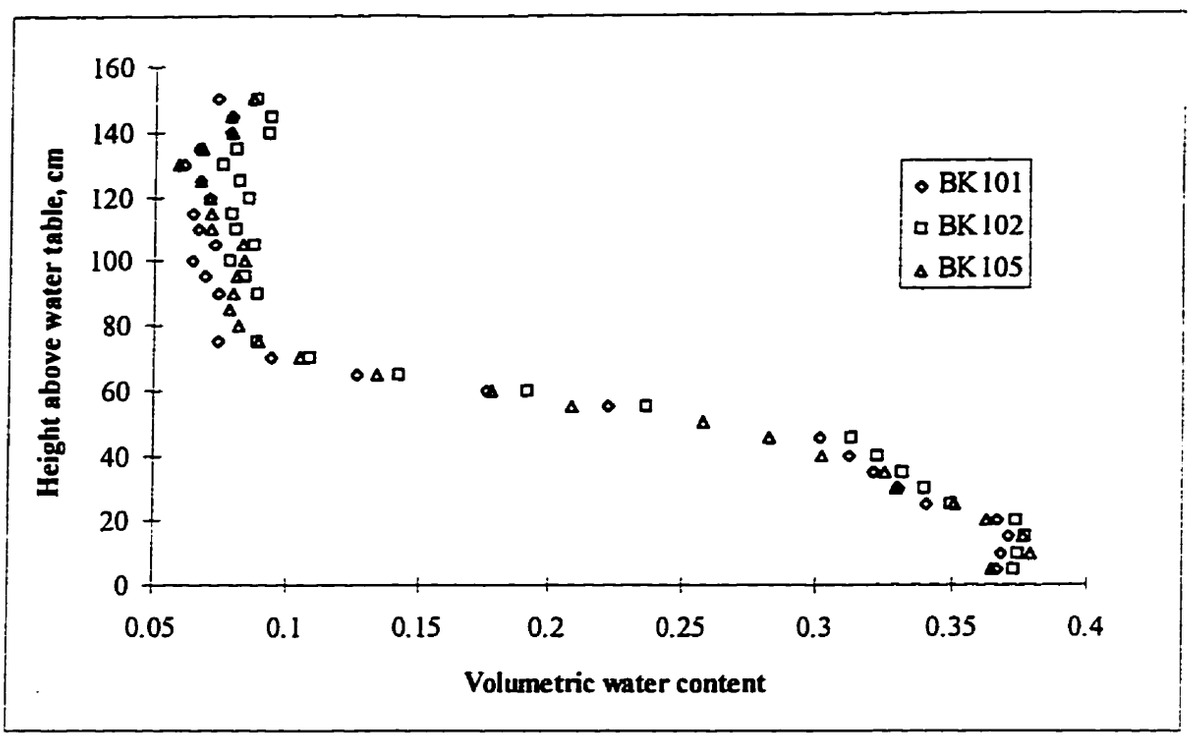

Figure 4-18. Water contents determined from responses of multilevel probe ML4 under fully drained conditions as a function of the elevation above the water table collected during operation of the central pumping well (BK102) and both before (BK101) and after (BK105) pumping.

For direct comparisons among these data sets, the water contents calculated using Equations 1-3 and 4-2 are plotted against the elevation above the water table in Figure 4-18. The results show the high degree of repeatability and the vertical sampling resolution attainable with the multilevel probe.

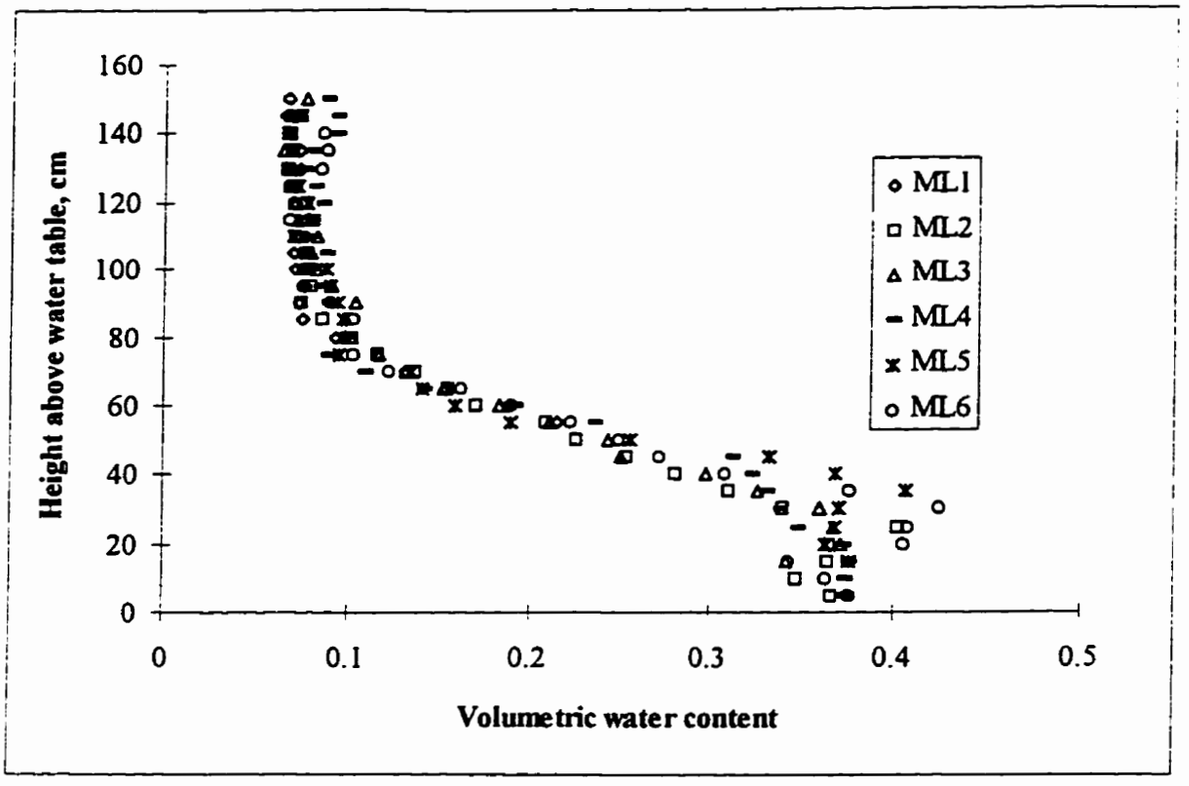

Figure 4-19. Water content determined from responses of the six multilevel probes under fully drained conditions as a function of the elevation above the water table.

Figure 4-19 shows the water contents calculated from the responses of all six multilevel TDR probes under fully drained conditions. Although there is some variability in the deeper, higher water content regions, the agreement among the probes through most of the profile is very good.

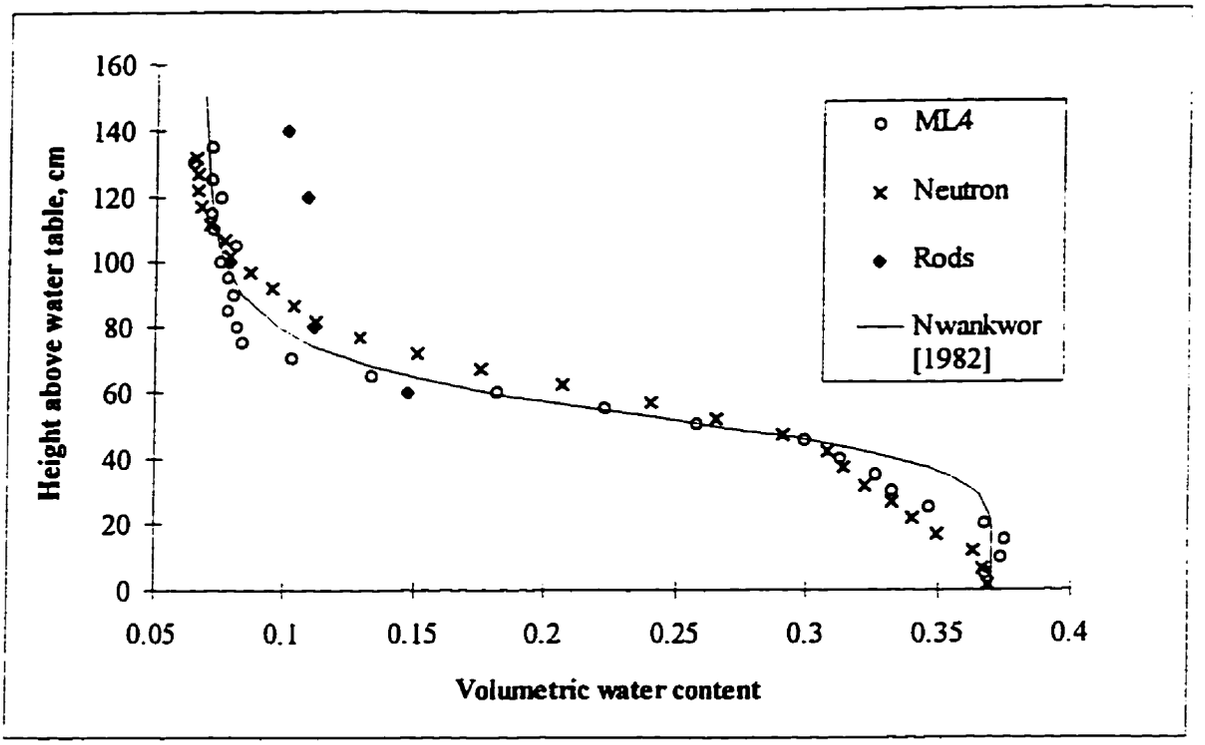

Figure 4-20. Water contents determined from the responses of multilevel probe ML4, the neutron probe, and by interval differencing of the responses of the continuous-rod probes under fully drained conditions as a function of the elevation above the water table. The water contents determined in the laboratory by *Nwankwor* [1982] are plotted as a function of the water-phase suction in cm of water as a solid line.

Figure 4-20 shows the water content profiles measured with the continuous rods, the neutron probe and multilevel probe ML4 under fully-drained conditions. Both the multilevel and neutron probes show good agreement with the laboratory measured drainage curve presented by *Nwankwor* [1982]. The neutron probe profile is slightly smoother, possibly due to its larger sampling volume. Interval differencing of the continuous rod responses shows general agreement with the other methods; however, the depth of investigation was insufficient for full comparison.

4.4.6 Calibration of the Water Content Response during Drainage

The water contents calculated from the responses of the 40 cm long continuous-rod probes using Equation 1-3 suggest that the drained water content may have been greater than the residual water content measured in the lab; this would introduce error into the absolute water contents calculated using the two-point

calibrations of the multilevel and neutron probes. Therefore, a more complete method of calibration of the multilevel probe was examined.

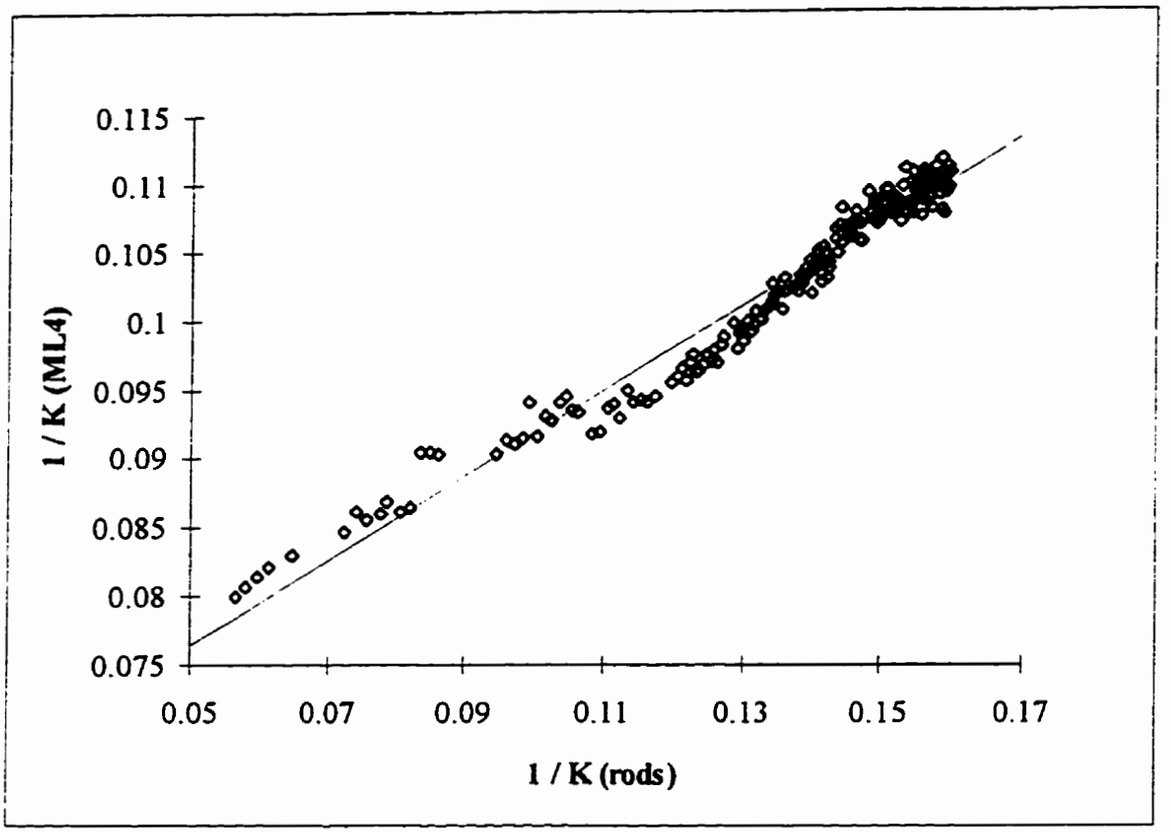

Figure 4-21. Inverse of the relative dielectric permittivity measured with multilevel probe ML4 with the target rods centered 90 cm below the ground surface as a function of the inverse of the relative dielectric permittivity measured with the 80 cm continuous-rod probe collected during drainage. The linear regression of the data to Equation 4-2 is shown as a solid line.

After establishing steady-state infiltration conditions with the drip-line irrigation system, the water content was monitored during drainage with an 80 cm long pair of continuous rods, and with multilevel probe ML4 and the neutron probe both centered at 90 cm depth. The water table was located 2.2 m below the ground surface. For the relatively homogeneous site conditions, the water content should be nearly constant with elevation during drainage within a meter of the ground surface, allowing for direct comparison of all of the probe responses. Figure 4-21 shows a direct comparison of the inverse of the relative dielectric permittivity measured with the 80 cm continuous-rod pair to the inverse of the relative dielectric permittivity measured with the multilevel probe centered at 90 cm depth. The figure also includes a linear regression of Equation 4-2 to the data. The data are well represented by the linear relationship with an r^2 value of 0.96.

The slope and intercept of this relationship are 3.25 and -0.20, respectively, which compare reasonably well with those found by the two-point calibration for probe ML4 shown in Table 4-1.

The linearity of the relationship between the inverses of K_m and K_{soil} justifies the application of Equation 4-2 to describe the response of the multilevel probe despite the concentric gap geometry of the probes. However, as explained in the preceding analysis of coated rod probes, the inverse dielectric mixing model underlying this equation leads to incorrect averaging of the water content if the water content varies along the rods. For the multilevel probe, this potential error can be minimized by using the shortest target rods that will still clearly separate the characteristic reflections defining the travel time through the target interval and by altering the design to maximize the soil weighting factor.

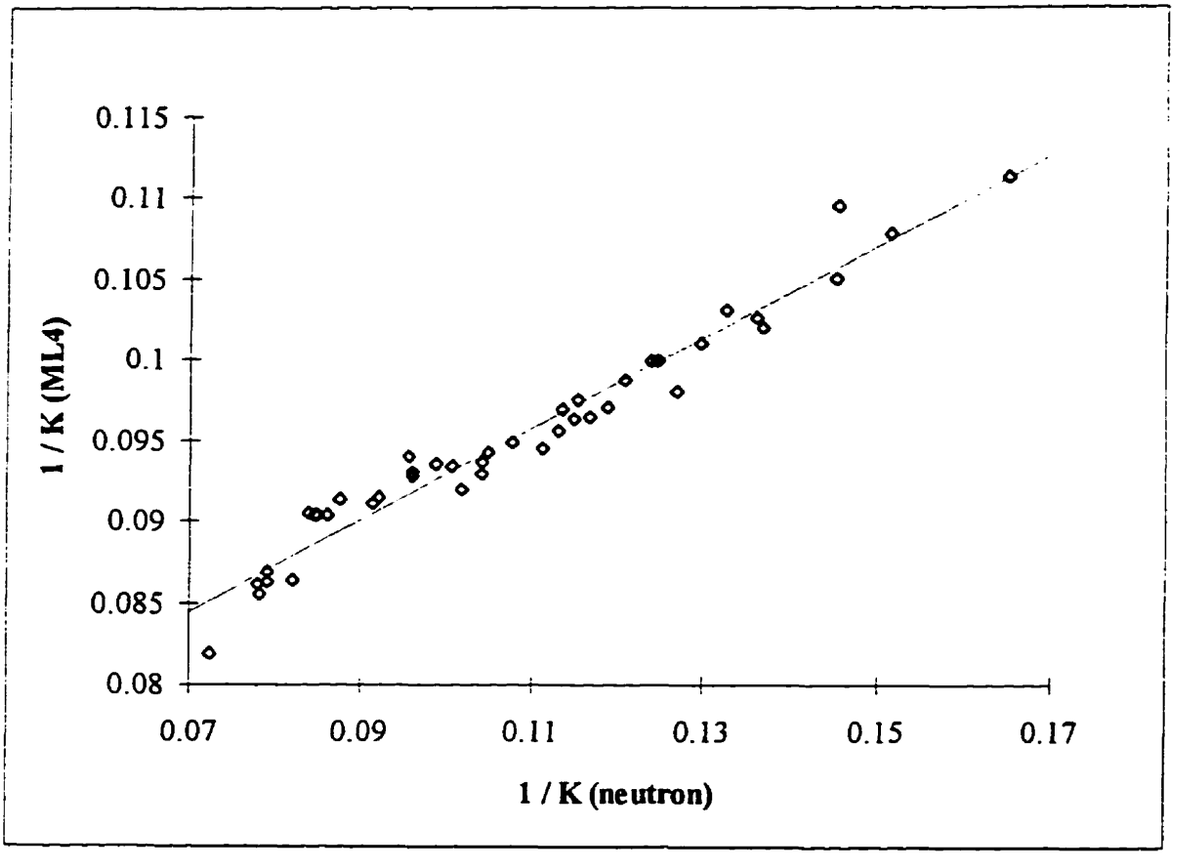

Figure 4-22. Inverse of the relative dielectric permittivity measured with the multilevel probe ML4 with the target rods centered 90 cm below the ground surface as a function of the inverse of the relative dielectric permittivity calculated from the water content measured during drainage with the neutron probe centered at 90 cm below ground surface.

A comparison of the responses of the multilevel TDR and neutron probes is shown on Figure 4-22. The linear two-point calibration was used to determine the water content from the neutron probe response. Equation 1-2 was then applied to relate these water contents to the relative dielectric permittivity of the soil, K_{soil}. There is a highly linear relationship between the inverses of K_m and K_{soil} with a linear regression to Equation 4-2 showing an r^2 value of 0.96. The slope and intercept of the regression are 3.56 and -0.23, respectively, which are in very close agreement with those found using the linear two-point calibration of probe ML4 shown in Table 4-1.

4.4.7 Measured Water Content Profiles during Infiltration

The drip-line irrigation system provided constant flux infiltration onto the fully-drained soil. During infiltration, the water content was measured with depth using the continuous-rod probes, the neutron probe and multilevel probe ML4.

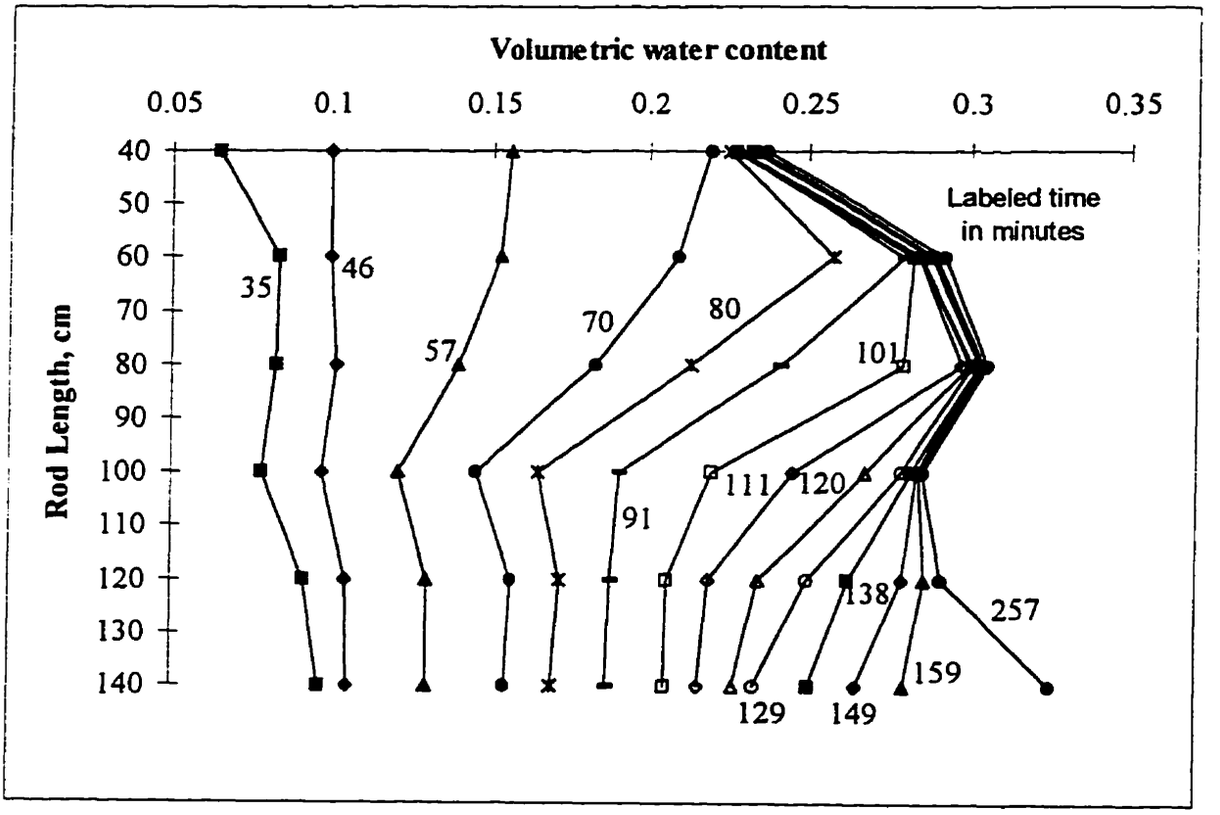

Figure 4-23. Volumetric water content calculated during infiltration plotted as a function of the length of the continuous-rod probes. Profiles are labeled with the elapsed time, in minutes, since the beginning of infiltration.

The water content measured with each continuous-rod probe is plotted against the length of the rod-pair on Figure 4-23. Each rod-pair measures the average water content from the ground surface to the end of the rods; therefore, the water content measured with all of the rod-pairs increased immediately with the onset of infiltration. The water content increased in time for all of the rod-pairs until late time when the profiles become nearly constant in time. At each depth, the water content increased continuously in time until steady-state flow was established.

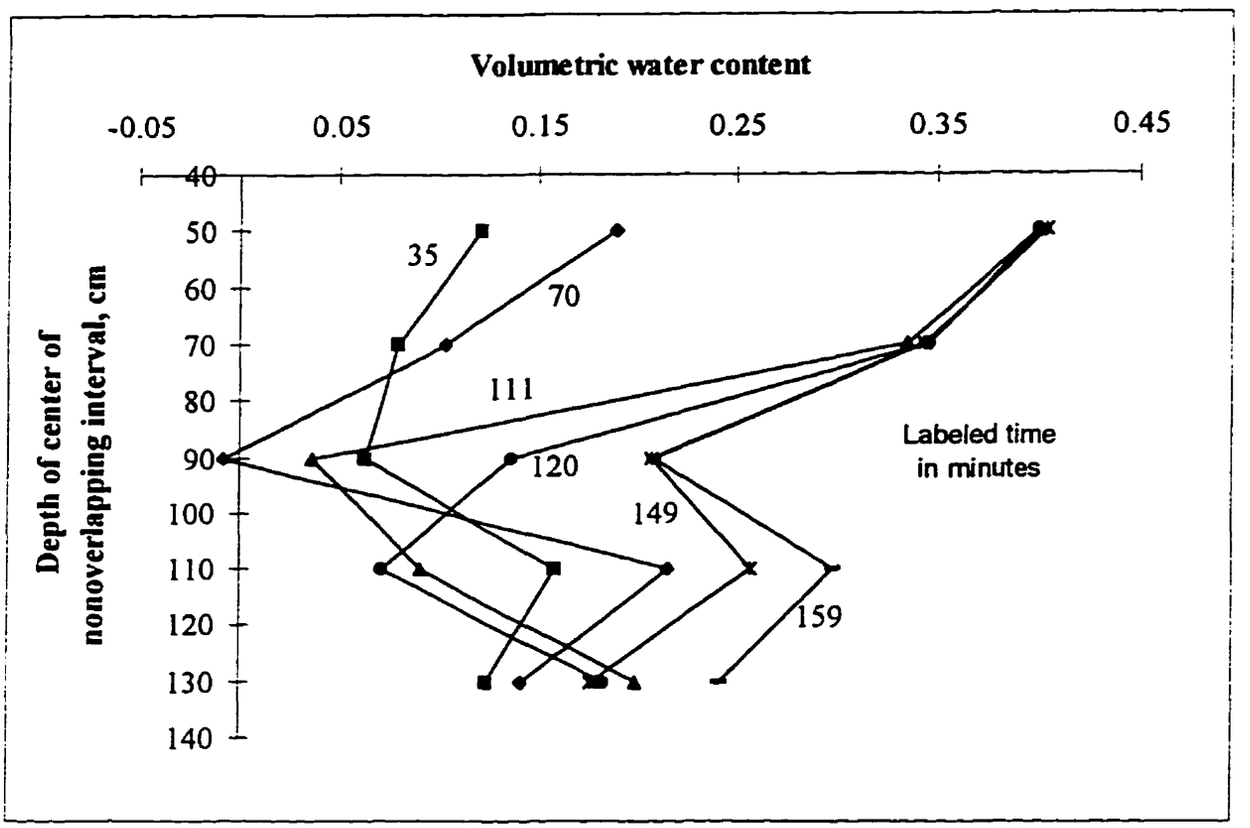

Figure 4-24. Volumetric water content calculated by interval differencing of the responses of the continuous-rod probes during infiltration plotted as a function of the center of the nonoverlapping depth interval. Profiles are labeled with the elapsed time, in minutes, since the beginning of infiltration.

Equation 1-4 must be applied to the continuous-rod results to produce water content profiles. Some of the interval differenced profiles determined from the continuous-rod measured water contents are shown on Figure 4-24. The data show the wetting front advancing in time. Except for a negative water content determined at 90 cm depth after 70 minutes of infiltration, the minimum and maximum water contents are in

reasonably good agreement with the residual and saturated water contents found in the laboratory. However, the water content does not increase continuously in time for each depth and the water content beneath the wetting front does not remain constant before the arrival of the wetting front, clearly demonstrating the limitations of water content profiling with continuous-rod probes.

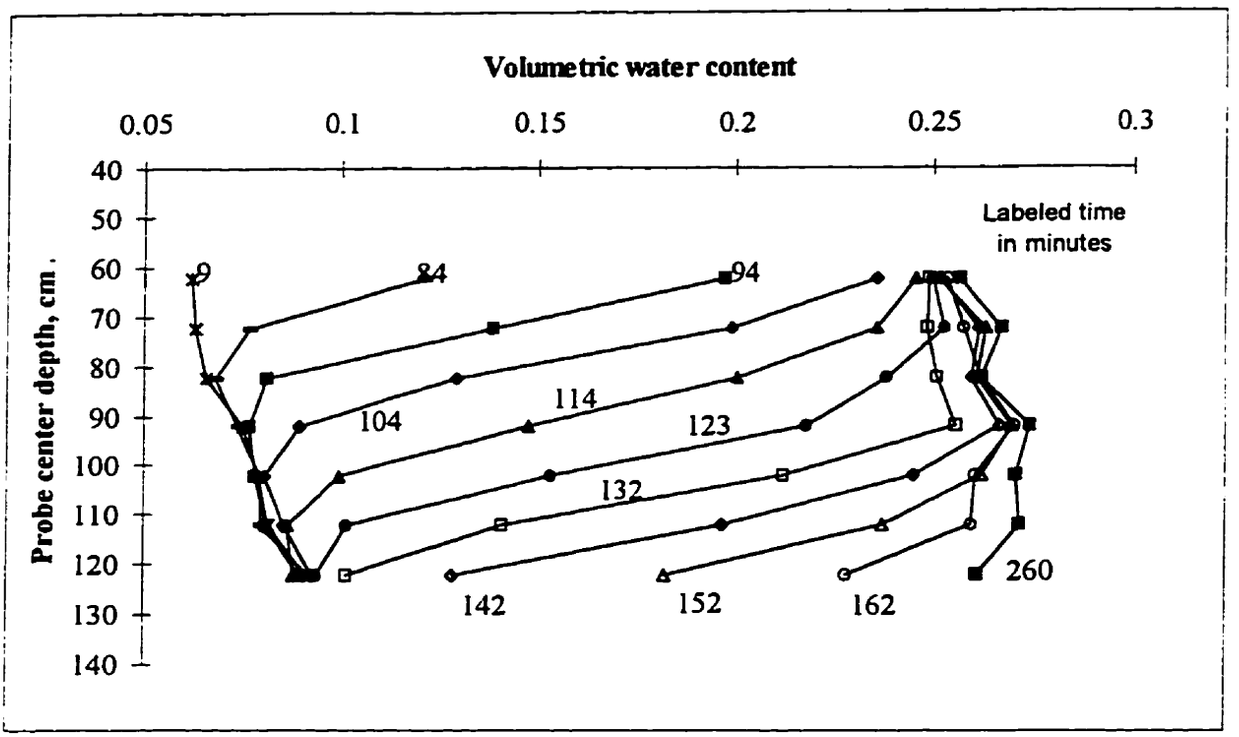

Figure 4-25. Volumetric water content calculated during infiltration plotted as a function of the depth of the center of the neutron probe. Profiles are labeled with the elapsed time, in minutes, since the beginning of infiltration.

Water content profiles collected with the neutron probe are shown on Figure 4-25. In contrast to the interval-differenced continuous-rod profiles, the water content increases continuously at each depth and the water content at depth is constant before the arrival of the wetting front. The probe clearly shows the advance of the wetting front throughout the profile, establishing a final water content of approximately 0.27.

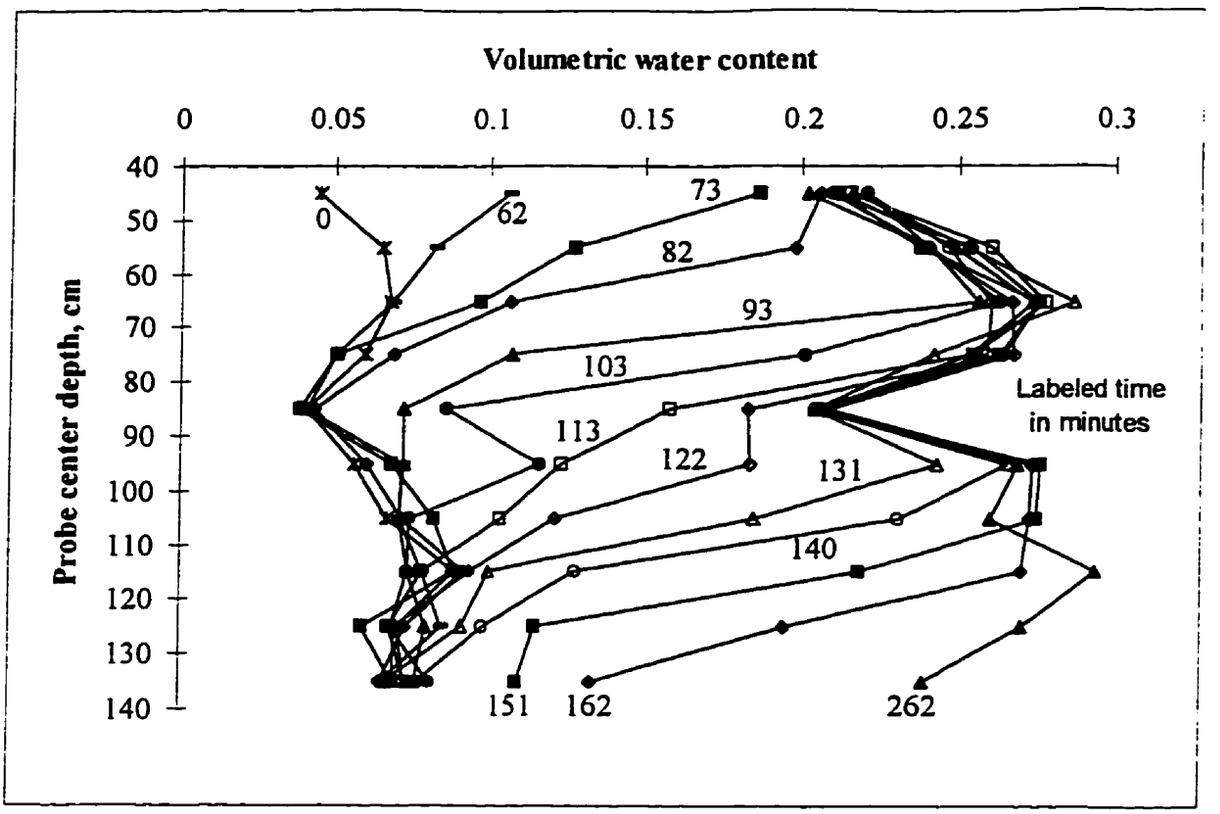

Figure 4-26. Volumetric water content calculated during infiltration plotted as a function of the depth of the center of the target rods of multilevel probe ML4. Profiles are labeled with the elapsed time, in minutes, since the beginning of infiltration.

The results of monitoring the advance of the wetting front with multilevel probe ML4 are shown on Figure 4-26. The water contents are nearly constant with time below the wetting front and the water content rises consistently with time at each depth. The wetting profiles are less smooth than those measured by the neutron probe. Specifically, there appears to be a consistent low water content at 90 cm depth that was also identified with the continuous-rod probes. The waveforms do not have any unusual reflections at this depth, suggesting that this may be a true measure of the water content distribution that the neutron probe failed to identify due to its larger sample volume.

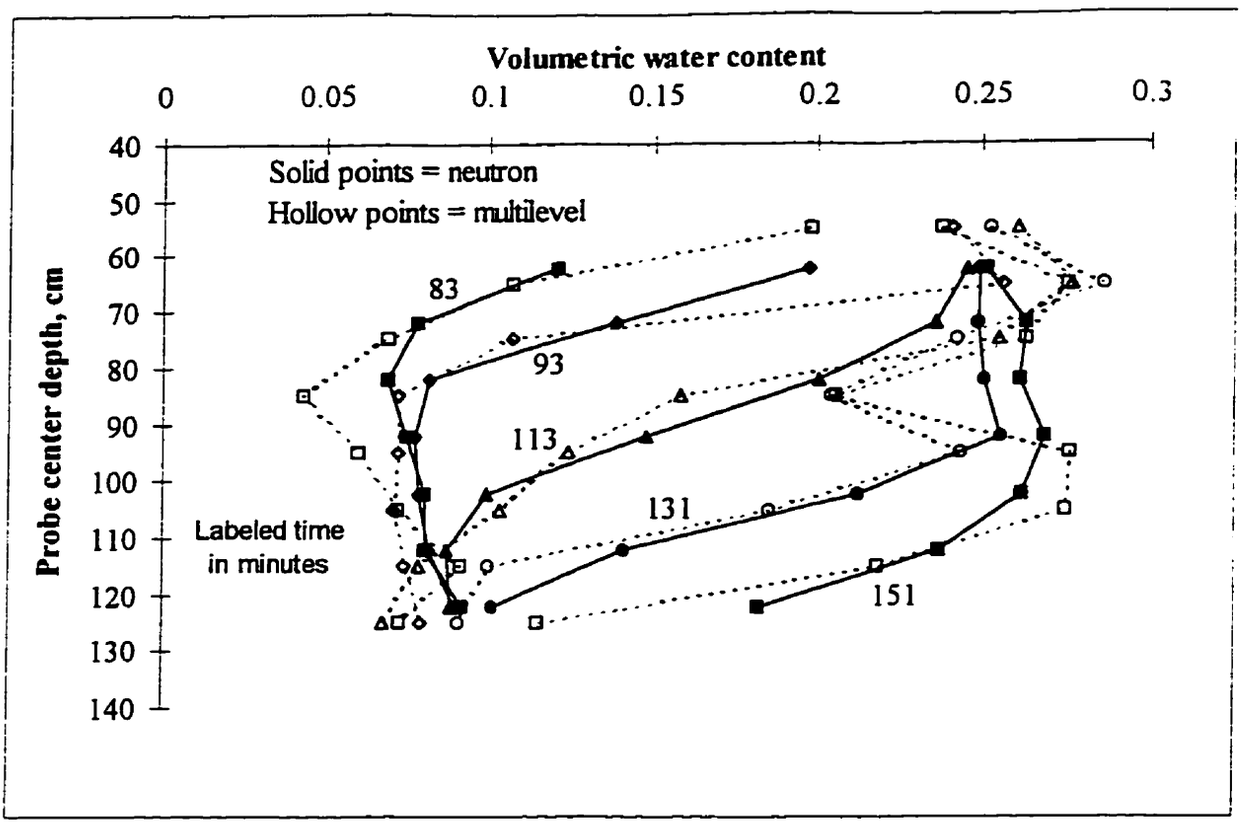

Figure 4-27. Comparison of the volumetric water content calculated from the responses of multilevel probe ML4 to those calculated from the neutron probe responses during infiltration plotted as a function of the depth of the center of the probes. Profiles are labeled with the elapsed time, in minutes, since the beginning of infiltration.

Several water content profiles measured with the neutron probe and multilevel probe ML4 are compared on Figure 4-27. The water contents differ slightly, perhaps due to differences in the sample sizes of the instruments or in the exact times of measurement. However, the location of the wetting front is very similar for both probes throughout the infiltration event.

4.4.8 Summary and Conclusions

An alternative multilevel TDR probe has been designed based on the description of the spatial sensitivity of TDR probes presented by *Knight* [1992]. The probe is only sensitive to the surrounding medium over a limited depth interval. Six prototype probes built using readily available components showed a consistent sensitivity to the soil, receiving approximately 30% of the total probe response from the medium around the access tubes in the sample interval.

Two methods of field calibration are shown. Water content profiles calculated from the responses of the multilevel probe are compared to those determined with continuous-rod TDR probes and a neutron probe during the advance of a wetting front. The neutron probe produced the most consistent water content profiles with highly repeatable water contents below the wetting front. The multilevel probe showed more variability in the water contents below the wetting front; however, the multilevel probe also showed consistent, small scale variations in the water content with depth that may not have been present in the neutron profile due to its larger sample volume. The location of the wetting front with time was very similar for the neutron and multilevel probes. Interval differencing of continuous rod measured water contents did not produce satisfactory water content profiles.

4.5 *Bulk Electrical Conductivity Response of an Alternative Multilevel Probe*

4.5.1 Field Experimental Design

In addition to profiling the water content with depth, the limited sensitivity of the alternative multilevel TDR probe to a distinct depth interval should allow for profiling of the bulk EC. A field experiment was performed to examine the EC response of the multilevel probe. The soil was preflushed with the municipal source-water with no added tracer (EC = 0.040 S/m) to displace any resident pore water and then allowed to drain. After five days of drainage, municipal-water flushing was restarted and continued until steady-state flow was established. Then, a KCl tracer (EC = 0.085 S/m) was applied through a separate irrigation system at the same flux and waveforms were collected during the advance of the tracer step. When the tracer front passed the ends of the rods, the infiltration gallery was turned off and waveforms were collected during drainage. The municipal-water flushing, tracer step and drainage were repeated using a solution with an EC of 0.142 S/m. Finally, a long duration (45 minute) pulse of KCl tracer (EC = 0.142 S/m) was applied during steady-state flow. Waveforms were collected with the multilevel probe during each of these experimental steps.

4.5.2 Continuous-rod Probe Waveforms

Energy losses are cumulative along TDR rods. Therefore, longer rod-pairs will show greater reductions in the amplitudes of the reflections on the waveform than shorter rod-pairs placed in the same medium. Figure 4-28 shows waveforms collected with the six continuous-rod pairs after 195 minutes of steady-state infiltration of a tracer solution (EC = 0.142 S/m). The final amplitude of the waveform generally decreased with increasing rod lengths. However, there is no clear relationship between the rod length and the final amplitude, demonstrating that the response of each rod-pair must be independently calibrated to

determine the EC of the medium. The small amplitude of the characteristic reflection from the ends of the 140 cm rods (located at approximately 45 ns on the figure) suggests that further conductive losses due to an increase in the water content, pore water EC or rod length would make an accurate measure of the travel time of the pulse along the rods impossible.

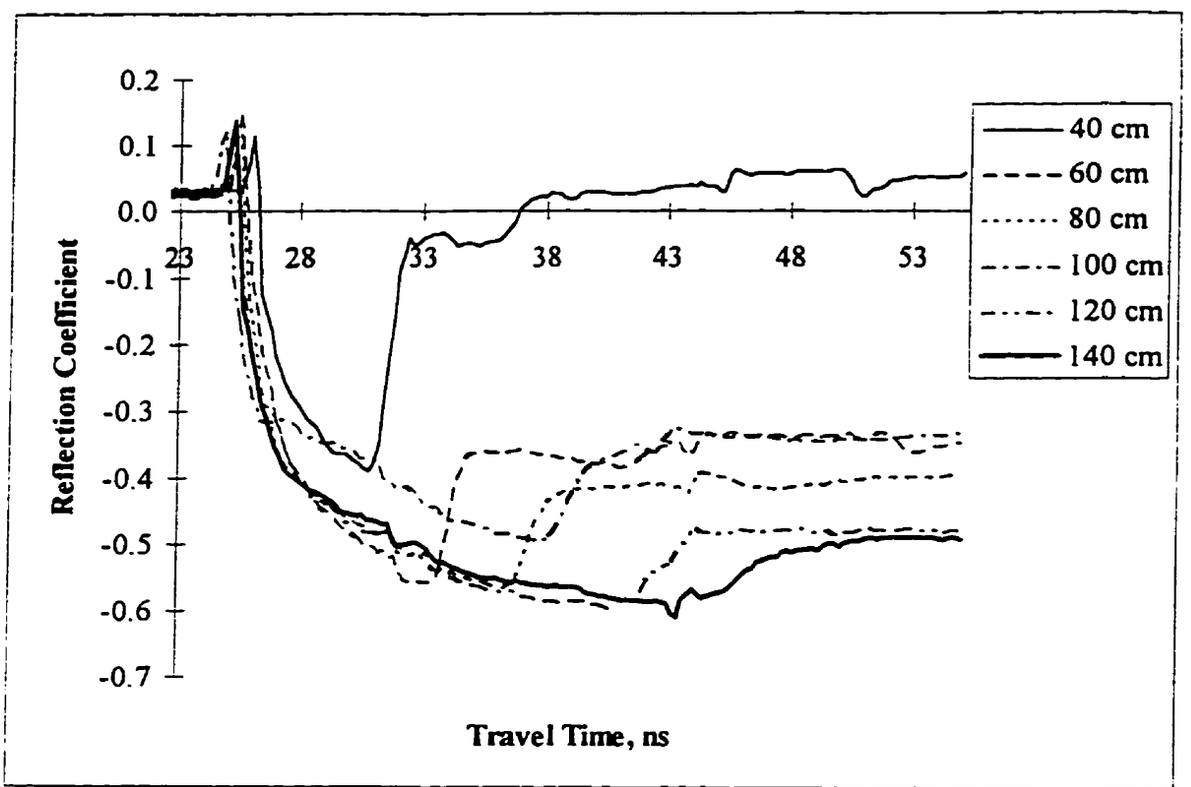

Figure 4-28. Waveforms collected with continuous-rod probes, labeled by their length, after 195 minutes of steady-state infiltration of a tracer solution (EC = 0.142 S/m).

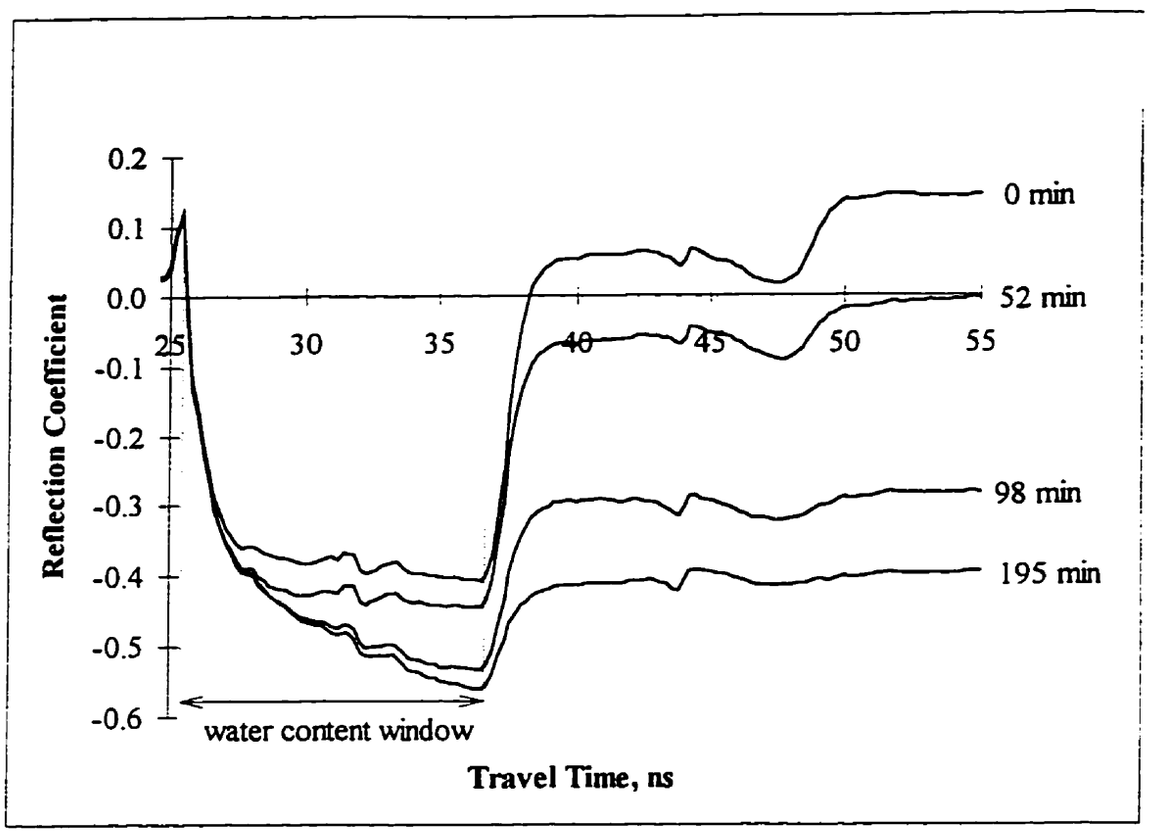

Figure 4-29. Waveforms collected with an 80 cm long continuous-rod probes during the advance of a tracer step (EC = 0.142 S/m) under steady-state infiltration. Waveforms are labeled with the elapsed time since the beginning of the application of the tracer step.

Figure 4-29 shows waveforms collected with the 80 cm rod-pair during the advance of a tracer step under steady-state infiltration. The travel time between the characteristic reflections at the ground surface and at the end of the rods, referred to as the water content window on Figure 4-29, remained constant for the steady-state infiltration conditions. The final amplitude of the waveforms decreased with time because the total mass of the tracer in the measurement volume of the rods increased as the tracer step advanced, increasing the average solute concentration along the rods.

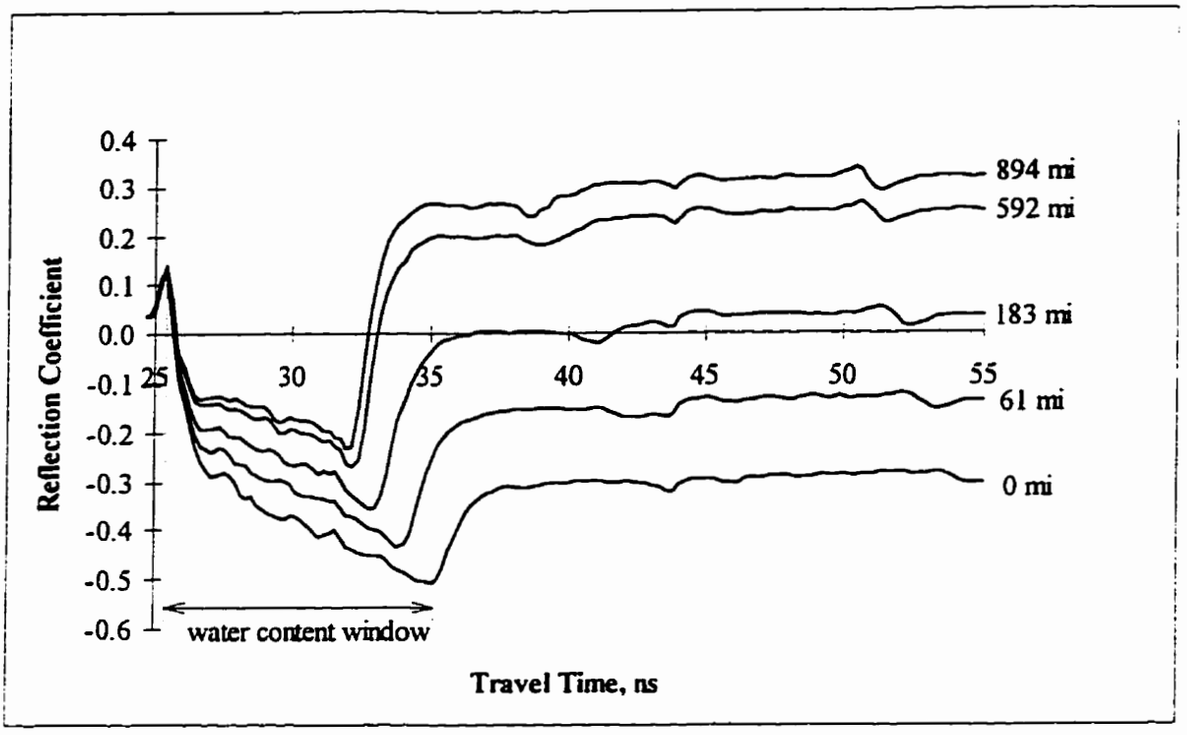

Figure 4-30. Waveforms collected with an 80 cm long continuous-rod probe during drainage of a tracer solution. Waveforms are labeled with the elapsed time from the beginning of drainage.

Figure 4-30 shows waveforms collected with the 80 cm rod-pair during drainage following steady-state infiltration of a tracer solution (EC = 0.142 S/m). Both the relative dielectric permittivity and the bulk EC of the medium decreased as the medium drained; the pore water EC remained constant throughout the drainage event. The decrease in the duration of the water content window with the decreasing relative dielectric permittivity during drainage is evident on the waveforms. The increase in the final amplitude of the waveform with decreasing water content is also clear.

4.5.3 Multilevel Probe Waveforms

The quality of the waveforms collected with any TDR probe for water content measurement can be judged on the clarity of the characteristic reflections that define the water content window. The calibrations of the water content response of the multilevel probes shown above are applied to calculate the water content from the multilevel waveforms. The sensitivity of the amplitude of the waveform to changes in the water content and pore water EC demonstrate the ability of a probe to monitor the bulk EC.

The depth of placement of the target rods alters the response of the multilevel probe. Figure 4-31 shows waveforms collected with the multilevel probe with the target rods placed at three different depths after 143 minutes of infiltration of the KCl solution (EC = 0.142 S/m). The travel time to the top of the water content measurement window increased as the rods were lowered in the access tubes because a section of the small diameter wire was lowered from the low dielectric air into the higher dielectric water-filled access tubes. The waveforms collected from all three target rod depths show very similar durations of the water content window. There is no clear relationship between the shapes and amplitudes of the waveforms and the depth of measurement suggesting that each depth will have to be calibrated separately to the EC of the medium.

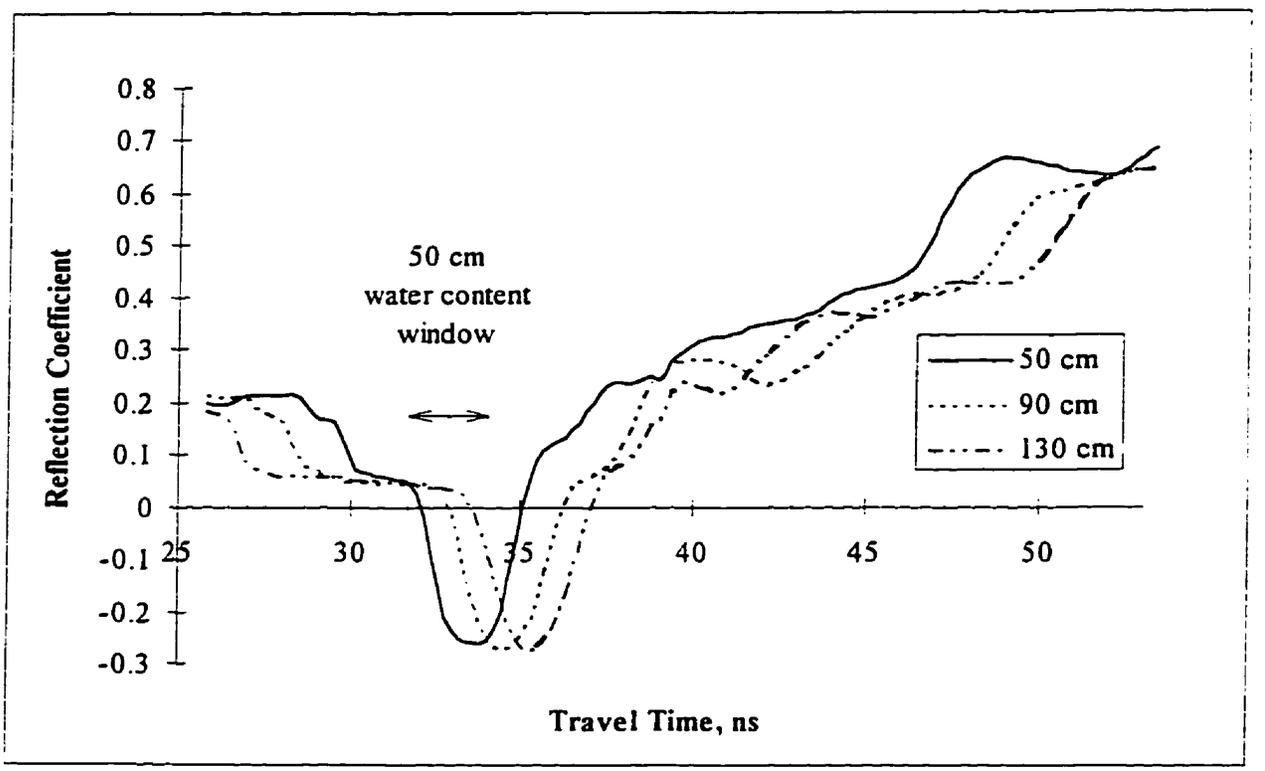

Figure 4-31. Waveforms collected with the multilevel probe, labeled by the depth of the center of the target rods, after 143 minutes of steady-state infiltration of a tracer solution (EC = 0.142 S/m).

Even under steady-state infiltration of the tracer solution, the terminal reflection collected with the target rods centered at 130 cm depth is very clear. In contrast, the reflection from the ends of the 140 cm long continuous rods (Figure 4-28) is just large enough to be identified reliably. This difference demonstrates that the insensitivity of the multilevel probes to the region above the target rods can be an advantage when monitoring water contents at depth in electrically conductive media.

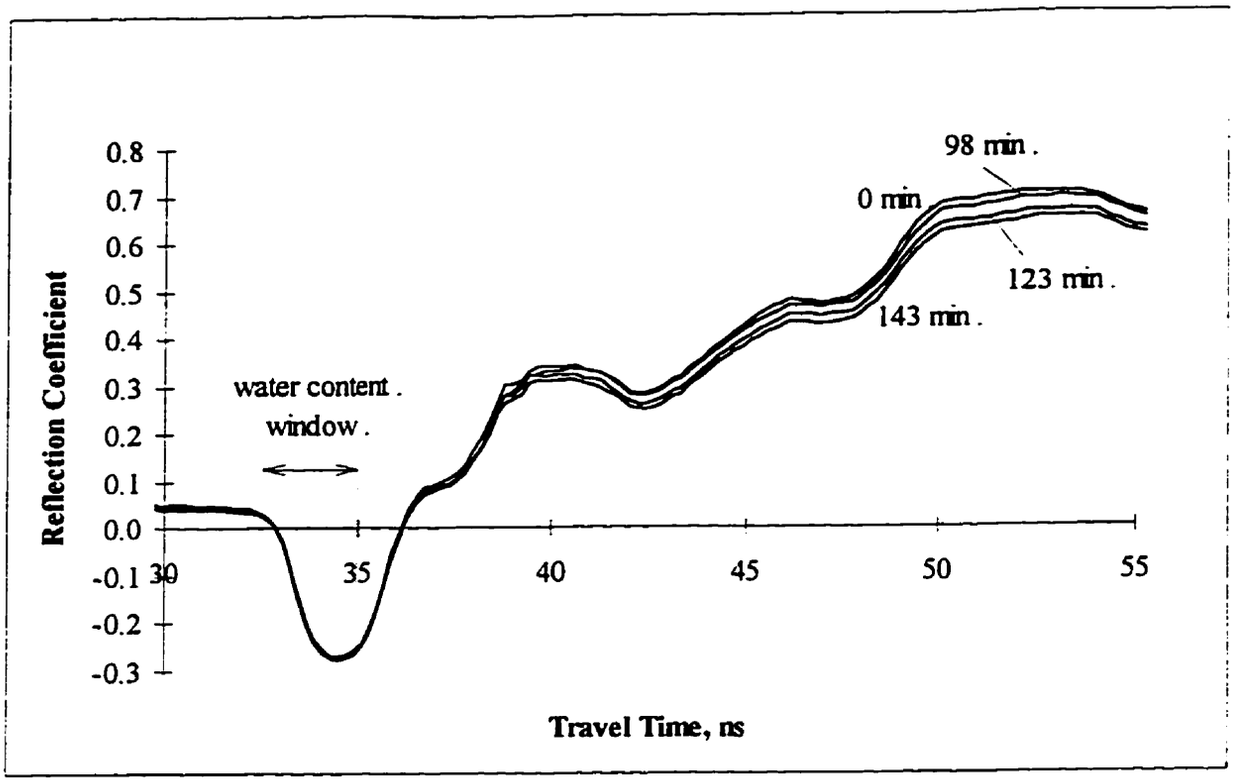

Figure 4-32. Waveforms collected with multilevel probe with the target rods centered at 90 cm depth during the advance of a tracer step (EC = 0.142 S/m) under steady-state infiltration. Waveforms are labeled with the elapsed time since the beginning of application of the tracer step.

The duration of the water content measurement window on the waveforms collected with the multilevel probe centered at 90 cm depth remained constant during the advance of the tracer solution (Figure 4-32). The final amplitudes of the waveforms decreased with time as the total mass of tracer between the target rods increased. The decrease in the final amplitude is far less pronounced than that seen with the continuous rods because of the minimal lengths of the target rods and the insulating effects of the access tubes. Isolation of the probe sensitivity to the medium in the target region is demonstrated by the near constant amplitude of the waveforms at the travel time corresponding to the beginning of the water content window despite the increase in tracer mass above the target region. In addition, the amplitude at late time on the waveform during the first 90 minutes of infiltration of the tracer step is nearly constant; there is a rapid decrease in the late-time amplitude over the next 60 minutes, demonstrating that the probe was sensitive to the presence of the tracer mass within the target region.

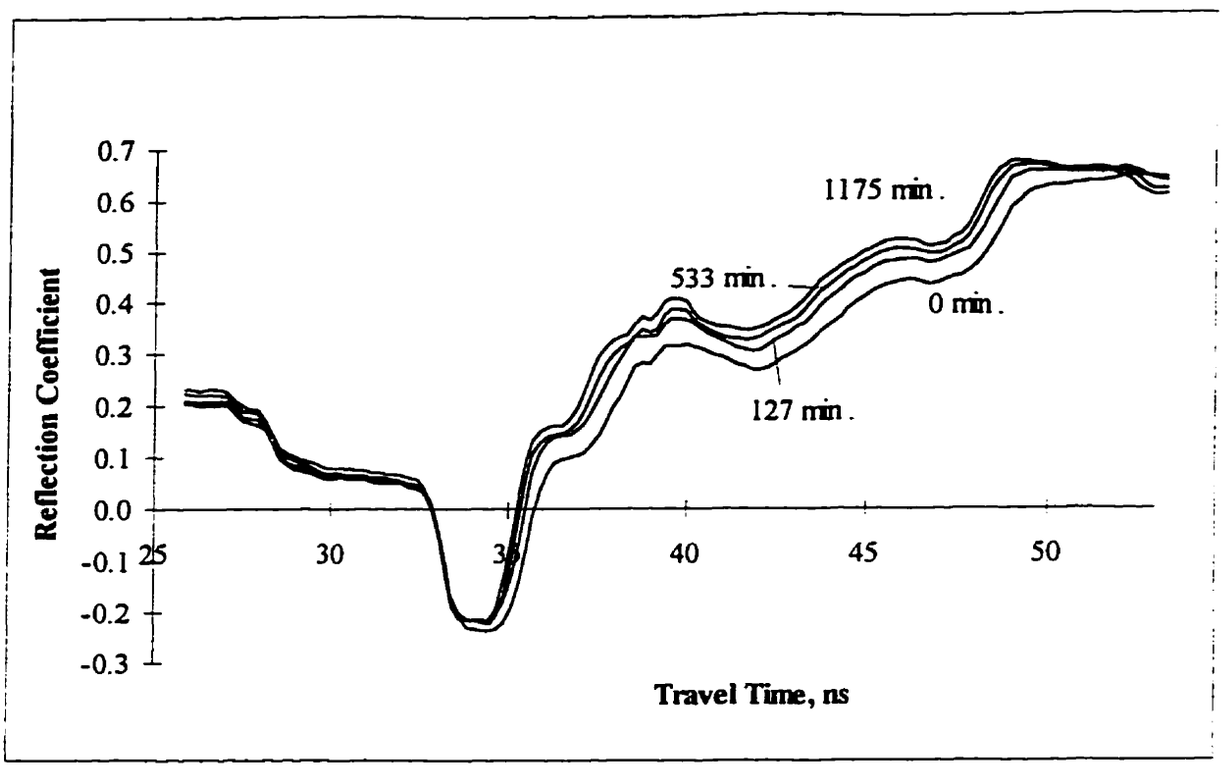

Figure 4-33. Waveforms collected with the multilevel probe with the target rods centered at 90 cm depth during drainage, labeled with the elapsed time from the beginning of drainage.

Waveforms collected with the multilevel probe with the target rods centered at 90 cm depth during drainage following steady-state infiltration of the tracer solution are shown on Figure 4-33. There is no consistent change in the amplitude at late times on the waveform ($t > 50$ ns) with changes in the water content. However, a decrease in the water content does cause a consistent increase in the amplitudes of the waveforms over the section of the waveform following the water content measurement window ($t < 50$ ns). Most methods of EC analysis require amplitude measurements made at late time on the TDR waveforms [*Topp et al.*, 1988, *Nadler et al.*, 1991]. For a more consistent response, we relate the bulk EC of the medium to the inverse of the average impedance, in ohms, measured from 45 to 50 ns on the waveform following the approach of *Nadler et al.* [1991].

4.5.4 Dependence of the Bulk EC Response on the Water Content

Figure 4-34 shows paired measurements of the EC response of the multilevel probe and the water content. Unlike the results shown in the field for continuous-rod probes, there is a nonlinear relationship between the EC measured by the multilevel probe and the water content for spatially uniform pore water EC

conditions. As a result, there will not be a unique relationship between the EC response of the multilevel probe and the length-weighted average solute mass if the water content varies along the probes. Therefore, the target rods should be as short as possible to minimize spatial variability of the water content within the sample volume.

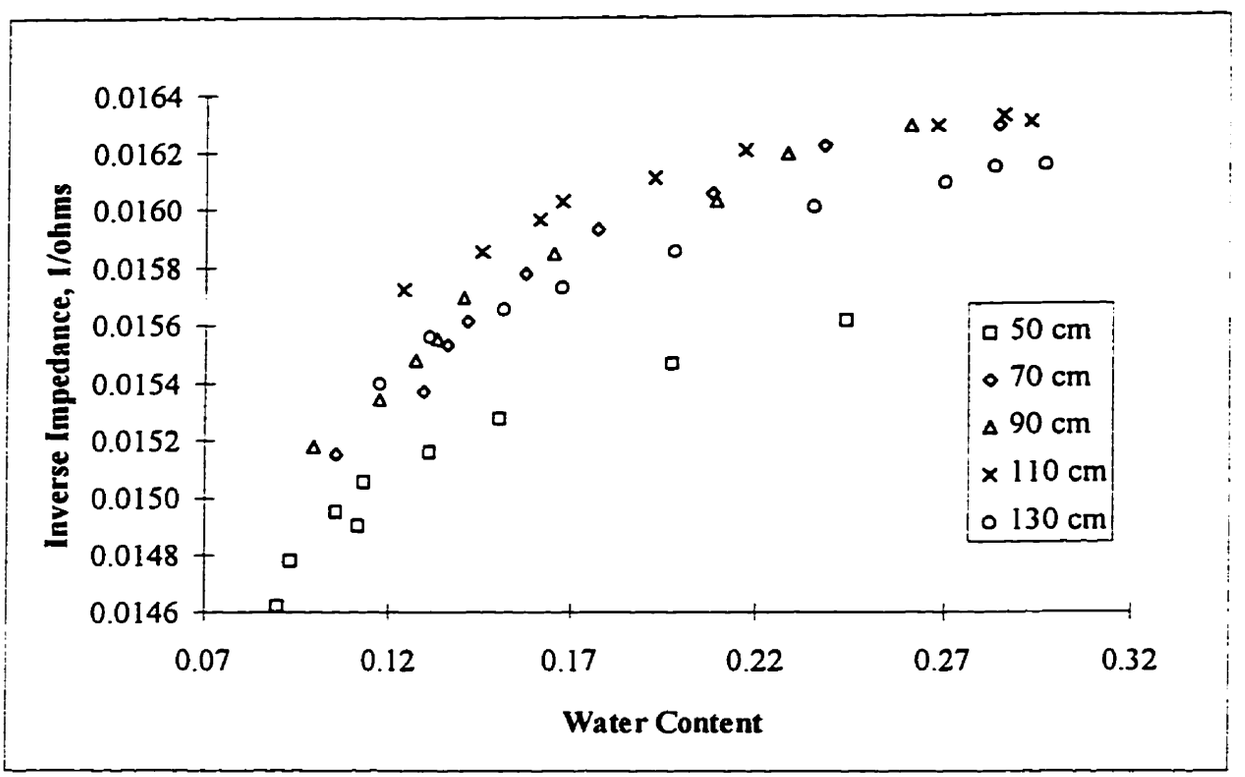

Figure 4-34. Paired measurements of the water content and the average the inverse of the impedance measured with multilevel probe ML4 at five depths during drainage.

The design of the multilevel probe includes an electrically resistive polyvinyl chloride coating around the target rods. The water content response of rods with dielectric coatings follows an inverse dielectric mixing model, leading to a linear relationship between the inverse of the measured relative dielectric permittivity and the inverse of the relative dielectric permittivity of the medium. This finding arises from the description of the averaging of dielectric permittivities around the rods based on a solution of Laplace's equation. Given that the electric field around the rods is also described by Laplace's equation, a similar averaging of the electrical conductivities of the materials surrounding the target rods is expected. Figure 4-35 shows the inverse of the EC response as a function of the inverse of the water content for all five target rod depths. The linear regressions shown on the figure all show r^2 values greater than 0.97.

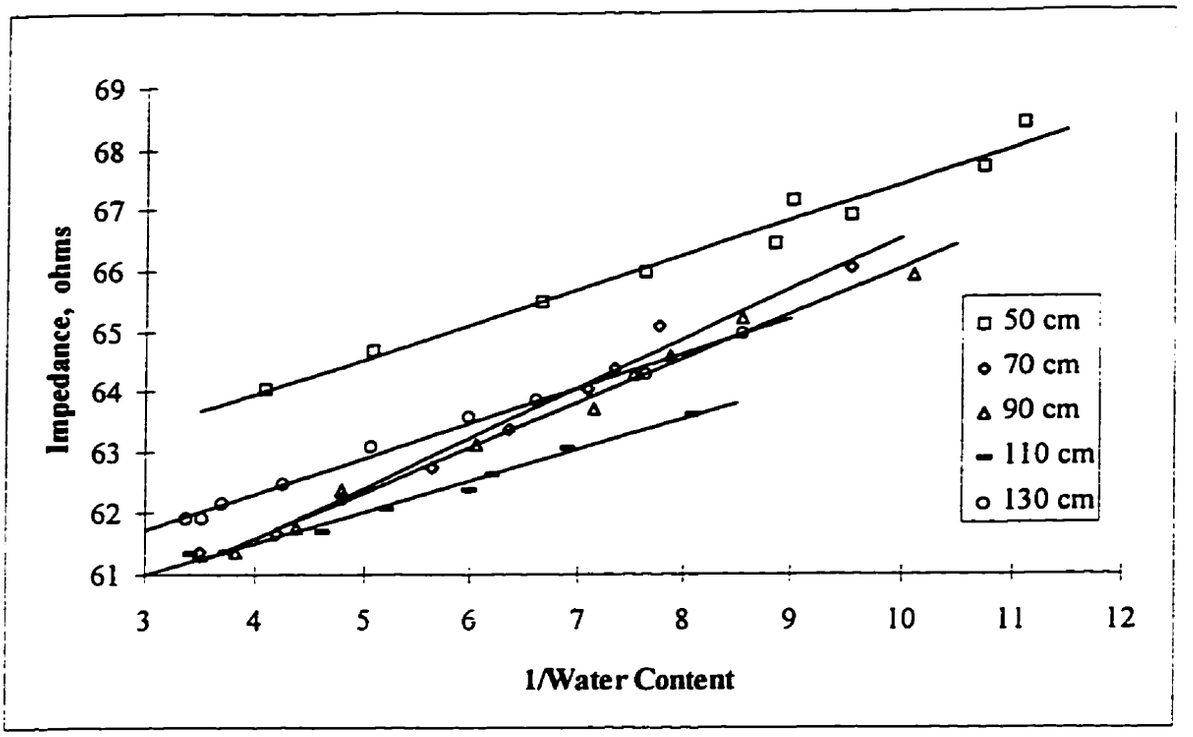

Figure 4-35. Inverses of the water content and the average impedance (1/ohms) measured with the multilevel probe at five depths during drainage.

Based on the linear relationships shown on Figure 4-35, if the pore water EC is constant, the EC response of a given probe, σ_{TDR}, is related to the water content, θ, by,

$$\frac{1}{\sigma_{TDR}} = \frac{a_1}{\theta} + c_1, \tag{4-3}$$

where the probe specific constants a_1 and c_1 are independent of the water content, but a_1 is a function of the pore water EC.

4.5.5 Dependence of the Bulk EC Response on the Pore Water EC

To complete the calibration of the EC response to the water content and pore water EC, the EC and the water content were measured with the multilevel probe during steady-state infiltration of three different KCl solutions (0.040, 0.085 and 0.142 S/m). The water content varied slightly among the infiltration events. From Equation 4-3, if the pore water EC is constant, the TDR-measured EC values measured at some water content, θ, can be corrected to the value that would be measured at a common water content of 0.25 using,

$$\frac{1}{\sigma_{TDR}(0.25)} = \frac{1}{\sigma_{TDR}(\theta)} + a_1(0.25-\theta). \qquad (4\text{-}4)$$

Table 4-2 shows the slopes, intercepts and goodness of fit values of linear regressions of the inverse of the water content corrected TDR-measured EC as a function of the inverse of the EC of the pore water, σ_w, measured with a standard conductance cell.

	slope	intercept	r^2
50 cm	0.142	62.78	0.917
70 cm	0.150	59.7	0.988
90 cm	0.143	59.7	0.999
110 cm	0.153	59.5	0.999
130 cm	0.174	59.7	0.999

Table 4-2. Linear regressions of the inverse of the TDR-measured EC as a function of the inverse of the pore water EC.

The linearity of the relationships shown on Table 4-2 suggests a relationship of the form,

$$\frac{1}{\sigma_{TDR}} = \frac{a_2}{\sigma_w} + c_2. \qquad (4\text{-}5)$$

where the soil-specific constant, a_2, is a function of the water content; c_2 is independent of both the water content and the pore water EC.

4.5.6 Determination of the Pore Water EC from the Probe Responses

Equations 4-3 and 4-5 can be combined to relate the EC response to the water content and pore water EC as,

$$\frac{1}{\sigma_{TDR}} = \frac{m}{\theta\sigma_w} + b. \qquad (4\text{-}6)$$

For each probe, m equals the slope reported on Table 4-2 multiplied by the constant water content of 0.25; b is equal to the intercept shown on Table 4-2. Equation 4-6 can be rearranged to define the pore water EC from the EC and water content responses of the probe as,

$$\sigma_w = \frac{m}{\theta\left[\frac{1}{\sigma_{TDR}} - b\right]}. \tag{4-7}$$

4.5.7 Independent Calibration of the EC Response

Mallants et al. [1996] compared three methods of calibrating the EC response of TDR probes: independent calibration of the EC response, normalization to the response of a long-duration tracer step, and numerical integration of a tracer pulse. These methods are compared for the multilevel probe below.

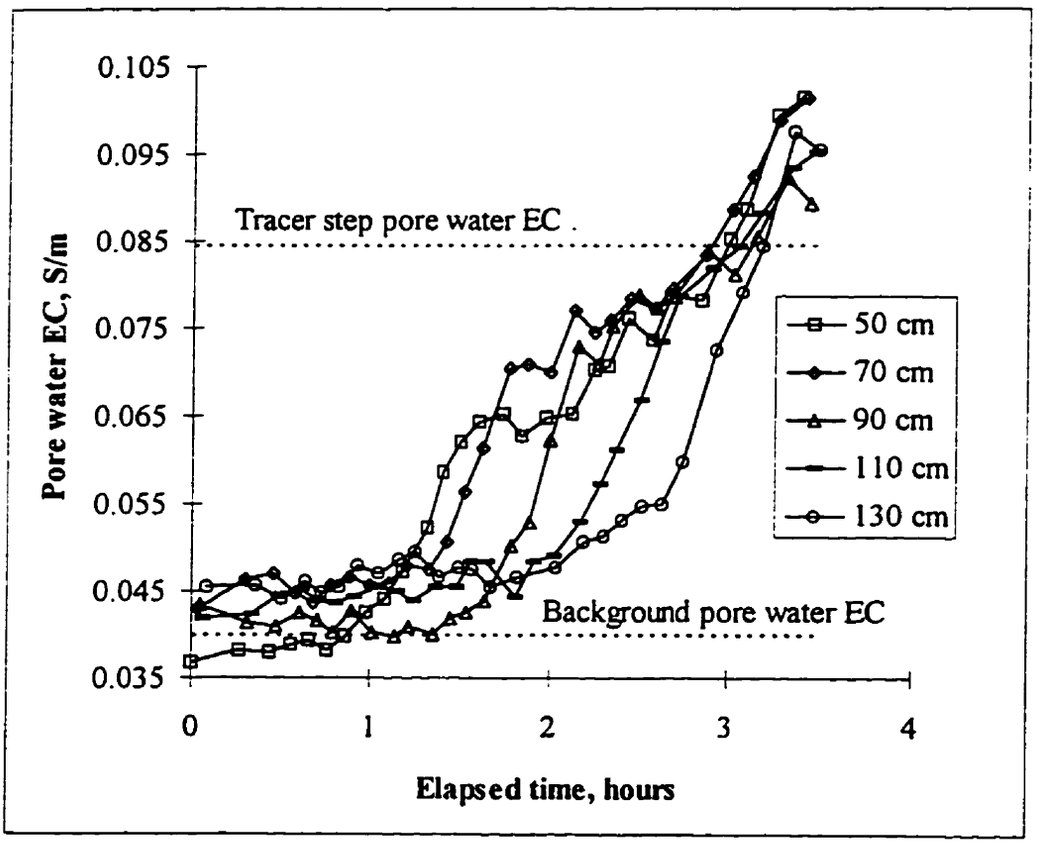

Figure 4-36. The pore water EC calculated using the independent probe calibration method.

The preceding analysis leads to an independent calibration of the EC response of the multilevel probe. Figure 4-36 shows the pore water EC calculated using Equation 4-7 and the constants shown on Table 4-2 for the waveforms collected during the advance of a tracer step (EC = .085 S/m). The breakthrough curves show the arrival of the tracer mass at each depth with time. At early times, the calculated pore water EC values vary about the known EC of the municipal water. At the end of the tracer step application, all of the probes overestimate the calculated pore water EC.

4.5.8 Normalization of the EC Response using a Tracer Step

The EC response of the multilevel probe can be calibrated specifically for the conditions of the tracer step. Under steady-state flow, the water content remains constant for each depth throughout the experiment. Preceding the tracer step, the medium was preflushed with the unamended municipal water, resulting in a constant pore water EC throughout the medium of 0.040 S/m. Assuming that the resident pore water was replaced completely by the tracer by the end of the experiment, the pore water EC will be spatially uniform and equal to 0.0845 S/m. For these conditions, the EC response at each depth can be correlated with the pore water EC using a two point calibration to these two known pore water EC values.

Figure 4-37 shows the pore water EC values determined using the long-duration tracer step method of calibration. The multilevel probe clearly defines the arrival of the solute front at each depth. The measured EC remains constant for the initial 45 minutes of tracer step application, demonstrating that the multilevel probe is only sensitive over a limited depth range. However, the pore water EC does not achieve a constant value by the end of the tracer step, even for the shallowest target rod depth. The slowly increasing pore water EC values calculated with time after the arrival of the tracer front may be due to redistribution of the tracer mass into inactive regions of the flow field. This mass redistribution, even in a clean sand, demonstrates the main limitation to the two point probe calibration as discussed by *Mallants et al.* [1996]. However, this level of probe sensitivity to the resident tracer mass also shows the potential usefulness of the multilevel probe for solute monitoring.

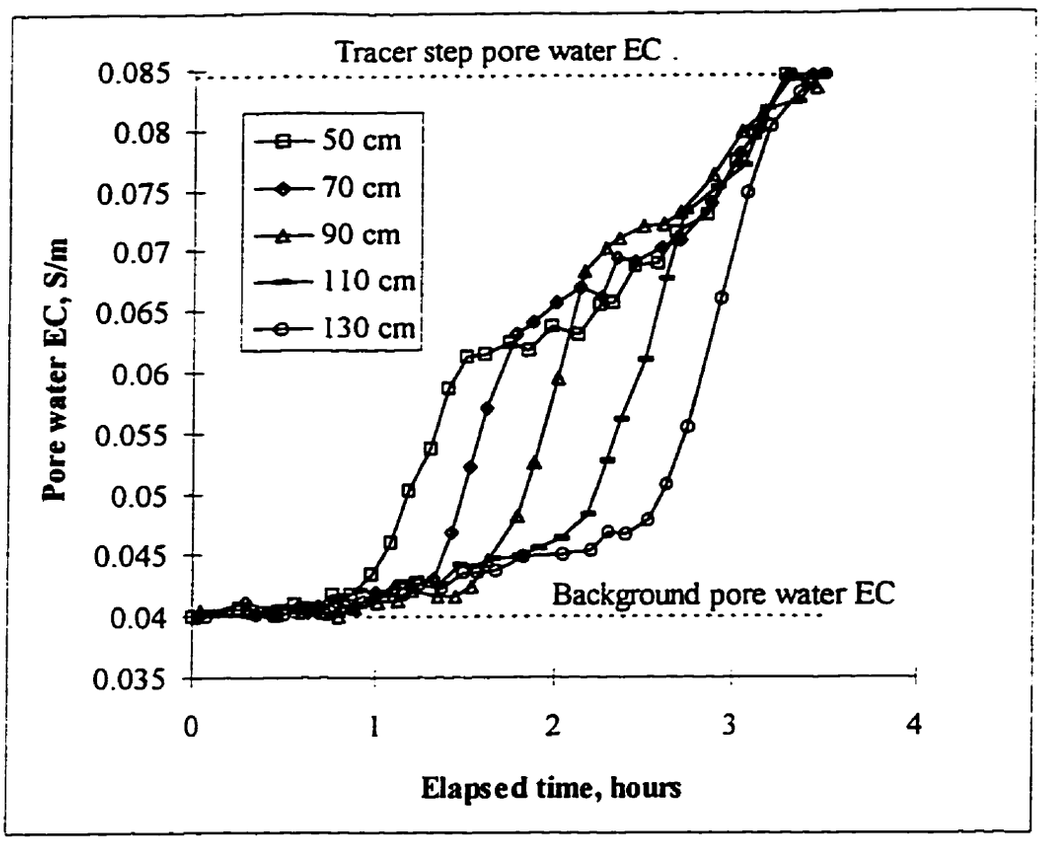

Figure 4-37. The pore water EC calculated with the long-term solute step calibration method.

4.5.9 Calibration by Numerical Integration of a Tracer Pulse

Ward et al. [1994] demonstrated that the EC response of horizontally installed rods can be calibrated to return the resident mass by numerical integration of the probe responses during the advance of a tracer pulse; *Mallants et al.* [1996] found that this method produced the most accurate probe calibrations for a relatively homogeneous soil. To produce a measurable solute pulse in the field, we applied municipal water until steady-state flow was achieved, followed by a 45 minute pulse of tracer-amended water (EC = 0.142 S/m), followed by further infiltration of the municipal water. To increase the density of the data set, we monitored the EC rapidly with the target rods at a single depth of 90 cm below ground surface. The results of applying this method of calibration to the responses of the multilevel probe are shown on Figure 4-38. The calculated EC values are unchanged before the arrival of the pulse, rise to a reasonable value and then return to the background level, clearly demonstrating the ability of the probe to monitor the bulk EC over a limited depth range. Unfortunately, no independent measure of the tracer concentration was made for independent calibration of the probe response during this pulse experiment.

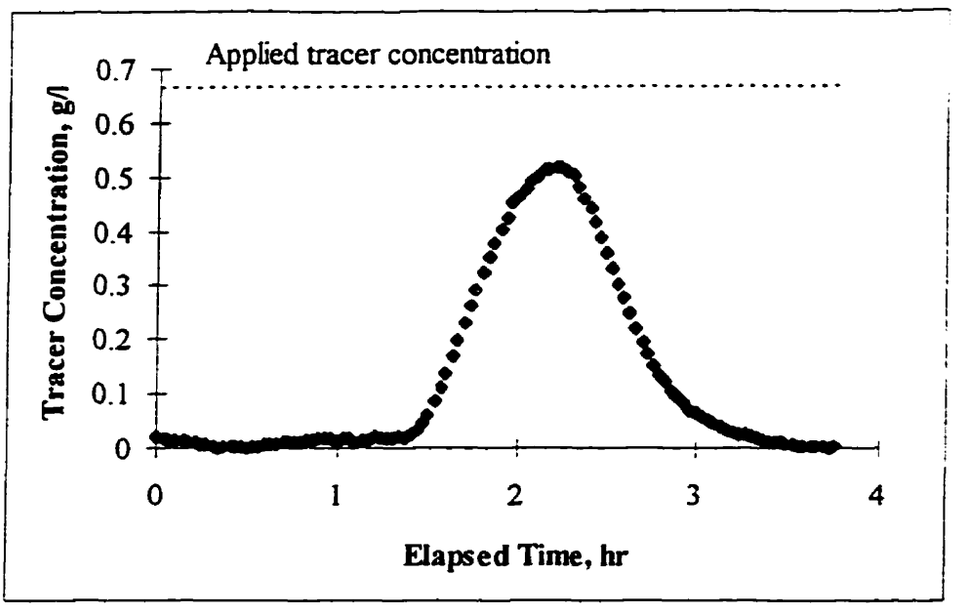

Figure 4-38. The pore water EC calculated with the numerical integration method.

4.5.10 Summary and Conclusions

A comparison of the responses of continuous-rod TDR probes and a prototype alternative multilevel TDR probe shows that the waveforms of standard continuous-rod probes are more sensitive to changes in the pore water EC and water content than those produced by the multilevel probe. The decreased sensitivity of the multilevel probe is due to the short target rod length and the electrical insulation of the access tubes.

There is a linear relationship between the inverse of the water content and the inverse of the EC response of the multilevel probe under constant pore water EC conditions. There is also a linear relationship between the inverses of the EC response and the pore water EC for a given water content. Based on these findings, we describe a general calibration of the EC response to the water content and pore water EC that allows for determination of the pore water EC from the probe responses. Calibrating the EC response with a long-duration solute step gives improved solute breakthrough curves at each depth. Finally, the numerical integration method of calibration produces excellent results for monitoring the resident solute concentration.

The EC response of the multilevel probe is nearly insensitive to the properties of the medium above the target region, offering the possibility of solute concentration profiling. The reduced sensitivity of the multilevel probe above the target region also allows for EC and water content monitoring in media that are too electrically conductive for measurement with standard continuous-rod TDR probes. In addition, the probe clearly identified solute breakthrough within the target region and may have detected redistribution of the solute mass to inactive regions of the flow field as well.

4.6 *Numerical Analysis of TDR Probes*

4.6.1 Numerical Approach

Due to the geometry of TDR probes, analytical descriptions of the effects of heterogeneous distributions of dielectric materials in the transverse plane have been possible only for a few restrictive cases. *Annan* [1977a] derived an analytical formula for the response of coaxial probes with concentric circular gaps around the inner and outer conductors. For the two-rod probe with nonconcentric circular gaps around the rods, *Annan* [1977b] also found an analytical result. *Knight et al.* [1994] presented an analytical solution for the case in which a continuous-rod probe is placed with the centers of the rods located on the boundary between two media with different relative dielectric permittivities.

To address the limitations of the existing analytical solutions, *Knight et al.* [1997] presented a steady-state, two-dimensional finite element numerical solution of Laplace's equation to analyze the response of TDR probes to dielectric materials distributed in the plane perpendicular to the rods. This approach uses the numerically determined electrostatic potential distribution and boundary fluxes based on the finite element numerical model of *Pinder and Frind* [1972] to calculate the equivalent relative dielectric permittivity measured by TDR.

The time harmonic electric field along a transmission line can be derived from the potential function. For a TDR pulse applied to parallel rods embedded in a heterogeneous medium, the pulse velocity is governed by the electrostatic potential, ϕ, in the plane perpendicular to TDR rods, which satisfies a generalization of Laplace's equation in the (x,y) plane,

$$\nabla \cdot (K \nabla \phi) = 0 . \qquad (4\text{-}8)$$

The domain Ω has a boundary S consisting of an external boundary S_3, and, in the case of a two-rod probe, two internal boundaries, S_1 and S_2, as shown in Figure 4-39. The relative dielectric permittivity varies over the region as $K=K(x,y)$. A direct parallel can be drawn to the equation for the steady-state flow of water, for which K and ϕ in Equation 4-8 are replaced by the hydraulic conductivity and hydraulic head, respectively. This analogy allows for the use of existing groundwater flow software to analyze the electrostatic problem for TDR.

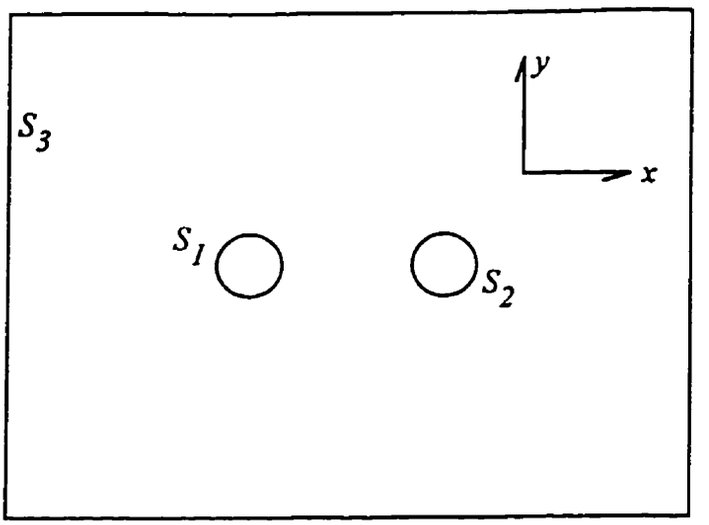

Figure 4-39. Domain used for the numerical model.

In the solution, the potential, ϕ, is set to constant values of V_1 on S_1 and V_2 on S_2. In his analysis, *Knight* [1992] implicitly assumed that at large distances from the probe the boundary condition was such that the energy decayed to zero. This assumption is physically reasonable, as discussed by *Whalley* [1993] and *White et al.* [1994] who investigated the question of the boundary condition at infinity in more detail. In the numerical approach, a sufficiently large domain was chosen such that the energy flow across the outer boundary will be negligible, giving the boundary condition,

$$\frac{\partial \phi}{\partial n} = 0, \tag{4-9}$$

where n is the outward pointing unit normal vector on the S_3.

In the development of the numerical solution, *Knight et al.* [1997] define a vector, **F**, as,

$$\mathbf{F} = -\phi(K\nabla\phi). \tag{4-10}$$

Applying the divergence theorem to **F** over the domain, Ω, and the surfaces S_1, S_2 and S_3 gives,

$$-\iint_{\Omega} \nabla \cdot \left(\phi(K\nabla\phi)\right) dA = -\int_{S} \phi(K\nabla\phi) \cdot \mathbf{n} dS. \tag{4-11}$$

Expanding the left hand side gives,

$$-\iint_{\Omega} \phi \nabla \cdot (K \nabla \phi) dA - \iint_{\Omega} (K \nabla \phi) \cdot (\nabla \phi) dA = -\int_{S} \phi (K \nabla \phi) \cdot \mathbf{n} dS . \qquad (4\text{-}12)$$

The first term on the left hand side is equal to zero by Equation 4-8. Eliminating this term and expanding the surface integral to integrals over the three boundaries gives.

$$\iint_{\Omega} (K \nabla \phi) \cdot (\nabla \phi) dA = \int_{S_1} \phi (K \nabla \phi) \cdot \mathbf{n} dS + \int_{S_2} \phi (K \nabla \phi) \cdot \mathbf{n} dS + \int_{S_3} \phi (K \nabla \phi) \cdot \mathbf{n} dS . \qquad (4\text{-}13)$$

Applying the surface boundary conditions gives,

$$\iint_{\Omega} K |\nabla \phi|^2 dA = V_1 \int_{S_1} K \left(\frac{\partial \phi}{\partial n} \right) dS + V_2 \int_{S_2} K \left(\frac{\partial \phi}{\partial n} \right) dS . \qquad (4\text{-}14)$$

The total energy in the electrostatic field, W, is defined as,

$$W = \frac{1}{2} \varepsilon_0 \iint_{\Omega} K |\nabla \phi|^2 dA = \frac{1}{2} \varepsilon_0 \left(V_1 \int_{S_1} K \left(\frac{\partial \phi}{\partial n} \right) dS + V_2 \int_{S_2} K \left(\frac{\partial \phi}{\partial n} \right) dS \right) . \qquad (4\text{-}15)$$

where ε_0 is the relative dielectric permittivity of free space.

For a two-rod probe in a lossless medium, a no-flux outer boundary requires that the flux out of one interior boundary must equal the flux into the other interior boundary for the electrostatic case. Therefore, the two integrals on the right hand side of Equation 4-15 have opposite sign and equal magnitude. As a result, Equation 4-15 can be simplified to,

$$W = \frac{1}{2} \varepsilon_0 (V_1 - V_2) \left(\int_{S_1} K \left(\frac{\partial \phi}{\partial n} \right) dS \right) . \qquad (4\text{-}16)$$

Equation 4-16 describes the total electrostatic energy in a medium with a spatially heterogeneous K. For a domain with a uniform relative dielectric permittivity, K_{eq}, the resulting potential is $\phi_0(x,y)$ and Equation 4-16 simplifies to,

$$W = \frac{1}{2}\varepsilon_0 (V_1 - V_2) K_{eq} \left(\int_{S_1} \left(\frac{\partial \phi_0}{\partial n} \right) dS \right). \tag{4-17}$$

As in *Knight* [1992], a value of K_{eq} can be defined such that the total energy in the field with this uniform relative dielectric permittivity is equal to the total energy in the field with a spatially variable relative dielectric permittivity, $K(x,y)$, for the same boundary conditions.

$$W = \frac{1}{2}\varepsilon_0 (V_1 - V_2) K_{eq} \left(\int_{S_1} \left(\frac{\partial \phi_0}{\partial n} \right) dS \right) = \frac{1}{2}\varepsilon_0 (V_1 - V_2) \left(\int_{S_1} K \left(\frac{\partial \phi}{\partial n} \right) dS \right). \tag{4-18}$$

From Equation 4-18 an expression defining K_{eq} for the equivalent homogeneous distribution is,

$$K_{eq} = \frac{\left(\int_{S_1} K \left(\frac{\partial \phi}{\partial n} \right) dS \right)}{\left(\int_{S_1} \left(\frac{\partial \phi_0}{\partial n} \right) dS \right)}. \tag{4-19}$$

Notice that this expression is independent of the voltages V_1 and V_2. Therefore, when calculating K_{eq} from Equation 4-19, the voltages applied to S_1 and S_2 can be taken to be 1 and -1, respectively, without loss of generality. A similar development is possible for any number of rods, regardless of the shapes or distribution of the rods.

Knight [1992] developed an analytical expression for the spatial sensitivity of TDR probes based on the distribution of energy in the electrostatic field. He defined a spatial weighting factor at each point in the domain, $w(x,y)$, equal to the square of the gradient of the potential in the heterogeneous medium divided by the integral of the square of the voltage gradient for a homogeneous medium (with any arbitrary K value) and the same boundary conditions,

$$w(x,y) = \left[\nabla \phi(x,y) \right]^2 \Big/ \iint \left[\nabla \phi_0(x,y) \right]^2 dx\,dy. \tag{4-20}$$

where $\phi(x,y)$ is the potential in the heterogeneous medium and $\phi_0(x,y)$ is the potential in the homogeneous medium.

The value of K_{eq} was chosen such that the total energies in the two media are equal,

$$\iint K|\nabla\phi|^2 dA = K_{eq}\iint|\nabla\phi_0|^2 dA. \tag{4-21}$$

By combining Equations 4-20 and 4-21, the equivalent uniform relative dielectric permittivity is defined as the spatially weighted sum of the relative dielectric permittivity values in the heterogeneous field over the domain,

$$K_{eq} = \iint w(x,y)K(x,y)\,dx\,dy. \tag{4-22}$$

It can be seen from the form of Equations 4-20 and 4-22 that the weighting function depends on the distribution of $K(x,y)$ around the probe. Although his analysis allowed for the investigation of the spatial sensitivity of different rod geometries, the application of the analytical approach of *Knight* [1992] is restricted to uniform media with small perturbations in the relative dielectric permittivity in the transverse plane. With the use of a numerical model, this approach can be extended for more general applications.

It is important to note that the spatial weighting factors defined by *Knight* [1992] are not equivalent to the weighting factors presented in Chapter 2 for the dielectric mixing models. To compare the two weighting factors, Equation 4-22 can be rewritten as two integrals, one over the areas occupied by the rings and the other over the soil outside of the rings,

$$K_{eq} = \iint_{rings} w(x,y)K(x,y)\,dx\,dy + \iint_{soil} w(x,y)K(x,y)\,dx\,dy. \tag{4-23}$$

The relative dielectric permittivity in the rings is uniform, as is the relative dielectric permittivity outside of the rings. Therefore, Equation 4-23 can be simplified to,

$$K_{eq} = K_{rings}\iint_{rings} w(x,y)\,dx\,dy + K_{soil}\iint_{soil} w(x,y)\,dx\,dy. \tag{4-24}$$

A comparison of Equations 2-15 and 4-24 demonstrates the difference between these weighting factors. In effect, the numerical approach assumes an arithmetic mean dielectric mixing model, regardless of

the distribution of dielectric media, and then calculates the weighting factors that must apply to the materials distributed throughout the transverse plane to return the correct average relative dielectric permittivity for the given distribution of materials and imposed boundary conditions. In order to achieve this, the weighting factors throughout the transverse plane are altered to account for both the distribution of materials and the relative dielectric permittivities of those materials. In contrast, for a specific distribution of materials, the dielectric mixing model approach integrates the spatial weighting throughout each region that applies specifically for the probe geometry, materials distribution and boundary conditions. As a result of applying the mixing model that applies directly to the distribution of dielectric media, the weighting factors need only account for the geometry; therefore, the weighting factors for the dielectric mixing model are independent of the dielectric permittivities of the media in the transverse plane.

The distributions of hydraulic potential and electrostatic potential in response to similar boundary conditions are both described by Equation 4-8. Therefore, existing analytical or numerical groundwater flow models can be used to investigate the response of TDR pulses propagating along probes placed in a medium with a heterogeneous distribution of relative dielectric permittivity in the plane perpendicular to the rods. A two-dimensional, finite element groundwater flow model [*Pinder and Frind*, 1972] was used to investigate the distribution of electrostatic potential in the plane perpendicular to TDR rods. A grid generator [*McLaren*, 1996] created a triangular mesh within a rectangular domain. A zero flux boundary condition was imposed on the nodes on the outer boundary of the domain. Two or three holes were cut in the mesh to represent the two or three rods of a TDR probe. For two-rod probes, the nodes on one rod were set to a constant potential of -1; the potential on the second rod was set to 1. Nodes on the central rod of a three-rod probe were set to a constant potential of 1 with the outer rods set to -1. To model coated continuous-rod probes, nodes were located on circles around the rods to ensure that elemental properties could be defined separately for the coatings and for the surrounding medium.

The numerical analysis allows for complete generality in both the geometry of the probe and the distribution of relative dielectric permittivities in the transverse plane. The equivalent relative dielectric permittivity, K_{eq}, is determined for any heterogeneous distribution of K using Equation 4-19. Initially, the potential distribution is determined for the specific rod geometry and boundary conditions for a medium with a constant relative dielectric permittivity, K_0. For the homogeneous case, the potential distribution is not dependent on the value of the relative dielectric permittivity; therefore, any positive value for K_0 can be chosen with the same result. The denominator of Equation 4-19 is equivalent to the flux into the homogeneous system divided by K_0. The numerator of Equation 4-19 is equivalent to the flux out of the interior boundary for the heterogeneous relative dielectric permittivity distribution with the same boundary conditions.

4.6.2 Effects of Gaps and Coatings on Continuous Rod Probes

Using this numerical analysis, *Knight et al.* [1997] found that the analytical solution due to *Annan* [1977b] for nonconcentric gaps (Equation 2-12) can be used as a good approximation to predict the effect of concentric gaps or coatings that completely surround twin rods. For two-rod probes, the impact of a coating of a given thickness and relative dielectric permittivity decreases with an increase in the rod diameter and, to a lesser degree, with an increase in the rod separation. A gap or coating of a given thickness and relative dielectric permittivity will have a greater impact on the response of a three-rod probe than on that of a two-rod probe with the same rod diameter and separation of the outermost rods. Finally, they showed that partial air gaps surrounding less than 30 degrees of the rod circumference are not likely to affect the probe response significantly.

4.7 *Sample Area of TDR Probes*

4.7.1 Definition of the Sample Area

In addition to the ability to accurately measure a soil property, the volume of porous medium sampled is an important characteristic of any sampling method. The spatial weighting concept proposed by *Knight* [1992] and the numerical approach of *Knight et al.* [1997] can be used to define the area in the plane perpendicular to TDR rods that contributes to the response of a TDR probe.

The sample volume is the region of the porous medium that contributes to the total probe response; changes in the properties of the porous medium outside of this volume do not have a measurable influence on the response of the instrument. Ignoring any effects arising from the distribution of the electrostatic field at the ends of the rods, the sample volume is defined as the projection along the length of the rods of the sample area in the plane perpendicular to the long axis of the rods.

For convenience of calculation and use, sample areas are often defined using some regular shape such as an ellipse [*Baker and Lascano*, 1989] or circles [*Knight*, 1992] surrounding the rods. A sample area so defined is affected by the arbitrary choice of a regular shape. The numerical analysis allows for a more exact definition of the sample volume. Given the distribution of spatial weighting factors, the sample area enclosing the regions of greatest spatial sensitivity can be identified, thereby uniquely defining the smallest region contributing to the probe response.

The numerical analysis of *Knight et al.* [1997] defines the weighting factor for each element in a finite element mesh for a representative cross section of any probe with a given distribution of relative dielectric permittivities in the surrounding porous medium. The weighting factors define the relative contribution per unit area of the medium located at each point in the plane. The sum of the product of the

elemental spatial weighting factors, w_i, and elemental areas, A_i, define the fraction of the total probe response contributed by any area within the domain. To uniquely define the sample area containing the regions of highest sensitivity, the product of w_i and A_i is summed beginning with those elements with the highest weighting factors, w_{hi}, and continuing over progressively less heavily-weighted elements until the desired percent of the total response, f, is achieved.

$$f = 100\% * \sum_{w_{hi}}^{w} w_i A_i \ . \tag{4-25}$$

The elements included in the summation define the area contributing any fraction of the total probe response.

In reality, the sensitivity of a continuous-rod probe will decrease to an unmeasureable level some distance from the rod surfaces. In the numerical analysis, the region contributing 100% of the probe response will, by definition, fill the entire finite element domain, regardless of the size of the domain. Therefore, some large fraction of the total contribution must be chosen to define the sample area. The 90% level was chosen to represent the sample area in this study because it was the highest level that was insensitive to the size of the finite element domain. The 50 and 70% sample areas are also shown to demonstrate the distribution of probe sensitivity within the sample volume.

4.7.2 Continuous-rod Probes

Continuous-rod TDR probes are comprised of two or three parallel metal rods. As shown in Figure 4-1, the separation of the outer rods, S, and the rod diameter, D, define the representative cross section of standard continuous-rod probes.

Figure 4-40 shows the equipotentials surrounding two- and three-rod probes with separation to diameter ratios (S:D) of 5 and 10. For direct comparison, only one quadrant is shown for each configuration. For conventional probes in a homogeneous medium, the distribution of equipotentials is independent of the relative dielectric permittivity of the medium; the potential distribution is only a function of the probe geometry. Analogously, under steady state, one-dimensional downward flow through a saturated, homogeneous soil column with fixed potential boundary conditions, the distribution of equipotentials is independent of the magnitude of the hydraulic conductivity of the porous medium. The spatial weighting factors are based on the square of the gradient of the potential. Therefore, for conventional rods in a homogeneous medium, the weighting factors and, therefore, the sample area are only a function of the probe geometry.

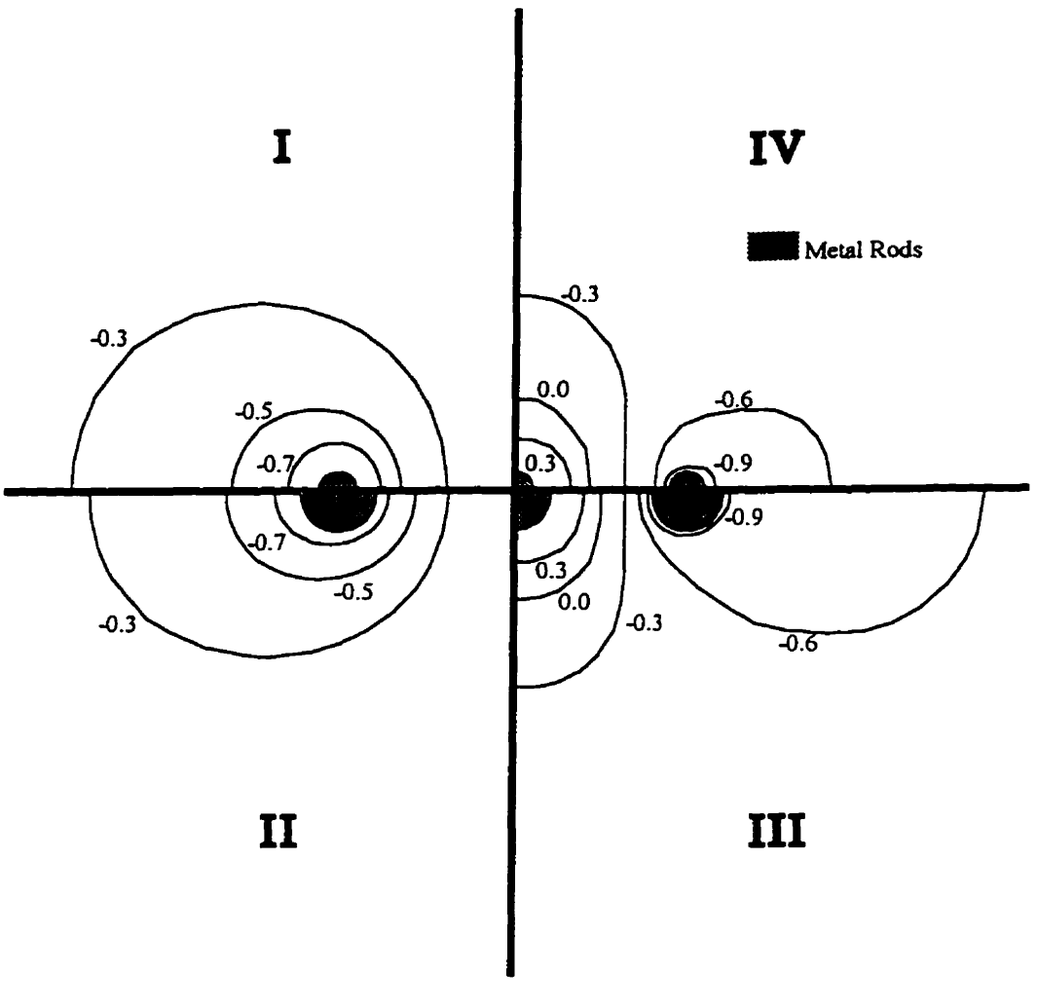

Figure 4-40. Equipotentials surrounding conventional rod probes with, (I) two rods, $S:D$=10, (II) two rods, $S:D$=5, (III) three rods, $S:D$=5, (IV) three rods, $S:D$=10.

The sample areas determined for two- and three-rod conventional probes with $S:D$ values of 5 and 10 are compared in Figure 4-41. Comparison of cases I and II shows that the sample area of two-rod probes is controlled by the separation of the rods; an increase in the rod diameter for a constant rod separation marginally improves the uniformity of the distribution of sensitivity within the sample area. For the dimensionless plots shown, the sample area of a two-rod probe with the same rod diameter as case I and half the separation can be envisioned as case II reduced in both directions by a factor of 2. In other words, as suggested by *Knight* [1992], the spatial sensitivity of a continuous-rod probe in a homogeneous K field can be defined uniquely for a given rod separation to diameter ratio. Case IV shows the results of adding a third rod to the probe shown as case I. The three-rod design has a drastically reduced the sample area. The size of the sample area of a three-rod probe is controlled by the rod separation as well; however, for a constant rod

separation, the sample area and uniformity of the probe sensitivity decrease with an increase in the rod diameter.

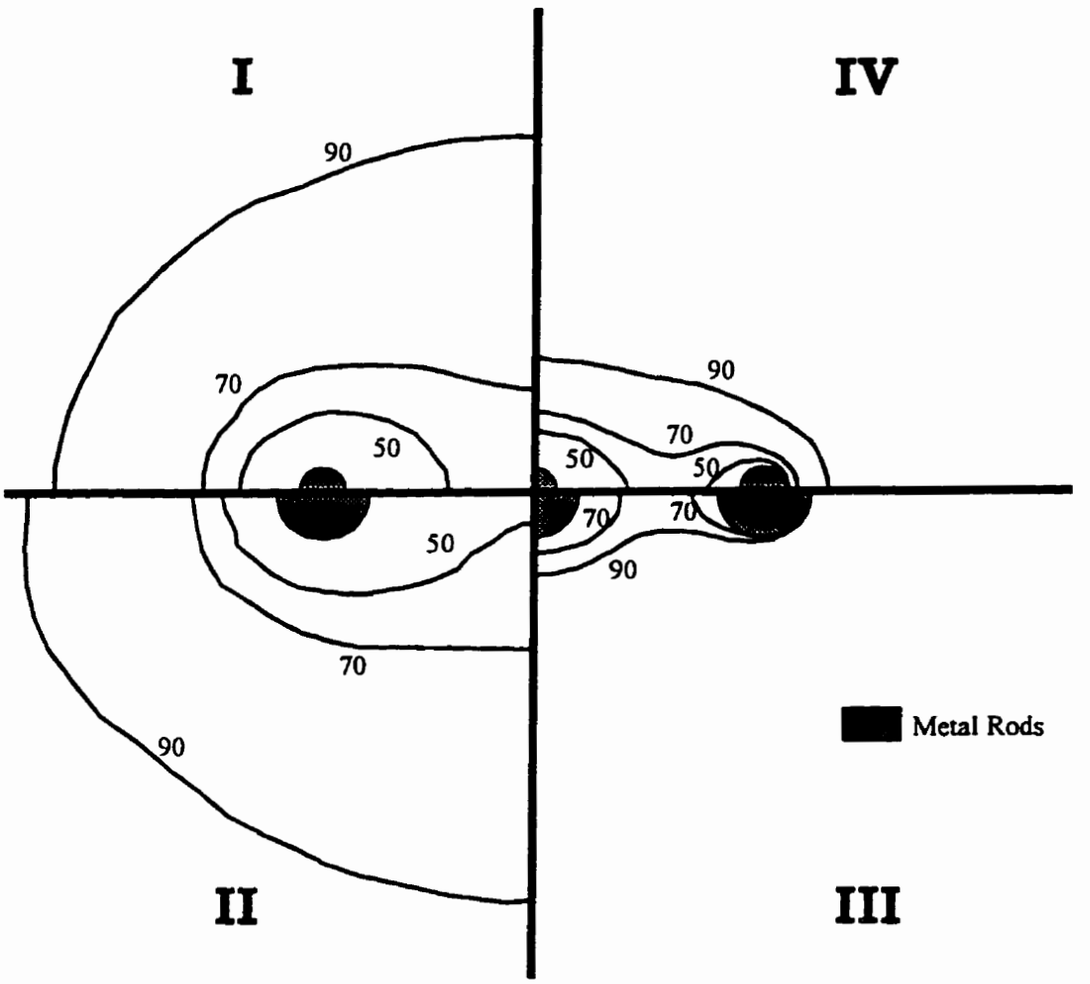

Figure 4-41. Percent sample areas of conventional rod probes with, (I) two rods, S:D=10, (II) two rods, S:D=5, (III) three rods, S:D=5, (IV) three rods, S:D=10.

4.7.3 Coated Continuous-rod Probes

Electrically resistive coatings can be applied to metal TDR rods to reduce signal losses through electrical conduction; these coating materials generally have low relative dielectric permittivities. Figure 4-3 shows the representative cross section of coated rod probes. The separation of the outer rods, S, the rod diameter, D, and the outer diameter of the rod coatings, G, define the probe configuration. For generality, the probe dimensions are described using nondimensional ratios of the separation and coating outer diameter to

the rod diameter, *S:D* and *G:D*, respectively. We use a relative dielectric permittivity for the coatings of 2.8, equal to that of PVC measured at 3 GHz [*Musil and Zacek*, 1986].

Annan [1977b] recognized that the equipotentials around uncoated two-rod probes, shown in Figure 4-40, conform to the bipolar coordinate system. He considered nonconcentric, circular air- or water-filled gaps with their boundaries placed on equipotentials. In the bipolar coordinate system, these gaps are perfectly in series with the soil and, therefore, do not change the shape of the equipotentials. As a result, the distribution of equipotentials around rods with nonconcentric circular gaps or coatings can be treated analytically using a bipolar coordinate transformation. Although the shape of the equipotentials is unchanged, if the relative dielectric permittivity of the gap or coating is fixed, the gradients throughout the system will be a function of the relative dielectric permittivity of the surrounding medium. Therefore, unlike conventional rod probes, the sampling area of coated continuous-rod probes will be a function of both the probe geometry and the dielectric permittivities of the medium and of the coating. For the analogy drawn to the one-dimensional vertical soil column discussed above, this is equivalent to placing a horizontal layer of a different material in the column; the resulting equipotentials will still be horizontal, but the gradients throughout the column will be a function of the hydraulic conductivities of both the added layer and the original medium. *Knight et al.* [1997] showed numerically that the analytical solution of *Annan* [1977b] closely approximates the apparent relative dielectric permittivity measured by rods with concentric coatings, demonstrating that concentric circular coatings are approximately in series with the soil. Similarly, thin coatings around three-rod probes approximately conform to the equipotentials shown in Figure 4-40, suggesting that the coatings on three-rod probes are also nearly in series with the soil.

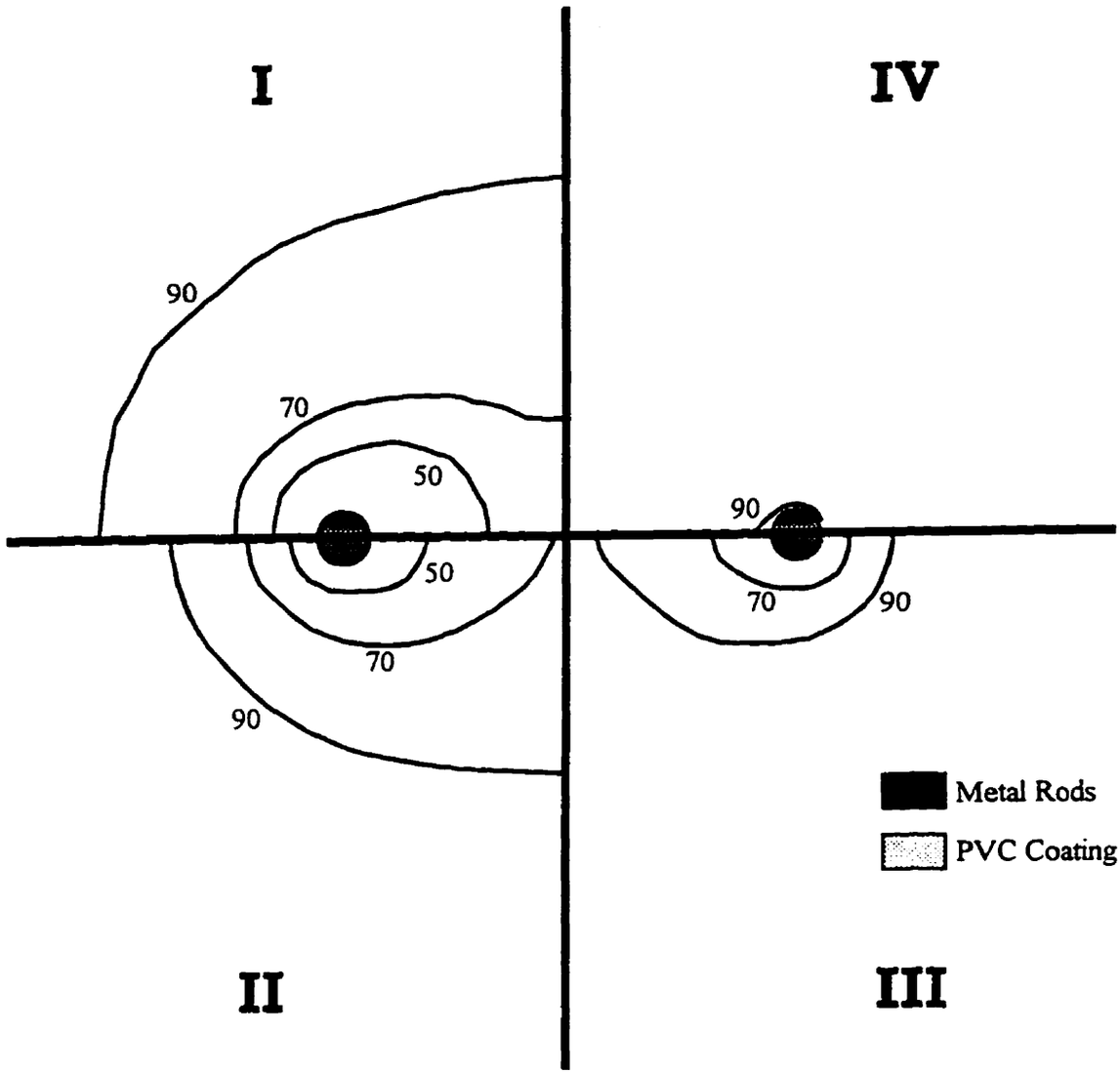

Figure 4-42. Percent sample areas of coated two-rod probes with, $S:D$=10, $G:D$=1.1 surrounded by a porous medium with a relative dielectric permittivities of (I) 5, (II) 7.5, (III) 12 and (IV) 18.

Figure 4-42 shows the sample areas of coated continuous-rod probes with an S:D of 10 and a G:D of 1.1 as a function of the relative dielectric permittivity of the surrounding medium. The gradient of the potential through the PVC coating increases with increases in the relative dielectric permittivity of the surrounding medium, increasing the relative weighting of the coating in the spatial average. As a result, the sample area for this configuration of coated continuous-rod probes is limited to a very small region adjacent to the rods for soil dielectric permittivities greater than 15, corresponding to a water content of 0.276 by Equation 1-3.

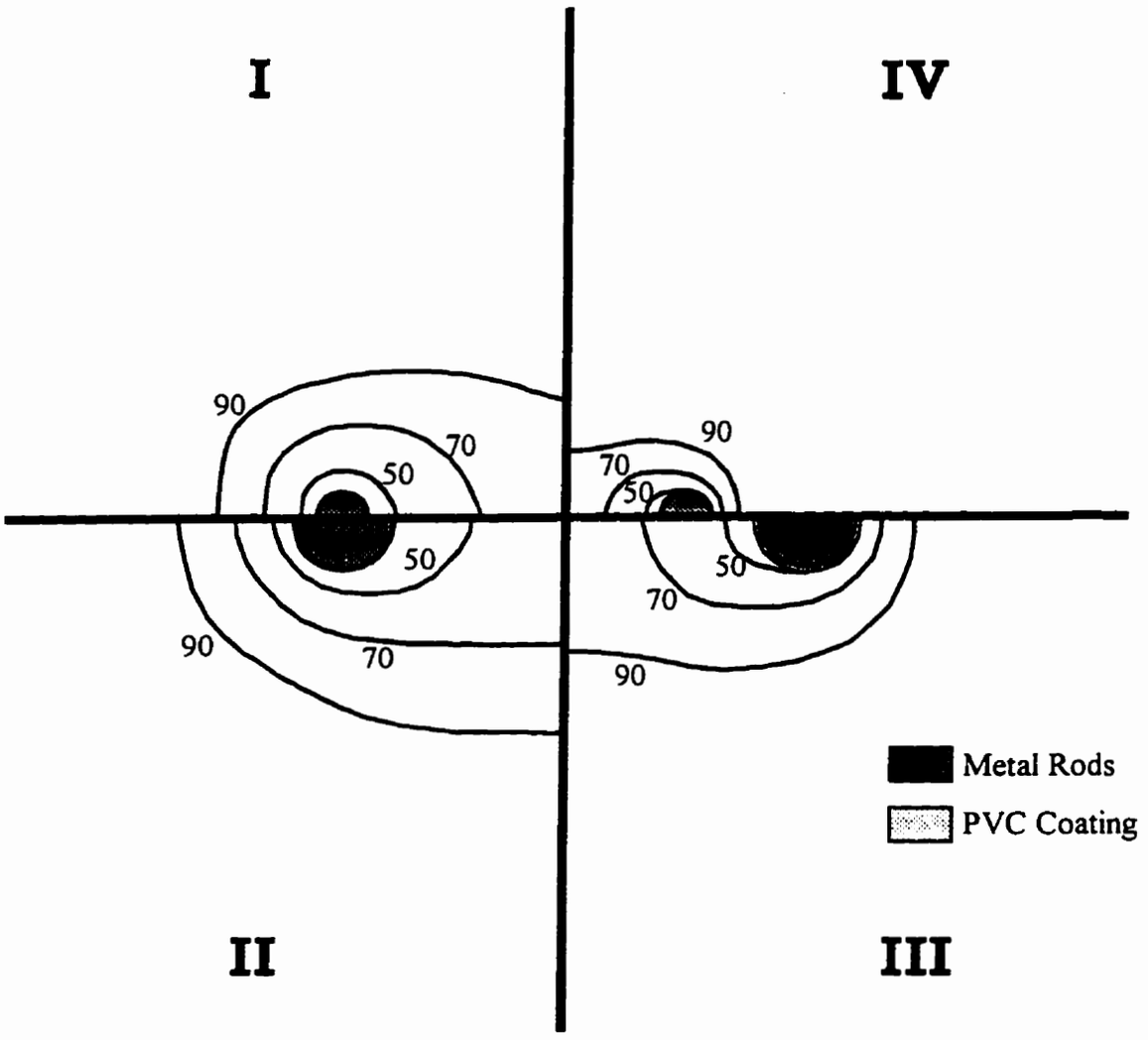

Figure 4-43. Percent sample areas of two-rod coated probes surrounded by a porous medium with a relative dielectric permittivity of 10 with, (I) *S*:*D*=10, *G*:*D*=1.1, (II) *S*:*D*=5, *G*:*D*=1.05, (III) *S*:*D*=5, *G*:*D*=1.1, (IV) *S*:*D*=5, *G*:*D*=1.1.

The configuration of a coated continuous-rod probe influences the impact of rod coatings on the sample area. Figure 4-43 shows four configurations of two-rod coated probes. Comparison of cases I and II shows that, as with the uncoated continuous-rod probes, the size of the sample area is controlled by the rod separation. Table 4-3 details the reduction in the sample area caused by the rod coatings. The area of surrounding medium sampled by each of the two-rod coated probe configurations shown on Figure 4-43 was calculated. The ratio of the size of this sample area to the size of the sample area for the same configuration with no coating present describes the relative area sampled by the coated probes. Comparison of the results for configurations I and II on Figure 4-43 show that for a constant rod separation, the use of larger diameter rods

has little influence on the impact of a coating of a given thickness. The sample area decreases with an increase in the thickness of the coating, as seen by comparing the results for configurations II and III on Figure 4-43. Notice that the dimensionless descriptions of configurations III and IV are identical, only the absolute size of the rods and coatings differ. These configurations differ from case I in the rod separation only. Comparison of the relative sample areas of configurations I, III and IV shows that, for a given rod diameter and coating thickness, a decrease in the rod separation causes a greater reduction in the relative sample area size. In summary, using thin coatings, high relative dielectric permittivity coating materials and a large rod separation will minimize the reduction in the sample area due to coatings on two-rod probes. These results must be balanced with the results for uncoated rods that showed that the probe sensitivity will be more uniformly distributed if the ratio of the rod separation to the rod diameter is small.

Nondimensional Parameters	Figure	Configuration(s)	Coated Area/ Uncoated Area
S:D=10, G:D=1.1, 2 rod	4-43	I	.32
S:D=5, G:D=1.05, 2 rod	4-43	II	.33
S:D=5, G:D=1.1, 2 rod	4-43	III,IV	.23
S:D=10, G:D=1.1, 3 rod	4-44	V	.41
S:D=5, G:D=1.05, 3 rod	4-44	VI	.92
S:D=5, G:D=1.1, 3 rod	4-44	VII,VIII	.54

Table 4-3. Effects of coatings on the sample area of continuous-rod TDR probes.

The impacts of the configuration of a three-rod coated probe on the sample area differ from those of two-rod probes. Figure 4-44 shows four configurations of three-rod coated probes; Table 4-3 includes the relative sample areas of these probes. As with uncoated three-rod probes, the sample size is controlled by the rod separation. Thin, high relative dielectric permittivity coatings will reduce the impact of coatings on the sample size. In contrast to the two-rod probes, the relative sample area of three rod probes increases with a decrease in the rod separation or an increase in the rod diameter.

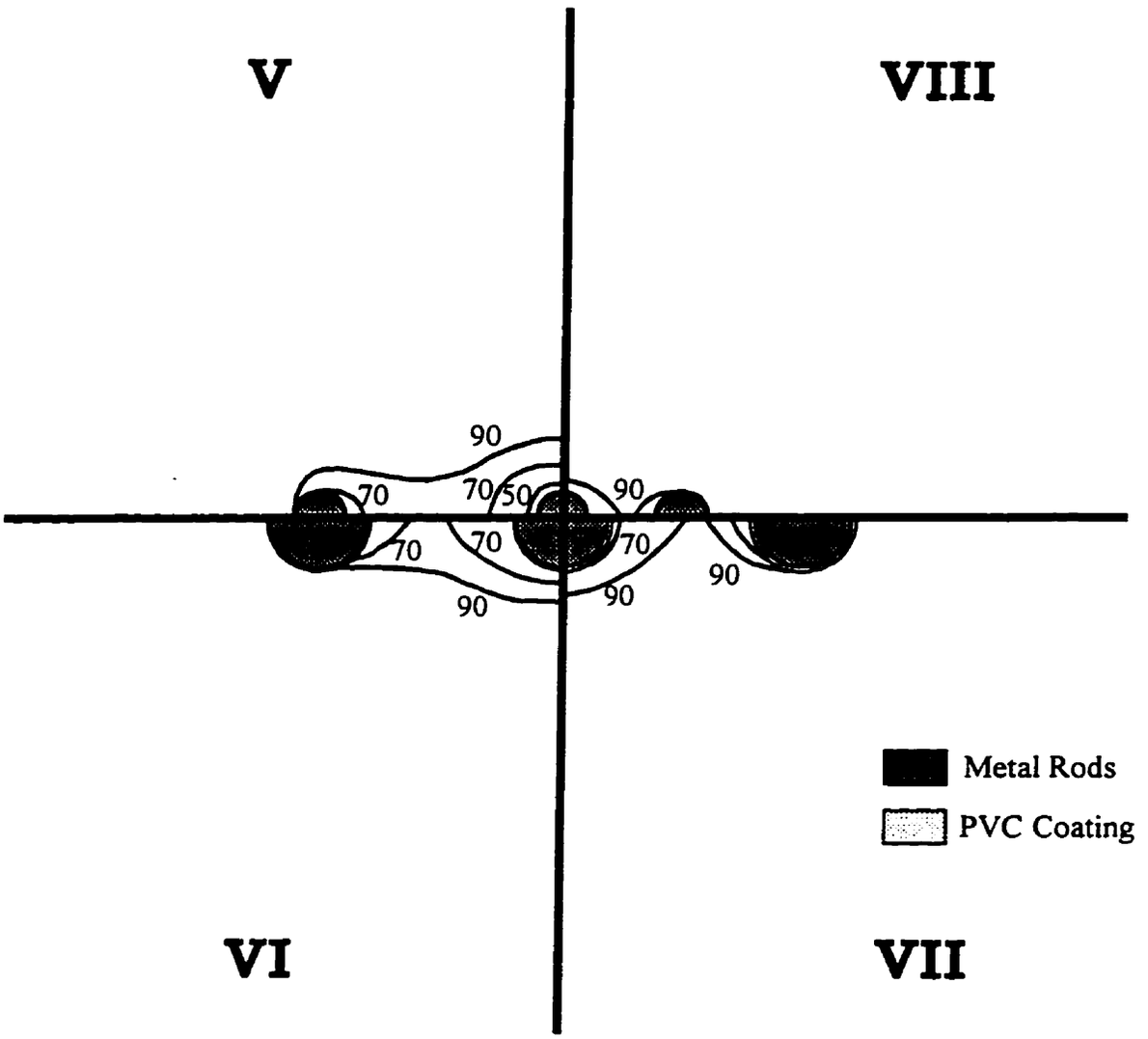

Figure 4-44. Percent sample areas of three-rod coated probes surrounded by a porous medium with a relative dielectric permittivity of 10 (I) *S*:*D*=10, *G*:*D*=1.1, (II) *S*:*D*=5, *G*:*D*=1.05, (III) *S*:*D*=5, *G*:*D*=1.1, (IV) *S*:*D*=5, *G*:*D*=1.1.

4.7.4 Hook et al. Multilevel Probe

Hook et al. [1992] designed a probe to measure the water content profile below a single surface location. The probe includes rectangular metal rods and a nonmetallic probe body housing remotely-activated shorting diodes. As shown in Figure 4-3, the height, H, width, W, and separation, S, of the rods define the representative cross section of the probe. A unitless description of the probe dimensions as ratios of the rod height to the rod width, $H:W$, and the rod separation to the rod width, $S:W$, is used here. The probe body is assumed to have a relative dielectric permittivity equal to that of PVC.

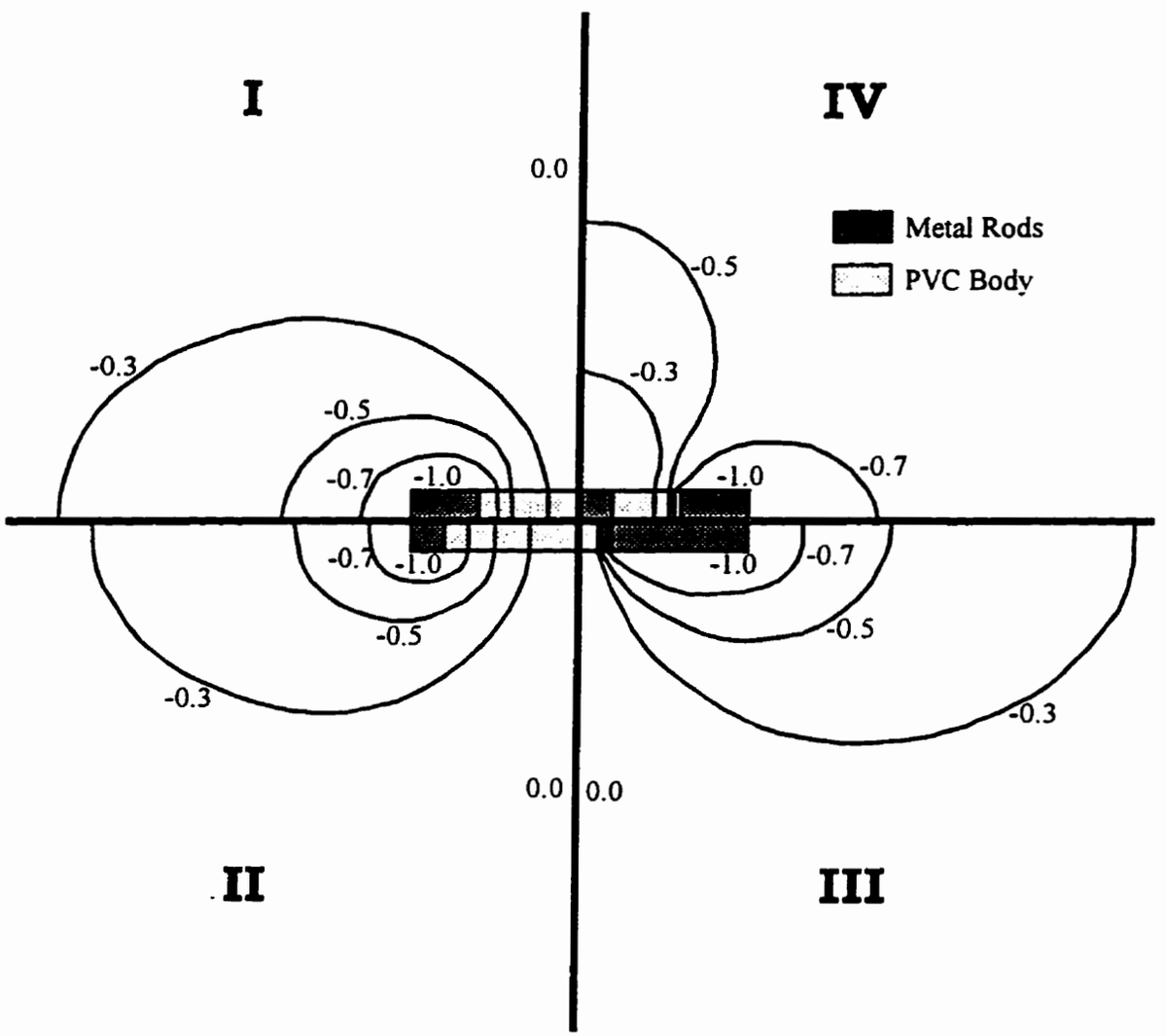

Figure 4-45. Equipotentials surrounding *Hook et al.* [1992] probes with, (I) two rods, $H:W$=1, $S:W$=4, (II) two rods, $H:W$=2, $S:W$=9, (III) two rods, $H:W$=0.5, $S:W$=1.5, (IV) three rods, $H:W$=1, $S:W$=4 if the nonmetallic probe body was not present.

Figure 4-45 shows the equipotentials that would surround the metallic rods used in four configurations of the *Hook et al.* [1992] probe placed in a homogeneous porous medium if the rods were inserted into the medium with no nonmetallic probe body present. The shapes of the equipotentials are similar to those around the circular rods shown in Figure 4-40. However, the equipotentials in the region between the rectangular rods are straight lines, parallel to the edges of the rods. The boundaries of the probe body are perpendicular to these equipotentials; therefore, relative to the geometry of the probe, the probe body is placed in parallel with the surrounding medium. The geometry of this probe is analogous to a vertical column undergoing one dimensional, steady-state saturated flow that includes a vertical soil layer with a different hydraulic conductivity. The addition of this layer will not change the distribution of equipotentials throughout the column. Therefore, the gradient of the potential will be spatially uniform, leading to a constant spatial weighting and an arithmetic averaging of the hydraulic conductivities. Furthermore, this result applies regardless of the hydraulic conductivities of the layer and of the background material. As a result, the sample area of the probe is independent of the relative dielectric permittivities of the probe body and the surrounding porous medium.

The sample area of a *Hook et al.* [1992] probe is controlled by the configuration of the probe. The sample areas of four designs with a constant overall probe size are shown in Figure 4-46. Two-rod probes have much larger sample areas than the three-rod design. Among these two-rod designs, the sample area increases with decreases in the width of the rods. Three other two-rod designs were analyzed to determine which design parameters controlled the size of the sample area. Configurations I and V, shown on Figure 4-47, have the same rod separation and height with different rod widths; configurations I and VII differ only in their rod separations. Direct comparison of the sample areas of these designs shows that the rod separation controls the sample size; changes in the rod width only introduce slight changes in the distribution of probe sensitivity. Similarly, comparison of configurations VI and VII shows that the sample area is not highly sensitive to the rod height. In summary, to maximize the sample area while maintaining a reasonable distribution of probe sensitivity, two-rod probes with large rod separations and small rod widths and heights should be used.

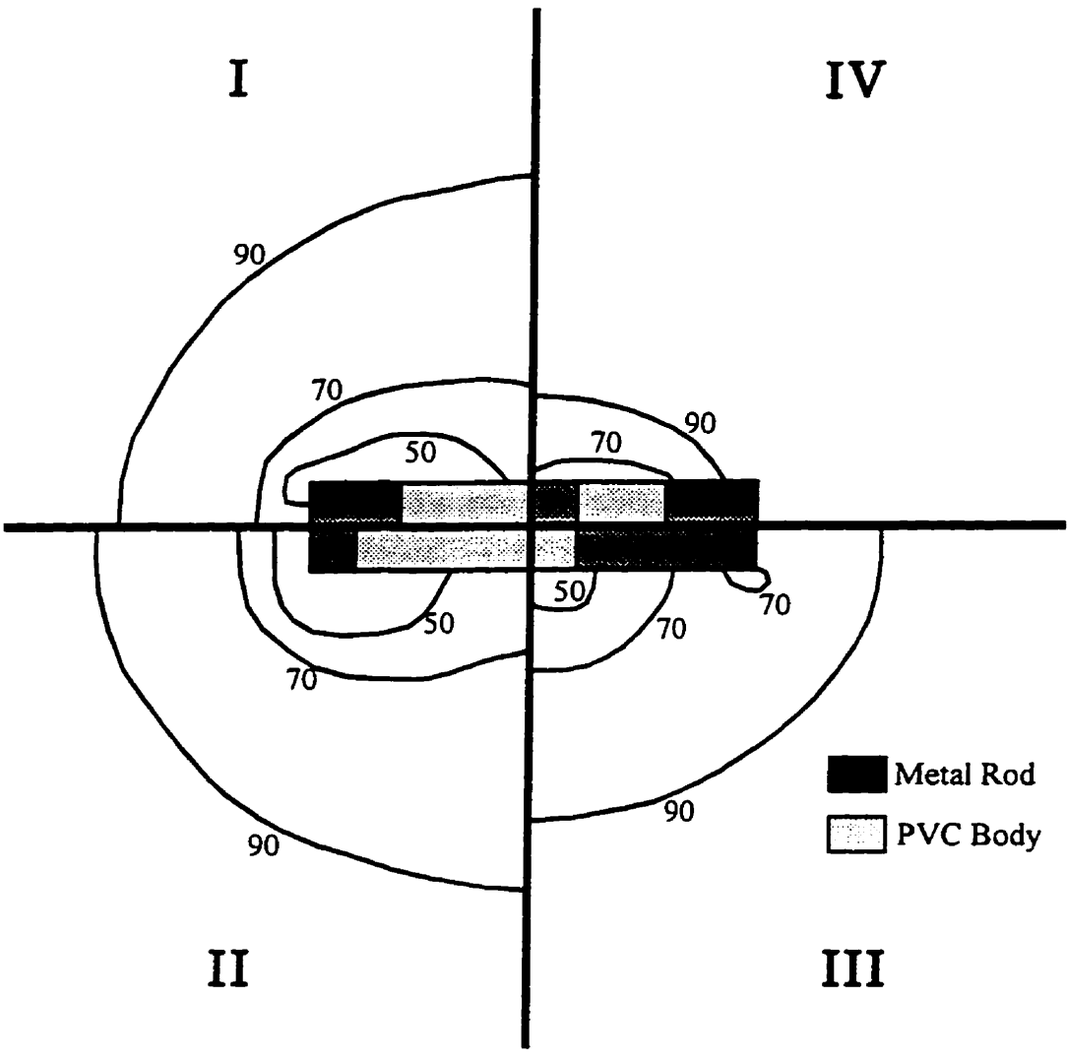

Figure 4-46. Percent sample areas of *Hook et al.* [1992] probes surrounded by a porous medium with a relative dielectric permittivity of 10 with, (I) two rods, $H:W$=1, $S:W$=4, (II) two rods, $H:W$=2, $S:W$=9, (III) two rods, $H:W$=0.5, $S:W$=1.5, (IV) three rods, $H:W$=1, $S:W$=4.

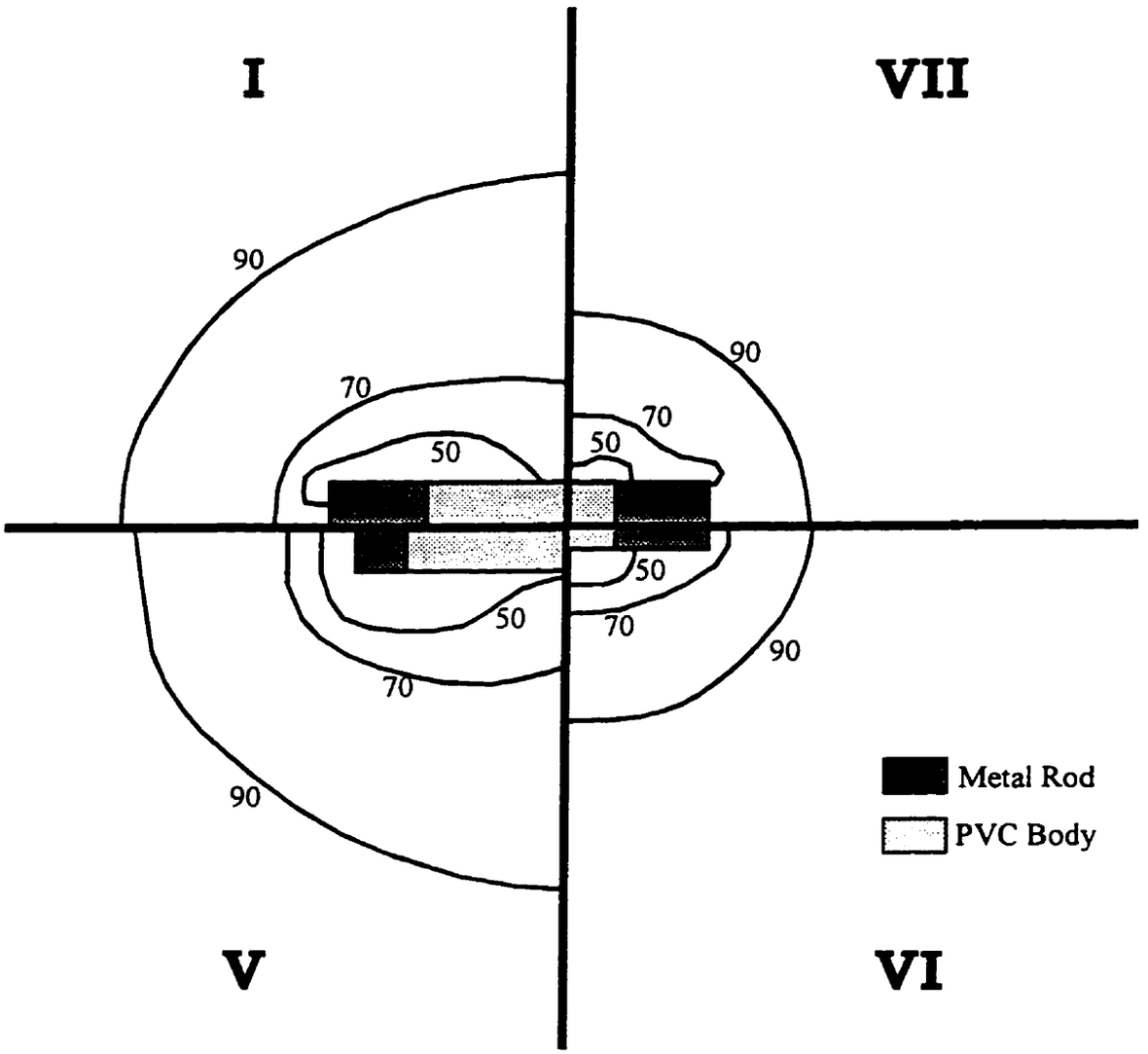

Figure 4-47. Percent sample areas of *Hook et al.* [1992] probes surrounded by a porous medium with a relative dielectric permittivity of 10 with, (I) two rods, H:W=1, S:W=4, (V) two rods, H:W=2, S:W=8, (VI) two rods, H:W=1, S:W=2, (VII) two rods, H:W=2, S:W=4.

4.7.5 Alternative Multilevel TDR Probe

Like coated continuous-rod probes, the alternative multilevel TDR probe places the probe materials approximately in series with the surrounding medium. As a result, this probe and other designs that include coatings on the metal rods should consider the results presented for coated continuous-rod probes. Specifically, two-rod designs should be used rather than three-rod designs. Thin, high relative dielectric permittivity gaps and access tubes will increase the sample size of the probe in the target region. Probe

sensitivity above the target region will be minimized by using small diameter wires surrounded by materials with low dielectric permittivities. Finally, as with a neutron probe, the sample size of the alternative multilevel probe will be a function of the water content of the medium, decreasing with an increase in the water content.

4.7.6 Redman and D'Ryck Multilevel Probe

Redman and D'Ryck [1994] designed a probe to measure the water content profile. The probe is comprised of a PVC access tube with two metal rods attached to its exterior, as shown in Figure 4-4. The probe dimensions include the inner diameter, *ID*, and outer diameter, *OD*, of the access tube, the rod diameter, *D*, and the angle between the rods on the surface of the access tube, *a*. Nondimensional parameters based on the ratios of the *ID* and *OD* to the rod diameter are used to describe the probe designs here.

The solid lines on Figure 4-48 show the sample areas of the probe configuration presented by *Redman and D'Ryck* [1994] and of a configuration with a smaller angular separation of the metal rods, both surrounded by a medium with a relative dielectric permittivity of 10. The sample area is controlled by the separation of the metal rods, which is a function of the outer diameter of the access tubes and the angular separation of the rods. The probe sensitivity is concentrated in close proximity to the rods. For larger rod separations, much of the probe sensitivity becomes restricted to two nonoverlapping areas. The figure also includes the sample area of configuration 1 surrounded by a porous medium with a relative dielectric permittivity of 25, showing that the sample area is not highly sensitive to the relative dielectric permittivity of the medium. The sample area is also insensitive to the rod diameter and the inner diameter of the access tube (not shown).

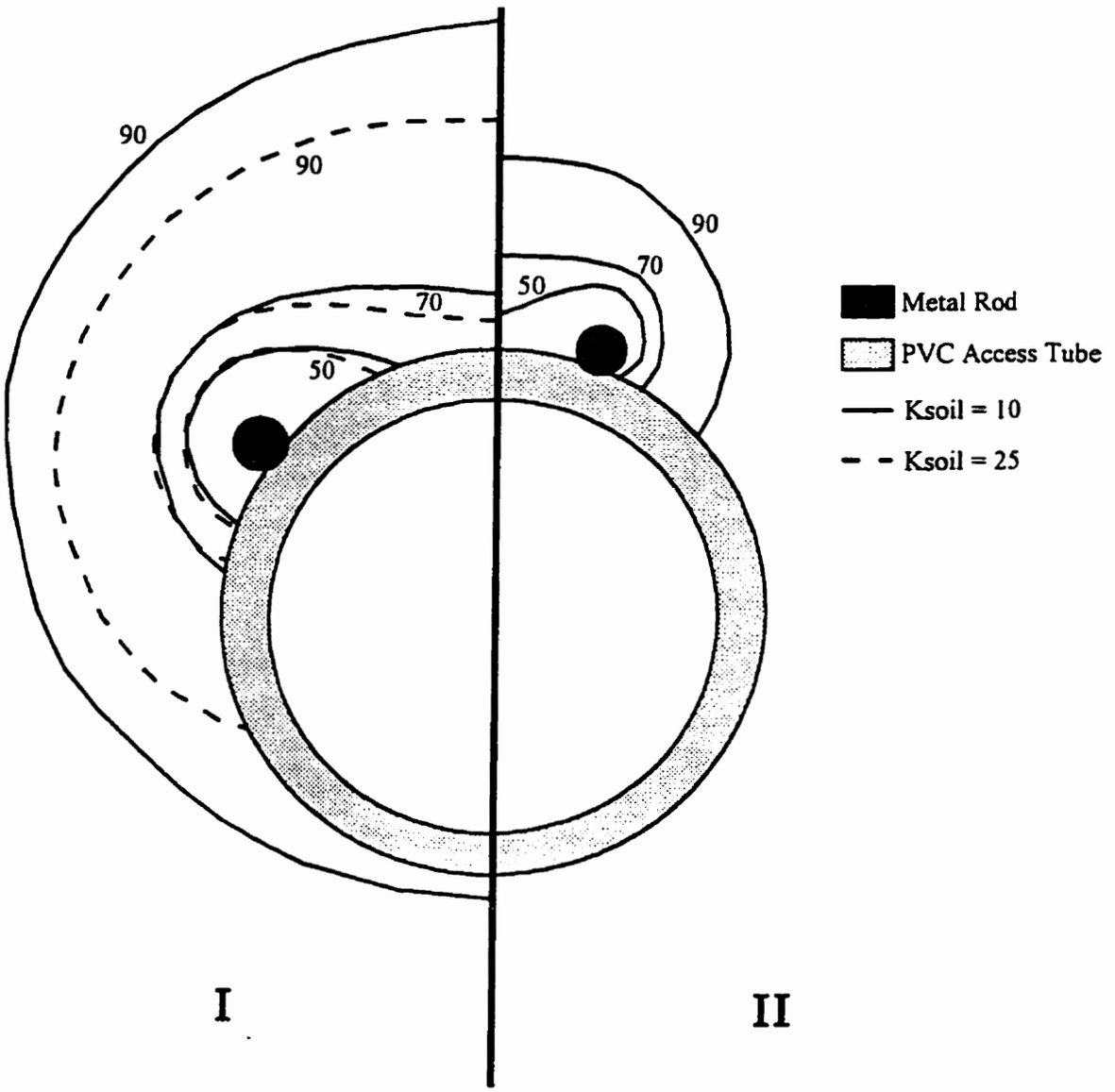

Figure 4-48. Percent sample areas of *Redman and DeRyck* [1994] probes with (I) an *OD:D* of 11.1, *ID:D* of 13.4 and *a* of 110 degrees surrounded by a porous medium with a relative dielectric permittivity of 10 (solid line) or a K_{soil} of 25 (dashed line), (II) an *OD:D* of 11.1, *ID:D* of 13.4 and *a* of 45 degrees surrounded by a porous medium with a relative dielectric permittivity of 10.

4.7.7 Selker et al. Surface Probe

Selker et al. [1993] designed a probe to measure the water content at the ground surface. The probe is comprised of metal rods embedded in an acrylic body. As shown in Figure 4-6, in cross section, the probe body has a height, *Hb*, and a width, *Wb*. The rectangular rods have a width, *W*, a height, *H*, and are separated by a distance, *S*. The height of the rods extending out of the base, into the soil, is H_o. Unitless dimensions relative to the width of the rods are used to describe the probe dimensions. Acrylic (Plexiglas) has a relative dielectric permittivity of 2.7 at $3x10^8$ Hz [*von Hippel*, 1954].

In a homogeneous medium, the equipotentials around the rectangular rods without any surrounding probe materials would be the same as those shown in Figure 4-45. The probe design described by *Selker et al.* [1993] had an H_o:H of 0.5. Taking the porous medium to be homogeneous and the probe body to be large compared to the rod separation, the rods for this probe lie on the boundary between two uniform half-spaces. This boundary is perpendicular to the equipotentials around the rods; therefore, the soil and probe body are in parallel with respect to the probe geometry and the measured relative dielectric permittivity will be the arithmetic average of the K of the probe materials and K_{soil}. Furthermore, the sample area will be independent of the relative dielectric permittivities of the porous medium and the material used for the probe body. Numerical analysis has shown that the sample areas of probes with fully embedded rods (H_o = 0.0) such as case II on Figure 4-49 are insensitive to the relative dielectric permittivities of the medium and probe body as well.

Figure 4-49 compares the sample areas of two probes with consistent design parameters, differing only in the fraction of the rod extending into the soil. Although the sample area of the probes is marginally reduced by fully embedding the rods in the probe body, the advantage of minimizing disturbance to the soil will outweigh this result for many applications. The results also show the size of the probe body required to isolate the probe from the influence of the conditions above the ground surface.

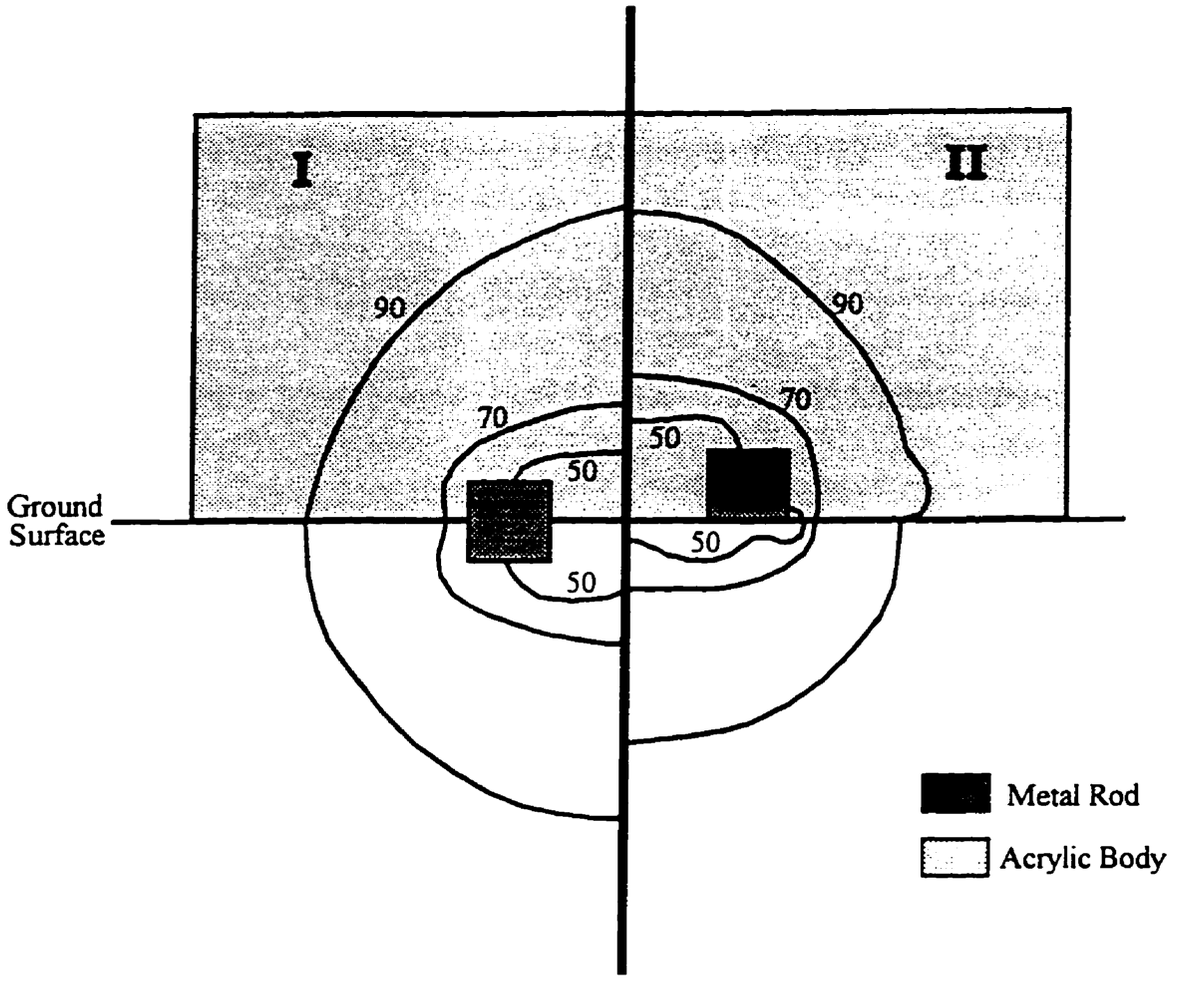

Figure 4-49. Percent sample areas of *Selker et al.* [1993] probes above a porous medium with a relative dielectric permittivity of 10 with, (I) two rods, H:W=1, S:W=4, H_o:W=0.5, Wb:W=7, Hb:W=3.5 (II) two rods, H:W=1, S:W=4, H_o:W=0.0, Wb:W=7, Hb:W=3.5.

The sample areas of nonintrusive probes (H_o = 0.0) with reduced rod heights or increased rod separations were also investigated. Comparison of case II on Figure 4-49 and case III on Figure 4-50 shows that reducing the height of the rods has no effect on the sample area or the distribution of probe sensitivity in the medium; however, this design allows for the use of a smaller probe body. Case IV on Figure 4-50 is identical to case II on Figure 4-49 except that the separation of the rods has been increased slightly. As a result, the sample volume has increased, but the probe sensitivity has become concentrated beneath the rods and a larger probe body is required.

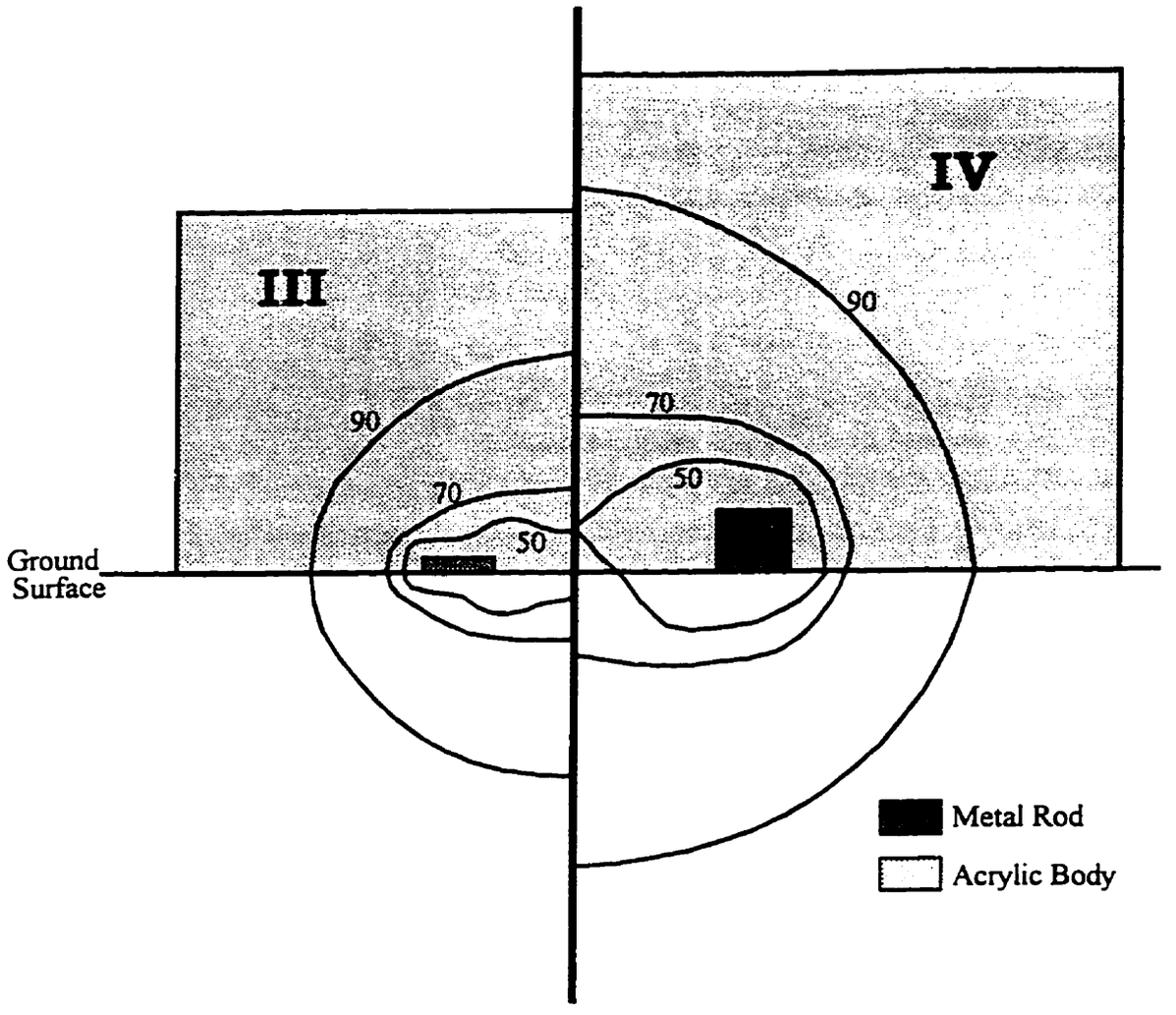

Figure 4-50. Percent sample areas of *Selker et al.* [1993] probes above a porous medium with a relative dielectric permittivity of 10 with, (III) two rods, H:W=0.25, S:W=4, H_o:W=0.5, Wb:W=7, Hb:W=3.5 (IV) two rods, H:W=1, S:W=5, Ho:W=0.0, Wb:W=7, Hb:W=3.5.

4.7.8 White and Zegelin Probe

White and Zegelin [1992] designed a probe to measure the water content at the ground surface based on a semicoaxial design. Figure 4-5 shows a representative cross section of the probe. The outer diameter of the semicircular shield, S, diameter of the semicircular rod, D, shield thickness, t, and length of wings extending from the body, W, define the probe configuration. Unitless dimensions are defined relative to the diameter of the central rod. Beeswax, with a relative dielectric permittivity of 2.4 at $1x10^8$ Hz [*von Hippel*, 1954], fills the gap between the rod and the shield.

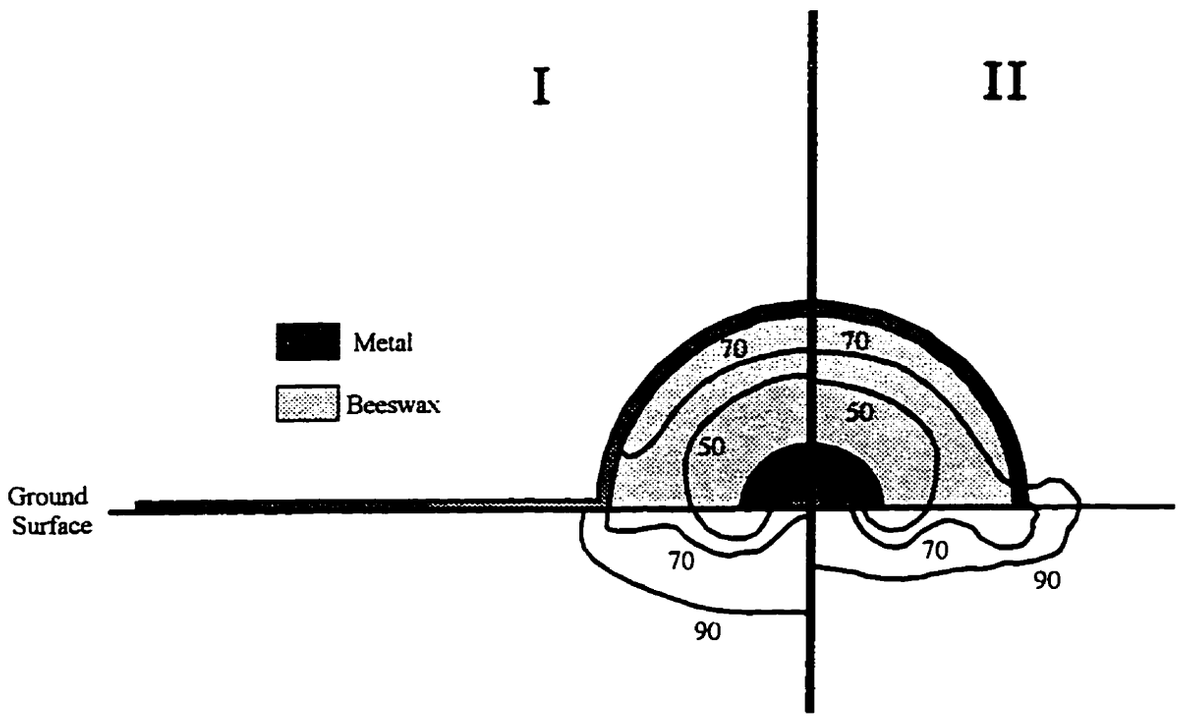

Figure 4-51. Percent sample areas of *White and Zegelin* [1992] probes above a porous medium with a relative dielectric permittivity of 10 with, (I) $S:D$=3, $W:D$=3.5, $t:D$=0.2, (II) $S:D$=3, $W:D$=0.0, $t:D$=0.2

The sample area of the probe configuration reported by *White and Zegelin* [1992] is shown as case I on Figure 4-51. The sample area in the porous medium is confined to the region beneath the shield, only extending a short distance along the wings. Removing the wings (case II) leads to a reduced sample size that is concentrated at the edges of the central rod. Maintaining a constant shield inner radius, the size of the sample area is unchanged by reducing the rod radius (case III, Figure 4-52). However, the smaller rod results in a more even distribution of probe sensitivity in the porous medium. A similar design, using a rectangular rod and shield is shown as case IV; this probe has a slightly smaller sample area, but does not require wings.

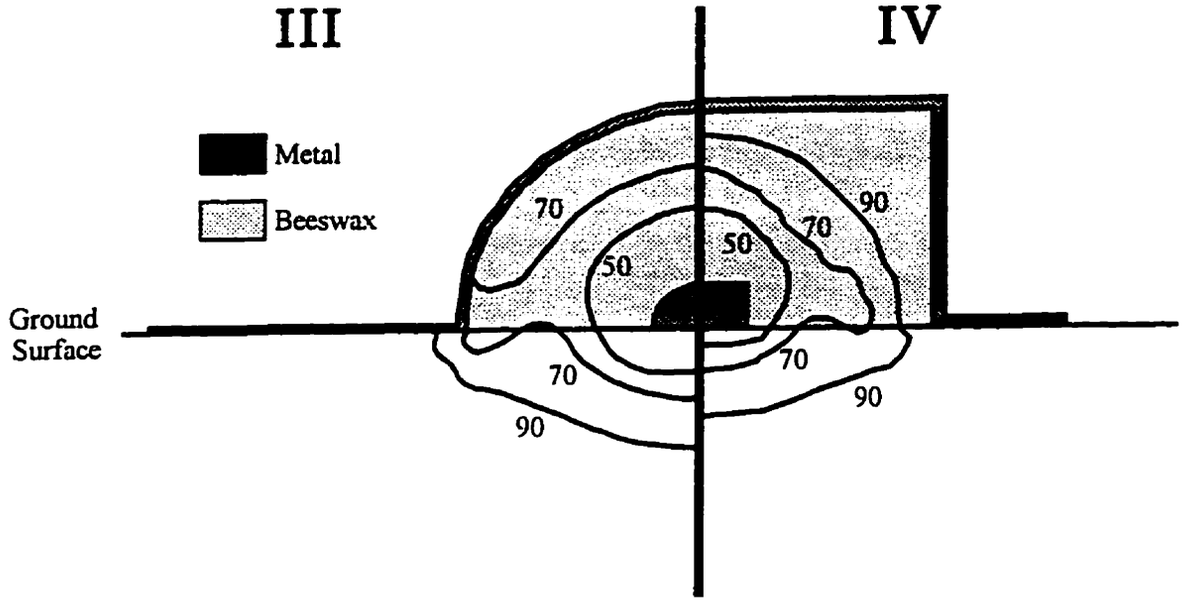

Figure 4-52. Percent sample areas of *White and Zegelin* [1992] probes above a porous medium with a relative dielectric permittivity of 10 with, (III) S:D=5, W:D=2.5, t:D=0.2, (IV) rectangular probe, S:D=5, W:D=2, t:D=0.2

4.7.9 Summary and Conclusions

The numerical analysis of *Knight et al.* [1997] and the definition of spatial sensitivity of *Knight* [1992] combine to provide a powerful tool for designing probes for specific water content measurement objectives. The results of applying this analysis to published alternative probes has shown the strengths and limitations of each design as well as identifying design changes to improve the probe responses.

The sample area of two-rod conventional probes is controlled by the separation of the rods; an increase in the rod diameter with a constant rod separation only causes a slight increase in the sample area and a minor improvement in the distribution of sensitivity within the sample area. The addition of a central rod drastically reduces the sample area. For three-rod probes, an increase in the rod diameter for a given rod separation reduces the sample area.

The influence of the nonmetallic components of alternative probes on the sensitivity of the sample area to the relative dielectric permittivity of the surrounding porous medium has been explained. Coated continuous-rod probes and the alternative multilevel probe presented in this chapter place the probe materials in series with the porous medium relative to the probe geometry. As a result, these probe designs have sample areas that vary with the relative dielectric permittivity of the surrounding medium. Even PVC coatings with a thickness as small as one twentieth of the rod diameter restrict the sample area of coated continuous-rod probes to the region immediately adjacent to the coatings for a soil with a volumetric water content greater

than 0.28. The presence of coatings has a greater impact on the sample area of coated two-rod probes than on the sample area of three-rod probes; but, coated two-rod probes still have larger sample areas than coated three-rod designs. For two-rod probes, the impact of coatings on the sample area decreases for probes with thin coatings, high relative dielectric permittivity coating materials, and large rod separations. Decreased coating thicknesses, increased relative dielectric permittivities of the coating material, decreased rod separations and increased rod diameters minimize the impact of coatings on the sample area of coated three-rod probes. These results extend to other probe designs that include coatings on the metal rods.

The sample area of a *Hook et al.* [1992] probe with uncoated metal rods is not a function of the dielectric permittivity of the medium or the material used for the probe body. The separation of the metal rods controls the size of the sample area; reducing the rod height and width improves the distribution of sensitivity within the sample area. Similarly, the separation of the metal rods on the surface of the access tubes controls the sample area of *Redman and DeRyck* [1994] probes.

The sample areas were calculated for two alternative probes designed to measure the soil water content at the ground surface [*White and Zegelin*, 1992; *Selker et al.*, 1993]. Nonintrusive configurations of these probes have similar sample areas, concentrated beneath the probe, very close to the ground surface. The size of the probe body required to isolate the *Selker et al.* [1993] probe from the air above the soil must be altered for each probe configuration; the coaxial design of *White and Zegelin* [1992] only requires the inclusion of short wings on the ground surface to eliminate the influence of the conditions above the soil surface. The size of the sample area of the *Selker et al.* [1993] probe increases with an increase in the rod separations; however, the resulting sample area becomes focused in two regions beneath the rods. Increasing the diameter of the outer shield increases the sample area of the *White and Zegelin* [1992] probe; decreasing the diameter of the central rod improves the distribution of probe sensitivity within the sample area.

4.8 *Sensitivity of TDR Probes*

4.8.1 Numerical Determination of Probe Sensitivity

TDR probes must perform three functions: connection to a coaxial line from a cable tester, transmission of a voltage pulse through a sample, and termination at the end of the probe. The following analysis focuses solely on the influence of the probe design on the pulse propagation through the sample.

Most of the published alternative probe designs include nonmetallic components. These components commonly have a relative dielectric permittivity that contrasts strongly with that of the surrounding soil. Given that these materials are located within the sample volume of the probes, the measured apparent relative dielectric permittivity will be some average of the relative dielectric permittivities of the probe materials and the soil.

In this study, the numerical analysis of *Knight et al.* [1997] is used to determine the apparent relative dielectric permittivity, K_m, that a representative cross section of an alternative probe would measure under a wide range of relative dielectric permittivities of the surrounding porous medium. These results are used to construct calibration curves of calculated values of K_m versus given values of K_{soil} for several configurations of each alternative probe. Differences in the calibration curves among configurations of a single probe demonstrate the sensitivity of the response of that probe to changes in each design parameter. In addition, these calibration curves are related to the probe sensitivity as defined in Chapter 2.

The numerically determined calibration curves are compared with published laboratory or field calibrations where available. In addition, the numerical and direct calibrations are compared with analytical solutions if applicable. These comparisons are limited by the ability to describe the probe with a single cross section. Variations in the probe geometry, typically at the top of the probe, and end effects at the termination of the probe cannot be modeled with this approach. Recommendations are made based on the modeling results with the assumption that the optimization of an alternative probe will require a minimization of the impacts of these other, poorly understood influences.

4.8.2 Continuous-rod Probes

Standard continuous-rod probes do not have any nonmetallic probe materials in the sample volume; therefore, the apparent relative dielectric permittivity of a representative cross section of conventional rods in a homogeneous medium is equivalent to the relative dielectric permittivity of that medium, regardless of the probe configuration. Each alternative probe calibration curve includes the response of continuous-rod probes for comparison.

4.8.3 Coated Continuous-rod Probes

Figure 4-53 shows the relative dielectric permittivity that would be measured with coated continuous-rod probes as a function of the relative dielectric permittivity of the surrounding medium. Applying thinner coatings increases the measured relative dielectric permittivities. Two-rod probes have greater responses than three-rod designs. An increase in the ratio of the rod separation to the rod diameter (S:D) with a constant coating to rod diameter ratio (G:D) gives a response that more closely approximates the response of uncoated continuous-rod probes for two-rod probes; a decreased S:D improves the response of three-rod designs. All of the coated probe configurations show a nonlinear response to changes in K_{soil}. This nonlinearity results from the placement of the probe materials in series with the soil relative to the probe geometry.

A direct calibration of coated continuous-rod probes has not been presented in the literature. However, as discussed above, *Knight et al.* [1997] demonstrated that the numerical analysis of the response of coated continuous-rod probes agrees with an analytical solution presented by *Annan* [1977b].

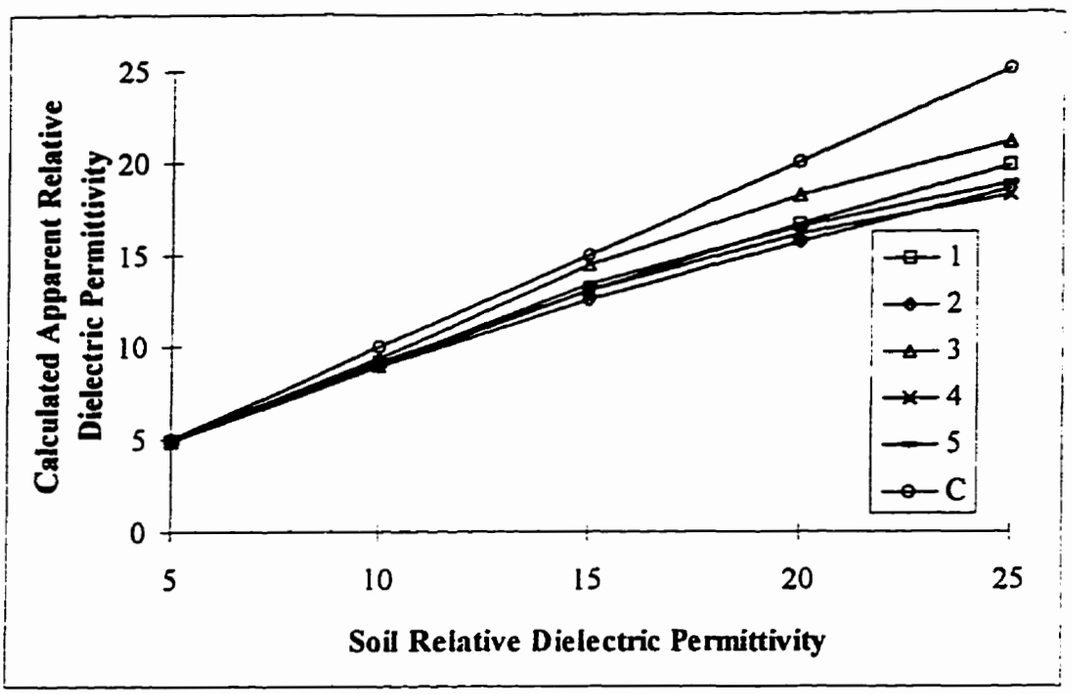

Figure 4-53. Numerically determined calibration curves for coated continuous-rod probes. (1) *S:D*=10, *G:D*=1.1, 2 rods; (2) *S:D*=5, *G:D*=1.1, 2 rods; (3) *S:D*=5, *G:D*=1.05, 2 rods, (4) *S:D*=10, *G:D*=1.1, 3 rods; (5) *S:D*=5, *G:D*=1.1, 3 rods; and (C) conventional metal rod probe.

4.8.4 Alternative Multilevel TDR Probe

Calibration curves for the alternative multilevel TDR probe described above are shown in Figure 4-54. The base case has water-filled tubes, an *S:D* of 5, a *G:D* of 1.83, and a *W:D* of 2.8, representing 1/2 inch ID (1.27 cm) SCH80 PVC access tubes with 0.76 cm OD metal rods. Filling the annulus between the rods and the access tubes with air rather than water causes a drastic reduction in the apparent relative dielectric permittivity measured by the probe. A thinner-walled probe with a *G:D* of 2.08, representing 1/2 inch (1.27 cm) SCH40 PVC access tubes, performs better than the base case probe. Increasing the *S:D* also improves the probe response. All configurations show a nonlinear response to changes in the soil relative dielectric permittivity because the probe materials are placed in series with the surrounding porous medium.

The apparent relative dielectric permittivities measured with the alternative multilevel probe are plotted as a function of the soil relative dielectric permittivity determined with the conventional rods on Figure 4-54 as well. The relative dielectric permittivities measured with the probe with water-filled access tubes have been presented previously on Figure 4-10. The relative dielectric permittivity was also calculated from waveforms collected with the probe with air-filled access tubes during the field testing of the probe. The

numerical analysis correctly predicts the drastic reduction in apparent relative dielectric permittivity measured with air-filled access tubes. It is unclear why the response of the water-filled probe is not as well represented by the numerical model. Under low water content conditions, the discrepancy between the measured and modeled relative dielectric permittivites may be due to inaccuracies in the determination of travel times from the alternative probe waveforms; these inaccuracies are exacerbated by the short travel times measured for the short rod lengths (20 cm) under low water content conditions.

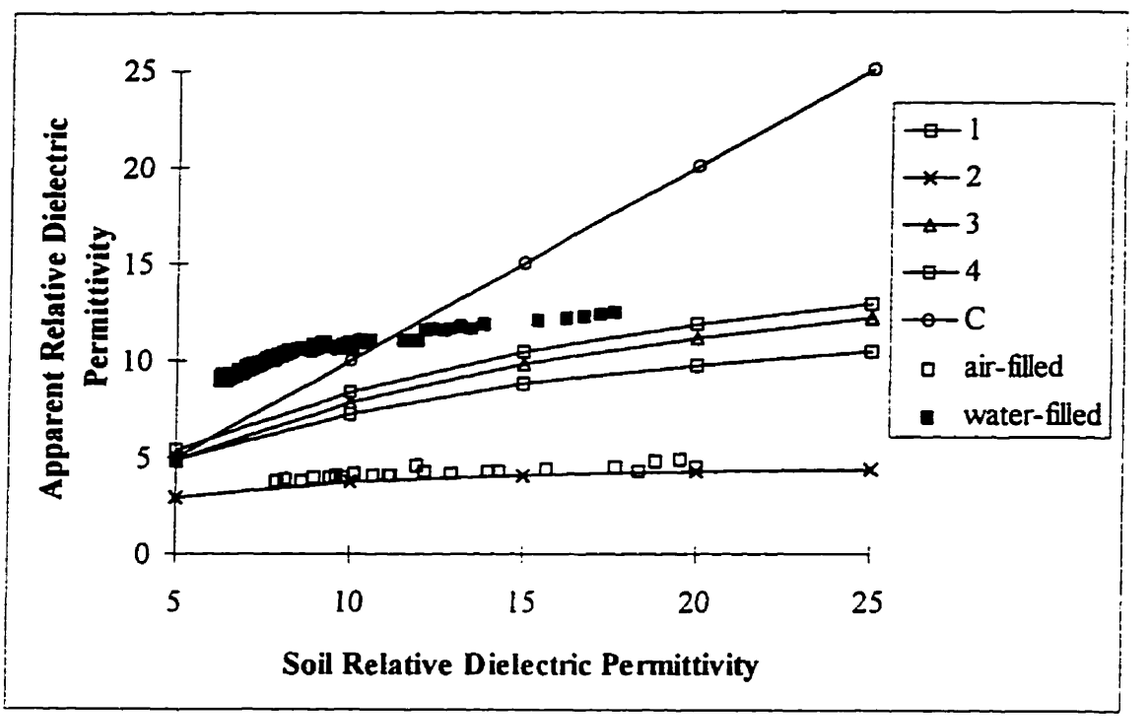

Figure 4-54. Numerically determined and field-measured calibration curves for our multilevel probe, (1) *S*:*D*=5, *G*:*D*=1.35, *W*:*D*=2.08, water-filled access tubes; (2) *S*:*D*=5, *G*:*D*=1.35, *W*:*D*=2.08, air-filled access tubes; (3) *S*:*D*=10, *G*:*D*=1.35, *W*:*D*=2.08, water-filled access tubes; (4) *S*:*D*=5, *G*:*D*=1.53, *W*:*D*=2.08, water-filled access tubes; (C) conventional metal rod probe; (open squares) field measurements with air-filled access tubes; and (filled squares) field measurement with water-filled access tubes.

4.8.5 Redman and D'Ryck Multilevel Probe

Calibration curves calculated for the *Redman and DeRyck* [1994] probe, Figure 4-55, show a linear response to changes in K_{soil}. The base case probe has an *ID*:*D* of 11.1, an *OD*:*D* of 14.27, and rods separated

by an angle, a, of 110 degrees. The probe response is insensitive to the rod diameter, angle of separation and thickness of the access tube walls.

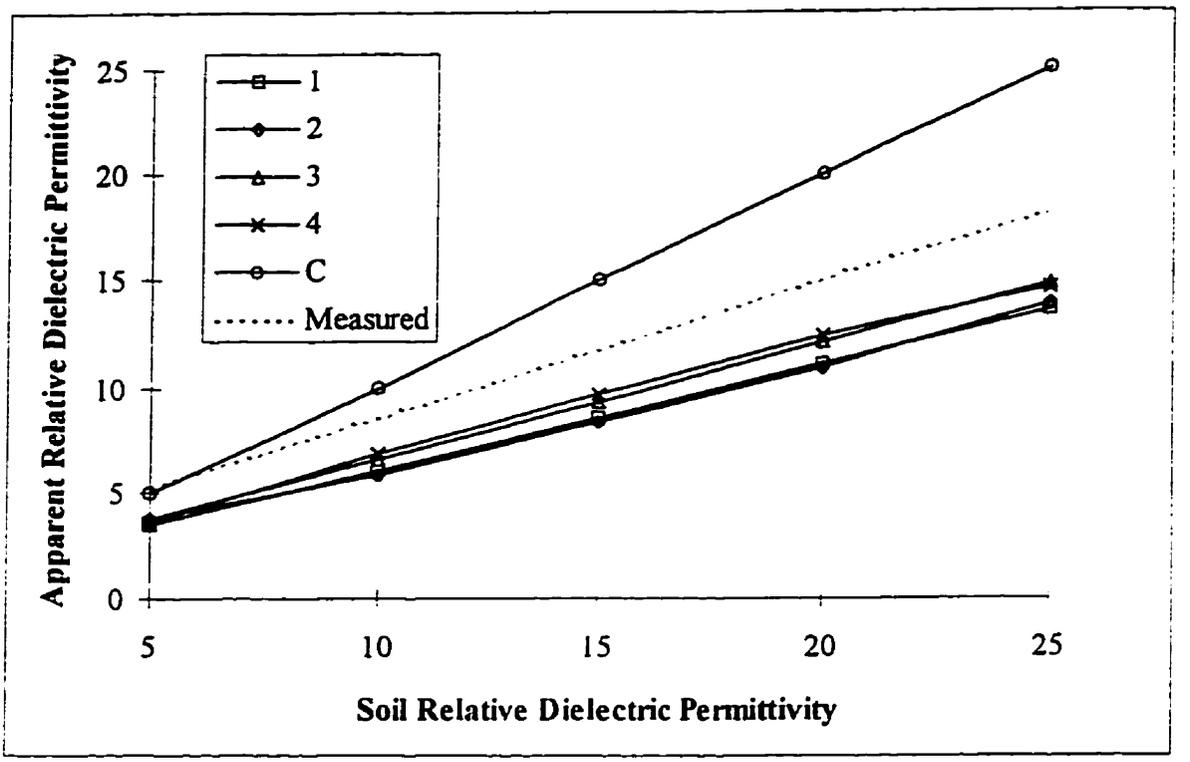

Figure 4-55. Numerically determined and laboratory-measured calibration curves for the *Redman and DeRyck* [1994] probe. (1) *ID*:*D*=11.1, *OD*:*D*=14.3, a=110; (2) *ID*:*D*=6.9, *OD*:*D*=14.3, a=110; (3) *ID*:*D*=11.1, *OD*:*D*=14.3, a=45; (4) *ID*:*D*=7.4, *OD*:*D*=9.5, a=110; (C) conventional metal rod probe; and (dashed line) laboratory calibration.

Redman and D'Ryck presented the results of a laboratory calibration of their probe using mixtures of water, ethanol and hexane. This calibration procedure has the advantages of providing numerous calibration points over a wide range of relative dielectric permittivities while allowing for a convenient, accurate measurement of the relative dielectric permittivity of the surrounding medium in a coaxial cell. The numerical and direct calibrations show linear relationships between K_m and the relative dielectric permittivity of the medium with similar slopes; but, the direct calibration shows consistently higher measured relative dielectric permittivities than those predicted by the numerical model. The direct calibration shows that the probe will measure an apparent relative dielectric permittivity greater than the soil relative dielectric permittivity for K_{soil} values as high as 6. Given that the probe materials have relative dielectric permittivities less than 3, this result suggests that the some aspect of the probe design or waveform interpretation has resulted in an overestimation of the apparent relative dielectric permittivity in the measured data.

4.8.6 Hook et al. Multilevel Probe

The *Hook et al.* [1992] probe also shows a linear response to the soil relative dielectric permittivity (Figure 4-56). The base case has two rods with an $H:W$ of 1 and an $S:W$ of 2. The apparent relative dielectric permittivity decreases with a decrease in $S:W$ or the inclusion of a central rod. A decrease in $H:W$ improves the probe response.

In their analysis of the response of their probe, *Hook et al.* [1992] presumed that a linear relationship existed between the travel time measured by their probe, t_m, and the travel time that would be measured by a continuous-rod probe, t_c.

$$t_c = \left(\frac{t_m}{B}\right) + A. \tag{4-26}$$

where A and B are defined by *Hook et al.* [1992] as the offset and interaction efficiency, respectively.

This assumption leads to the following relationship between the measured and soil relative dielectric permittivities for a probe of length, L,

$$K_m = B^2 K_{soil} - \frac{2cAB^2}{L}\sqrt{K_{soil}} + \left(\frac{cAB}{L}\right)^2. \tag{4-27}$$

The authors apply this model using a two point calibration of the probe in air and in water. Although this calibration procedure has the advantage of being easy to perform, it would be more appropriate to calibrate the probe with two fluids with relative dielectric permittivities closer to the range of relative dielectric permittivities of typical soils.

The measured calibration curves for two segments of a strip line probe with cross sections approximately equivalent to the modeled case 4 are included on Figure 4-56. The direct calibration is similar to the modeled response although the predicted apparent relative dielectric permittivities are consistently lower than the measured values. As with the *Redman and DeRyck* [1994] probe, measured relative dielectric permittivities higher than the soil relative dielectric permittivity suggest some error in the measured propagation velocity unless the probe materials have a relative dielectric permittivity that is unusually high for plastics. For this probe, the improved interpretation of the terminal reflection using the shorting diodes suggests that the discrepancy is due to the interpretation of the location of the beginning of the probe, represented by the constant, A.

The highly linear relationship between K_m and K_{soil} determined numerically suggests that the assumption underlying the form of Equation 4-26 is not appropriate. Given that the probe materials and

surrounding porous medium are placed in parallel for this design, the calibration relationship should be of the form of an arithmetic averaging model,

$$K_m = w_{soil} K_{soil} + (1 - w_{soil}) K_{probe}, \tag{4-27}$$

where K_{probe} and K_{soil} are the relative dielectric permittivities of the probe materials and the surrounding soil and w_{soil} is the weighting factor on the soil. Therefore, the square of the interaction efficiencies reported by *Hook et al.* [1992] approximately describe the fractional sensitivity of their probes to the soil.

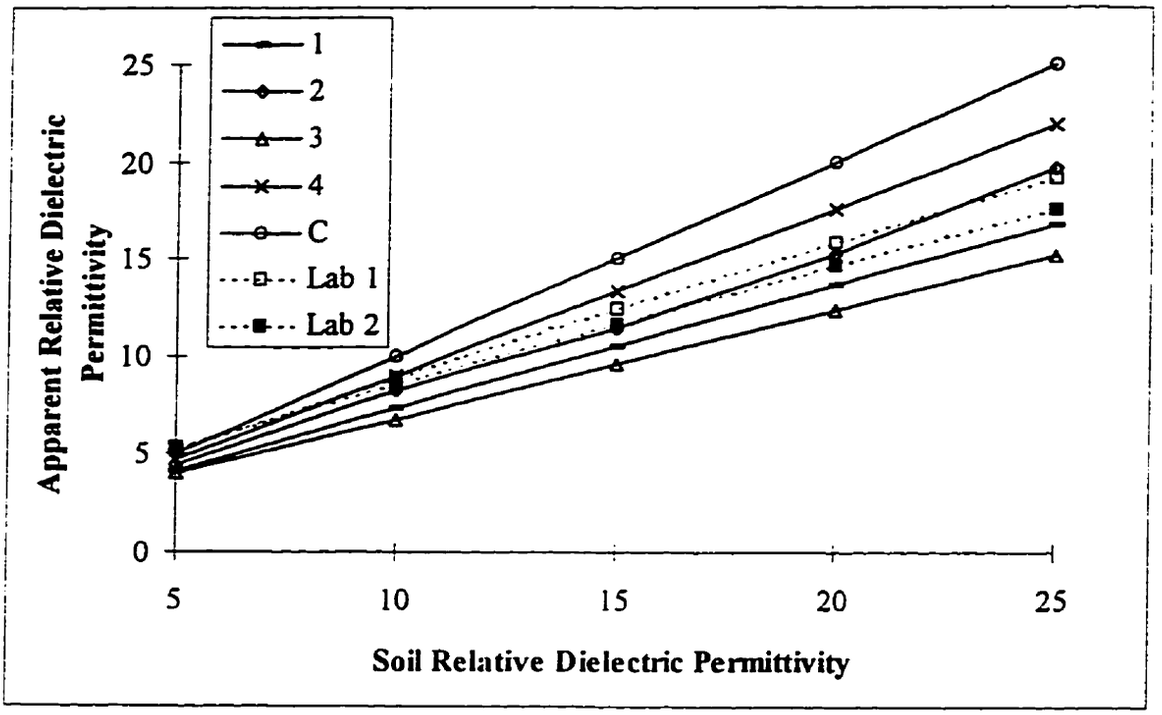

Figure 4-56. Numerically determined and laboratory-measured calibration curves for the *Hook et al.* [1992] probe, (1) H:W=1, S:W=2, two rods; (2) H:W=1, S:W=4, two rods; (3) H:W=1, S:W=4, 3 rods; (4) H:W=0.5, S:W=2, 2 rods; (C) conventional metal rod probe; (open squares) laboratory calibration of strip line probe segment 1; and (closed squares) laboratory calibration of strip line probe segment 2.

4.8.7 Selker et al. Surface Probe

The base case *Selker et al.* [1993] surface probe has two square rods with an S:W of 3, H_b:W and W_b:W are equal to 4.5 and 9, respectively and the rods do not extend below the base of the box into the soil (H_o

= 0). As shown in Figure 4-57, the probe measures higher apparent dielectric permittivities if *S*:*D* is increased or *H*:*W* is decreased; a third rod decreases the K_m values.

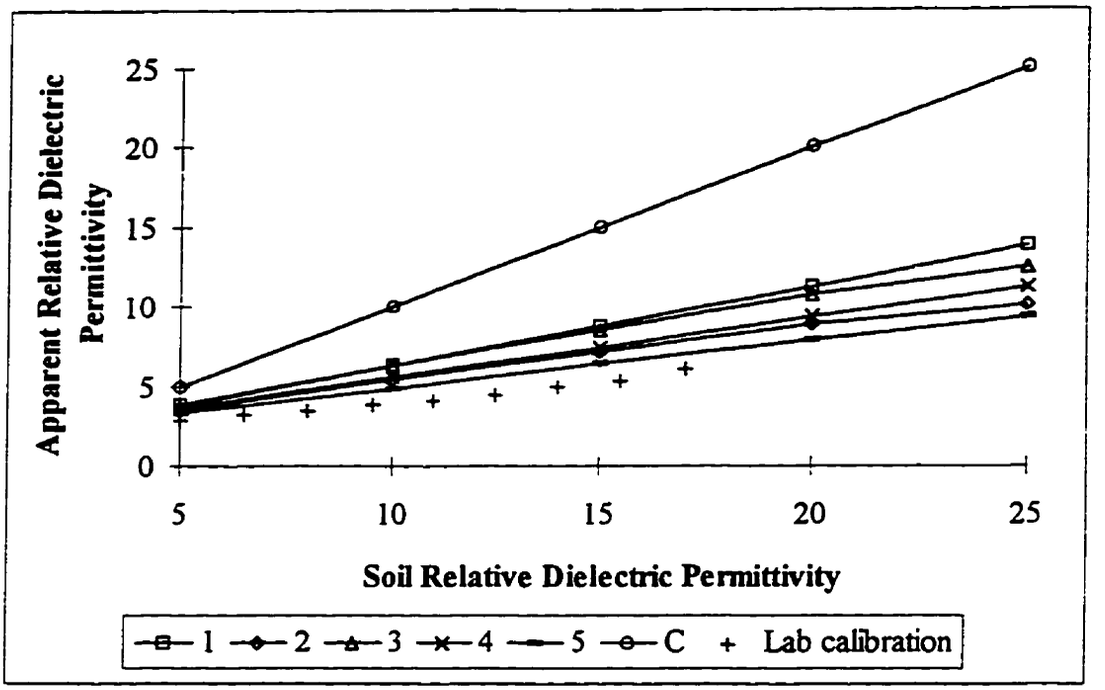

Figure 4-57. Numerically determined and laboratory-measured calibration curves for the *Selker et al.* [1993] surface probe, (1) *H*:*W*=1, *Ho*:*W*=0, *S*:*D*=3, *Wb*:*W*=9, *Hb*:*W*=4.5, 2 rods; (2) *H*:*W*=1, *Ho*:*W*=0.5, *S*:*D*=3, *Wb*:*W*=9, *Hb*:*W*=4.5, 2 rods; (3) *H*:*W*=0.25, *Ho*:*W*=0, *S*:*D*=3, *Wb*:*W*=9, *Hb*:*W*=4.5, 2 rods; (4) *H*:*W*=1, *Ho*:*W*=0, *S*:*D*=5, *Wb*:*W*=9, *Hb*:*W*=4.5, 2 rods; (5) *H*:*W*=1, *Ho*:*W*=0, *S*:*D*=5, *Wb*:*W*=9, *Hb*:*W*=4.5, 3 rods; (C) conventional metal rod probes; and (+) laboratory calibration.

If the box surrounding the rods in the *Selker et al.* [1993] surface probe is sufficiently large to eliminate the influence of the surrounding air and half of the rod height extends into the soil, the probe response can be defined by a simple analytical description of rods placed on the boundary between two half-spaces of different relative dielectric permittivities. *Knight et al.* [1994] showed that for this case the apparent relative dielectric permittivity, K_a, will follow,

$$K_a = 0.5K_p + 0.5K_s, \tag{4-28}$$

where K_p and K_s are the relative dielectric permittivities of the probe body and soil, respectively. As seen in Figure 4-57, the modeled apparent relative dielectric permittivities agree with the analytically determined

linear response ranging from 3.9 to 13.9 for the case 2 design. *Selker et al.* [1993] fit a second order polynomial to values of the apparent relative dielectric permittivity measured with a case 2 probe configuration and gravimetrically determined soil water contents measured in a quartz sand. Although this function described the relationship between the sets of measured values adequately, it is an inappropriate form for general use because it has a maximum at a water content of 0.31. For comparison, the measured water contents were replaced with soil relative dielectric permittivities using Equation 1-2. The numerical and analytical approaches do not agree with the measured response of the *Selker et al.* [1993] probe. Potential differences may be due to overestimating the appropriate physical length of the probes because of their serpentine layout of the metal rods on the face of the probe (see Figure 4-8), poor contact with the soil surface, or inaccuracies in the gravimetrically determined soil water contents used for calibration.

4.8.8 White and Zegelin Probe

The semicoaxial design of this surface probe is not highly sensitive to the probe dimensions.

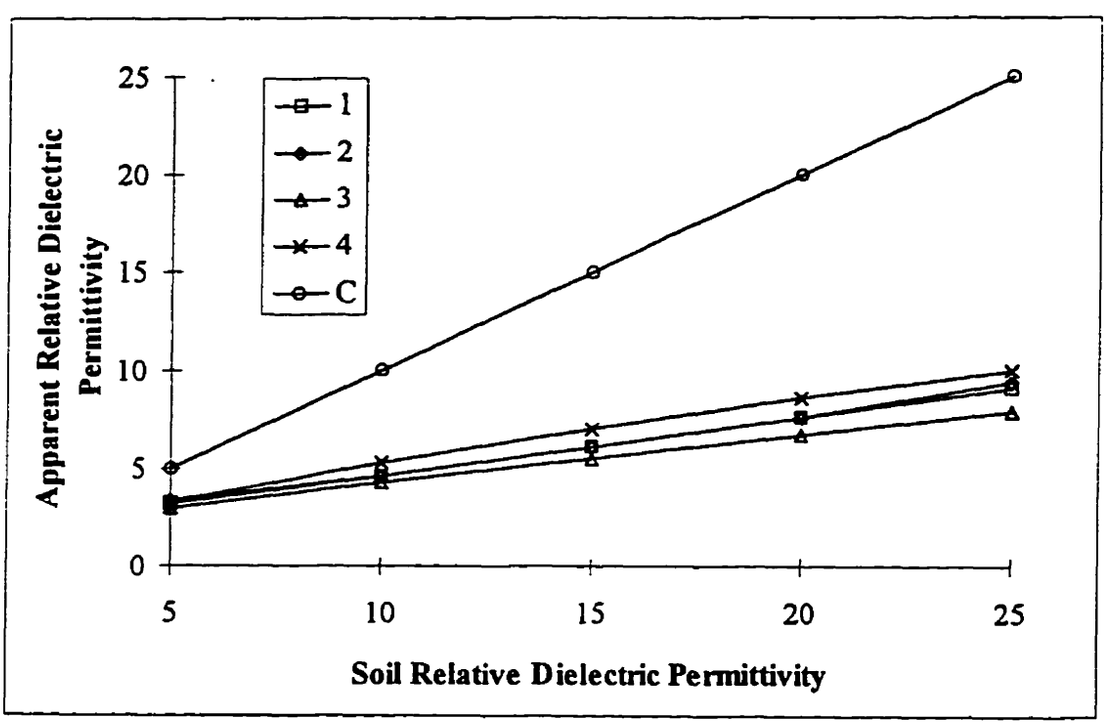

Figure 4-58. Numerically determined calibration curves for the *White and Zegelin* [1992] surface probe, (1) OD:D=3, W:D=3.5, t:D=0.17, K_{fill}=2.4; (2) OD:D=3, W:D=3.5, t:D=0.17, K_{fill}=2.8; (3) OD:D=5, W:D=2.5, t:D=0.17, K_{fill}=2.4; (4) OD:D=5, W:D=0.0, t:D=0.17, K_{fill}=2.4, rectangular rod and shield; and (C) conventional metal rod probes.

Figure 4-58 shows the responses of several configurations of the *White and Zegelin* [1992] probe. The probe response improves if PVC (K=2.8) is used to fill the gap between the conductors rather than beeswax (K=2.4). Increasing the diameter of the shield decreases the response of the probe. However, a rectangular probe design with the increased *OD:D* shows an improved response. The outer conductor acts as a constant potential boundary; therefore, the thickness of the shield, t, has no effect on the probe response (not shown).

4.8.9 Comparison of Probe Sensitivities

Equation 2-24 defines the sensitivity of a probe from the slope of a plot of the square root of the measured relative dielectric permittivity as a function of the square root of the relative dielectric permittivity of the soil. A similar development defines the sensitivity as a function of the slope of the numerically determined calibration curves, dK_m / dK_{soil}, as,

$$\frac{dt}{d\theta} = \frac{dK_m}{dK_{soil}} \frac{dt}{dK_m} \frac{dK_{soil}}{d\theta} = \frac{dK_m}{dK_{soil}} \frac{La}{c} \sqrt{\frac{K_{soil}}{K_m}} . \qquad (4\text{-}29)$$

For direct comparison among the probe designs, sensitivities were calculated for probes of an arbitrary length of 1 m. These sensitivities are plotted as a function of the water content on Figure 4-59.

The results demonstrate that all of the alternative probes show a reduced sensitivity compared to conventional probes. Most of the probes show near constant sensitivity over the range of soil water contents. Only the coated continuous-rod probes and the alternative multilevel probe show clearly varying sensitivities; as discussed in the development of the analytical solution above, this behavior is due to the placement of nonmetallic probe materials in series with the surrounding medium with respect to the probe geometry. Only those probes that show a sensitivity that is independent of the water content will measure the correct length-weighted water content if the water content varies along their length.

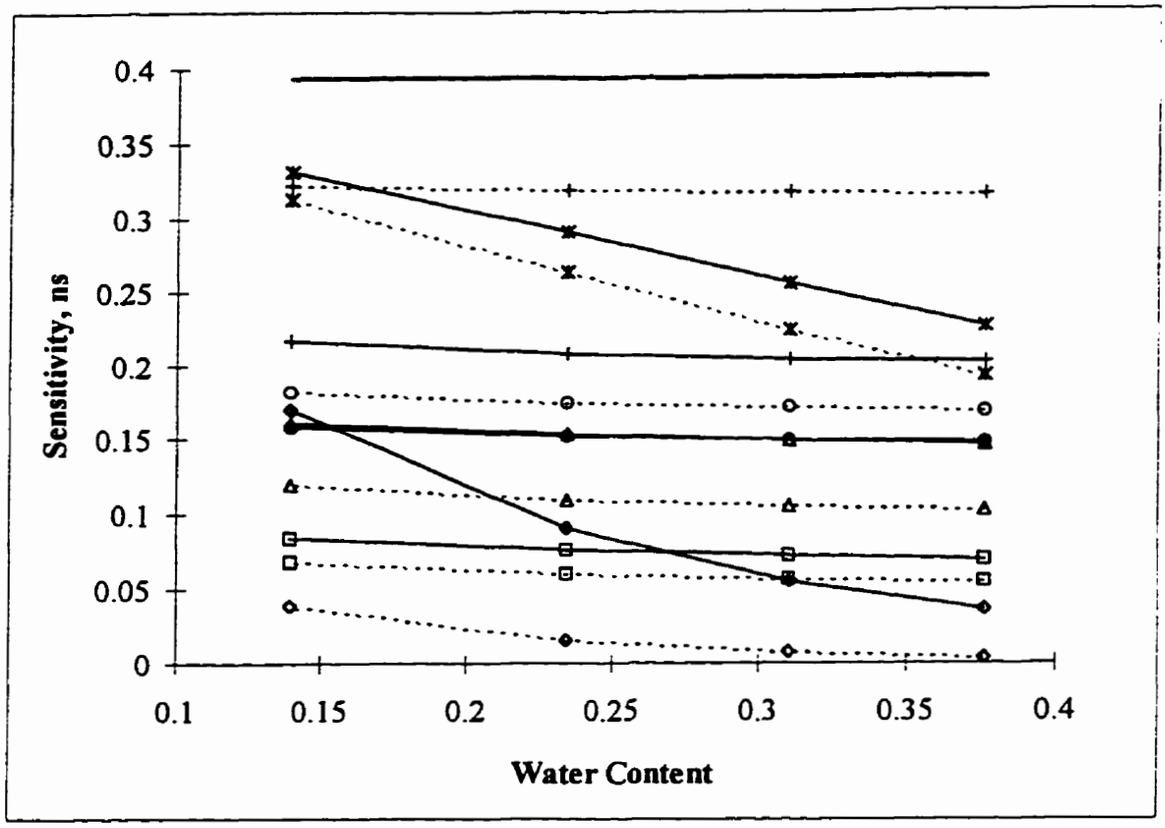

Figure 4-59. Sensitivities of conventional and alternative TDR probes as a function of the volumetric soil water content. (star - solid line) PVC coated continuous-rod probes case 1; (star - dashed line) PVC coated continuous-rod probes case 2; (diamond - solid line) our multilevel probe case 1; (diamond - dashed line) our multilevel probe case 2; (plus - solid line) the *Hook et al.* [1992] probe case 1; (plus - dashed line) the *Hook et al.* [1992] probe case 4; (circle - solid line) *Redman and DeRyck* [1994] probe case 1; (circle - dashed line) *Redman and DeRyck* [1994] probe case 3; (triangle - solid line) *Selker et al.* [1993] probe case 1; (triangle - dashed line) *Selker et al.* [1993] probe case 4; (square - solid line) the *White and Zegelin* [1992] probe case 1; (square - dashed line) the *White and Zegelin* [1992] probe case 3.

The numerical calibration curves presented on Figures 4-53 through 4-58 show that all of the alternative probe designs measure relative dielectric permittivities lower than those that would be measured with standard, continuous-rod probes. The optimal probe design will combine a high probe response to minimize the impact of travel time measurement errors and a high sensitivity to distinguish among soil water contents with greater precision.

4.8.10 Summary and Conclusions

The probe response and the level and uniformity of the probe sensitivity are only partial criteria for the choice of a design of a TDR probe. Other factors affecting the selection of a probe design may include the minimization of conductive losses, the desired sample area, the ease of interpreting travel times from the waveforms, the achievable vertical resolution of the water content or EC profile and the ease of installation for the site soil. However, some general recommendations on probe design can be made based on the results presented above.

Conventional probes have the highest probe response and the highest, most constant sensitivity. Therefore, conventional probes should be used for all applications unless specific measurement objectives require the use of an alternative probe design.

The presence of thin coatings on rods greatly influences the behavior of the probes. Even this simple design results in a dependence of the probe sensitivity on the soil water content. To minimize their impact, rod coatings should be as thin as possible and constructed from high relative dielectric permittivity materials. Furthermore, given that the response of coated continuous-rod probes is a function of the separation to diameter ratio, the separation must be constant along the length of the rods, unlike conventional rods.

The alternative multilevel TDR probe presented above is a specialized case of a coated rod probe. This design offers very precise vertical resolution of the water content profile. However, because of the strong dependence of the sensitivity on the soil water content, this probe should not be used in conditions of highly variable water contents over the length of the metal rods. The access tubes should be water-filled to maximize the sensitivity and probe response.

The use of low-loss coaxial cables within the access tubes of the *Redman and DeRyck* [1994] probe can allow water content profiling to extended depths, even in electrically conductive soils. Using large rods separated by a small angle will marginally improve the probe response.

The case 4 *Hook et al.* [1992] probe with two thin, wide blades with a large separation shows the greatest sensitivity and highest measured apparent dielectric permittivites of all of the alternative probes modeled. The rods can be electrically shorted, allowing for the depth profiling of water content beneath a single surface point. In addition, shorting improves the interpretation of the pulse travel time, leading to more accurate water content determinations. To maximize the response and sensitivity of this probe, the rods should have a width equal to or greater than their height, only two rods should be used and the rod separation should be large. The main limitation on the use of this probe will be conductive losses in electrically conductive soils because the metal rods are in direct contact with the soil along their entire length.

Both surface probe designs analyzed show near-constant probe sensitivities, regardless of the water content of the medium. The *Selker et al.* [1993] probe configurations modeled showed higher probe sensitivities. However, the serpentine probe layout on the base of the probe may introduce uncertainties into interpretations of the probe response.

There appear to be limitations to the accuracies of the published physical calibrations of alternative probes. Discrepancies between the modeled and observed responses may be due to the behavior of the EM wave at the ends of the rods, inaccuracies in the method of waveform analysis, limitations to the standard methods used for baseline water content measurements, or interactions between the pulse and the surrounding medium that are currently not understood and, therefore, not considered in the model. The mixed fluid method described by *Redman and DeRyck* [1994] appears to provide the best range of well-defined, controlled relative dielectric permittivities for laboratory calibrations. Measurement during drainage in a homogeneous medium offers the widest range of relative dielectric permittivities for calibration of larger probes in the field.

5. CHAPTER FIVE

IMPLICATIONS FOR WATER CONTENT AND EC MONITORING WITH TDR

The relative dielectric permittivity measured by TDR using standard, continuous-rod probes can be directly related to the water content of the surrounding medium without the need for soil-specific calibration in a wide range of soils. This property makes TDR a very useful tool for water content measurement in the field. In addition, the signal loss measured by TDR can be related to the bulk EC of the surrounding medium, indicating their ability to monitor transport of electrolytic solutes.

TDR is used in both the laboratory and the field to measure the water content and bulk EC. This wide range of applications requires a variety of probe designs; laboratory probes generally use thin rods, with small separations while field probes require thicker rods for ease of installation. Previous laboratory studies and analytical descriptions showed that the probe configuration affects the sample size and spatial distribution of probe sensitivity. The results of a numerical investigation presented here specifically show the sample area of two- and three-rod probes. Two-rod probes have a much larger sample area with a more uniformly distributed sensitivity than three-rod probes. In addition, the analysis shows that the sample area of two-rod probes is largely controlled by the rod separation; an increase in the rod diameter improves the uniformity of the spatial distribution of probe sensitivity. The sample area of a continuous-rod probe is independent of the soil water content if the water content is uniform throughout the sample area.

To infer the concentration of an electrolytic solute from the TDR measured water content and EC under spatially and temporally variable water content conditions requires an understanding of the relationship between the TDR-measured bulk EC and the soil water content. The results of this work demonstrate the dependence of the EC response of standard, continuous-rod TDR probes on the soil water content. In addition, the laboratory results presented here show that two-rod probes either with or without baluns can be used to measure the bulk EC as well as three-rod designs. The results of a field experiment show that the EC response of long, continuous-rod probes can be related directly to the solute mass residing between the rods, even if the water content and pore water EC are spatially variable. This finding supports the application of TDR to solute monitoring under transient flow conditions.

In the field, standard continuous-rod probes are commonly installed vertically from the ground surface, measuring the water content and the bulk EC over large sample volumes. As a result, these probes face limitations in profiling either the water content or the bulk EC with depth. Similarly, the long metal rods face excessive power losses through electrical conduction, limiting the maximum depth of investigation using TDR. Finally, the standard probes require a minimum length of approximately 10 cm to clearly identify the reflection from the ends of the rods, making water content measurement in the very

shallow subsurface impractical. Several alternative TDR probes have been designed to address these limitations.

Despite the availability of alternative probes for specific measurement needs, there is still a need for a probe that can profile both the water content and the bulk electrical conductivity with depth. A probe is presented that can make these measurements with a very fine vertical profiling interval. A field trial shows that the water content profiling capabilities of the probe are comparable to a neutron probe. In addition, the probe is shown to be able to monitor the advance of a pulse of an electrolytic solute. Using this probe, solute transport can be studied over discrete depth intervals in the field under transient flow conditions.

Most of the published alternative probe designs have nonmetallic probe components within their sample area. As a result, the relative dielectric permittivity measured by the probes will be some average of the relative dielectric permittivities of the probe components and the surrounding soil. Thus, each probe requires a specific calibration to relate the measured relative dielectric permittivity to the soil water content. Unfortunately, building and calibrating alternative probes is difficult and time consuming, making optimization of the probe design difficult. This investigation presents a numerical approach to defining the sensitivity of an alternative TDR probe based on a representative cross section through the probe. In addition to allowing for the direct comparison of the performance of alternative probes, this approach can be used to optimize the design of a probe without the need for multiple calibrations. In addition, the dependence of probe sensitivity on the soil water content can be determined numerically; this is an important quality of a probe because any probe with a water content-dependent sensitivity will not measure the correct length-weighted average water content if the water content varies along its length. Recommendations are made for changes in the configurations of all published alternative probes to improve their sensitivities.

The sample area of each of the alternative probes was determined numerically. This approach adds an additional criterion on which to compare probe designs and by which a probe design can be optimized for specific sampling objectives. Given that most nonmetallic probe components are plastics, with very low relative dielectric permittivities, the sample areas of probes that place their nonmetallic components in series with the soil will vary with the soil water content, becoming smaller with increases in the soil water content. Probes that place their nonmetallic components in parallel have larger, more uniformly distributed sensitivities that are less dependent on the relative dielectric permittivity of the surrounding medium. Design changes are recommended for all published probes to increase their sample size, increase the uniformity of the spatial distribution of their sensitivity and to reduce the dependence of their sample size on the soil water content.

REFERENCES

Annan, A. P. **1977a.** Time-domain reflectometry — air-gap problem in a coaxial line, in Report of Activities, Part B, Pap. 77-1B, Geol. Surv. Can., Ottawa, ON, 55-58.

Annan, A. P. **1977b.** Time-domain reflectometry — air-gap problem for parallel wire transmission lines, in Report of Activities, Part B, Pap. 77-1B, Geol. Surv. Can., Ottawa, ON, 59-62.

Archie, G.E. **1942.** The electric resistivity log as an aid in determining some reservoir characteristics, Trans. AIME 146, 54-62.

Baker, J.M., and R.J. Lascano. **1989.** The spatial sensitivity of time domain reflectometry, Soil Sci., 147, 378-384.

Baker, J.M. and E.J.A. Spaans. **1993.** Comments on "Time domain reflectometry measurements of water content and electrical conductivity in layered soil columns", Soil Sci. Soc. Am. J., 57, 1395-6.

Barthel, J., F. Feuerlein, R. Neueder, and R. Wachter. **1980.** Calibration of conductance cells at various temperatures, J. Solution Chem., 9, 209-219.

Birchak, J.R., C.G. Gardner, J.E. Hipp, and J.M. Victor. **1974.** High dielectric constant microwave probes for sensing soil moisture, Proc. IEEE, 62, 93-98.

Dalton, F.N., W.N. Herkelrath, D.S. Rawlins, and J.D. Rhoades. **1984.** Time-domain reflectometry: simultaneous measurement of water content and electrical conductivity with a single probe, Science, 224, 989-990.

Dasberg, S. and W. Hopmans. **1992.** Time domain reflectometry calibration for uniformly and nonuniformly wetted sandy and clayey loam soils, Soil Sci. Soc. Am. J., 56, 1341-5.

Fellner-Feldegg, H. **1969.** The measurement of dielectrics in the time domain. J. Phys. Chem. 73, 616-623.

Giese, K. and R. Tiemann. **1975.** Determination of the complex permittivity from thin-sample time domain reflectometry improved analysis of the step response waveform. Advances in Molecular Relaxation Processes 7, 45-59.

Heimovaara, T.J. 1992. Comments on "Time domain reflectometry measurements of water content and electrical conductivity of layered soil columns." Soil Sci. Soc. Am. J. 56, 1657-8.

Heimovaara, T.J., A.G. Focke, W. Bouten and J.M. Verstraten. 1995. Assessing temporal variations in soil water composition with time domain reflectometry. Soil Sci. Soc. Am. J. 59, 689-98.

Herkelrath, W.N., S.P. Hamburg, and F. Murphy. 1991. Automatic real-time monitoring of soil moisture in a remote field area with time domain reflectometry, Water Resour. Res., 27, 857-64.

Hook, W.R., N.J. Livingston, Z.J. Sun and P.B. Hook. 1992. Remote diode shorting improves measurement of soil water by time domain reflectometry, Soil Sci. Soc. Am. J., 56, 1384-1391.

Kachanoski, R.G., E. Pringle and A. Ward. 1992. Field measurement of solute travel times using time domain reflectometry, Soil Sci. Soc. Am. J., 56, 47-52.

Kachanoski, R.G., L. Thony, M. Vauclin, G. Vachaud and R. Laty. 1994. Measurement of solute transport during constant infiltration from a point source, Soil Sci. Soc. Am. J. 58, 304-9.

Knight, J.H. 1991. Discussion of "The spatial sensitivity of time-domain reflectometry" by J.M Baker and R.J. Lascano, Soil Sci. Soc. Am. J., 151, 254-255.

Knight, J. H. 1992. Sensitivity of time domain reflectometry measurements to lateral variations in soil water content. Water Resour. Res., 28, 2345-2352.

Knight, J.H., P.A. Ferré, D.L. Rudolph and R.G. Kachanoski. 1997. A numerical analysis of the effects of coatings and gaps upon relative dielectric permittivity measurement with time domain reflectometry. Accepted in Water Resour. Res., 33, 1455-60.

Knight, J. H., I. White, and S. J. Zegelin. 1994. Sampling volume of TDR probes used for water content monitoring, in Proc. of the Symposium and Workshop on Time Domain Reflectometry in Environmental, Infrastructure and Mining Applications, Special Publication SP 19-94, US Department of Interior Bureau of Mines, Minneapolis, MN, 93-104.

Kramer, J.H., S.J. Cullen, and L.G. Everett. 1992. Vadose zone monitoring with the neutron moisture probe. Ground Water Mon. Rev. Summer, 177-187.

Ledieu, J., P. De Ridder, P. De Clerck, and S. Dautrebande. 1986. A method of measuring soil moisture by time-domain reflectometry, J. of Hydrol., 88, 319-328.

MacFarlane, D.S., J.A. Cherry, R.W. Gillham and E.A. Sudicky. 1983. Migration of Contaminants in Groundwater at a Landfill: A Case Study, 1. Groundwater Flow and Plume Delineation, J. of Hydrol., 63, 1-29.

Malicki, M.A., R. Plagge, M. Renger, and R.T. Walczak. 1992. Application of time-domain reflectometry (TDR) soil moisture miniprobe for the determination of unsaturated soil water characteristics from undisturbed soil cores. Irrig. Sci., 13, 65-72.

Mallants, D., M. Vanclooster, N. Toride, J. Vanderborght, M. Th. van Genuchten, and J. Feyen. 1996. Comparison of three methods to calibrate TDR for monitoring solute movement in undisturbed soil, Soil Sci. Soc. Am. J., 60, 747-754.

McLaren, R. 1996. GRIDBUILDER User's Manual, Waterloo Centre for Groundwater Research, Waterloo, ON, Canada.

Mualem, Y, and S.P. Friedman. 1991. Theoretical prediction of electrical conductivity in saturated and unsaturated soil. Water Resour. Res., 27, 2771-7.

Musil, J. and F. Zacek. 1986. Microwave measurement of complex permittivity by free space methods and their application, Elsevier, Amsterdam, 275 p.

Nadler, A., S. Dasberg, and I. Lapid. 1991. Time domain reflectometry measurements of water content and electrical conductivity of layered soil columns. Soil Sci. Soc. Am. J., 55, 938-943.

Nwankwor, G.I. 1982. A comparative study of specific yield in a shallow unconfined aquifer. M.Sc. Thesis, University of Waterloo, 63 p.

Pinder, G. F., and E. O. Frind. 1972. Application of Galerkin's procedure to aquifer analysis, Water Resour. Res., 8, 108-120.

Redman, J.D. 1995. User's manual for WATTDR software, Waterloo Centre for Groundwater Research, University of Waterloo, Waterloo, ON 10 p.

Redman, J.D. and S.M. D'Ryck. 1994. Monitoring nonaqueous phase liquids in the subsurface with multilevel time domain reflectometry probes. Proc. of the Symposium and Workshop on Time Domain Reflectometry in Environmental, Infrastructure and Mining Applications, Sept., 1994, 207-14.

Rhoades, J.D., P.A.C. Raats and R.J. Prather. 1976. Effects of liquid-phase electrical conductivity, water content, and surface conductivity on bulk soil electrical conductivity, Soil Sci. Soc. Am. J., 40, 651-655.

Risler, P.D., J.M. Wraith and H.M. Gaber. 1996. Solute transport under transient flow conditions estimated using time domain reflectometry, Soil Sci. Soc. Am. J., 60, 1297-1305.

Roth, K., R. Schulin, H. Fluhler, and W. Attinger. 1990. Calibration of time domain reflectometry for water content measurement using a composite dielectric approach, Water Resour. Res., 26, 2267-2273.

Rudolph, D.L., R.G. Kachanoski, M.A. Celia, D.R. LeBlanc and J.H. Stevens. 1996. Infiltration and solute transport experiments in unsaturated sand and gravel, Cape Cod, Massachusetts: Experimental design and overview of results, Water Resour. Res., 32, 519-532.

Selker, J.S., L. Graff and T. Steenhuis. 1993. Noninvasive time domain reflectometry moisture measurement probe. Soil Sci. Soc. Am. J., 57, 934-6.

Spaans, E.J.A. and J.M. Baker. 1993. Simple baluns in parallel probes for time domain reflectometry, Soil Sci. Soc. Am. J., 57, 668-73.

Topp, G.C. 1987. The application of time domain reflectometry (TDR) to soil water content measurement. Proc. Intl. Conf. on Meas. of Soil and Plant Water, 85-93.

Topp, and G.C., J.L. Davis. 1985. Measurement of soil water content using time-domain reflectometry (TDR): A field evaluation. Soil Sci. Soc. Am. J., 49, 19-24.

Topp, G.C., J.L. Davis, and A.P. Annan. 1980. Electromagnetic determination of soil water content; measurement in coaxial transmission lines. Water Resour. Res., 16, 574-582.

Topp, G.C., J.L. Davis, and A.P. Annan. 1982a. Electromagnetic determination of soil water content using TDR: I. Applications to wetting fronts and steep gradients. Soil Sci. Soc. Am. J., 46, 672-674.

Topp, G.C., J.L. Davis and A.P. Annan. 1982b. Electromagnetic determination of soil water content using TDR: II. Evaluation of installation and configuration of parallel transmission lines. Soil Sci. Soc. Am. J., 46, 678- 684.

Topp, G.C., M. Yanuka, W.D. Zebchuk, and S.J. Zegelin. 1988. Determination of electrical conductivity using time domain reflectometry: soil and water experiments in coaxial lines, Water Resour. Res., 24, 945-52.

Von Hippel, A.R. (Ed.). 1954. Dielectric materials and applications, The Technical Press of MIT and John Wiley and Sons, Inc, NY, 438p.

Van Loon, W.K.P. 1991. Application of dispersion theory to time domain reflectometry in soils, Transport in Porous Media, 6, 391-406.

Ward, A.L., R.G. Kachanoski and D.E. Elrick. 1994. Laboratory measurements of solute transport using time domain reflectometry. Soil Sci. Soc. Am. J., 58, 1031-1039.

Ward, A.L., R.G. Kachanoski and I.J. van Wesenbeeck. 1988. Solute transport during three dimensional unsaturated water flow: Axisymmetric measurements using time domain reflectometry. In Agronomy abstracts, ASA, Madison, WI, 192.

Weast, R.C. (Ed.). 1990. CRC Handbook of Chemistry and Physics, 71st ed., CRC Press, Boca Raton, FL.

Whalley, W. R. 1993. Considerations on the use of time-domain reflectometry (TDR) for measuring soil water content, J. Soil Sci., 44, 1-9.

White, I., J. H. Knight, S. J. Zegelin, and G. C. Topp. 1994. Comments on 'Considerations on the use of time-domain reflectometry (TDR) for measuring soil water content' by W. R. Whalley, European J. Soil Sci., 45, 503-508.

White, I. and S.J. Zegelin. 1992. Measurement of moisture content and electrical conductivity. U.S. Patent 5,136,246.

Wygal, R.J. 1963. Construction of models that simulate oil reservoirs. Soc. of Pet. Eng. J., 281-286.

Wyllie, M.R.J., and M.B. Spangler. 1952., Bull. Am. Assoc. Pet. Geol., 36, 359.

Yanuka, M., G.C. Topp, S. Zegelin and W.D. Zebchuk. 1988. Multiple reflection and attenuation of time domain reflectometry pulses: theoretical considerations for applications to soil and water. Water Resour. Res., 24, 7, 939-944.

Zegelin, S.J., I. White, and D.R. Jenkins. 1989. Improved field probes for soil water content and electrical conductivity measurement using time domain reflectometry, Water Resour. Res., 25, 2367-76.